UNIVERSITY OF SOUTHAMPTON

DOCTORAL THESIS

Design of Electric Vehicle Warning Sound Systems to Minimise Drive-by Noise

Author:
Nikolaos KOURNOUTOS

Supervisor:
Dr. Jordan A. H. CHEER

Thesis submitted for the degree of
Doctor of Philosophy

Signal Processing, Audio and Hearing Group
Institute of Sound and Vibration Research

October 29, 2020

UNIVERSITY OF SOUTHAMPTON

Abstract

Faculty of Engineering and Physical Sciences
Institute of Sound and Vibration Research

Doctor of Philosophy

Design of Electric Vehicle Warning Sound Systems to Minimise Drive-by Noise

by Nikolaos KOURNOUTOS

Electric and hybrid-electric vehicles are required to emit artificial warning sounds at low speeds, as their quiet operation poses a potential hazard for vulnerable road users. At the same time, concerns have been expressed over the increase in environmental noise levels this measure might bring. This thesis aims to design a warning sound system that can both fulfil its role as a safety measure while minimising its noise contribution. In addition, the proposed system must be viable for a wide scale implementation by keeping the manufacturing and maintenance costs low, and ensuring that it is physically robust for long-term operation within a vehicle.

For this purpose, a directional sound system based on structural vibration has been designed, utilising an array of inertial actuators forcing the structure upon which they are attached to vibrate and radiate a sound field of controllable directivity. An analytical model was formulated to describe the physical system, combining existing models of structural vibration and sound radiation. A simulations-based parametric study performed using this model provided insight into the design parameters, indicating that a larger number of actuators distributed evenly along the entire radiating surface ensures the greatest possible bandwidth and steerability for the system.

The construction and measurement of a simple physical prototype system allowed for the experimental validation of the analytical model. The proposed system was evaluated in its intended implementation by installing the array in a test vehicle and measuring the directivity of the radiated sound field for different arrangements of the actuators on the vehicle. Experimental results indicated that an actuator array installed in the bumper of the vehicle can achieve directivity of at least 10 dB in terms of acoustic contrast level, for a bandwidth from 300 Hz to 5 kHz, while minimising interior and drive-by noise.

An additional approach to reducing the impact of warning sounds was also investigated, in the form of an environmentally adaptive warning sound system. The proposed system employs an algorithm that estimates the auditory thresholds due to a changing sonic environment, and uses this information to adapt the warning sound. This aims to render the vehicle detectable in all environments without unnecessarily increasing its level, therefore limiting noise pollution. The adaptation algorithm was tested in a simulation-based application study for a variety of environmental noise scenarios, showing that it is capable of selectively adjusting the output of the warning sound at specific frequency bands to match the audibility threshold.

Contents

List of Figures

List of Tables

Declaration of Authorship

I, Nikolaos KOURNOUTOS, declare that this thesis titled "Design of Electric Vehicle Warning Sound Systems to Minimise Drive-by Noise" and the work presented in it are my own. I confirm that:

- This work was done wholly or mainly while in candidature for a research degree at this University.
- Where any part of this thesis has previously been submitted for a degree or any other qualification at this University or any other institution, this has been clearly stated.
- Where I have consulted the published work of others, this is always clearly attributed.
- Where I have quoted from the work of others, the source is always given. With the exception of such quotations, this thesis is entirely my own work.
- I have acknowledged all main sources of help.
- Where the thesis is based on work done by myself jointly with others, I have made clear exactly what was done by others and what I have contributed myself.
- Parts of this thesis have been published as:
  - N. Kournoutos, J. Cheer, and S. J. Elliott, "The design of a low-cost directional warning sound system for electric vehicles," in *Proceedings of the 28th International Conference on Noise & Vibration Engineering (ISMA)*, (Leuven, Belgium), 2018.
  - N. Kournoutos and J. Cheer, "Directivity control using a structural actuator array," in *Proceedings of the 26th International Congress on Sound and Vibration*, (Montreal, Canada), 2019.
  - N. Kournoutos and J. Cheer, "An Environmentally Adaptive Warning Sound System For Electric Vehicles," in *Proceedings of the 48th International Congress and Exhibition on Noise Control Engineering (INTER-NOISE)*, (Madrid, Spain), 2019.
  - N. Kournoutos and J. Cheer, "A system for controlling the directivity of sound radiated from a structure," *Journal of the Acoustical Society of America*, vol. 147, pp. 231-241, 2019.
  - N. Kournoutos and J. Cheer, "Design and realisation of a directional electric vehicle warning sound system," in *Proceedings of meetings on acoustics Acoustical Society of America*, vol. 39, 040001, 2020.
  - N. Kournoutos and J. Cheer, "Investigation of a directional warning sound system for electric vehicles based on structural vibration," *Journal of the Acoustical Society of America*, vol. 148, pp. 588-598, 2020.

Signed: _____

Date: _____

Acknowledgements

The completion of this thesis and all the work involved around it would have been impossible without certain people, who, either through helping with technical aspects of the research or forming part of a pleasant and motivational environment, helped and supported me in these past few years. The mention of their names on a page of this thesis is the least amount of gratitude that I could show to all of them as a sincere thank you.

- Jordan Cheer has been more than a supervisor during my time in this project, and a large part of the input work presented in this thesis is owed to him. I thank him wholeheartedly for trusting this research upon me and being there to advise and provide both help and motivation to carry out this task. I can honestly say that I could not have asked for a better supervisor.
- Steve Elliott for enabling all of this by his role in organising the project, and for his valuable help as a co-supervisor.
- Angelis Karlos for being a colleague and above all a close friend to discuss things I couldn't with anyone else.
- Aaron Poole, the person who first welcomed me in Southampton and a close friend ever since.
- Thanasis Papaioannou, together with whom we shared the full experience, including the highs and lows, of going through the PBNv2 project.
- The Spanish-speaking friends met in the ISVR - Felipe Vasquez, Ander Biguri and Xavi Garcia. I hope we meet again for more adventures.
- Charlie House, Marcos Simon and all the people in the ISVR and SPCG who aided me in carrying out my experimental work.
- Juan Jesus Garcia and Xavi Montane from Applus+IDIADA for their hospitality and assistance, thanks to which I was able to carry out some of the most valuable experimental work.
- Jacques Cuenca, Laurent De Ryck and Mansour Alkmim, again for their hospitality and assistance in carrying out my secondment in SIEMENS.
- All of the people involved in organising and realising the Innovative Training Network, and enabling the funding necessary for this project, provided by the European Commission through the ETN PBNv2 project (GA 721615).
- The rest of the friends in Southampton, for the music we made together.
- My parents, who although far away, have always been close to me , believed in me more than I did myself, and supported me no matter what.

List of Abbreviations

AVAS	**A**coustic **V**ehicle **A**lerting **S**ystems
DML	**D**istributed **M**ode **L**oudspeaker
EV	**E**lectric **V**ehicle
eVADER	**e**lectric **V**ehicle **A**lert (for) **D**etection (and) **E**mergency **R**esponse
HEV	**H**ybrid **E**lectric **V**ehicle
ICE	**I**nternal **C**ombustion **E**ngine
ISVR	**I**nstitute (of) **S**ound (and) **V**ibration **R**esearch
JASIC	**J**apan **A**utomobile **S**tandards **I**nternationalization **C**enter
NHTSA	**N**ational **H**ighway **T**raffic **S**afety **A**dministration
NVH	**N**oise **Vibration** and **Harshness**
PWM	**P**ulse **W**idth **M**odulation
RMS	**R**oot **M**ean **S**quare
SPL	**S**ound **P**ressure **L**evel
TRL	**T**ransport **R**esearch **L**aboratory
UNECE	**U**nited **N**ations **E**conomic **C**ommission (for) **E**urope
VESS	**V**irtual **E**ngine **S**ound **S**ystem
VSP	**V**ehicle **S**ound for **P**edestrians

List of Symbols

$A_{1,2}$	Amplitudes of forward travelling plane waves	
AE	Array effort	dB
a	Effective radius of dust cap (Ch. 3)	m
	Plate length (Ch. 4)	m
a_r	Total absorption coefficient	
$B_{1,2}$	Amplitudes of reflected plane waves	
b	Plate width	m
C	Acoustic contrast	dB
c_0	Speed of sound	$\mathrm{m\,s^{-1}}$
E	Young's modulus of elasticity	GPa
F	Driving force amplitude	N
f	Frequency	Hz
f_{LC}	Cut-on frequency	Hz
f_S	Resonance frequency	Hz
$\boldsymbol{G_B}$	Complex transfer response matrix for the bright zone	
$\boldsymbol{G_D}$	Complex transfer response matrix for the dark zone	
g_i	Gain coefficient for the i-th frequency band	
^{H}	Complex conjugate transpose of vector or matrix	
H_{er}	Transfer function between emitter and receiver	
H_{nr}	Transfer function between noise source and receiver	
H_{rp}	Transfer function between receiver and pedestrian location	
h	Plate thickness	m
I	Number of actuators in structural array	
I_M	Moment of inertia	$\mathrm{kg\,m^{-2}}$
L	Array length	m
$\mathfrak{L}$	Lagrangian function	
L_x	Panel length	m
L_y	Panel width	m
L_z	Panel thickness	m
l	Spacing between array elements	m
k	Wavenumber	$\mathrm{rad\,m^{-1}}$
k_m	Wavenumber of the m-th mode	$\mathrm{rad\,m^{-1}}$
k_n	Wavenumber of the n-th mode	$\mathrm{rad\,m^{-1}}$
M	Number of modes considered along the x-axis (Ch. 4)	
M_B	Measurement points in the bright zone	
M_D	Measurement points in the bright zone	
m	Structural mode number along the x-axis	
N	Number of sources in loudspeaker array (Ch. 3)	
	Number of modes considered along the y-axis (Ch. 4)	
n	Structural mode number along the y-axis	
p	Acoustic pressure	Pa
p_0	Reference acoustic pressure	Pa

p_n	Acoustic pressure at n-th hole	Pa
$\boldsymbol{p_B}$	Vector of complex pressure in the bright zone	
$\boldsymbol{p_D}$	Vector of complex pressure in the dark zone	
p_{En}	Signal for the environmental noise SPL at its source	
p_{Er}	Signal for the environmental SPL at the receiver	
p_{We}	Signal for the warning sound SPL at the emitter	
p_{Wr}	Signal for the warning sound SPL at the receiver	
$\hat{p}_{Ep}$	Signal for the environmental SPL estimate at pedestrian location	
$\hat{p}_{Er}$	Signal for the environmental SPL estimate at the receiver	
$\hat{p}_{Wp}$	Signal for the warning sound SPL estimate at pedestrian location	
$\hat{p}_{Wr}$	Signal for the warning sound SPL estimate at the receiver	
$\boldsymbol{q}$	Vector of complex source strengths	
r	Distance	m
S	Area of the cross section of the pipe	m^2
s_W	Base warning sound signal	
$\tilde{s}_W$	Adapted warning sound signal	
Th_i	Audibility threshold at i-th frequency band	dB
t	Time	s
t_h	Thickness of pipe	m
U_d	Downstream volume velocity	$\mathrm{m}^3\,\mathrm{s}^{-1}$
U_u	Upstream volume velocity	$\mathrm{m}^3\,\mathrm{s}^{-1}$
$\boldsymbol{u}$	Vector of complex input signal	
u_m	Input signal for single source to generate equivalent pressure	
W_{mn}	Modal amplitude of transverse velocity	$\mathrm{m\,s}^{-1}$
w	Transverse velocity	$\mathrm{m\,s}^{-1}$
Z_d	Downstream impedance	$\mathrm{Pa\,s\,m}^{-3}$
Z_u	Upstream impedance	$\mathrm{Pa\,s\,m}^{-3}$
α_b	Radius of hole	m
η_s	Hysteretic damping coefficient	
θ	Polar angle	rad
λ	Wavelength	m
$\lambda_{1,2}$	Lagrange multiplier	
ρ	Panel density	$\mathrm{kg\,m}^{-3}$
ρ_0	Air density	$\mathrm{kg\,m}^{-3}$
ϕ	Azimuthal angle	rad
ω	Angular frequency	rad
ω_{mn}	Resonant angular frequency of the m-th and n-th modes	rad

Chapter 1

Introduction

1.1 Motivation

Over the past decade, Electric Vehicles (EVs) and Hybrid-Electric Vehicles (HEVs) have increased their share of the passenger vehicle market, and given the desire and support of public and authorities alike for ecologically friendlier means of transportation, it is reasonable to assume that this presence is only going to grow stronger in the future (Fortune, 2019; Wagner, 2020; Harrop and Gonzalez, 2018). A wider integration of EVs in public and private transport should result in better living conditions for urban areas, with reduced air pollution due to lower carbon dioxide emissions, and reduced noise pollution, due to the quiet operation of electric motors. In a society that prioritizes environmental and public health concerns, this gives EVs a significant edge over their Internal Combustion Engine (ICE) counterparts.

One point of concern regarding this quiet operation of EVs is the lack of detectability it may provide for pedestrians, cyclists and other vulnerable road users. A number of surveys have been made investigating the extent to which this lack of audible cues may pose a safety issue (Wogalter et al., 2001), (Hanna, 2009). Legislative bodies in Europe, Japan and the US have issued regulations that require EVs and HEVs to be fitted with systems capable of producing audible warnings for pedestrians. Still, scepticism regarding the necessity of such systems persists, with a major argument against them being the potential increase in noise pollution caused by such warning sounds (Sandberg et al., 2010).

For this reason a part of the existing literature on the matter has focussed on the design of warning sound systems that can provide detectability of the vehicle while avoiding unpleasant and unnecessary noise emissions. Apart from characteristics inherent to the sound itself, a major factor in determining the above balance is the directivity of the radiated sound field. Systems that take into account the above consideration have been developed and tested in the past. However, up to this point, the solutions either fail to perform consistently enough throughout the necessary bandwidth (Cheer et al., 2013), or have been deemed too costly for a wider implementation by the industry (Quinn et al., 2014; You et al., 2020).

The key motivation for this research is to find a compromise between the public safety concerns and the limitation of noise pollution caused by vehicles. A success in meeting the objectives of this work would mean that one of the obstacles regarding the wider adoption of EVs in society will be overcome, making for an easier path towards a more ecological solution to transportation.

1.2 Objectives

The main question that the research in this thesis sets to answer can be formulated as follows.

Given the requirement in electrically powered vehicles for an audible warning so that they can be detected by vulnerable road users, and the necessity to maintain environmental noise emissions at a low level, can a warning sound system be developed to satisfy both points?

Taking into account existing research in the field regarding both the content of warning sound signals and the systems through which they are radiated to the environment, the following objectives are set:

- Develop a warning sound system that is capable of rendering the vehicle detectable by pedestrians and other vulnerable road users in its path.
- The system should be able to transmit the above information, while having a minimal overall contribution to the environmental noise level.
- The system should provide sufficient bandwidth, so as to accurately emit a detectable warning sound, whose harmonic content must be within the 100 Hz to 5 kHz frequency range, in accordance with current international guidelines.
- The components of the system should be appropriate for installation on a passenger vehicle, and robust enough to withstand long-term use.
- The manufacturing and maintenance costs of the system should be kept as low as possible, so as to ensure that it is a viable as a solution for wide implementation in commercial passenger vehicles.

1.3 Contributions

The contributions of this doctoral research thesis are:

- An analytical model for the vibration of a structure and the resulting radiation of sound that offers simplicity in terms of calculations while maintaining accuracy in its predictions across a significant frequency range.
- The utilisation of the existing acoustic contrast maximisation method to control the directivity of the sound field produced by the vibration of a structure excited by an array of inertial actuators.
- A fundamental investigation into the design of a directional sound radiator based on the direct structural excitation of a plate, with consideration for the directivity performance, the required operational bandwidth of 100 Hz to 5 kHz, and cost.
- The experimental implementation and evaluation of the proposed system installed in a vehicle, thus demonstrating its potential as a directional warning sound system for EVs and HEVs.

- The development of an algorithm for the adaptation of the warning sound levels across frequency, depending on the audibility thresholds imposed by the sonic environment, as estimated through the implementation of an auditory masking model.

1.4 Thesis Structure

Chapter 2 constitutes an introduction to the subject of EV warning sounds in the form of a literature review. Results of published studies are used to show the differences between noise generated by electric motors and ICEs, and the safety concerns stemming from the quiet operation of EVs and HEVs. The relevant legislation currently in effect world wide is also presented. The rest of the chapter is devoted to past research on the development of warning sounds and the design of warning sound systems that are currently in use or have been suggested as high performance solutions.

Chapter 3 focuses on the aspect of directional sound radiation, with the introduction of acoustic contrast as a means of quantifying and comparing directivity performance. A number of methods for achieving directivity are then presented and commented on for their suitability as warning sound systems, which considers both cost and performance. Two directional sound systems, the loudspeaker array and the low-cost end-fire acoustic radiator, which have been developed and evaluated in previous research for integration in a warning sound system, are then evaluated through a series of simulations to serve as reference points for the system developed as part of this project.

Chapter 4 introduces the structural actuator array as a system for achieving a directional sound field. A mathematical model is presented and a simulation based parametric study is then performed in order to determine the effect of different design attributes on the performance of the system. Under the conclusions drawn from this study, the specifications for the structural array to be constructed and physically tested are determined.

Chapter 5 is devoted to the experimental validation of the structural actuator array. A prototype system is built and measured in an anechoic environment. The results are compared to those obtained via simulations to evaluate the accuracy of the mathematical model, and provide insight into the performance capabilities of the proposed system.

Chapter 6 presents the experimental evaluation of the structural actuator array as an EV warning sound system. The array of actuators is installed in a test vehicle and its resulting directivity is measured. A number of different arrangements of the array on the body of the vehicle are tested to determine the most suitable configurations. In addition to directivity, the suitability of the system is evaluated by measuring the noise from its operation leaking into the cabin of the vehicle.

Chapter 7 investigates a different approach in achieving the minimisation of unnecessary noise generated by the warning sound, through the introduction of an algorithm for the frequency band-specific environmental adaptation of the warning

sound. Such a system can function independently, or can be used in conjunction with the directional warning sound system. The key components and operational principles are presented, and a simulation-based application study is conducted, which employs a masking model to estimate the audibility thresholds for a given sample of environmental noise.

Chapter 8 summarises the results of the studies conducted within the project and lists the conclusions of this research. In addition, ideas for future work and the further development of the concepts investigated are presented.

Chapter 2

Warning Sound Systems for Electric Vehicles

This chapter constitutes an introduction to the main topic addressed in this thesis. This is done in the form of a literature review, which aims to present the reasoning behind the conceptualisation of artificial warning sounds for EVs and HEVs, the regulations dictating the content of such warning sounds, and existing research on the development of warning sound systems. Section 2.1 presents the sources and nature of noise generated by EVs and HEVs, and the way in which these differ from internal combustion engines. The results from studies on the effects and potential risks this difference in noise emissions causes, and the introduction of artificial warning sounds as a safety measure are presented in Sec. 2.2. Section 2.3 is dedicated to the presentation of international regulations on the inclusion of warning sounds, their content, and the required evaluation process for warning sound systems. An overview of research performed on the development of warning sound systems, and of systems currently in use is given in Sec. 2.4. Lastly, the concept of a warning sound system that aims to minimise environmental noise emissions, and a number of proposed systems aiming to achieve this objective are presented in Sec. 2.5.

2.1 Noise from Road Vehicles

The necessity of artificial warning sounds for EVs stems from the difference in the noise generated between EVs and HEVs and vehicles equipped with conventional internal combustion engines (ICEs). It is therefore important to have an understanding of how the noise coming from vehicles equipped with electric motors differs from that of ICE vehicles. This section presents results of studies performed on the sources of noise in road vehicles, how these are different depending on the type of vehicle, and their effect on the generated noise.

2.1.1 Sources of Noise in Road Vehicles

The noise generated by road traffic has been a concern since the adoption of the car as the most used means of transportation, and the identification of noise sources (Heckl, 1986; George, 1990) as well as strategies for its reduction (Grad et al., 1975; Rimondi, 1995) have been the subject of research during the development of many generations of road vehicles. A comprehensive study on NVH (Noise, Vibration and Harshness) analysis techniques for design and optimization of HEVs and EVs supported by the European Cooperation in Science and Technology (Parizet et al., 2016a) offers an identification and classification of the primary sources of pass-by noise found in a typical passenger vehicle. With the exception of the engine, which will be addressed

separately, the following components are found in both ICE equipped vehicles and EVs, and constitute sources or important factors in the generation of pass-by noise.

Tyres: The tyres constitute the contact surfaces between the road and the vehicle, and contribute to the generation of noise in multiple ways. Firstly, the nature of the tyre surface in contact with the road is an important source of airborne noise, dependent on both the geometry of the tyre tread and its material composition. In addition, the dynamic behaviour of the tyres allows for the transmission of forces between the road and the wheels, transmitting vibrations to the vehicle by means of the structure borne path. The tyre-road noise becomes an increasingly important factor of overall pass-by noise as the speed of the vehicle, and therefore the velocity at which the wheels rotate, increases (Heckl, 1986).

Suspensions: The suspension is the principal connecting component between the tyres and the vehicle body (Takahashi et al., 1987). It is therefore a crucial structure borne transmission path, transmitting vibrations produced by the tyre-road contact. Suspensions are normally engineered with the goal of minimising this transmission, but there is a complicated trade-off between handling and NVH performance.

Aerodynamic Sources: The aerodynamics of the vehicle are the main source of airborne noise at high speeds, with the intensity of the aerodynamic noise being proportional to the sixth power of the speed (George, 1990). Aerodynamic sources can be distinguished into three types (Parizet et al., 2016a): a global flow which influences the low-frequency range; a local flow, mainly present at mid-to-high frequencies; and turbulence, which generates a broadband noise.

Other Sources: Vehicle components such as brakes and miscellaneous electrical and mechanical accessories can by considered as secondary sources of noise. Although their contribution to overall noise levels produced is minimal compared to the other sources listed, they should still be considered when studying the acoustic behaviour of a vehicle.

Noise Characteristics of the Engine

ICEs and electric motors display fundamental differences in their components and operation, and thus the characteristics of the resulting noise generated. In addition to the motor itself, each type also requires a different powertrain, also characterised by unique noise sources.

ICE and powertrain: In ICE equipped vehicles, the reciprocating and rotational masses within the engine, such as the pistons, connecting rods and shafts, are the primary sources of vibration. Additional sources in the corresponding powertrain are the exhaust system, and the gearbox and differential when the vehicle is in motion.

Electric motors: Research into the noise produced by the operation of electric motors has found that the noise signature is characterised by tonal components mainly at frequencies above 2 kHz (Allam et al., 2007; Florentin et al., 2011; Lennström et al., 2013). These components are speed dependent, resulting from the dominating electromagnetic harmonics and covering a wide rpm range. The most widely

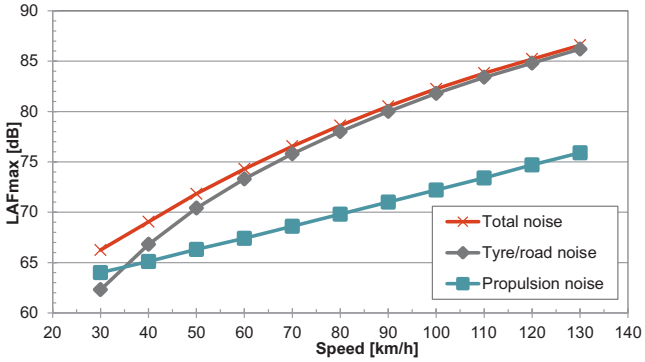

FIGURE 2.1: The propulsion noise, the tyre/road noise and the total noise from a passenger car calculated with the Nord2000 noise prediction model (Kragh, 2006) as presented in (Iversen et al., 2013).

used type of electric motor is the permanent magnet synchronous motor. In this system, the battery provides a DC voltage. This is in turn converted to a magnitude and frequency controlled AC voltage on the inverter via pulse-width modulation (PWM) (Ojo et al., 2006). The switching frequency for the PWM is located for the majority of EVs in the 5 kHz to 20 kHz range. This switching frequency is the primary contributor to the audible noise produced by an electric motor and powertrain system, followed by the magnet noise from the powertrain and the cooling system.

2.1.2 Noise Measurements from EVs and ICE Vehicles

Noise Measured from ICE Vehicles

Many of the different sources of noise presented above are dependent on the speed of the vehicle, and, in the case of the ICE, factors such as the rpm and the gear in which the vehicle is being driven. This means that the contribution of each source to the overall pass-by noise generated depends on the driving conditions. In particular, the main contributors to noise in an ICE vehicle are the engine and the tyre-road interaction. The latter becomes more influential as the speed of the vehicle increases. Figure 2.1 shows a prediction of the noise generated by the propulsion system and the tyres of an ICE car, calculated using the Nord 2000 noise prediction model (Kragh, 2006). The term LAF_{max} denotes the maximum A-weighted and time weighted sound pressure level over the measured time period. The plot used has been presented as part of an existing literature survey on noise from EVs by Iversen and Marbjerg (Iversen et al., 2013; Marbjerg, 2013).

It can be seen from this figure that at low speeds, the propulsion system, which consists of the ICE and the corresponding powertrain, is the primary source of noise. However, from speeds of around 35 km/h and up, the tyre-road interaction becomes the main source of noise, reaching a 10 dB difference at 50 km/h and up to 20 dB as the speed increases. For speeds above 90 km/h, both sources of noise rise linearly with speed. It is therefore apparent that differences in the engine will only yield a significant difference in the noise generated at speeds below the 35 km/h threshold, especially since an electric motor is generally understood to be quieter in operation than an ICE.

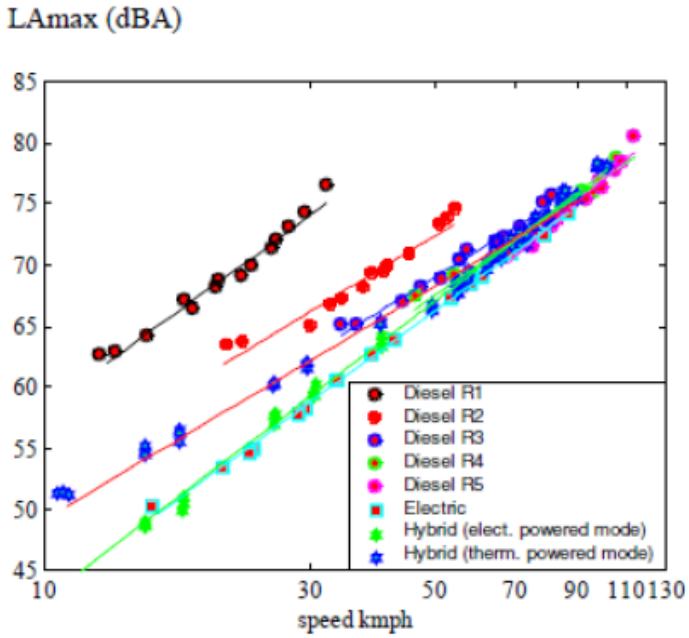

FIGURE 2.2: Overall noise levels at different speeds for an ICE vehicle, an EV and a HEV driven at different modes, as presented in (Lelong and Michelet, 2001).

Comparison Between EV and ICE Vehicle Noise

A study conducted in 2001 by Lelong and Michelet (Lelong and Michelet, 2001) investigated noise at different speeds from an ICE vehicle, an EV and a HEV driven in electric and in conventional mode. The cars were driven at constant speed when the measurements were performed. No separation between the tyre-road interaction and the propulsion noise was considered, and it is worth noting that the ICE vehicle chosen for the study ran on diesel fuel.

Figure 2.2 shows results of the study in terms of the overall noise generated by the vehicles at different speeds. Similarly to the preceding figure, the term LA_{max} denotes the maximum A-weighted sound pressure level over the measured time period. The notations R1 to R5 in the figure stand for different gears. It is evident that at low speeds, the EV and HEV achieve an overall noise reduction of about 15 dB, and it is worth noting that the HEV driven in electrically powered mode displays the same noise behaviour as the EV. Even when driven in conventional mode, the HEV still produces significantly less noise at low speeds. For increasing speeds above 35 km/h, the overall noise produced is similar for all of the measured vehicles, which suggests that the tyre-road interaction and aerodynamics become the dominant sources of noise instead of the engines, as suggested in the previous section.

A more recent study conducted by the National Traffic Safety and Environment Laboratory and the Ministry of Land, Infrastructure, Transport and Tourism in Japan, compared the noise from a HEV operated in electric mode and from two ICE vehicles (Sakamoto et al., 2010, 2012). All vehicles were classified as small passenger cars. Pass-by measurements performed at different constant speeds were made, and the results are shown in Fig. 2.3. As this study is focused on low speeds up to 30 km/h, the difference between the noise produced by the HEV and the ICE vehicles is more

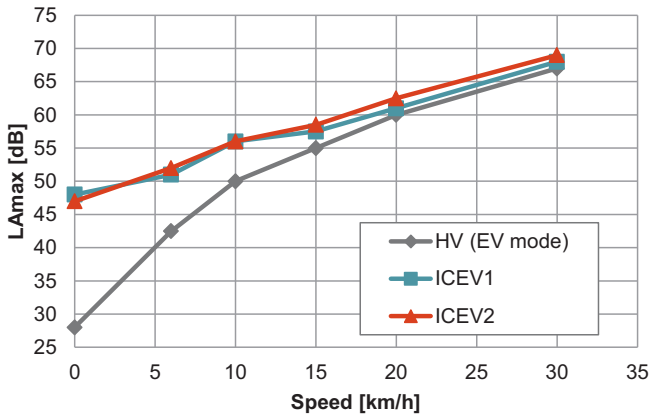

FIGURE 2.3: The maximum sound pressure level from two different ICE vehicles and one hybrid vehicle operated in electric mode when the cars pass-by at different constant speeds with the microphone at a distance of 2 m. Results from (Sakamoto et al., 2010), as presented in (Marbjerg, 2013).

prevalent. The HEV produces a noise level reduced by over 15 dB compared to the ICE vehicles when stationary, and remains quieter up to a speed of 20 km/h. The increase in noise measured at these low speeds for the HEV was interpreted as being caused by the tyre-road interaction.

The results of the two studies presented above are clear in showing that the quiet operation of electric motors results in EVs and HEVS being significantly quieter than ICE vehicles at low speeds. As measurements shown thus far have only considered the overall noise levels, it could be useful to have a picture of the sound pressure levels across frequency. The study presented in (Sakamoto et al., 2012) also provides an insight into the frequency spectrum of the noise produced by the investigated vehicles. An example is shown in Fig 2.4, which contains the A-weighted frequency spectra for the noise from the vehicles driven at constant speeds of 10 km/h and 20 km/h. In the 10 km/h case, the EVs generate a lower overal level of noise compared to the ICE vehicles. Only in the lower frequencies up to 315 Hz the levels of both types are similar. It was not elaborated to what extent the low frequency components were due to non-engine related factors, but the conclusion from this was that ICEs emit higher noise levels at all frequencies over 315 Hz compared to electric motors. At 20 km/h both types of vehicle display a very similar noise spectrum. This is indicative of how noise from tyres and aerodynamics overcomes the engine by a significant amount as the speed increases.

The study results showcased in this section indicate that EVs and HEVs driven in electric mode are significantly quieter than conventional petrol vehicles. This is due to the quiet operation of the electric motor compared to the internal combustion engine. From a threshold of roughly 20 km/h and above, the noise generated by either type of vehicle tends to be similar, due to the prevalence of aerodynamic and tyre-related noise at such higher speeds.

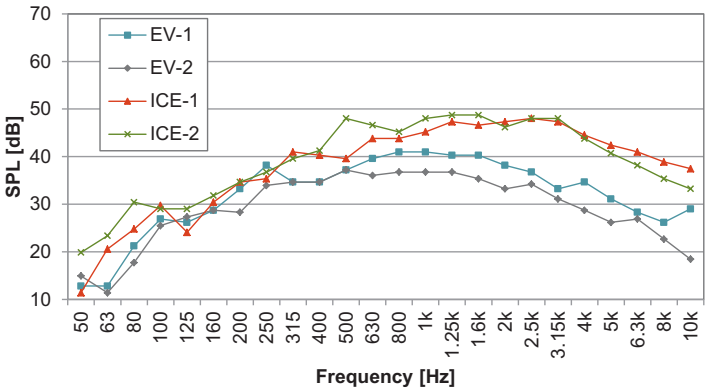

(A) Vehicles driven at a constant speed of 10 km/h.

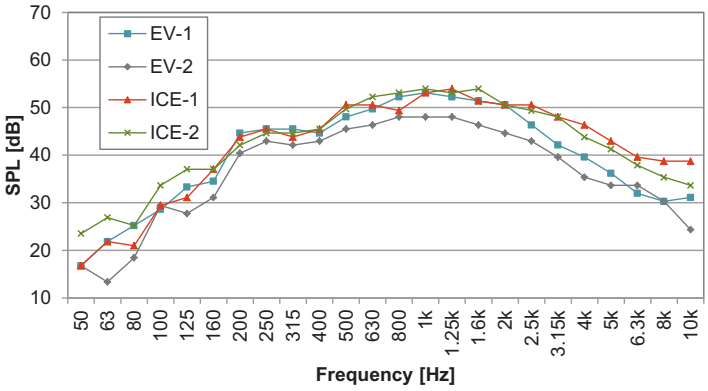

(B) Vehicles driven at a constant speed of 20 km/h.

FIGURE 2.4: The A-weighted frequency spectra for vehicles driven at different constant speeds. From (Sakamoto et al., 2012), as presented in (Marbjerg, 2013).

2.2 Electric Vehicles and Pedestrian Safety

The fact that EVs have proven to be substantially quieter than ICE vehicles at low speeds has raised concerns over increased collision incidents involving pedestrians and other vulnerable road users, particularly during low speed manoeuvres, due to the lack of auditory warning. The motivation of the two Japanese studies presented in the previous section (Sakamoto et al., 2010, 2012) was partly to determine whether these vehicles pose a safety risk to pedestrians due to their low noise level, especially in consideration of visually impaired people. Similarly, a number of studies have solely focussed on determining the extent of this issue. This section presents the findings of studies regarding the increased risks that the quiet operation of EVs brings, and the resulting necessity for an artificial auditory warning system.

Wogalter et al. (2001)

One of the earliest mentions of the potential risks of wide EV use was in a 2001 study by Wogalter (Wogalter et al., 2001), which focussed on a survey exploring interest and concerns over the then emerging technology of EVs. The study considered the pre-existing auditory alarms installed in automated guided vehicles (Egawa, 1988), as well as the effectiveness of alarms found in emergency vehicles (Robbins, 1995). Findings of the survey indicated that the public, though supportive of the adoption of EVs and HEVs, expressed worries over the reduced auditory cues to the presence of a moving vehicle. Aside from the issue of detection by pedestrians and other vulnerable road users, the study also addressed factors crucial to the evaluation of danger and collision avoidance, such as speed estimation, which are heavily dependent on sound (Evans, 1970). In addition, the importance of auditory cues to aid the performance of the driver of the vehicle was considered (Nelson and Nilsson, 1990). Lastly, the study offered suggestions for the nature of potential artificial warning sound sources to be installed in EVs.

Hong et al. (2009)

A 2009 study by Hong (Hong et al., 2013) investigated the auditory recognition distance for different types of vehicles, which included diesel and petrol ICE vehicles, EVs and HEVs, based around two experiments. The first experiment was conducted at speeds of 20 km/h and 30 km/h on a public road, while the second experiment was performed using an idle engine setting in an underground car park. In both cases, the objective was to determine the maximum distance at which the vehicle could be reliably perceived through noise. The participants were split into two age groups, those below 60 years and those above.

Results indicated that the younger group could more easily recognise the EVs and HEVs driving at a speed of 30 km/h. The study estimated the collision probability of the younger group to be 20% lower than the older group regardless of vehicle type. Overall probability of collision for EVs and HEVs were increased by 31% compared to the ICE vehicles. Lastly, during the static experiment 80% of participants were unable to perceive the HEV at a distance greater than 0.1 m, while the percentage was as high as 97% for the case of the EV.

NHTSA (2009)

In USA, the National Highway Traffic Safety Administration (NHTSA) performed a study which collected data from twelve states covering pedestrian or cyclist incidents with HEVs or ICE vehicles between the years 2000 and 2007 (Hanna, 2009). The sample was limited to vehicles which had both ICE and Hybrid-Electric versions. A total of 8,287 HEVs and 559,703 ICE vehicles were included. Incidence rates were calculated as the number of a given vehicle type involved in an incident divided by the total number of vehicles of its type in the sample. The findings of the survey are summarised as follows:

- A total of 0.9% of HEVs and 0.6% of ICE vehicles were involved in incidents with pedestrians.
- For cyclists the rates were 0.6% with HEVs and 0.3% with ICE vehicles.
- Regarding incidents recorded at speeds below 35 mph, the rates were 1.8% for HEVs and 1.2% for ICE vehicles. There were substantially fewer incidents with pedestrians for speeds above 35 mph.
- For speeds under 35 mph, incidence rates with cyclists were: HEV:1.0%, ICE: 1.6%.
- Collisions that occurred while the vehicle was travelling straight were the most common manoeuvres, although no significant difference between the incidence of HEV and ICE vehicle crashes was shown in the data.
- The second most common manoeuvre prior to a pedestrian involving collision was making a turn, with incidence at 1.8% for HEVs and 0.6% for ICE vehicles.
- Low speed manoeuvres such as slowing down, stopping, reversing and entering or leaving a driveway were grouped together. Pedestrian incidence rates were found to be 1.2% for HEVs and 0.6% for ICE vehicles.
- The same types of manoeuvres showed for cyclists the incidence rates of 0.8% for HEVs and 0.4% for ICE vehicles.

The study concluded that HEVs were more likely to be involved in collisions with pedestrians or cyclists than ICE vehicles at speeds below 35 mph. However, as the small sample size, in part due to the newly emerging market presence of HEVs during the years investigated, the results were deemed questionable. A second survey under the same guidelines was performed in 2011, with a sample of 24,297 HEVs and 1,001,000 ICE vehicles (Wu et al., 2011). Its summarized results are as follows:

- Total incidence rates for pedestrian collisions were 0.77% with HEVs and 0.57% with ICE vehicles.
- For cyclists, the total rates were 0.48% against 0.30% with HEVs and ICE vehicles respectively.
- At speeds under 35 mph, the HEV incidence rate was 1.39% and the ICE vehicle rate was 1.01%.
- For the low speed manoeuvres defined as in the previous study, rates were 1.24% for HEVs and 0.75% for ICE vehicles.

Overall, this repetition came to verify the initial conclusions that at lower speeds, HEVs tend to be less safe for pedestrians as well as cyclists. These surveys, however, have been subject to criticism for their methodology by published literature. Namely, the neglect of mileage for each vehicle, of the population composition between car owners and the fact that the studies do not indicate whether the HEV was being driven in electric mode at the time of the incident are factors stressed in question of the above conclusion (Verheijen and Jabben, 2010).

JASIC (2009)

A 2009 study by the Japan Automobile Standards Internationalization Center (JASIC) (JASIC, 2009) mentioned that no accidents resultant from lack of audible warning had been recorded until then in Japan; however no further information on the methods under which this survey was conducted were provided. Also mentioned was the lack of difference between the noise produced by EV/HEVs and ICE vehicles at speeds above 20 km/h.

Transport Research Laboratory, UK (2011)

The Transport Research Laboratory (TRL) performed a statistical study for the UK Department for Transport based on police reports of pedestrian-vehicle collisions between the years 2005 and 2008 (Morgan et al., 2011). Among these results it was found:

- Pedestrian-vehicle involvement density in per 10,000 registered vehicles was overall between 2005-2008: 4.9 incidents for EV/HEVs and 5.5 incidents for ICE vehicles.
- Regardless of vehicle type, the majority of incidents involving pedestrians occur at speeds below 30 mph, with both categories of vehicles displaying similar rates when it comes to injuries sustained.
- Considering relative rates of vehicles sampled, it was deduced that EV/HEVs were less likely to be involved in a general collision by 30%.

The study also conducted surveys with vision impaired participants in vehicle detection during drive-by scenarios such as moving straight, turning and parking; manoeuvres for which EV/HEVs showed a high rate of incidence in the NHTSA report (Hanna, 2009). The TRL report concludes that although EV/HEVs might pose an increased risk for pedestrians, not enough data is included in the statistics, such as mileage of each vehicle, and whether an HEV involved was operating in electric or ICE mode. A further point for consideration was that during the sound level measurements conducted, it was found that differences in the noise produced by EV/HEVs and contemporary ICE equipped vehicles is negligible, even at these rather low speeds (Morgan et al., 2011).

TRL subsequently conducted a complementary study with extra focus on the correlation of sound levels emitted from the vehicle and the likelihood of incidents involving pedestrians (Muirhead and Walter, 2011). Results, as seen in Table 2.1, show that apart from vehicles with exceptionally high noise levels, the proportion of vehicles involved in incidents with pedestrians at lower speeds is fairly constant at the order of 91%. The conclusion of both UK based studies is that the evidence for the increased risk to pedestrians posed by EV/HEVs is insufficient to reach a verdict. A noteworthy point put forth is the fact that as newer ICE models display

Pass-by noise dB(A)	No. of vehicles	Percentage of vehicles	Density *1000
$\leqslant$71	4,698	92.0%	0.54
71	12,330	91.5%	0.57
72	14,662	91.7%	0.62
73	8,424	90.8%	0.56
74	5,342	90.7%	0.54
75	586	91.0%	0.45
$\geqslant$ 75	393	83.4%	0.28

TABLE 2.1: Vehicles involved in pedestrian accidents at speeds below 30 mph, as presented in (Muirhead and Walter, 2011)

similar sound levels to EVs even when at low speeds, the use of warning sounds might as well be considered for all quiet cars regardless of propulsion system.

Kim et al. (2012)

A study was conducted in 2012 (Kim et al., 2012) to investigate the difference that an artificial warning sound makes in the perceptibility of a HEV by vision impaired adults. Fourteen participants with visual impairments attempted to detect three different vehicles: a HEV without any artificial warning sounds, a HEV with a Vehicle Sound for Pedestrians (VSP) installed (Konet et al., 2011), and a comparable ICE vehicle. The characteristics of the VSP warning sound system will be presented in more detail in Sec. 2.4. Two test sites were used, a parking lot and a road way, which provided an overall background sound level difference of roughly 10 dBA. Results indicated that the HEV with the added VSP system was detected at a distance greater than that corresponding to the HEV without the artificial warning sound by over 10 m, and on occasion even surpassed that corresponding to the ICE vehicle. The study concluded that equipping HEVs and EVs with a sound system that emits an alerting sound in certain low-speed manoeuvres is crucial for the safety of blind pedestrians.

2.3 Regulations on Warning Sound Systems

The potential risks arising from the quiet operation of EVs and HEVs, addressed in studies such as the ones presented in the previous section, have incited legislative bodies around the world to draft regulations making the use of artificial warning sounds by quiet vehicles mandatory. Even though not all of the studies have found strong associations between the noise from EVs and increased collision rates (Morgan et al., 2011; Muirhead and Walter, 2011; JASIC, 2009), organisations such as the National Federation of the Blind (NFB) in USA and the World Blind Union (WBU) (Sandberg, 2012), have pressured for the adoption of measures for the protection of the more vulnerable groups. This section provides an overview of the legislation that has been coming into effect regarding the use of warning sounds from EVs and HEVs.

Europe

The United Nations Working Party on Noise (GRB), which is a subsidiary body of the World Forum for Harmonization of Vehicle Regulations, has been convening regularly since 1999 to develop noise requirements for vehicles. The proposal for guidelines on audibility ensuring measures for EVs was brought forth in 2011 and has since been kept up to date with the participation of the World Blind Union (GRB, 2011). The European Commission commenced the drafting of regulations for an Acoustic Vehicle Alerting System (AVAS) in 2011, under the suggestions made by the GRB, with the purpose of presenting recommendations to manufacturers for the introduction of warning signal systems on their electric and hybrid models that would comply with a uniform guideline.

The regulation eventually came to form in 2014, defining the specific requirements for the AVAS as well as a transitional period of five years, after which the fitting of the warning sound systems becomes mandatory for all EVs and HEVs (European Council, 2014). Aside from the European Union authorities, specifications of the AVAS have also been kept up to date by the Economic Commission for Europe of the United Nations (UNECE), with the intent of providing a global set of guidelines for manufacturers and public alike (UNECE, 2017).

Japan

As the country with the leading role in the development of EVs and HEVs, Japan was the first to express concern and conduct studies on the potential issues stemming from quiet vehicles at a national level (JASIC, 2009). Many of the findings of the resulting research were utilised in forming the UNECE legislation on the matter, and, in turn, Japan has fully incorporated the AVAS regulations (JASIC, 2010; Arima, 2015).

China

China announced as of 2018 that it was researching guidelines on acoustic alerting systems for EVs and HEVs driven at low speeds, and has reportedly been implementing these measures since September 2019 (Code of China, 2018). However, no further information on the specifics of these guidelines was available to the author at the time of this work.

United States

In the United States, the results of the studies conducted by the NHTSA showed a measurable increase in collision incidents involving EVs and HEVs (Hanna, 2009; Wu et al., 2011). A proposal rule was thus published for comment in 2013 (NHTSA, 2013). The rule required EVs and HEVs travelling at less than 30 km/h to emit warning sounds that pedestrians could hear over background noises. According to the initial proposal, vehicle manufacturers would be able to pick the sounds the vehicles make from a range of choices, and similar vehicles would have to make the same sounds.

After feedback from the industry, the rule was revised to include more specific guidelines on the technical aspects of the warning sounds, and compliance was delayed to 2018. The final rule was published in 2016 (NHTSA, 2016), however, since then the compliance date has been postponed to 2020, and adjustments to the requirements have been made to approach the AVAS guidelines, thus pointing towards a global standard for EV warning sounds.

AVAS Guidelines

The majority of EV manufacturing countries form their legislation on the matter under the standards of the AVAS, and as a result, the warning sound systems that are currently being developed are designed and evaluated following the guidelines given by the AVAS regulations. It is therefore useful to provide an overview of these guidelines prior to the presentation of existing warning sound systems and the suggestion for development of novel systems.

The AVAS is evaluated using the system fully integrated within an EV, with sound pressure level measurements performed outdoors and indoors. Two microphones, standing at 1.2 m above the ground and at a distance of 2 m from the centreline of the vehicle at each side are used to measure any noise produced by the vehicle. Outdoor measurements involve the vehicle moving forward at a constant speed of 10 km/h and at 20 km/h as well as a reversing test with no specific speed defined. Figure 2.5a shows the positions from which measurements are to be taken. In the forward tests the measurement begins at the point in time the front plane of the vehicle crosses the line AA' until the point in time the rear plane crosses the line BB', following a straight course as set by line CC'. Lines AA' and BB' are both distanced 10 m from the plane PP' defined by the placement of the two microphones. The reversing test is similarly performed, with the measurements being taken between the points in time the rear plane crosses the line BB' until the front plane crosses the line AA'.

Indoor measurements are intended to be taken within a semi-anechoic environment with the vehicle in standstill condition; a constant speed is instead simulated for a minimum of 5 seconds. Figure 2.5b shows how the front plane of the car is positioned to coincide with the plane PP' defined by the two microphones for the forward tests, and the rear plane is likewise used for the reversing test. Table 2.2 shows the minimum sound pressure levels required to be achieved at specific frequency bands for each type of test. UNECE Regulations specify that a warning sound must have components covering at least two of the $1/3^{rd}$ octave frequency bands included in the table, with at least one of them below or within the 1600 Hz $1/3^{rd}$ octave band.

As with other regulations regarding EVs and HEVs, the AVAS guidelines have undergone a number of revisions since they were first presented, due to the rapid

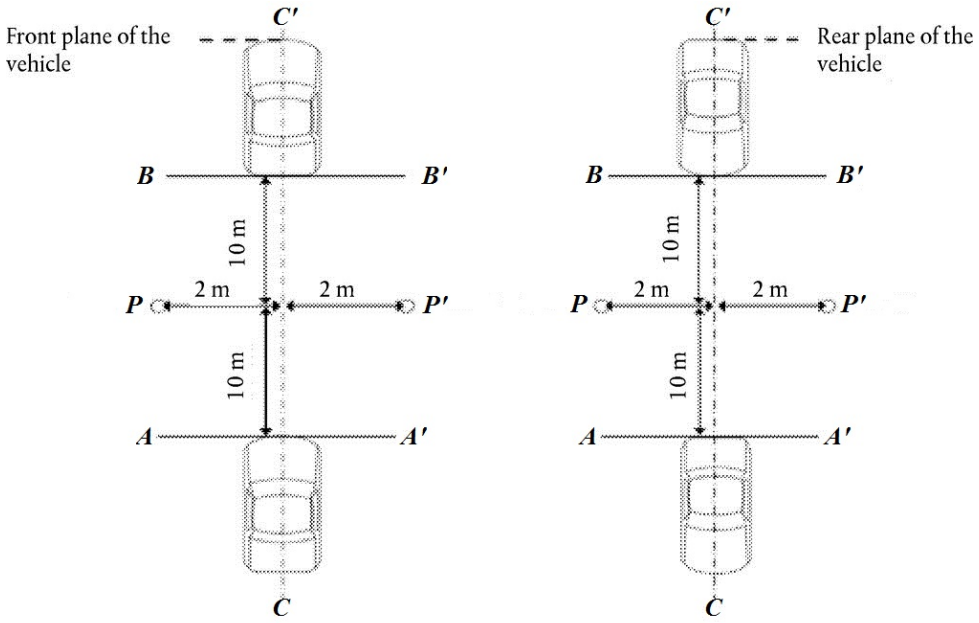

(A) Measuring positions for vehicles in motion outdoor in accordance with UNECE guidelines for the AVAS, presented in (UNECE, 2017).

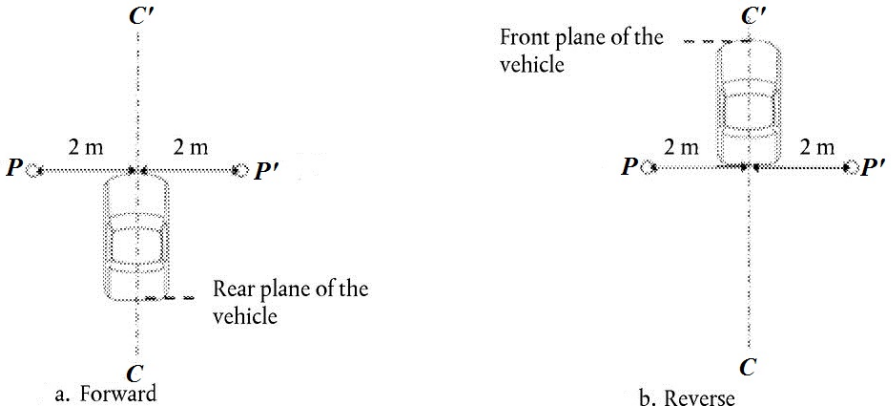

(B) Measuring positions for vehicles in standstill for indoor testing in accordance with UNECE guidelines for the AVAS, presented in (UNECE, 2017).

Frequency [Hz]	dB at 10 km/h	dB at 20 km/h	dB Reversing
OVERALL	50	56	47
160	45	50	
200	45	49	
250	43	48	
315	44	49	
400	45	50	
500	45	50	
630	46	51	
800	46	51	
1000	46	51	
1250	46	51	
1600	44	49	
2000	42	47	
2500	39	44	
3150	36	41	
4000	34	39	
5000	31	36	

TABLE 2.2: Minimum Sound Level Requirements, overall and at specific $1/3^{rd}$ octave bands, in dB(A) for the AVAS in accordance with UNECE Regulation 138 (UNECE, 2017), for constant forward speed tests at 10 km/h and 20 km/h, and reversing.

development of technologies around warning sounds in the last few years. It could therefore be expected that the guidelines for AVAS presented in this section may be subject to change in the face of new findings, or if novel relevant technologies become available for wide implementation within the vehicle industry.

The short presentation of legislation on mandatory auditory warnings for EVs in this section showed that, although initial efforts were taken by each country individually, there has been a tendency towards a global standard in the last few years. The point of convergence can be considered to be in the regulations proposed for the AVAS guidelines. Under these guidelines, the bandwidth in which warning sounds are expected to operate, and the minimum SPL necessary at each frequency band are dictated. Also included are instructions on the measurements for the evaluation of the warning sounds. However, as EV technologies progress, the exact form of such regulations is expected to change in the near future.

2.4 Development of Warning Sound Systems

Artificial sounds have been designed and installed in EVs and HEVs even before the issue of pedestrian safety was officially addressed. Differences in the design philosophy of warning sounds can also be seen in the time between identifying their necessity and finalising the guidelines for their attributes. This section gives an overview of studies on the identification of characteristics in warning sounds that may render them more efficient in their role, as well as investigations on the impact that warning sounds might have on the environment. In addition, warning sounds currently used by EV and HEV manufacturers are presented, to the extent that such information has been openly published.

2.4.1 Characteristics of Warning Sounds

Wogalter (2001) & Nyeste (2008)

The study of Wogalter that was previously mentioned (Wogalter et al., 2001) included a survey intended to obtain an insight into the type of sounds that the public associated with road vehicles, and would prefer to characterise the sound of an EV or HEV. Results of this survey indicated an overwhelming preference for the sound of a conventional ICE, followed by sounds like wide band noise and humming. The least preferred sound was that of an ICE vehicle exhaust.

A similar study was performed in 2008 (Nyeste and Wogalter, 2008) with a focus on the evaluation of potential warning sounds. In this instance, the survey presented participants with the actual sound samples instead of their description. The results of this study showed high correspondence with the results of the earlier study, with a conventional engine noise being rated as the most preferable sound, followed by the sounds characterised as hum and white noise.

For both studies, this preference was interpreted as a result of the familiarity the public has with such sounds, and the instinctive association with road vehicles. It is worth mentioning however, that other types of noise associated with ICE vehicles, such as the sound of an exhaust, were considered most undesirable. In general, the sounds that were least preferred were characterised by strong tonal components, especially at higher frequencies.

Petiot (2013)

With the concept of artificial EV warning sounds established and the planning of regulations in progress, researchers in the Technical University of Denmark (DTU) conducted a survey in 2013 to determine which types of sound were most appropriate for use as warning sounds (Petiot et al., 2013). The survey separated participants in two subgroups, one consisting of 34 “novice users” and the other of six “experts” with technical knowledge in the subject of EVs and artificial warning sounds. In the first part of the survey participants were asked their opinion on the matter of warning sounds for EVs with results indicating an approval of warning sounds as a safety measure, and a preference of sounds that would be associated with ICE vehicles to be used.

The experimental part of the survey had the participants evaluate different synthesized sounds on the bases of appropriateness and pleasantness. 17 different sounds were designed and put to evaluation. The tests also simulated the movement of the car by adjusting the frequencies and amplitudes of the sounds to recreate a pass-by effect. Upon analysis of the quantitative ratings on pleasantness and

appropriateness, it was found that little agreement (28.4%) existed between the subjects. The researchers' explanation for this was the fact that still few propositions exist on the market for EV sounds, and the absence of context for judgement.

Singh (2013)

A survey conducted by researchers from the University of Warwick (Singh et al., 2013) considered both the detectability, as well as the subjective evaluation and suitability of different warning sounds. The study employed simulation software to recreate visual and audio stimuli of EVs moving through an urban environment and carrying out different manoeuvres, as would have been heard by a pedestrian. Although the published results from this study did not provide details on the characteristics of each sound, nor did the conclusions point out a trend in the qualities that render a warning sound more detectable, a finding that is worthy of note was that the A-weighted SPL of the warning sound did not show association with its detectability. Such a finding suggests that pass-by SPL measurements might be insufficient as the sole means for the assessment of the effectiveness of warning sounds. The conclusions from this research pointed out the necessity of evaluating warning sounds through more subjective criteria such as familiarity and association of the sound with a vehicle, as well as annoyance.

Parizet (2014, 2016)

Between 2011 and 2014, the European Commission and a number of EV manufacturers in part funded the eVADER project (electric Vehicle Alert for Detection and Emergency Response), which aimed to develop a next generation warning sound system solution for EVs and HEVs (Quinn et al., 2014). The key objective for this system was to achieve the communication of an auditory warning to a vulnerable road user while minimising the overall contribution of the vehicle to environmental noise. An overview of the complete system that was developed is given in Sec. 2.5. In the scope of warning sound design within the project, the work of Parizet (Parizet et al., 2014) aimed to develop warning sounds that are effective at being easily detectable by a recipient, without causing annoyance.

On the topic of determining the qualities that would make the warning sounds themselves suitable, a series of psychoacoustics experiments were performed (Parizet et al., 2014). The survey involved a sample of 100 normal vision and 53 visually impaired participants. A drive-by scenario was simulated in order to evaluate each sound. Warning sounds were synthesized according to a three factor design, for each of which three levels of variation were defined. Therefore, each sound used was characterised by three indices, corresponding to a specific level for each factor; these were:

- Number of components: Each component referring to a "harmonic" frequency, with the lowest fixed at 300 Hz. Three frequencies were separated by 300 Hz for level 1, six "harmonics" were separated by 150 Hz for level 2 and nine "harmonics" at 150 Hz apart were generated for level 3, all at the same initial level.

- Frequency modulation: At level 1 all components had fixed frequencies. At level 2 the frequencies of the higher two components were modulated at 5 and 4 Hz respectively. Level 3 included level 2 with a saw tooth modulation applied to the rest of the components.

Stimulus	Frequency Modulation	Harmonics	Amplitude Modulation
s1	None	3	None
s2	None	6	8 Hz
s3	None	9	Random
s4	Sinusoidal	3	None
s5	Sinusoidal	6	8 Hz
s6	Sinusoidal	9	Random
s7	Sawtooth	3	None
s8	Sawtooth	6	8 Hz
s9	Sawtooth	9	Random

TABLE 2.3: Characteristics of warning signals that were used in the experiment of (Parizet et al., 2014).

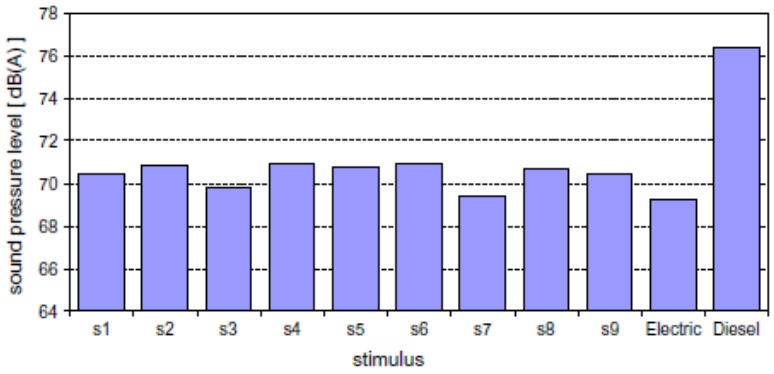

FIGURE 2.6: Peak level (A-weighted SPL) of the vehicle sounds with (s1–s9) and without added warning signals (the two rightmost bars), as presented in (Parizet et al., 2014).

- Amplitude modulation: No amplitude modulation was applied for level 1. At level 2, the signal amplitude was sinusoidally modulated at 8 Hz. At level 3, the lower two components were modulated with a variable modulation frequency of unspecified range. This last level was designated as "random" amplitude modulation.

Table 2.3 contains the list of sounds that were evaluated in the survey and their characteristics. The sound pressure level (SPL) of the synthesized sounds are shown in Fig. 2.6. It can be seen that compared to a diesel ICE, all synthesized sounds maintained a lower level, and in certain cases the levels were comparable to the operation of an EV without a warning sound system installed.

The evaluation of the effectiveness of each sound was performed in a simulated environment, where participants attempted to identify by sound the approaching vehicles. The measured reaction times of participants were converted to the corresponding distance of the vehicle in the simulated scenario. Figure 2.7 depicts the mean distance at which the vehicle was detected using each synthesized sound. It is evident that certain synthesized sounds worked efficiently enough to be just as detectable as a standard ICE. Added to the fact that the overall sound level for all the samples was 5 to 7 dB lower than that of the conventional engine, the successful sound types offer an ideal solution that combines both detectability and lower noise emissions.

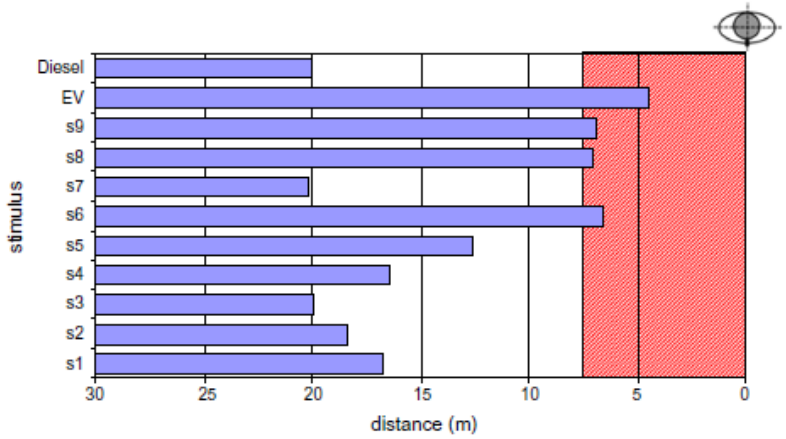

FIGURE 2.7: Distance in m at which the vehicles were detected in the virtual scenario, as presented in (Parizet et al., 2014). The shaded area corresponds to unsafe distances.

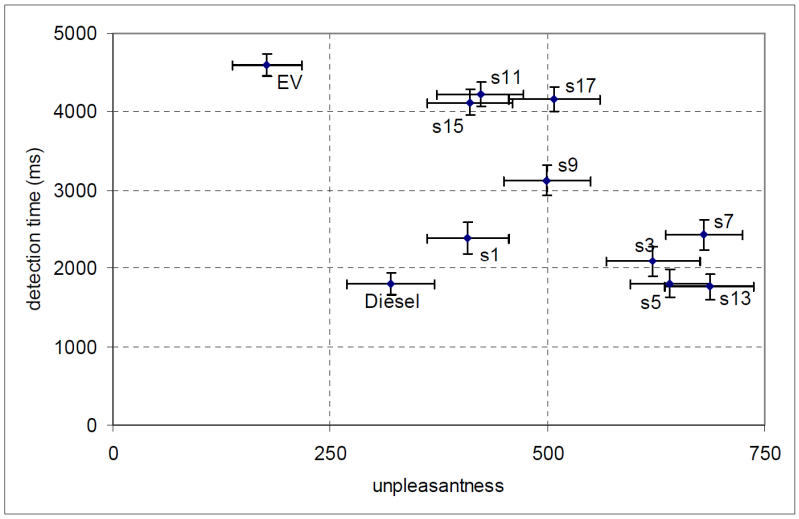

FIGURE 2.8: Mean detection time and rated unpleasantness for various synthesized warning sounds, as presented in (Parizet et al., 2016b).

An extended presentation of the same study, published in (Parizet et al., 2016b), provides a view of the effectiveness of each synthesized sound in relation to the annoyance caused by its perception. Figure 2.8 shows this in terms of the mean detection time versus the perceived unpleasantness as rated by the participants. The figure includes warning sounds for which details were not explicitly presented in the paper. For sounds with the naming convention s1 to s7, the characteristics defined in Table 2.3 apply. It is apparent that synthesized sounds that are more easily detectable are also characterised by a high unpleasantness factor, therefore necessitating a compromise when choosing the optimum sound. As the study concludes, s1, which consists of three tonal components and no frequency or amplitude modulation offers a satisfactory combination of detectability and limited annoyance caused.

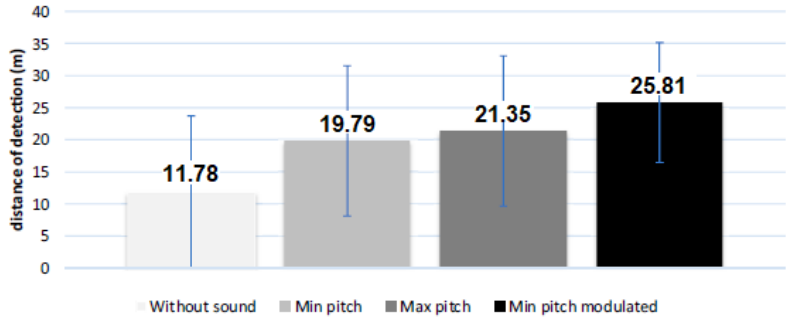

FIGURE 2.9: Mean detection distances and standard deviations for the four types of sounds tested in (Fleury et al., 2016), as presented in the published article.

Fleury (2016)

A publication by Fleury (Fleury et al., 2016) investigated the effect that the pitch of a warning sound had on its detectability. Three sample sounds were used for the test: two static sounds that were characterised by a difference in pitch, and a third one based on the lower pitched sound, with added frequency modulation. In the first study, blindfolded participants had to detect an approaching EV with either no warning sounds at all or one of three types of sound tested. The second study aimed to replicate the results of the first in an ecological setting; for that purpose the EV was driven along a road as conductors of the experiment counted the number of people who turned their heads towards its direction.

Figure 2.9 shows the results of the first study with the mean distance of detection for each of the warning sounds investigated. It can be seen that raising the pitch of a sound made it detectable from a greater distance; however, a modulated pitch proves even more effective in that regard, as its distance of detection increases despite its base pitch being lower.

The second study was unique in comparison to existing ones at featuring the sounds tested in a natural context. Participants were unaware of their involvement in a survey, and therefore could not concentrate their perceptual and cognitive resources on detection. Overall, results showed that when the vehicle was travelling at 10 km/h, it was detected 2.88 s earlier for the minimum pitch sound (which corresponds to a safety margin of 6.02 m), and 5.05 s earlier in the modulated pitch (8.01 m).

2.4.2 Warning Sounds and the Sonic Environment

The work presented so far has studied warning sounds in an isolated environment. However the implementation of such systems more often than not regards a sonic environment which contains a multitude of other sounds. Under this consideration, the subject of the research presented in this section has been the detectability of EVs through their warning sounds in presence of existing background noise, and the contribution of such warning sounds to the overall environmental noise levels.

Yamauchi (2014)

A 2014 study by researchers from the University of Nagasaki (Yamauchi, 2014) reviewed the issue of EV and HEV quietness, with focus on the design of feasible warning sounds. Attention was given to the impact of environmental sounds to the

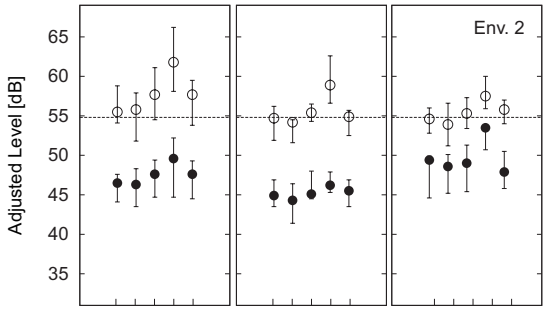

FIGURE 2.10: Minimum level requirements for warning sounds (dark points), and levels necessary for a reliable detection given a background noise, as estimated using different methods (white points). The level of the background noise is marked by the horizontal line. From (Yamauchi, 2014).

perceptibility of the warning signals, including the factors such as the variability in time of said interfering sounds. Examples were given of warning sounds evaluated as reliably detectable proving inaudible when used in environments significantly louder than the testing tracks. A characteristic example is displayed in Fig. 2.10, where the minimum required levels for the warning sound are shown to be well below the estimated levels necessary for a reliable detection of the sound over a background noise. The variation in detecting capabilities by persons of different age was also addressed. The study concluded that revisions on the guidelines for warning sounds are necessary if auditory warnings are to be the solution to vehicle detectability, otherwise non-acoustical measures should be considered.

Poveda-Martinez et al. (2017)

Poveda-Martinez et al. (Poveda-Martínez et al., 2017) analysed in detail the characteristics of a number of warning sounds proposed by the industry and conducted a comparative study to determine their effectiveness in different urban environments. Soundscapes from static traffic, a busy pedestrian area and the vicinity of a playground were used. 8 warning sound samples were used, classified into four groups based on their characteristics: flat/tonal spectrum, unmodulated/modulated. As can be seen in Fig. 2.11, the A-weighted level of these sounds varies, but in all cases is lower than that of the ICE in operation.

Figure 2.12 shows the distance at which the vehicle was detected using each warning sound, within the different simulated environments. The minimum safe distance is also marked with a horizontal dashed line. The results revealed a significant difference between detection errors committed depending on the sonic environment. The noisiest urban areas with the presence of idling vehicles (Environment 1) led to a higher number of detection errors, while in the pedestrian area (Environment 2) and especially the playground area (Environment 3) the vehicle can be more reliably detected at a greater distance.

Regarding the warning sound features, reaction time was reduced in the presence of stimuli with a small number of harmonic components. The incorporation of modulation, either in amplitude or in frequency, did not significantly improve the reaction time. However, it is noted that incorporation of pure tonal components may also result in an increase in annoyance from the sound. The study concludes that warning sounds more similar to those generated by traditional vehicles, where high spectral density bands are combined with pronounced tonal components, can

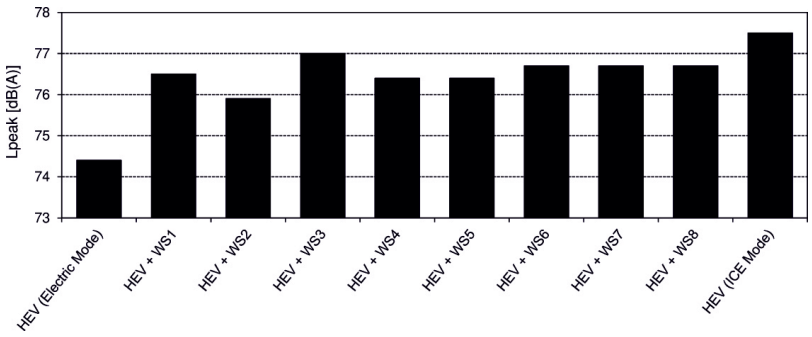

FIGURE 2.11: Overall A-weighted sound pressure levels generated by the different warning sounds, and HEVs in ICE mode and in electric mode without artificial noise. From (Poveda-Martínez et al., 2017).

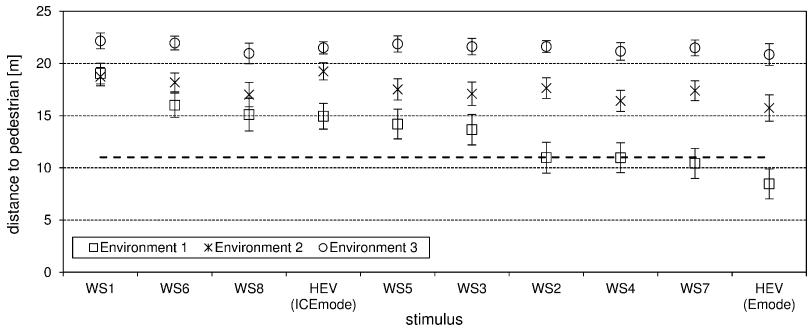

FIGURE 2.12: Distance at which the vehicle was detected using different warning sounds at the three environments. The dashed line denotes the minimum safe distance. From (Poveda-Martínez et al., 2017).

offer the most successful solution to the problem. Overall, the sound that proved to be most successful is an engine simulation characterized by a main wide band component in the 100 Hz to 300 Hz range, with additional narrow band components at 275, 550 and 800 Hz, with no amplitude or frequency modulation.

Campello-Vicente et al. (2017)

A Spanish study from 2017 (Campello-Vicente et al., 2017) investigated the expected noise effects of EVs and HEVs on noise maps in an urban environment through measurement and simulation. The noise emitted from the selected vehicles was measured and used in conjunction with the NMPB ROUTES noise prediction model (Abbaléa et al., 2009) to simulate a traffic environment and estimate the resulting noise levels and effects on the population.

Results from the study displayed in Fig. 2.13 show the estimated noise reduction in dB at different speeds that is achieved by having a vehicle population of EVs with and without AVAS, compared to ICE vehicles. The difference in either case decreases with speed, as expected from the predominance of the tyre-road interaction and other noise sources at higher speeds. Between 10 km/h and 20 km/h, the EVs without AVAS achieve a noise reduction from 10 dB to 4 dB. The reduction is not as significant when AVAS is equipped, in which case it ranges from 7 dB to 3 dB.

Figure 2.14 shows the results from the simulations regarding the number of citizens affected by high noise levels, given a street traffic consisting of EVs without warning sounds, EVs with AVAS, and ICE vehicles. Though the results for the AVAS

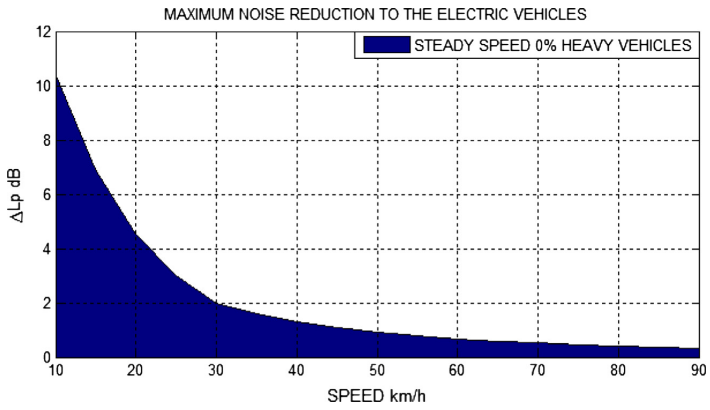

(A) Difference between EVs with no warning sounds and ICE vehicles.

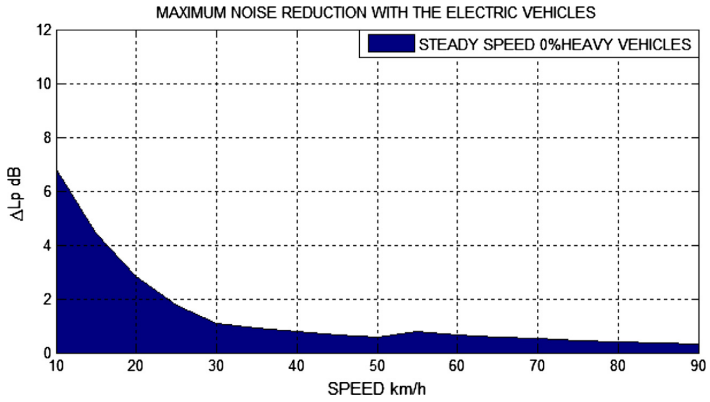

(B) Difference between AVAS equipped EVs and ICE vehicles.

FIGURE 2.13: Estimated difference in noise levels between a traffic constisting entirely of EVs with either no warning sound or equipped with AVAS, and of entirely ICE vehicles. As presented in (Campello-Vicente et al., 2017).

equipped EVs indicate that more people are exposed to higher noise levels than would be without AVAS, the situation still shows noticeable improvements compared to ICE vehicles. Thus, a reduction in noise pollution could still be achieved even with the current guidelines for AVAS in effect.

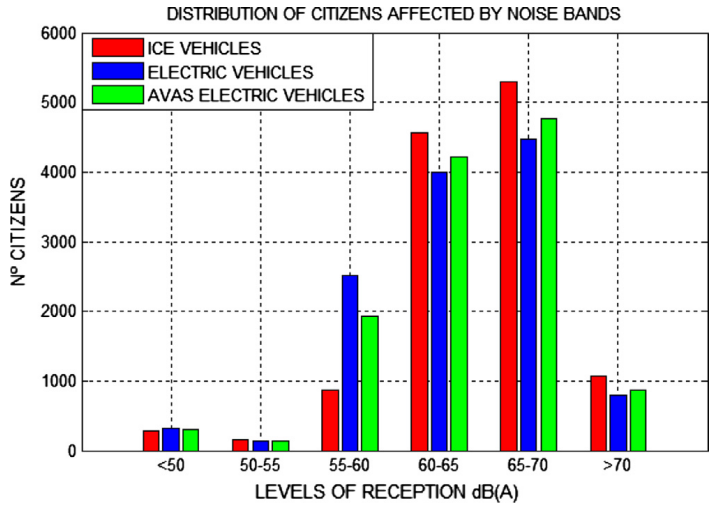

FIGURE 2.14: Number of citizens affected by different sound levels of the noise generated from EVs, EVs equipped with AVAS and ICE vehicles. From (Campello-Vicente et al., 2017).

2.4.3 Warning Sound Systems in Commercial Use

As the inclusion of artificial warning sounds has become mandatory in the majority of the world, manufacturers of EVs and HEVs produce their vehicles with pre-installed AVAS-compliant warning sound systems. Currently, warning sound systems in wide production use either a single or a pair of loudspeaker drivers installed usually under the bonnet in a forward facing orientation. This section will present a number of characteristic examples of such systems that are being used, or exist at a stage of development.

Nissan Vehicle Sound for Pedestrians

Nissan has so far been the first and only major EV manufacturer to openly publish the research around the development of the warning sound used for their vehicles (Konet et al., 2011; Tabata et al., 2011). The system has been named Vehicle Sound for Pedestrians (VSP). The system uses a single speaker placed under the bonnet of the vehicle, which is used to emit the warning sound both when moving forward and reversing. Under compliance to AVAS regulations, the system remains active as long as the vehicle is in operation, and produces the sound up to a speed of 30 km/h.

The VSP warning sound itself was designed with consideration to the frequency sensitivity of the human ear. For this reason a peak in the spectrum of the sound was included at 2.5 kHz. An additional peak was added at 600 Hz for better detectability from persons with age related hearing loss. This lower frequency component also displays an amplitude modulation to enhance its detectability in the presence of ambient noise. The VSP sound spectrum is also characterised by a dip at 1 kHz, as the ambient noise of traffic was found to consistently peak near that frequency. The system generates a sound pressure level ranging from 50 to 54 dB, which is lower than the 55 to 58 dB produced from a typical ICE.

Hyundai Virtual Engine Sound System

The Hyundai Motor Company, jointly with Kia Motors Corporation, have patented a Virtual Engine Sound System (VESS) for use in their EVs and HEVs (You et al., 2020). Currently, EVs and HEVs from Hyundai and Kia use a single loudspeaker mounted to the front bumper of the vehicle to emit the warning sound. The VESS is planned to incorporate various sub-systems in the vehicle to identify vulnerable road users and emit the warning sound towards their location. This is a system similar in principle to the one developed within the eVADER project, which was mentioned previously and will be further discussed in Sec. 2.5.

Figure 2.15 shows the schematic of the main functional components for VESS. An on-board camera and radar are able to detect the presence of a pedestrian or other vulnerable road user in the path of the vehicle. Along with information on the status of the vehicle, such as speed and steering, this data serves to determine the characteristics of the warning sound, and also the direction at which it will be emitted to match the location of the target. This aims to achieve a precise warning without generating noise that affects the rest of the environment. Such a system requires at least six loudspeakers in order to effectively control the sound beam, and, as alleged by the authors of (You et al., 2020), such a configuration would result in an increased production cost for the vehicle. For this reason, the necessity to develop new methods and apparatuses that are capable of achieving the same results at reasonable costs is acknowledged.

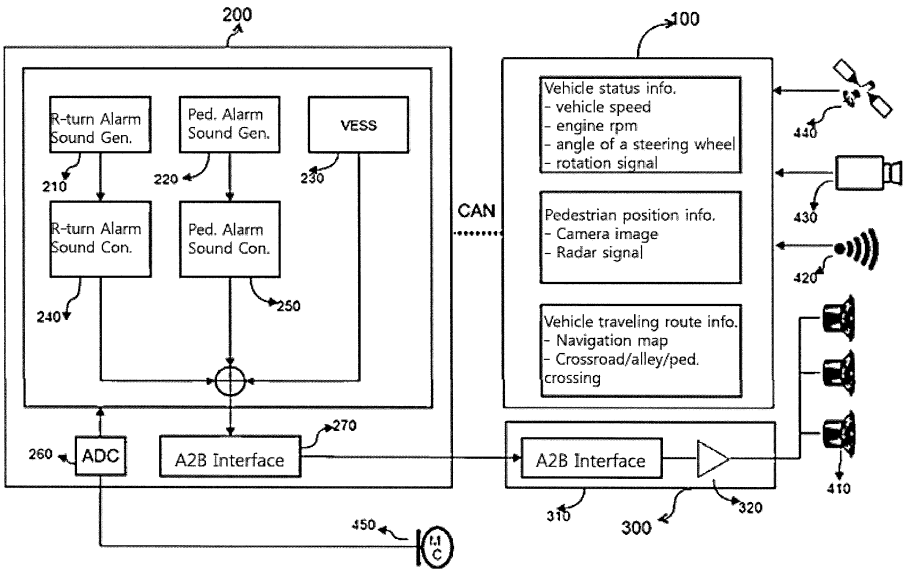

FIGURE 2.15: Schematic showing the components and operation sequence for VESS, as presented in (You et al., 2020).

Other Warning Sound Systems

Other EV and HEV manufacturers equip their vehicles with AVAS compliant warning sound systems, however no detailed information has been made publicly available regarding the composition of the sounds used or the particulars of their operation. The majority of systems that are currently used employ simple loudspeaker drivers, typically installed under the bonnet or near the front grille or bumper of the vehicle to emit the warning sound.

EV sound systems had been developed in the past prior to the AVAS regulations being formed. Either as warning systems, in response to the concerns voiced over safety issues, or purely as means of enhancing the driving experience.

- The Danish company EC Tunes developed a system capable of being retrofitted to a vehicle without an existing warning system (Oestergaards, 2013). Marketed both for the private users and automotive manufacturers the system used a control box with software, digital amplifiers and three external speakers, of which two mounted in the front and one in the rear of the vehicle. A selection of ICE simulating sound packs were available, which adapted with speed and acceleration of the vehicle.

- Lotus Engineering and Harman Becker, in cooperation, have been developing the HALOsonic system from an active noise control configuration used to cancel out intrusive noises inside a car (Peachy, 2013). The same system was adapted to simulate engine sounds to provide audible cues to the driver. This technology eventually shaped into the HALOsonic Internal and External Electronic Sound Synthesis system, which features a number of noise solutions, including an algorithm for pedestrian warning. The sounds are of simulated engines, and the option exists as above to have different settings externally and inside the car.

- Soundracer is a manufacturer of after-market electronic engine sound devices based in Sweden. Their EVEES product is aimed at providing a more enjoyable

driving experience by incorporating actual recorded engine sounds instead of synthesized ones. For the latter reason, the system provides the option of being deactivated or not at speeds chosen by the driver (Soundracer AB, 2017).

However, as the AVAS regulations have imposed strict guidelines on the characteristics of warning sounds, systems like the ones presented above are either becoming abandoned or limited to use as alternative engine sounds solely for use in the interior of the vehicle.

2.5 Warning Sounds and Drive-by Noise

Studies presented in the previous section indicate that artificial warning sounds lead to a perceivable increase in traffic noise generated by EVs, which, although lower in level than that generated by ICEs, potentially negates the benefit of reducing noise pollution that would otherwise be achieved.

Studies on the impact on environmental noise that artificial warning sounds on EVs and HEVs presented in the previous section indicate that the inclusion of AVAS technologies compromises the benefit of noise pollution reduction that quiet vehicles would otherwise bring. For this reason, concern and criticism over the mandatory use of auditory alarms has been voiced. This section gives an overview of such arguments, and presents solutions that have been suggested to achieve both objectives of safety and noise reduction.

2.5.1 Concerns Over the Use of Warning Sounds

Since the prospect of installing artificial sound generators in EVs and HEVs was first discussed, and in the years prior to the finalisation of the AVAS regulations, concerns have been voiced regarding the potential increase in noise pollution the measures might cause. From the results presented in Sec. 2.2, while the NHTSA study (Hanna, 2009; Wu et al., 2011) has found a significant relationship for incidents between quiet vehicles and pedestrians or cyclists, the studies from the UK (Muirhead and Walter, 2011) and Japan (JASIC, 2009) conclude that statistical evidence is too limited to identify such a relationship.

A Dutch study on the effect of EVs on traffic noise and the environment (Verheijen and Jabben, 2010) stresses how artificial warning sounds will negate numerous of the benefits that would normally be associated with the wide adoption of EVs and HEVs. In particular, efforts to curb noise pollution in urban centres may be ultimately undone as the noise of ICEs will merely be replaced by artificial sounds, and adverse health effects caused by noise annoyance will remain. In this respect, the study recommends the investigation of safety measures other than imposing minimum noise levels or continuous warning sounds.

A fact that has been addressed by Sandberg (Sandberg et al., 2010) is that the presence of quiet vehicles in traffic is not a phenomenon that first appeared with the arrival of HEVs. The study mentions that bicycles, another quiet means of transportation, are often cycled on pavements among pedestrians. In addition, trams and electrically powered trolley buses have also been present in urban environments for decades, and have developed to be increasingly quiet without sparking concern over the same issues.

Lastly, as has been put forward in (Muirhead and Walter, 2011), ICE vehicles have for some time been comparably quiet. An example of particular relevance to this argument can be found in a 2011 study on the sound characteristics of EVs (Govindswamy and Eisele, 2011). Here, a measurement of the noise from a standard petrol Fiat 500 was compared to an electrified version of the car named Liiondrive. Figure 2.16 shows the measured pass-by noise from the electric and ICE versions. The rolling noise was also measured with the engine switched off and, since everything except for the propulsion was identical about the cars, it was assumed as the same for both versions of the vehicle.

From the depicted example it can be seen that the difference between the electric and the ICE version of the Fiat 500 is very small, and in fact the Liiondrive is actually louder at high speeds. The latter observation can be explained by the fact that the

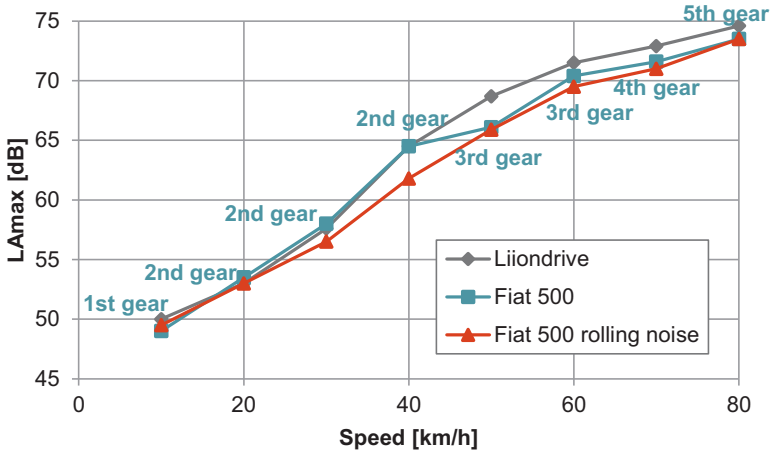

FIGURE 2.16: Exterior pass-by noise level of an electric car (Liiondrive) and a similar ICE car (Fiat 500). The Liiondrive is an electrified version of the Fiat 500 and is fixed in 2nd gear. The rolling noise of the two cars is assumed to be the same and the presented rolling noise is therefore for both vehicles. From (Govindswamy and Eisele, 2011), as presented in (Marbjerg, 2013).

electric version was fixed in second gear, which would mean an increase in noise at high speeds, as seen in the previously presented study by Lelong and Michelet (Lelong and Michelet, 2001), shown in Fig. 2.2. The rolling noise seems also to dominate at all speeds. These results indicate that ICE vehicles are occasionally just as quiet as EVs and HEVs. The conclusion here could be that either additional warning sources are unnecessary, as ICE vehicles are already quiet without an observable increase in collision incidents, or necessary for all quiet vehicles, regardless of propulsion means.

One last argument against the mandatory use of warning sounds, presented in (Sandberg, 2012), is the fact that headphone or earphone use has become increasingly common for pedestrians, cyclists and drivers alike. These devices, especially if used with noise-cancelling technolgy, effectively isolate the users from their environment. Thus, any auditory warning produced by an oncoming vehicle will have no effect on these individuals. A study conducted in the Netherlands (Stelling-Konczak et al., 2017) focussed on the impact that music listening and activities such as talking on the phone had on the incident involvement rates for Dutch cyclists. There was not any strong correlation found, however the study stresses that the majority of the cyclists seldom encountered quiet vehicles on the road. Therefore, as the number of EVs and HEVs is increasing, the question remains whether cyclists and pedestrians who listen to music or talk on the phone will sufficiently compensate for the limited auditory output of these vehicles.

The arguments presented above can be considered valid as to how artificial warning sounds might have limited positive impact for the majority of the public, and even cause more annoyance than convenience due to the resulting noise pollution. However, citizen groups such as the visually impaired, who are reliant on auditory cues for their safety, should not be isolated. The same could hold true for animals, domesticated or wild, that often find themselves near roads, though at this point, research on the effects of quiet vehicles on animal safety remains limited. Lastly, auditory warnings should not be ruled out as a means of ensuring the safety of the

wider public in specific circumstances, particularly starting and reversing manoeuvres.

It is therefore important to continue working towards the development of warning sound systems that render the vehicle detectable to any vulnerable person that might be affected by its presence, while at the same time minimising its contributions to environmental noise. The following sections present suggestions for warning sounds and warning sound system concepts that intend to achieve both of these objectives.

2.5.2 Adaptive Warning Sound Systems

Current AVAS regulations specify inflexible minimum sound levels for the warning sounds regardless of the sonic environment that surrounds the vehicle. As seen in studies presented in this chapter (Yamauchi, 2014; Poveda-Martínez et al., 2017), the level and spectrum of background noise has an effect in the perceptibility of a auditory warning. It would therefore mean that the warning sound needs to be emitted at a higher level to overcome increased environmental noise, and thus, if a global minimum level is defined by guidelines, the warning sound would be unnecessarily loud and intrusive in quieter environments.

A solution to this would be an adaptive warning sound, capable of amplifying or attenuating its signal depending on the current level of environmental noise. This has been investigated by SINTEF in Norway (Berge and Haukland, 2019b,a) in a study that evaluated the effect in detectability of the vehicle that a variance in background noise levels brings. The study was performed with a jury consisting of participants with both normal or impaired vision, using an EV with a speaker that emitted a warning sound at an adjustable level. The speed at which the tests were performed was 20 km/h. The results indicated that at the chosen speed, tyre noise had already become the primary noise source instead of the warning sound. In addition, for a background noise level of 60 to 65 dB, indicative for a busy urban street, the intended minimum level for the AVAS was found too low for detection. This last finding suggests that an adaptive AVAS might be necessary in order to achieve safety and limit noise pollution at the same time, as the level required to render the vehicle detectable in a loud environment would be a major source of noise in a more quiet situation.

One thing worth noting about the above study is that the adaptation of the warning sound is performed by adjusting the gain on the overall signal. As the usual composition of AVAS sounds is of discrete frequency bands, the extent to which the sound is masked by the background noise may not be an issue of its overall level, but the level of a specific frequency component which is masked by a sound in the current environment, in a tone masked by wide band noise scenario (Fastl and Zwicker, 2007). Masking effects have been considered in the evaluation of warning sounds (Lee et al., 2017), but not as part of an adaptive system. An adaptive system that considers the above effects, and is capable of adjusting specific components of the warning sound to avoid masking effects could potentially constitute a more refined and precise solution to the problem, and will be the focus of Chapter 7. In any case, however, such a system would require the alteration of current AVAS regulations to consider different minimum levels depending on the environment.

2.5.3 Directional Warning Sound Systems

A solution to the problem of ensuring the detectability of a vehicle by pedestrians and vulnerable road users, while keeping the overall sound emissions to a minimum, that could be achieved without interfering with the spectral content of the warning sound itself, would be to impose control over the shape of the radiated sound field. This would mean that the design of a warning sound emitting system that is capable of controlled directivity over a bandwidth sufficient to cover the contents of a warning sound.

Directional warning sound solutions have been suggested, including the filing of patents, for systems consisting of arrays of multiple loudspeakers (Kim and Moon, 2014) or parametric drivers (Pompei, 2006). A more in-depth look into such methods for achieving control over the directivity of the sound field will be presented in Chapter 3. However, despite the investigations of such concepts, no directional systems have been implemented in production vehicles of any type at the time of this research.

eVADER

An in-depth research into the design of a warning sound system aimed to maximise detectability and minimise its environmental impact was conducted and documented in the European project eVADER (Quinn et al., 2014). The project partly focussed on the development of a warning sound that could be easily detectable without causing annoyance, as reported in studies and surveys that have been reviewed in Sec. 2.4 (Parizet et al., 2014, 2016b). This section aims to give an overview of the full intended function of the proposed system, with focus on its approach to controlled directional sound radiation.

The project utilised an Environmental Perception System (EPS) incorporating a windscreen-mounted stereo camera and front chassis-mounted radar. In addition to the EPS, a Location Based System (LBS) was used to support risk estimation based on GPS position, time of day and a database of hotspots, critical areas and speed limits. The components are displayed as positioned in the test vehicle in Fig. 2.17. Similar to other warning sound systems mentioned here, the eVADER system only emitted sound at speeds below 35 km/h. On-board microphones measured the prevailing ambient noise levels so the overall level of the warning sound could be adjusted in response. The default condition, when no vulnerable road users are detected, had the system emit a low level sound in the general direction of travel of the vehicle. When a vulnerable road user was located, the warning sound was directed towards them, with the sound beam becoming spatially narrower and increasing in sound level, depending on the collision risk.

The eVADER system achieved directional sound radiation through a six loudspeaker array installed in the forward bumper of the vehicle. This array could be controlled via adjusting the phase and amplitude of the signals sent to each loudspeaker in order to control the width of the sound beam and direct it towards specific locations. To achieve this control, a sound-power minimisation algorithm was used, as presented in (van der Rots and Berkhoff, 2015). Figure 2.18 shows the beamforming performance of the array in terms of the resulting directivity patterns for settings directed forward and at angles of 30° and 60°. The system is seen to be capable of amplifying the sound by at least 10 dB at the location of a vulnerable road user, though the width of the beam increases at higher steering angle settings.

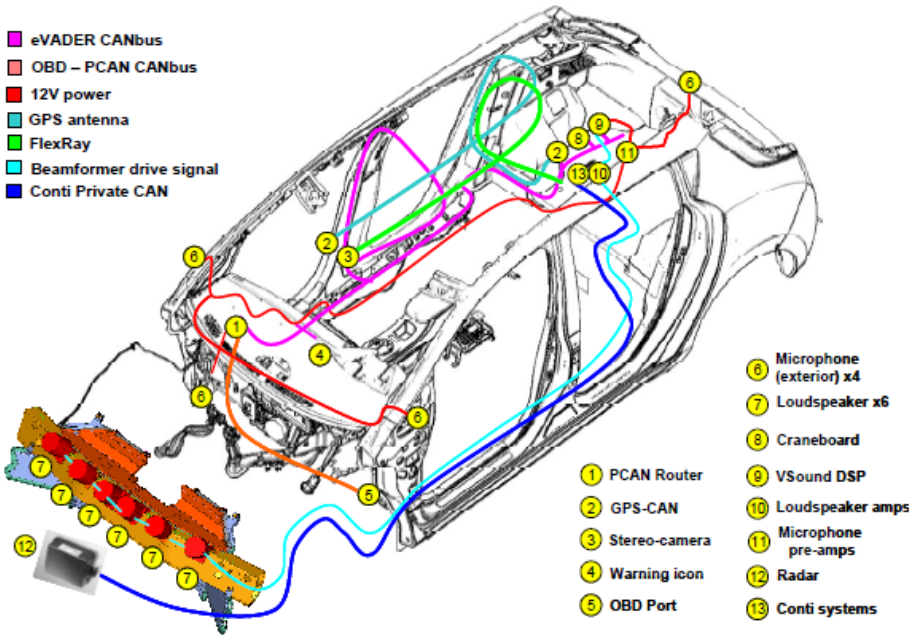

FIGURE 2.17: Schematic of the components comprising the full eVADER system. Note the six loudspeaker array arranged along the forward bumper (7), used to achieve a directional sound field. Figure as presented in (Quinn et al., 2014).

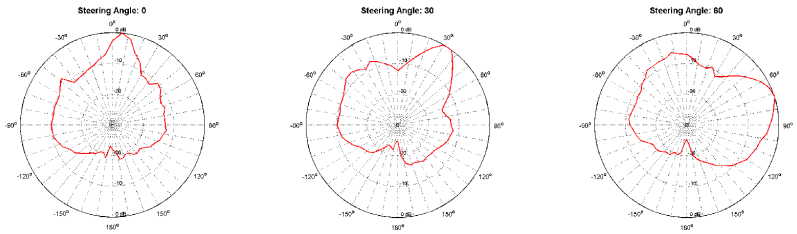

FIGURE 2.18: Resulting directivity patterns from the eVADER system, for the beamformer focussed on the forward direction and at 30° and 60° steering angles. Figure as presented in (Quinn et al., 2014).

Overall, eVADER offered a highly refined solution to the warning sound problem by focussing a sound only towards the locations where it is necessary to be conveyed, ensuring that the qualities of the warning sound render it detectable without causing annoyance, and even foreseeing for the adjustment of its level depending on the sonic environment. However, such a solution still has not seen a wide adoption by the industry, possibly due to the high production costs it encompasses, particularly when it comes to the installation of a full size loudspeaker array in a somewhat vulnerable position at the front bumper of the vehicle.

At this point, it is worth noting that all warning sound systems that are in use or have been experimentally investigated rely on the use of loudspeakers in order to generate sound. Given the drawbacks of cost and vulnerability, it is worth investigating the viability of alternative methods of sound generation, such as structural vibration, which will be the focus of Chapters 4, 5 and 6, as the basis of a more advanced warning sound system for EVs.

2.6 Summary

This chapter has presented a literature review aimed at introducing the topic of EV and HEV detectability through artificial warning sounds, presenting the global scale legislation dictating the implementation and evaluation of such safety measures, and providing an overview of the state of the art regarding the development of relevant technologies.

The quiet operation of electric motors on EVs and HEVs renders them significantly quieter than their ICE equipped counterparts in general. This has resulted in concern over the risks to pedestrians and vulnerable road users these vehicles might pose, especially during low speed manoeuvres. For this, regulations on a global scale have been coming into effect imposing guidelines on the inclusion of artificial warning sounds, that should ensure that the vehicles are detectable in all occasions.

Research on the development on warning sounds has focussed on investigating the properties that render a signal detectable by a recipient without being considered intrusive and causing discomfort. In order to address concerns over the potential increase in noise pollution that the mandatory use of warning sounds by EVs and HEVs might cause, suggestions were made for warning sound systems that adapt to the environment, or are capable of directing the emitted sound towards identified vulnerable individuals in the path of the vehicle.

Overall, it has been shown that research on the topic has produced synthesized warning sounds that are efficient in communicating the information of an approaching vehicle without being overbearing to a recipient. However, methods that ensure the minimisation of drive-by noise generated by the inclusion of such safety measures remain unimplemented, mainly due to suggested solutions requiring high production costs, despite their performance. For this reason, the focus of this research will be on the development of a practical and cost-effective solution for a warning sound emitting system capable of minimising drive-by noise.

Chapter 3

Directivity and Directional Sound Systems

A sound system that is capable of focussing the radiated sound field towards the direction of vehicle motion, or even individual vulnerable road users (Quinn et al., 2014; You et al., 2020), and minimising its output in all other directions, is potentially capable of achieving the desired compromise in between communicating an audible warning and keeping noise pollution contributions low. For this purpose, the research presented in this thesis will focus on the study and development of a directional sound system capable of emitting a detectable warning sound towards a vulnerable road user, while at the same time constituting a realisable configuration for integration within a production vehicle.

This chapter aims to introduce the concept of sound field directivity and go through some of the methods that have been used to achieve it. A brief overview of directional sound systems that are used in EVs or have been suggested as potential solutions is given in Sec. 3.1. Section 3.2 establishes a means of quantification for directivity in acoustic contrast, and presents the acoustic contrast maximisation method, which will be used throughout this research to control and evaluate the directivity of the investigated sound systems. A loudspeaker array is modelled and simulated in Sec. 3.3, with the intent of obtaining an insight into its performance and the effect that each design parameter has on it. The performance of the loudspeaker array can act as a point of reference during the evaluation of other systems presented in this research. Lastly, the low-cost endfire acoustic radiator, a directional sound system which was developed in the University of Southampton, and has been previously tested as a potential EV warning sound system, is presented in Sec. 3.4. The section covers a mathematical model and a simulation-based parametric study into the performance of this system.

3.1 Directional Sound Systems

There are numerous ways in which a directional sound field can be generated in practice, either by a solitary transducer or an array containing multiple elements. This section will present three basic systems that are either in use, or have been proposed and researched as EV warning sound systems. The directional performance, complexity and production cost, and viability for an in-vehicle implementation will be considered to determine the advantages and drawbacks of each system.

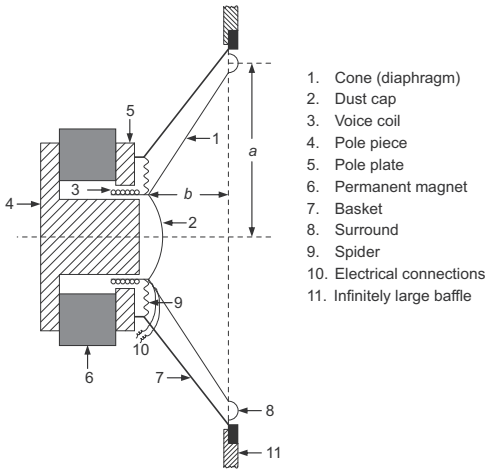

FIGURE 3.1: Cross-section sketch of an electrodynamic loudspeaker, as presented in (Beranek and Mellow, 2012).

3.1.1 Single Loudspeaker

Warning sound systems currently in use (Tabata et al., 2011; You et al., 2020) rely on a single loudspeaker placed under the bonnet or close to the front bumper of the vehicle, to emit the warning sound towards the direction of movement. The electrodynamic diaphragm loudspeaker is the most widespread transducer due to its relative simplicity and low cost, compact size, and stable response over a comparatively wide frequency range. In vehicle and mobile audio, where little acoustic power is necessary, the diaphragm based loudspeaker provides the optimal solution, despite its low efficiency and narrow directivity pattern at higher frequencies.

Figure 3.1 shows a cross sectional schematic of a typical loudspeaker, presented in detail in (Beranek and Mellow, 2012). In this instance, a brief overview of the components and the operation of such a loudspeaker will be given. The diaphragm (1) is in the shape of a cone, made by a light and stiff material. In the centre of the diaphragm, a dust cap(2) covers the voice coil (3), which lies in the gap of a magnetic path (4, 5, 6), held in place by a basket structure (7). The diaphragm is supported at the perimeter and near the voice coil by a surround (8) and spider (9). When a signal is applied through the electrical connections (10), the resulting current forces movement of the voice coil, and, hence, of the diaphragm cone to which it is attached. This entire drive unit is shown mounted in a flat baffle to acoustically isolate the front side of the diaphragm from the rear.

It is the movement of this cone that displaces the air molecules on its surface and produces sound waves. The cone is generally stiff at low frequencies and its motion is uniform. However, at high frequencies, travelling waves and resonances occur on the cone, resulting in irregularities in the frequency response. In terms of directivity, a loudspeaker is omnidirectional at lower frequencies, but its radiated sound field becomes more focused as the frequency increases past a certain point. As a general rule, for a larger driver, the limit at which radiation becomes directional is shifted towards lower frequencies.

A major factor in the resulting directivity is the baffle. As mentioned, a baffle acts to isolate the sound field radiated in the front from the field in the rear, effectively creating a dipole source (Olson, 1947). However, at lower frequencies, characterised by wave lengths large enough to be comparable to the extent of the baffle, the radiation in the far field can be considered omnidirectional. In particular, a single

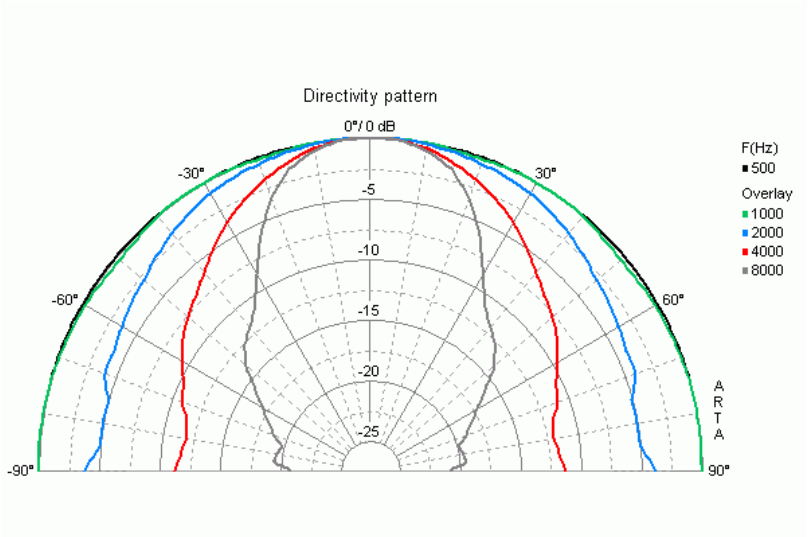

FIGURE 3.2: Directivity patterns at different frequencies for a 8 Ohm, 13 cm diameter commercial cone loudspeaker (VISATON MR 130) (VISATON GmbH & Co. KG, 2017).

loudspeaker system has been found in (Cheer et al., 2011) to become directional at frequencies closer to where the size of the baffle is comparable to one half of the corresponding wavelength. As a relevant example, if a loudspeaker utilised the entire width of a passenger car as a baffle, it would act as a monopole source for frequencies below roughly 100 Hz. However, systems in use do not utilise such large baffles, therefore they should be expected to be omnidirectional at significantly higher frequencies as well.

Figure 3.2 shows the measured directivity in the forward half-plane for a commercial loudspeaker driver with operational bandwidth between 1 kHz and 5 kHz (VISATON GmbH & Co. KG, 2017), at different frequencies. The loudspeaker is intended to be mounted on a baffle or enclosure. The behaviour at the lower frequencies is omnidirectional, and a clear trend of increasing directivity can be observed at the higher frequencies, with the sound field becoming more focused in the forward direction.

The typical on-axis SPL response of the same type of loudspeaker as above is shown in Fig. 3.3. The resonance frequency in this example, f_S, is located at 500 Hz. The frequency response displays a gradual rise until f_S, beyond which it remains relatively flat, for a range that constitutes the effective operational bandwidth of the loudspeaker (Newell and Holland, 2006), before performance eventually begins to deteriorate at higher frequencies.

The low cost and simplicity of an electrodynamic loudspeaker make it the choice for most manufacturers in their current implementations of EV and HEV warning sound systems Although satisfying the criteria imposed by regulations (GRB, 2011), the frequency dependent directivity of the loudspeaker means that the resulting sound field might vary in spatial coverage depending on the contents of the warning sound. The use of a horn could improve directivity across all frequencies, however such a configuration results in a poor frequency response (Newell and Holland, 2006), which would limit the bandwidth available for a warning sound, and would also require significant space in the vehicle, which might be reserved for other systems.

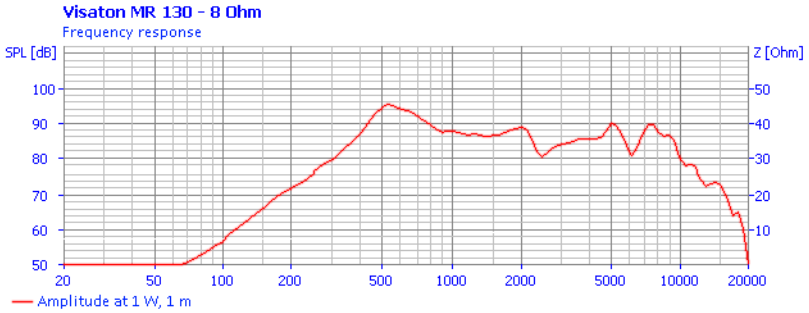

FIGURE 3.3: Frequency response of a VISATON MR 130 cone loudspeaker driver. From (VISATON GmbH & Co. KG, 2017).

3.1.2 Loudspeaker Arrays

Loudspeaker array as a term describes a number of usually identical loudspeaker elements arranged in a specific formation. Typically these arrangements have all elements standing in a line, hence the term line array often being used, although more complex geometries have also been explored and utilised in practice. The primary purpose of using loudspeaker arrays is to achieve a high degree of directivity towards a desired direction. Destructive and constructive interference between array elements shape the sound field, and effective beamforming can be achieved by controlling their relative phase and amplitude. This allows for a loudspeaker array to be optimised to maximise the radiated sound field in a specific direction, without any physical changes to the layout and orientation of the system. Loudspeaker array technology has often progressed alongside microphone array technology, on which a comparatively abundant bibliography exists (Soede et al., 1993; Elko, 2000; Brandstein and Ward, 2013). Due to acoustic reciprocity, the same principles that define the performance of microphone arrays also apply to loudspeaker arrays.

Depending on the desired properties of the generated sound field, different array geometries and can be used to achieve optimal performance for the system. In this work, only linear arrays will be investigated. Two basic configurations for linear arrays are defined, depending on the orientation of their main axis –either perpendicular or parallel relative to the intended directivity of the radiated sound field. A broadside configuration is the most straightforward application of a loudspeaker array; it has a number of identical elements placed along a line at equal spacing, and they are each fed with an identical signal in phase and amplitude. The resulting directivity pattern is beamed perpendicular to the array, while it remains narrow along its main axis, as can be seen in the example pictured in Fig. 3.4.

An endfire array is a line array where the intended directivity of the radiated sound field is along the axis on which the sources are distributed. As mentioned, a line array can be configured to change its directivity pattern by controlling the phase and amplitude of the signal emitted by each element (Holland and Fahy, 1991). A particular case is when a delay of $(n-1)l/c_0$ is introduced between the loudspeaker units, where n is the number of the loudspeaker, l is the distance between two sources and c_0 the speed of sound. Figure 3.5 shows that under this condition, the beam is steered so that sound radiates along the line of the arranged sources. In practice, the difference between a broadside and an endfire loudspeaker array is the direction of the generated sound beam relative to the axis of the array, which is ultimately a matter of controlling the relative phase and amplitude of the

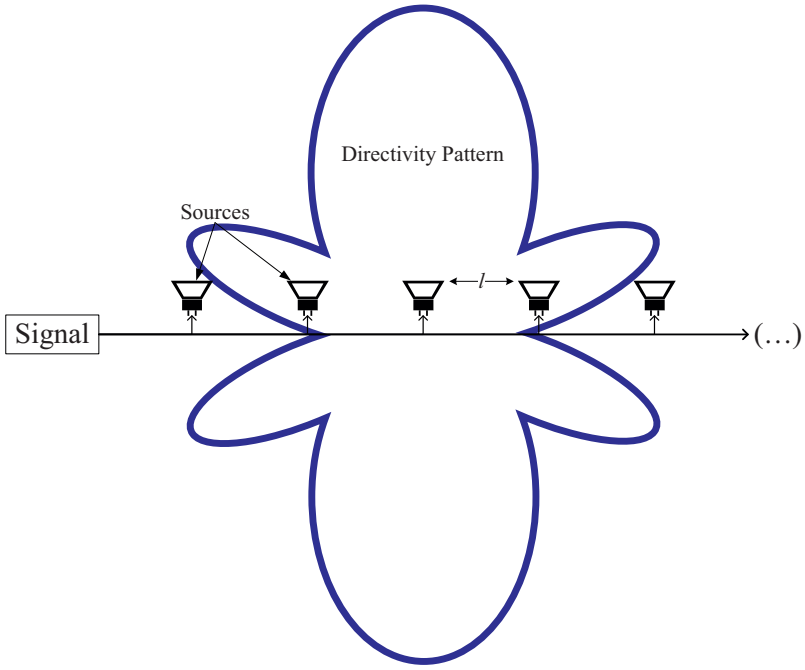

FIGURE 3.4: Generalised directivity of a five loudspeaker broadside array.

signals sent to each source.

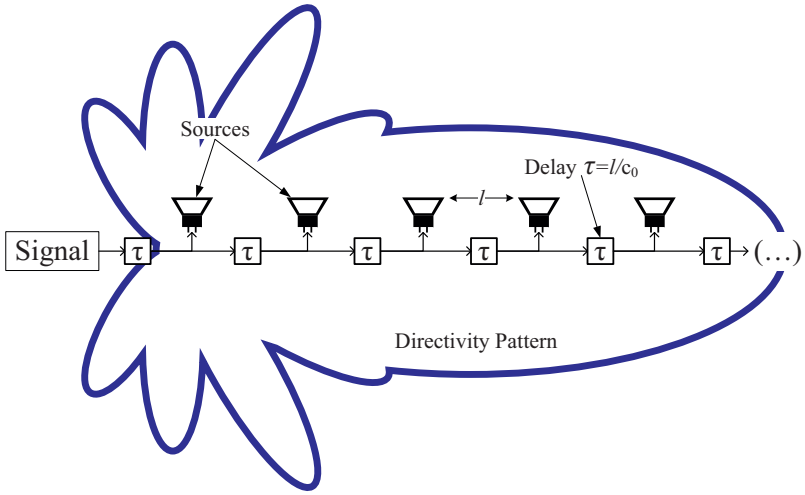

FIGURE 3.5: Generalised directivity pattern of an endfire array, where delay between sources is equivalent to l/c_0, presented in (Birchall et al., 2013).

Loudspeaker arrays have proven to be a capable means of achieving the directivity needed for an EV warning sound, attested by their experimental implementation in eVADER (Quinn et al., 2014) and VESS (You et al., 2020), which were presented in Sec. 2.5. A key drawback, however, is the high cost and complexity of having a multitude of individual loudspeakers on a vehicle. Additionally, the arrays display a low frequency limit tied to their overall length L, with the cut-on frequency f_{LC} given as

$$f_{LC} = \frac{2c_0}{L}. \tag{3.1}$$

The above means that the length of the array needs to be at least twice the wavelength of the lowest frequency of interest to achieve significant directivity. At the same time, loudspeaker arrays are also characterised by spatial aliasing artifacts at higher frequencies that impose a high frequency limit (Rabenstein and Spors, 2006). This limitation can be expressed as

$$f \leq \frac{c_0}{l(1+|\cos\theta|)}, \tag{3.2}$$

where θ is the incidence angle relative to the axis of the array. This angle, and the spacing between loudspeakers, l, are the parameters that affect the aliasing limit of the array. The cut-off frequency increases for lower values of l, corresponding to a narrow spacing, and as the incidence angle approaches a direction perpendicular to the axis of the array ($\theta = n\pi/2, n = 1, 2, 3...$). Together with the low frequency limitation, an array that is characterised by both a large overall length and narrow spacing between sources, therefore a greater number of loudspeakers, is necessary to improve performance in both ends of the frequency spectrum.

Given the available space and necessity for low cost during the production of a vehicle, limits need to be imposed on both the array length and number of loudspeakers used such an array, which in turn forces a compromise in the operational bandwidth of the warning sound system. An additional point of concern comes from the placement of an array. Such a configuration is presumed to be fitted at the front of the vehicle with the loudspeakers facing forward, becoming exposed to the environment and susceptible to damage and dust or dirt accumulation. Considering the fragility of a loudspeaker driver, this constitutes an issue when it comes to the durability and maintenance cost of the system. Moreover, the structure of the vehicle would need to be modified to allow the loudspeaker to radiate effectively, that is, openings with grilles would need to be incorporated into the design of the vehicle structure.

3.1.3 Parametric Loudspeaker

The parametric loudspeaker, pictured in Fig 3.6, is a type of directional loudspeaker which uses ultrasonic waves beyond the human hearing range as a unidirectional carrier to deliver audible sound to desired locations (Gan et al., 2012). The concept of the parametric acoustic array was introduced by Peter J. Westervelt in 1963 (Westervelt, 1963) and in 1975, Bennet and Blackstock proved that a parametric loudspeaker can work with air as the transfer medium (Bennett and Blackstock, 1975). More recently, steerable parametric loudspeakers have been developed and utilised in active noise control (Tanaka and Tanaka, 2010). Parametric loudspeakers have also been suggested and patented as part of a directional warning sound system for implementation in EVs (Pompei, 2006), though no further work in this direction has been published.

When two high intensity sinusoidal beams are radiated from an ultrasound source, a spectral component at the difference frequency is secondarily generated along the beams due to the non-linear interaction of the two primary waves. At the same time, superposition of the two waves results in a sum and difference frequency wave. Of these, only the difference frequency component can travel an appreciable distance, as sound absorption is generally increased with frequency, and amplitudes of higher frequency components decay fast in comparison. The difference frequency secondary beam is virtually created and distributed along the primary beam. Consequently, the directivity of the difference-frequency wave becomes very narrow.

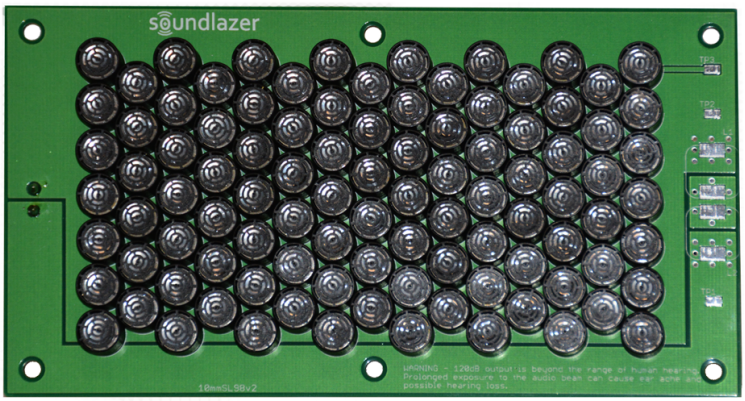

FIGURE 3.6: Example of a parametric array loudspeaker, consisting of numerous ultrasonic transducers. Picture as displayed in (Haberkern, 2020).

According to (Westervelt, 1963), when two primary waves of frequencies f_1 and f_2, where $f_2 > f_1$, are fully confined beams, the angular width, θ_w, at which the sound intensity of the difference frequency $f = f_2 - f_1$ is reduced by one-half (-3 dB), can be approximated as

$$\theta_w \approx \sqrt{2\alpha_r / k}, \tag{3.3}$$

where k is the wavenumber of the difference frequency wave, and a_r is the total sound absorption coefficient of the primary waves. When $f_1 \approx f_2$, $a_r \approx 2a_1$, where a_1 is the absorption coefficient of the primary wave of frequency f_1. The above equation essentially illustrates how the secondary beam is narrowed either by decreasing the primary frequencies or by increasing the secondary frequency.

Although capable of a high degree of beamforming, this method is not without drawbacks when it comes to its implementation within the context of a vehicle warning sound system. The cost of such an ultrasonic transducer is significantly higher than that of a conventional loudspeaker, and the same issues regarding robustness and maintenance are still present. In addition, concern over health issues associated with exposure to ultrasound with an SPL of 140 dB and over may constitute a deterrent in the perception of the public, although parametric arrays can operate at levels below this threshold (Pompei, 1999). For such reasons the parametric array might not be a suitable solution for this application.

This section presented in brief three sound emitter systems that have been investigated in the past as potential warning sound systems for EVs. In terms of directivity performance, an array of multiple sources is necessary to achieve a high enough directivity to minimise sound emissions towards the environment, and maintain a bandwidth large enough to include the frequency contents of potential warning sounds. A loudspeaker array, or a parametric array of ultrasonic transducers, are two systems capable of achieving such performance. However, due to their relatively high cost when it comes to manufacturing, difficulty integrating within a vehicle, as well as their fragility, such systems have yet to be adopted by the industry in spite of their capabilities. Thus far, the only emitter in use across wide production vehicles is the solitary loudspeaker driver, which, although incapable of acoustic beamforming, constitutes the practical solution due to its cost-effectiveness.

3.2 Acoustic Contrast and Directivity Control

Prior to introducing models and suggestions for warning sound systems, it is important to define a metric for their evaluation with regard to directivity and bandwidth. The most straightforward approach for this is through the delay and sum beamforming process, which offers a low computational cost and is easily implementable in real-time. However, research in both microphone and loudspeaker arrays has found that delay and sum beamforming is surpassed in effectiveness by more advanced methods, such as least-squares, superdirective array (Blanco Galindo et al., 2020), acoustic contrast control, and the acoustic energy difference method, which was employed in the case of the eVADER system (Berkhoff and Van der Rots, 2013). In this thesis, the approach for evaluating directivity and achieving control of the radiated sound field will be through the acoustic contrast maximisation process. The choice for this approach is due to the degree of control it offers not only in terms of the primary beam within which the output is maximised, but also in the minimisation of emissions in all other directions, something crucial within the context of minimising drive-by noise. This method has been utilised with success in the control of sound fields generated by multiple loudspeaker systems (Simón Gálvez et al., 2012, 2014).

The acoustic contrast maximization method was proposed by Choi and Kim (Choi and Kim, 2002) and aims to maximize the acoustic contrast between the mean squared pressure in two distinct zones defined as bright and dark, respectively referring to the regions where sound needs to be generated or attenuated. Two examples of such control zones, focussed at different directions, are illustrated in Fig. 3.7. The complex acoustic pressure generated by the array is measured at 180 evaluation points evenly distributed along a 2.8 m radius half circle covering the forward half space. A designated bright zone covering an angle $\theta_B = 36^\circ$ in the forward direction, and the dark zone defined by its supplementary angle θ_D, are used to calculate the acoustic contrast and optimise the outputs of both the loudspeaker and structural arrays to achieve the highest possible degree of directivity. Fig. 3.7a shows the schematic of this configuration in scale relative to an array length of 1 m. This bright zone example will be used in the remainder of this project for the simulation-based evaluation of all directional sound systems that are to be investigated. An additional bright zone is displayed in Fig. 3.7b, this time for a 45° steered setting. Again, the overall coverage of the bright zone is $\theta_B = 36^\circ$. This steered setting is to be used to evaluate the steerability and beamforming capabilities of a system.

3.2.1 Acoustic Contrast

For an array of N sources driven by a vector of complex input signals, $\boldsymbol{u}$, at a given frequency, the complex pressure amplitudes, $\boldsymbol{p}$, are given by vectors $\boldsymbol{p}_B$ and $\boldsymbol{p}_D$ for M_B measurement points in the bright and M_D points in the dark zone respectively. The complex transfer responses between the sources and the pressure measurement points in the bright and dark zones are $\boldsymbol{G}_B$ and $\boldsymbol{G}_D$, so that

$$\boldsymbol{p}_B = \boldsymbol{G}_B\boldsymbol{u} \qquad \boldsymbol{p}_B = \boldsymbol{G}_D\boldsymbol{u}. \tag{3.4}$$

Taking the above into account, the acoustic contrast is defined at a given frequency as the ratio of the mean of the squared pressures in the bright zone and the dark zone, which can be expressed as

$$C = \frac{M_D\boldsymbol{p}_B^H\boldsymbol{p}_B}{M_B\boldsymbol{p}_D^H\boldsymbol{p}_D} = \frac{M_D\boldsymbol{u}^H\boldsymbol{G}_B^H\boldsymbol{G}_B\boldsymbol{u}}{M_B\boldsymbol{u}^H\boldsymbol{G}_D^H\boldsymbol{G}_D\boldsymbol{u}}, \tag{3.5}$$

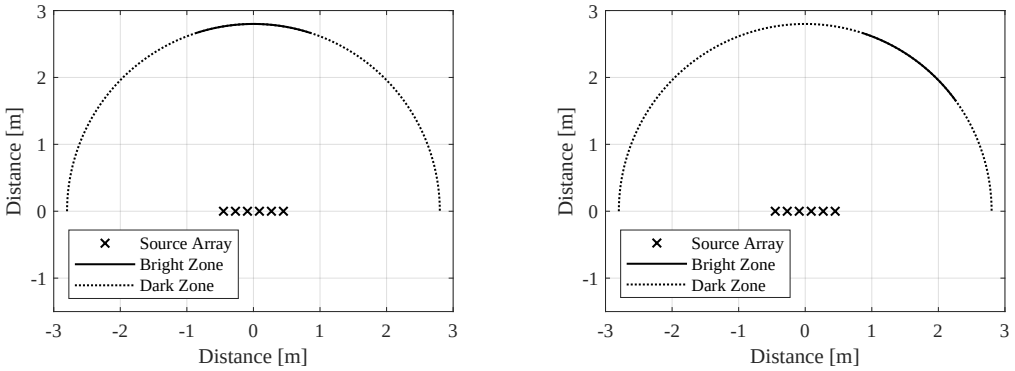

(A) Forward setting. (B) 45° steered setting.

FIGURE 3.7: Visualisation of designated pressure evaluation points and the defined bright zones, relative to the simulated arrays, for a forward and a 45° steered setting.

where the ^{H} superscript indicates the conjugate transpose operator. The acoustic contrast is a dimensionless quantity, which is usually expressed in decibels with its level defined as $10\log_{10} C$.

The above definition allows for the formulation of a constrained optimization problem. The most useful formulation aims to minimize $\boldsymbol{p}_D^H \boldsymbol{p}_D$ under the constraint that $\boldsymbol{p}_B^H \boldsymbol{p}_B$ is held constant, which also provides the practically useful solution (Elliott et al., 2012). The resulting Lagrangian is

$$\mathfrak{L} = \boldsymbol{p}_D^H \boldsymbol{p}_D - \lambda_1 (\boldsymbol{p}_B^H \boldsymbol{p}_B - B), \tag{3.6}$$

where λ_1 is the real and positive Lagrange multiplier, and B is the fixed constraint value. The vector $\boldsymbol{u}$ that minimizes this Lagrangian also maximizes the acoustic contrast. This solution corresponds to the eigenvector corresponding to the largest eigenvalue in the relation (Elliott et al., 2012)

$$\lambda_1 \boldsymbol{u} = \left[\boldsymbol{G}_D^H \boldsymbol{G}_D\right]^{-1} \left[\boldsymbol{G}_B^H \boldsymbol{G}_B\right] \boldsymbol{u}. \tag{3.7}$$

Using the values of this eigenvector to generate the driving signal for the array achieves the highest level of acoustic contrast in the radiated sound field that the system is capable of producing. It should be noted that alternative control methods, such as pressure matching (Olivieri et al., 2015) or planarity control (Coleman et al., 2014) may allow an improvement in the audio quality, and must be considered in high quality audio reproduction systems. However, this also comes at the expense of reduced contrast between the bright and dark zones and so it will not be considered further here, where the primary concern is the directional performance rather than the sound quality of reproduction.

3.2.2 Array effort regularization

Another quantity that is useful for both the performance evaluation and optimization of an array is the normalized array effort. This is defined here as the sum of the modulus squared signals driving the array, divided by the modulus squared signal required from a single element at the centre of the array to produce the same mean

squared pressure in the bright zone, u_m. This has the form

$$AE = \frac{\boldsymbol{u}^H \boldsymbol{u}}{|u_m|^2}, \tag{3.8}$$

and is proportional to the electrical power required to drive the array, if one assumes that no significant electroacoustic interactions between the transducers occur (Simón Gálvez et al., 2012). As with the acoustic contrast, the array effort is a dimensionless quantity, again expressed in decibels and with a level defined as $10 \log_{10} AE$.

When formulating the optimization problem defined by Eq. (3.6), it is generally of practical benefit in terms of the system robustness to introduce an additional constraint on the array effort and this has been investigated in (Elliott et al., 2012). In this case, the sum of the squared pressures in the dark zone, $\boldsymbol{p}_D^H \boldsymbol{p}_D$, is still minimized, but under the constraints that both $\boldsymbol{p}_B^H \boldsymbol{p}_B$ is equal to B and that $\boldsymbol{u}^H \boldsymbol{u}$ is equal to P, which represents a constraint on the total power of the signals driving the array. The corresponding Lagrangian has the form

$$\mathfrak{L} = \boldsymbol{p}_D^H \boldsymbol{p}_D + \lambda_1 (\boldsymbol{p}_B^H \boldsymbol{p}_B - B) + \lambda_2 (\boldsymbol{u}^H \boldsymbol{u} - P), \tag{3.9}$$

where λ_1 and λ_2 are the positive real values of the Lagrange multipliers. In the context of an EV warning sound system, the sound pressure constraint, B, would correspond to the sound pressure level that is required to render the sound audible in the bright zone, while the effort constraint, P, would be chosen under consideration of power availability and the capabilities of the actuators used. Seeking the minimum solution of this Lagrangian has been shown to lead to the relation

$$\lambda_1 \boldsymbol{u} = -\left[\boldsymbol{G}_B^H \boldsymbol{G}_B\right]^{-1} \left[\boldsymbol{G}_D^H \boldsymbol{G}_D + \lambda_2 \boldsymbol{I}\right] \boldsymbol{u}. \tag{3.10}$$

The optimal solution in this case can be obtained from the eigenvector corresponding to the largest eigenvalue of the inverse matrix, $\left[\boldsymbol{G}_D^H \boldsymbol{G}_D + \lambda_2 \boldsymbol{I}\right]^{-1} \left[\boldsymbol{G}_B^H \boldsymbol{G}_B\right]$. In this case, the Lagrange multiplier, λ_2, not only limits the array effort, but also regularizes the matrix being inverted, which can improve the robustness of the system in practice (Elliott et al., 2012).

3.3 Evaluation of the Loudspeaker Array

As the loudspeaker array is the most straightforward method for controlling the directivity of a radiated sound field, and it has been fully integrated as part of an experimental warning sound system previously (Quinn et al., 2014; You et al., 2020), a brief investigation of its capabilities and limitations can serve as a point of reference for alternative directional systems that will be subsequently investigated in this thesis. In this section, a simulations-based parametric study of the loudspeaker array is presented for this purpose. The directivity performance of each simulated array is evaluated through the resulting acoustic contrast across frequency. By modelling arrays with a varying number of loudspeakers and different overall length, the effects that these parameters bear on the response of the array are identified.

3.3.1 Radiated Sound Field in 2D and 3D

As mentioned in Sec. 3.1, a loudspeaker array can be controlled to steer its directivity towards a specific direction. A noteworthy aspect of the three dimensional geometry of the radiated sound field, is that any resulting directivity pattern is symmetrical around the main axis of the array. It is important to provide a view into this general behaviour of loudspeaker arrays, prior to defining the terms under which their performance is to be evaluated in a parametric study. Figure 3.8 shows the directivity of a simulated 8 source array, distributed along the y-axis, at 1 kHz, when optimised to radiate perpendicular to its main axis (broadside), at a 30 $^\circ$ angle, and along its main axis (endfire). The directivity patterns are displayed in three dimensional space, and on the azimuthal (xy) plane at the height of the sources.

In a two dimensional view, the broadside configuration (Fig. 3.8b) appears to be capable of a more focussed beam when compared to the endfire example (Fig. 3.8f), especially when one considers that the rear projected lobe in the former case can be ignored, as it is absorbed by the structure the array is installed in. However, when one examines the corresponding 3D view of the same radiated fields (Fig. 3.8a and 3.8e), it is evident that the broadside case actually generates a ring-shaped sound field, with significant output along the z-direction. The endfire configuration, in comparison, focusses its radiation in the forward direction. In the case of the intermediate angle steering setting, a 2D perspective indicates a single main lobe corresponding to the main beam. However, the three dimensional view shows that the actual shape of the sound field corresponding to this main lobe, is that of a conical surface, forming a 60° angle with the axis of the array, with its peak at the centre of the array. Through these examples, one can follow how, as the beamforming angle increases, the initial radiation pattern of a loudspeaker array in broadside configuration gradually assumes the single-main lobe shape characteristic of the endfire, always maintaining axial symmetry.

In terms of the acoustic contrast measured, the resulting levels also vary depending on whether three or two dimensional geometry has been considered. Figure 3.9 displays the acoustic contrast frequency response from a broadside and an endfire configuration of equal length and number of sources, when evaluated over two and three dimensional space. The bright zone is the circular arc in the 2D case, and spherical surface in the 3D case, defined by a 18° angle. It can be seen that the overall contrast level is lower when evaluated over 3D space. What is most noteworthy, is that while the endfire array achieves a higher contrast than the broadside throughout the entire frequency range in the 3D evaluation, in 2D the performance of the two configurations is rather more comparable at low frequencies, and the broadside array

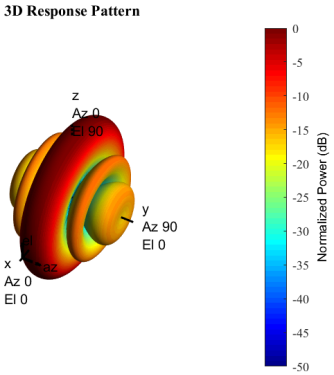

(A) Broadside configuration.

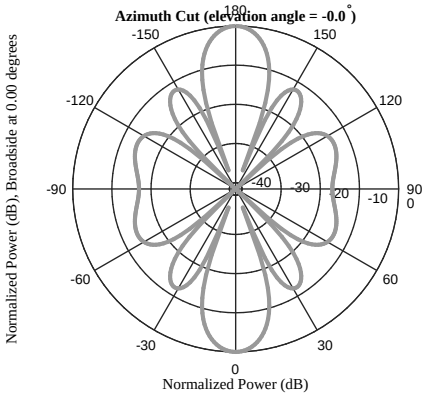

(B) Broadside configuration.

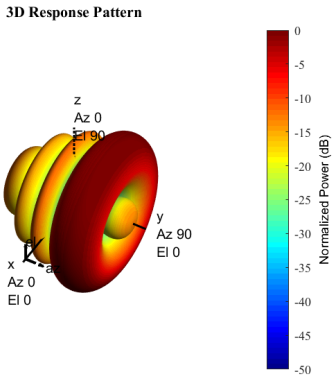

(C) 30 ° angle relevant to array.

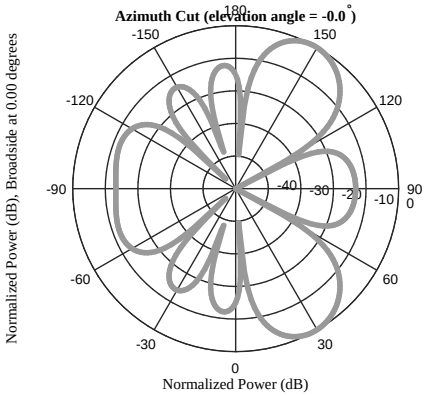

(D) 30 ° angle relevant to array.

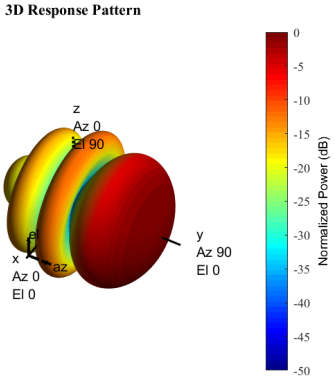

(E) Endfire confituration.

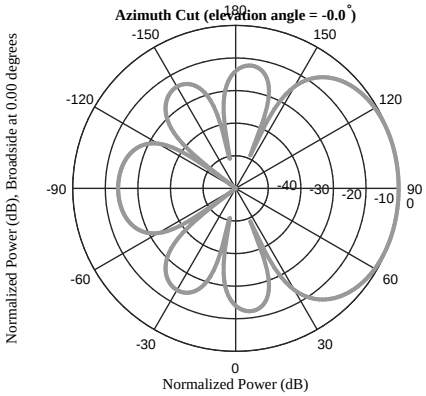

(F) Endfire confituration.

FIGURE 3.8: Directivity of eight loudspeaker array arranged along the *y*-axis at 1 kHz, for broadside, endfire, and intermediate steering setting.

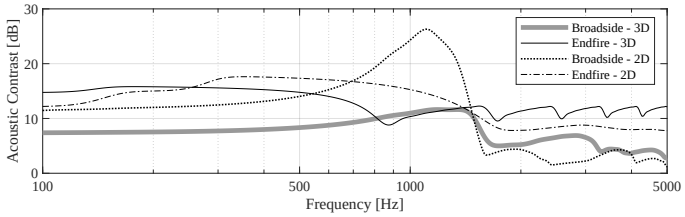

FIGURE 3.9: Acoustic contrast over frequency for broadside and endfire configurations of equal length and number of sources, evaluated using either a 2D or 3D geometry of control zones.

achieves a significantly higher contrast between roughly 500 Hz and 1.5 kHz. This is a further testament to the importance of the geometry considered for the evaluation of directivity when it comes to comparing different systems.

With the exception of the endfire configuration, the loudspeaker array produces a significant level of sound pressure along the z-direction. In the context of a vehicle moving on the xy plane, this means a significant amount of sound is directed upwards towards the sky and downwards towards the road. It can be considered that downwards emissions are mostly absorbed by the road, and the sound pressure levels generated from their reflection are negligible, and that upwards emissions do not affect environmental noise, which is measured roughly at the z-position of the vehicle. Under this assumption, the sound fields generated by a directional system intended as an emitter of EV warning sounds, can be evaluated solely on the xy-plane.

3.3.2 Basic Simulation Parameters

The loudspeaker array is modelled as an array of N point monopole sources, without the characteristics of mass and physical dimensions of individual loudspeakers. Since the primary concern of this study regards only the potential directivity performance of the loudspeaker array, particular properties inherent in a loudspeaker driver are not investigated in this model. Assuming an output volume velocity U_n, where n denotes the index of the loudspeaker in the array, the total sound field radiated by N loudspeakers is equivalent to the linear superposition of the sound fields radiated by each one individually; thus, the total pressure at position r is given by

$$p\left(r\right) = \frac{j\rho_0\omega_0}{4\pi}\sum_{n=1}^{N} U_n \frac{e^{-jkr_n}}{r_n}. \tag{3.11}$$

The values of U_n can be individually adjusted in accordance with the optimisation process presented in Section 3.2, in order to maximise the acoustic contrast at each frequency.

As mentioned in above, the directivity of the array is evaluated only on the plane of movement for the vehicle. In addition to that, only the forward half-plane will be considered, as the vehicle itself is expected to act as an absorber for any sound radiated by the array towards the rear. Figure 3.7 shows the two bright zone configurations that are used in this study to control the directivity of the array. As seen from the orientation of the source array relative to the control zones, the simulated system constitutes a broadside configuration. In either case, the overall control zone is defined as a semi-circle of 2.8 m radius, located in the forward half-space relative to the array. The resulting sound pressure is calculated using Eq. (3.11) at 180 points

along this semi-circle, arranged at single degree increments. The width of the bright zone is 36°, which corresponds to 37 points, with the respective dark zone comprising of the remaining 143 measurement points. The acoustic contrast is calculated for these sound pressure values using Eq. 3.5.

Broadside Array

Figure 3.10 shows the resulting SPL across frequency, as a function of the observation angle in the forward half plane, for a simulated broadside array of six loudspeakers with an overall length of 1 m and thus a spacing of 20 cm. The system is investigated over the frequency range between 100 Hz and 5 kHz. This range has been chosen to cover the bandwidth designated by regulations regarding the frequency contents of warning sound systems, presented in Sec. 2.3. The results for a forward bright zone setting (Fig. 3.10a) display symmetry around the forward direction, as expected from the geometry of the array. The sound field is directional up to a cut-off frequency at around 1.8 kHz, above which spatial aliasing artifacts in the form of high SPL side lobes occur in various angles. The cut-off frequency is reduced to around 1 kHz when using a bright zone steered by 45° (Fig. 3.10b).

The directivity of the above simulated array at specific frequencies for the two steering settings is shown in Fig. 3.11. At 300 Hz, as can also be observed in Fig. 3.10, the beam is focussed on the bright zone for both settings. Side lobes at different directions are observed, but their SPL is low compared to the main lobe. At 1.2 kHz, the array is capable of the highest directivity in the forward setting, but is past the cut-off frequency for the steered setting, producing high SPL in directions other than the designated bright zone. Lastly, at 2 kHz, the system is beyond its high frequency limit in both cases. Although a high SPL is still achieved in the bright zone, lobes in other directions have a comparable level which greatly reduces the directivity.

Endfire Array

An endfire configuration can be simulated by rotating the axis of the array by 90°, while maintaining the control zone distributions shown in Fig. 3.7. In this case, the SPL frequency response as a function of angle is shown in Fig. 3.12 for the forward directed and steered settings. In the forward setting, the resulting directivity behaviour is similar to the broadside configuration in Fig. 3.10a, with the sound beam focussed within the bright zone up to a cut-off frequency at around 1.8 kHz, after which side lobes reduce the directivity.

Using the endfire configuration and steering the bright zone by 45°, the symmetrical lobe that in the previous case would be considered as rear radiation and ignored is now in the designated forward half-plane. This results to a bilateral maximisation of sound pressure around the axis of the array. The resulting SPL for a 45° steered setting is shown in Fig. 3.12b, and it is evident that the symmetrical two-lobe behaviour is maintained throughout the investigated frequency range.

In order for the endfire array to steer the sound beam towards a specific angle, it would need to be positioned so that radiation on one side of the forward half-plane is absorbed by the vehicle, similarly to the broadside case. This would mean that the array would have to be placed on the side of a vehicle. Such an issue compromises the applicability of the endfire configuration, as full coverage of the forward half-plane would require two separate arrays, one on either side of the vehicle. Nevertheless, it is worth investigating the performance of this configuration when it

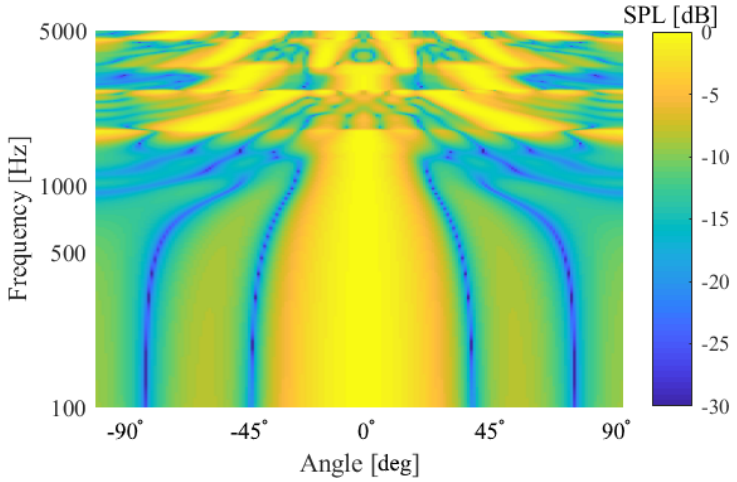

(A) Bright zone directed forward.

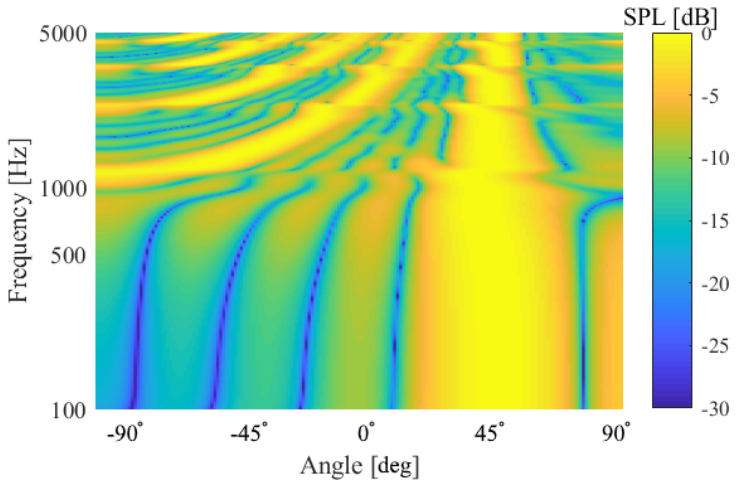

(B) Bright zone steered by 45°.

FIGURE 3.10: Normalised SPL frequency response as a function of the observation angle for a 1 m long six loudspeaker array. Optimised for directional radiation using different bright zones.

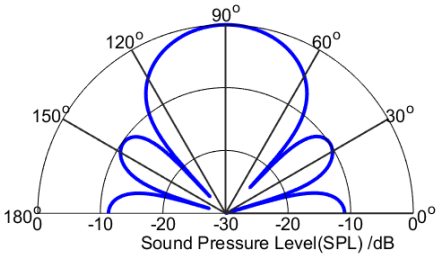

(A) 300 Hz; Forward directed setting.

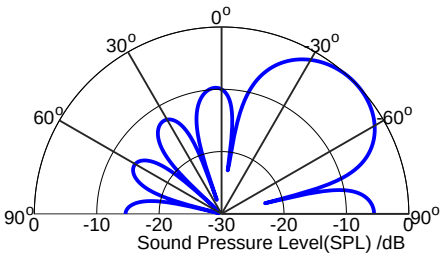

(B) 300 Hz; 45° steered setting.

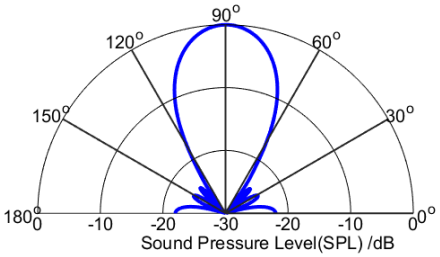

(C) 1.2 kHz; Forward directed setting.

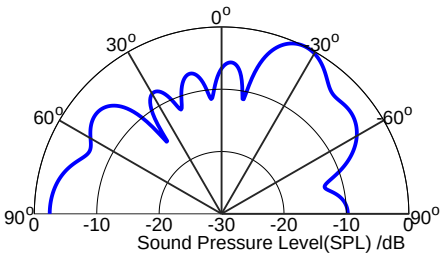

(D) 1.2 kHz; 45° steered setting.

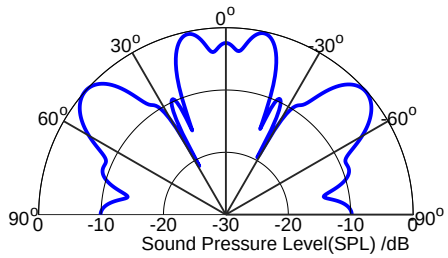

(E) 2 kHz; Forward directed setting.

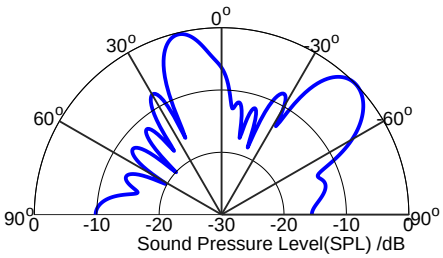

(F) 2 kHz; 45° steered setting.

FIGURE 3.11: Directivity of the simulated six loudspeaker array at specific frequencies, for a forward and a 45° steered bright zone setting.

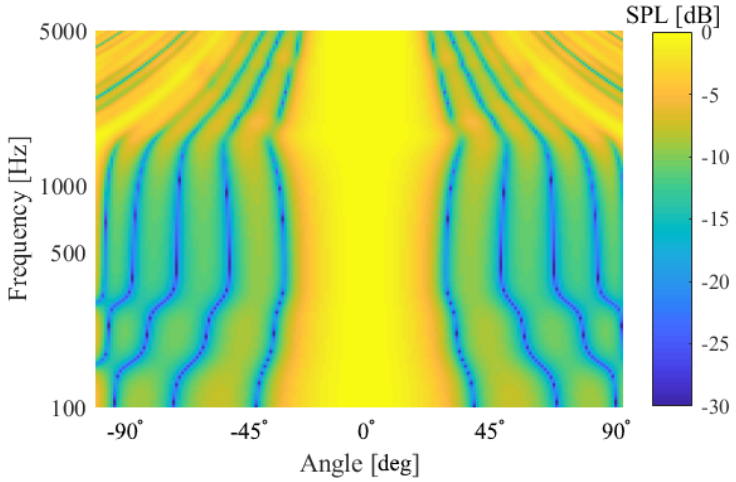

(A) Bright zone directed forward.

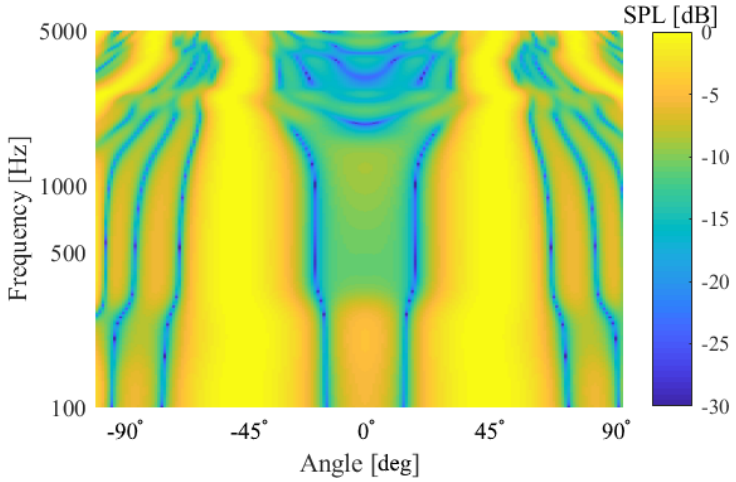

(B) Bright zone steered by 45°.

FIGURE 3.12: Normalised SPL frequency response as a function of the observation angle for a 1 m long six loudspeaker endfire array. Optimised for directional radiation using different bright zones.

comes to a forward directed sound field, as a point of reference and comparison to the broadside array and any other systems to be subsequently presented.

3.3.3 Parametric Study

From Eqs. (3.1) and (3.2) it is evident that the primary factors that influence the bandwidth of a loudspeaker array are its overall length and the spacing between its sources. Therefore, the focus of the parametric study presented in this section is on the effect that these two parameters have on the performance of the system. This is performed by changing the source spacing while keeping the overall array length fixed and vice versa. As a result, the number of sources forming the array also changes accordingly.

A broadside array will be simulated as optimised using the bright zones shown in Fig. 3.7, corresponding to the forward direction and a 45° steered setting. In addition, the forward directivity performance of a simulated endfire array, characterised by the same parameters, will also be evaluated and compared.

Array Length

Arrays of different overall lengths are simulated while keeping the spacing between sources fixed at 20 cm. The lengths considered, as well as the corresponding number of loudspeakers used in each case are displayed in Table 3.1. Figure. 3.13 shows the performance of the simulated arrays when optimised using the bright zone of Fig. 3.7a, to operate as broadside arrays. The acoustic contrast response, shown in Fig. 3.13a, demonstrates how longer arrays bear an improvement in directivity performance. Though a cut-off is maintained for all cases around 1.7 kHz, which imposes a high frequency limit on the operational bandwidth of the system, the level of contrast within this bandwidth consistently increases with the length of the array.

In order to offer a better indication of the sound as it reaches the targeted listener, the on-axis SPL frequency response, measured as the sound pressure at the single microphone in the centre of the designated bright zone, is shown in Fig. 3.13b. The response displays a roll-on behaviour which is similar to that of the baffled loudspeaker, though in this case the loudspeaker array is simulated through a number of monopole sources. This initial roll-on comes as a consequence of the regularization process expressed through Eq. (3.9), and in particular due to the constraint in array effort, which limits the output at lower frequencies. Beyond a cut-on frequency the response becomes flatter, as one would expect from the constraint on the mean square pressure in the bright zone set in Eq. (3.9). Irregularities at higher frequencies are likely due to the spatial averaging over the entire bright zone used in the consideration of the constraint, B, compared to the depicted case of the response at a single microphone. This frequency response is also representative of the other microphones covered by the bright zone.

Array Length	No. of Sources
0.6 m	4
0.8 m	5
1 m	6
1.2 m	7

TABLE 3.1: Different array lengths simulated, and corresponding number of loudspeakers used as sources considering a fixed spacing of 20 cm.

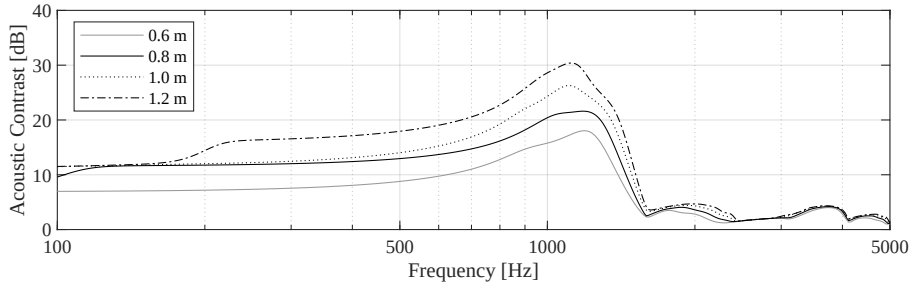

(A) Acoustic contrast frequency response.

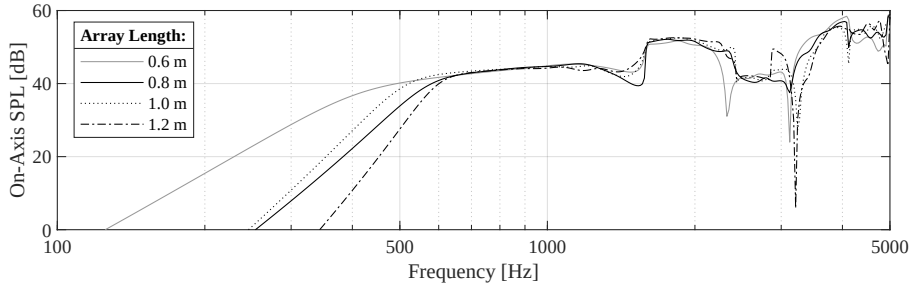

(B) On-axis SPL frequency response.

FIGURE 3.13: Acoustic contrast and on-axis SPL comparison for six loudspeaker arrays of varying length, operating in a broadside configuration.

Contrary to the acoustic contrast response, the SPL response at lower frequencies is highest for the shortest simulated array of 0.6 m length. The 0.8 m array displays a poorer low frequency performance with a steeper roll-on, which improves for a length of 1.0 m, while the 1.2 m long array provides the worst response of the group. The behaviour can be explained in that a shorter array will need to provide a higher SPL at lower frequencies to maximise its directivity. This is relatively negated when an odd number of sources is used, due to the position of a central source instilling a natural directivity to the system in the forward direction, which explains why low frequency SPL is increased when moving from 0.8 m length (5 sources) to 1.0 m.

The response of the simulated broadside arrays listed in Table 3.1, when optimised using a bright zone steered by 45° relative to their main axis, is shown in Fig. 3.14. In the case of the acoustic contrast response (Fig. 3.14a), a general decrease in directivity compared to Fig. 3.13a is clearly visible through the reduced levels of contrast for all cases. This is expected as, according to Eq. (3.2), the cut-off frequency decreases to around 1 kHz due to the angle of the bright zone relative to the axis of the array. Longer arrays still achieve higher contrast levels across all frequencies in this setting.

The on-axis SPL response (Fig. 3.14b) follows a behaviour similar to the broadside configuration, though in this case the flat region still displays constant slope, though reduced compared to the roll-on. The differences between the SPL response at the roll-on stage are not as significant as in the broadside setting, with the shortest array providing the highest levels, but no clear trend being discernible among the investigated array lengths.

Figure 3.15 shows the performance of the different arrays listed in Table 3.1 in the endfire configuration. In terms of acoustic contrast (Fig. 3.15a), longer arrays

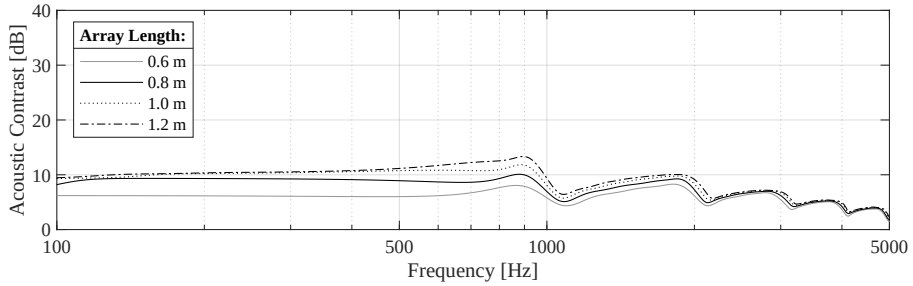

(A) Acoustic contrast frequency response.

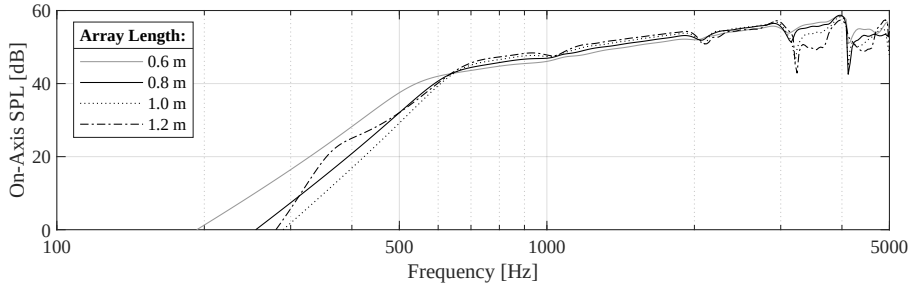

(B) On-axis SPL frequency response.

FIGURE 3.14: Acoustic contrast and on-axis SPL comparison for six loudspeaker arrays of varying length, optimised for a 45^o steered setting.

provide a higher directivity similarly to the broadside configuration, however the maximum levels of contrast achieved are lower in comparison. Although all arrays share a high frequency cut-off at around 1.8 kHz, the decrease in performance is not as significant as in the case seen in Fig. 3.13a, with all cases maintaining a contrast level in dB approximately half that of the maximum achieved.

The on-axis SPL frequency response (Fig.3.15b) shows that in the case of the endfire setting, the roll-on frequency is shifted towards higher frequencies. Comparing to the acoustic contrast response, the endfire configuration appears to provide the highest directivity at frequencies below its cut-on frequency limit. This means that the operational bandwidth of the system lies in frequencies where its directivity potential is relatively limited.

The above results indicate that the directivity performance of a loudspeaker array, in terms of acoustic contrast levels achieved and of its low frequency limitations, benefits from a greater overall array length. This is likely due to the better control over larger wavelengths facilitated by a longer array and the maximum distance available between sources. It should be stressed that, given the fixed spacing between sources considered, an increase in length also means an increase in the number of sources used in the array. The broadside configuration appears to be the one capable of the highest contrast levels. This performance, however, is reduced significantly when the system is optimised to steer its beam. The endfire configuration is characterised by a disparity between its operational bandwidth in terms of on-axis SPL, and the bandwidth at which it is capable of maximising directivity.

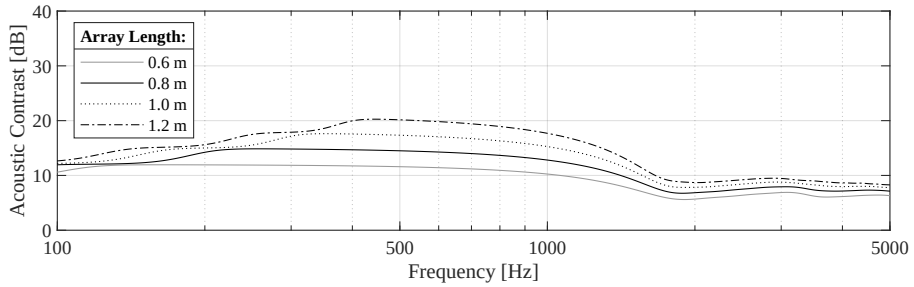

(A) Acoustic contrast frequency response.

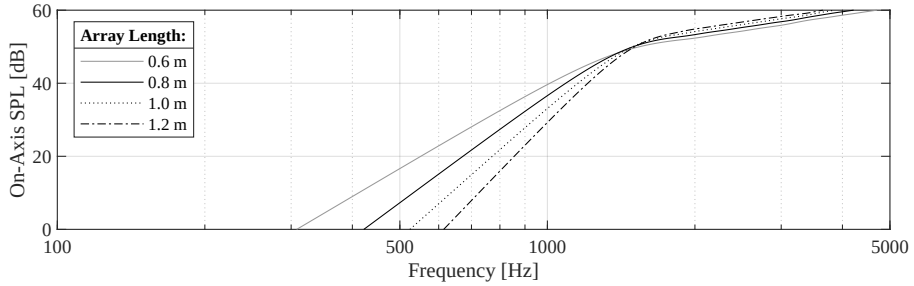

(B) On-axis SPL frequency response.

FIGURE 3.15: Acoustic contrast and on-axis SPL comparison for six loudspeaker arrays of varying length, operating in an endfire configuration.

Source Spacing

The second part of the parametric study regards the effect that the spacing between the sources in the array has on its performance. Table 3.2 shows the different spacing values considered, along with the corresponding number of sources given a fixed overall array length of 1 m. The choice of these particular values was due to the need to uniformly distribute the number of sources within the specified length, and at the same time ensure significant variance between the characteristics of the simulated arrays, which should help obtain a clearer view of any trends in the performance.

Figure 3.16 shows the responses of the simulated arrays, optimised using a forward directed bright zone to constitute a broadside array. The acoustic contrast frequency response (Fig. 3.16a) indicates a clear improvement in performance when the spacing between sources is decreased, both in the levels of contrast achieved but also over the high frequency limit. This latter improvement is due to the narrower spacing allowing better control over smaller wavelengths, and therefore higher frequencies, and overcoming aliasing related effects (Rabenstein and Spors, 2006).

The on-axis SPL response (Fig. 3.16b) displays the characteristic low frequency roll-on followed by a flat region and an irregular response at higher frequencies. Through this example, seen together with Fig. 3.16a, it is most visible how the on-axis SPL response correlates to the acoustic contrast response. The roll-on of the on-axis SPL response extends throughout the lower frequency range at which the acoustic contrast is maintained relatively constant, with a slight rate of increase along frequency. The flat SPL frequency response occurs within the frequency range where the highest levels of contrast are achieved, and the acoustic contrast follows a distinct peak over frequency. Lastly, the irregular SPL response corresponds to frequencies beyond the cut-off in acoustic contrast. Given these results, it can be noted how the narrower spacings, despite offering a higher directivity across all frequencies, may have their performance compromised due to their on-axis SPL response displaying a higher low frequency limit and narrower bandwidth.

Figure 3.17 shows the acoustic contrast and on-axis SPL frequency responses for the broadside arrays simulated above, in this instance optimised using a bright zone steered by 45° relative to the axis of the array. The acoustic contrast frequency response (Fig. 3.17a) displays the same general behaviour over frequency as in the previous part of the study (Fig. 3.14a). As with the broadside configuration, the narrower spacing between sources results in higher levels of contrast and a shift in the cut-off to higher frequencies. Compared to the corresponding arrays in Fig. 3.16a, the overall contrast levels are reduced due to the decrease in effective apperture size for the steered setting.

Source Spacing	No. of Sources
10 cm	11
20 cm	6
33 cm	4
50 cm	3

TABLE 3.2: Different source spacing settings simulated, and corresponding number of loudspeakers used as sources considering a fixed overall array length of 1 m.

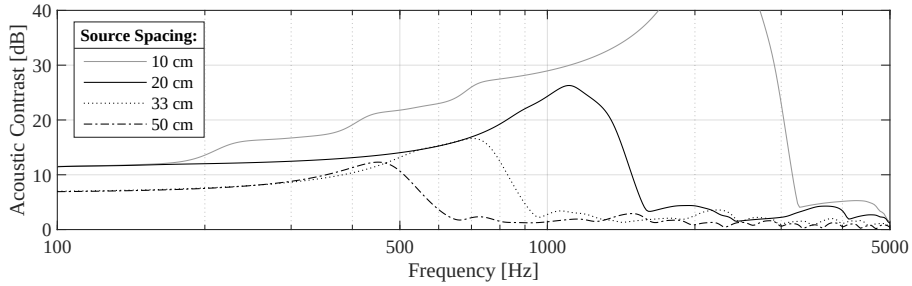

(A) Acoustic contrast frequency response.

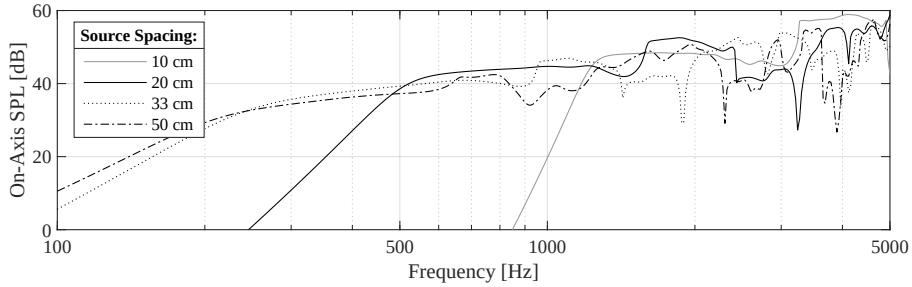

(B) On-axis SPL frequency response.

FIGURE 3.16: Acoustic contrast and on-axis SPL comparison for arrays with a varying number of loudspeakers and 1 m length, operating in a broadside configuration.

The on-axis SPL response (Fig. 3.17b) follows the same trend observed in the broadside case, with wider spacings improving the low frequency response and extending the bandwidth at which a relatively flat response is maintained. However, in this steered setting, the correlation between the different regions in the on-axis SPL and acoustic contrast responses is not as discernible as it was in the previous instance, as the acoustic contrast response does not display as clear a peak in levels, or a high frequency cut-off.

The performance of the same arrays in an endfire configuration is shown in Fig. 3.18. The acoustic contrast frequency response (Fig. 3.18a) displays the behaviour seen in the previous study, with a higher contrast level region characterised by a gradual increase and drop. A high frequency limit can be defined where the acoustic contrast level reaches its minimum value within the investigated frequency range. Narrower spacing between the sources of the array results in an increased acoustic contrast and an improvement of the cut-off frequency limit.

The on-axis SPL response (Fig. 3.18b) shows an improvement of the low frequency limit for wider spacings. As with the cases investigated in the array length study, the SPL roll-on can be associated with the initial high contrast stage in Fig. 3.18a, while the bandwidth where the on-axis SPL response is relatively flattened lies beyond the cut-off frequency of the acoustic contrast response.

Conclusions

From the investigation presented in this section, it is evident that the bandwidth of a loudspeaker array is primarily influenced by the separation between its sources when it comes to the upper frequency limit, and by its overall length when it comes to the lower frequencies. In particular, narrow spacing between the sources of the

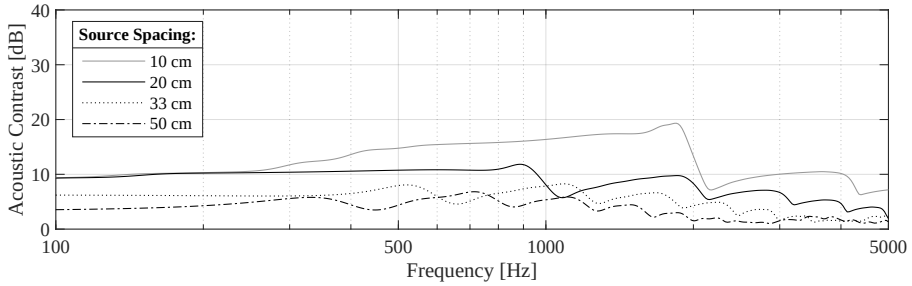

(A) Acoustic contrast frequency response.

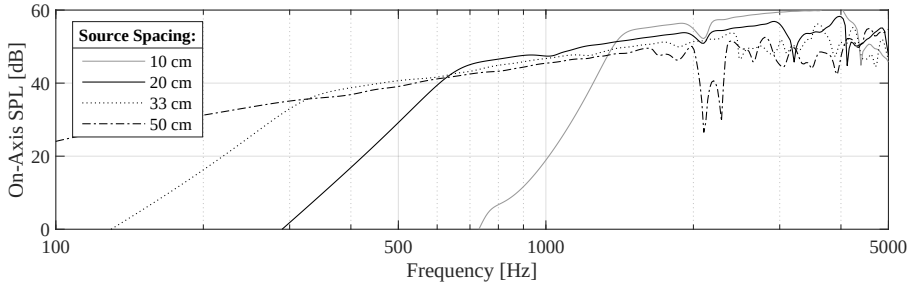

(B) On-axis SPL frequency response.

FIGURE 3.17: Acoustic contrast and on-axis SPL comparison for arrays with a varying number of loudspeakers and 1 m length, optimised for a 45^o steered setting.

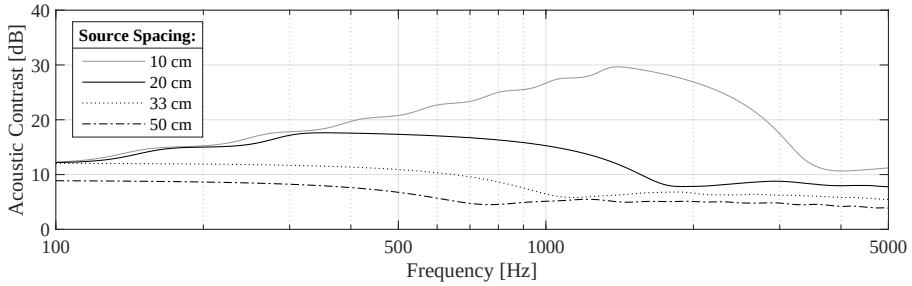

(A) Acoustic contrast frequency response.

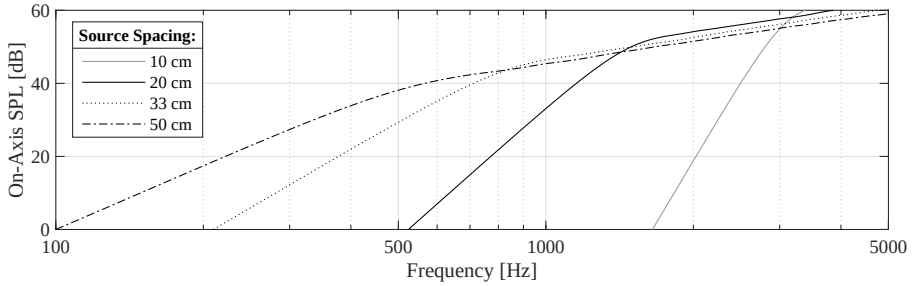

(B) On-axis SPL frequency response.

FIGURE 3.18: Acoustic contrast and on-axis SPL comparison for arrays with a varying number of loudspeakers and 1 m length, operating in an endfire configuration.

array ensures a better directivity performance and the shift of the cut-off limit towards higher frequencies. Longer arrays likewise result in higher levels of acoustic contrast and improve upon the low frequency response. Given these two factors, it can be concluded that a greater number of sources is necessary to maximise the overall directivity performance across all frequencies. The above parameters also impact the on-axis frequency response, meaning that a limitation is imposed upon the effective bandwidth of the array, which should be considered when designing a system intended to operate within a specific frequency range.

With the evaluation limited to the forward half-plane of movement, under the assumption that the vehicle itself may act as an absorber for any sound radiation towards the rear, it is the broadside configuration that was shown to achieve the best performance, with higher levels of acoustic contrast in the forward direction, and selective beamforming capabilities compared to the endfire configuration. The broadside array therefore constitutes the most effective system for integration in a vehicle in terms of generating a controllable directional sound field, as further evidenced by its successful implementation in experimental systems (Quinn et al., 2014; You et al., 2020).

To ensure a high enough directivity across a wide frequency range, however, a significant number of loudspeakers is necessary to be employed in the array. As a result, such a system would be characterised by a relatively high production and maintenance cost, increased weight, and relative fragility if positioned in the front end of a vehicle. Such drawbacks appear to have kept loudspeaker arrays from being adopted for by the industry. It is therefore crucial to consider these factors in the design of a directional sound system, with the aim of limiting the cost of manufacturing and integrating within a vehicle, towards offering a practical and applicable solution.

3.4 The Low Cost Endfire Acoustic Radiator

In 1991, K. R. Holland and F. J. Fahy developed a "Low-Cost Endfire Acoustic Radiator" in the Institute of Sound and Vibration Research (ISVR) of the University of Southampton (Holland and Fahy, 1991). The configuration consisted of an array of holes drilled in a pipe attached to a horn compression driver. Resulting directivity patterns are comparable to what would have been achieved by an array of multiple arranged sound sources, but thanks to this design, only a single powered source was used. This is a design equivalent to what is called a "shotgun" microphone, which consists of the same concept incorporating a microphone instead of a loudspeaker. Such microphones are used for their increased directivity (Olson, 1967).

Such a design offers a promising solution when it comes to generating a directive sound field for a vehicle warning sound system using fewer and simpler resources than other equivalents. However, it should be noted that the endfire acoustic radiator is not capable of selective beamforming in specific directions, unless the entire system is physically rotated. The principles behind this idea were incorporated in more recent projects carried out at the ISVR for the direct implementation of a directional warning sound system attached on a passenger vehicle (Cheer et al., 2013; Birchall et al., 2013). It would therefore be potentially valuable to investigate the directivity performance of the endfire acoustic radiator in a simulation based parametric study, as it may serve as a basis for the development of new warning sound systems, or, at the very least, provide an additional frame of reference in the evaluation of a different directional sound system.

3.4.1 Principle of the Endfire Radiator

As mentioned in Sec. 3.1, a number of identical sound sources arranged in a line will display directivity due to interference effects. This directivity is dependent on factors such as the total length of the array, the wavelength of the sound radiated, the number of sources and the differences in phase and amplitude of the signals emitted by them (Holland and Fahy, 1991). Considering a pipe along whose main axis a number of holes have been drilled as shown in Fig. 3.19, for any sound wave travelling along said pipe, each individual hole acts as a sound source in itself. Given that the output from each hole is delayed due to the propagation of the sound along the length of the pipe, these "sources" also display a delay between each other of approximately l/c_0, where l is the separation between holes. The end result is a

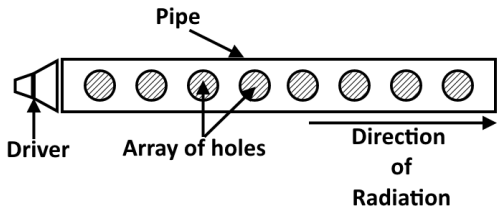

FIGURE 3.19: The endfire radiator.

configuration which behaves like a typical endfire array consisting of a number of sources equal to the number of holes drilled in the pipe. The directivity pattern, sensitivity and range of this array is primarily dependent on physical parameters such as the size, spacing and number of the holes as well as the dimensions of the pipe itself.

3.4.2 Mathematical Model

An analytical mathematical model can be constructed to simulate the operation of the endfire acoustic radiator, and thus offer a tool for the evaluation of its potential, and the optimisation of its design for the intended application. The model presented in this section is based on the one introduced in (Holland and Fahy, 1991). The system can be effectively modelled using acoustic transmission line theory, while approximating the fluid within the pipe as inviscid and ignoring any external coupling between holes.

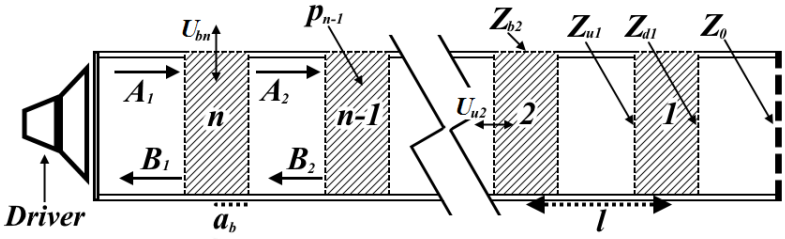

FIGURE 3.20: Diagrammatic representation of the mathematical model of the endfire radiator.

Upstream and Downstream Impedance

The complex acoustic impedances along the pipe are of particular interest at either edge of each hole - upstream and downstream in relation to the oncoming sound wave as shown in Fig. 3.20. Assuming that the impedance at the termination of the pipe can be taken as $Z_0 = \frac{\rho_0 c_0}{S}$, where ρ_0 is the air density and S is the cross-sectional area of the pipe, which constitutes an anechoic termination, the impedance transformation can be used to extract the impedance Z_{d1} downstream of the first hole as

$$Z_{d1} = \frac{\rho_0 c_0}{S} \left\{ \frac{Z_0 + j(\frac{\rho_0 c_0}{S} \tan(kl))}{\frac{\rho_0 c_0}{S} + jZ \tan(kl)} \right\}, \tag{3.12}$$

where $k = \omega / c_0$ is the acoustic wave number at the radial frequency of interest. It can be assumed that the acoustic pressure remains uniform in the area of the hole, given the small dimensions compared to the wavelength in question, and considering the continuity of volume velocity, the impedance upstream of the hole Z_{u1} is defined as

$$Z_{u1} = \frac{1}{1/Z_{d1} + 1/Z_b}, \tag{3.13}$$

where Z_b is the impedance of the hole. The above relation actually stands for any branch in the pipe in the downstream direction (Kinsler and Frey, 1962), in that the upstream impedance is equal to the downstream impedances of both divisions in parallel.

Under the assumption that the holes in the pipe are not wide enough for the volume velocity through each hole to cause viscous flow, the radiation impedance of the hole can be approximated as (Holland and Fahy, 1991)

$$Z_b = \rho_0 c_0 \left[\frac{k^2}{4\pi} + j \frac{k(t_h + 1.5\alpha_b)}{\pi \alpha_b^2} \right], \tag{3.14}$$

where variables t and α_b refer to the thickness of the pipe and the diameter of each hole respectively. The value of Z_b is the same for all holes considering they are identical. Using the value of Z_{u1} in place of Z_0 in Eq.(3.12), the downstream impedance from the second hole can be calculated, and subsequently all the respective impedances for every hole along the pipe.

Pressure inside the pipe

The value for acoustic pressure inside the pipe are calculated starting from the source end of the pipe. In the region between the sound source and hole n, part of plane wave of amplitude A_1 is reflected backwards with amplitude B_1, due to the impedance change caused by the hole as seen in Fig. 3.20. The pressure in said region is calculated as

$$p_n = A_1 + B_1, \tag{3.15}$$

and the volume velocity is

$$U_{un} = \frac{S}{\rho_0 c_0} (A_1 - B_1). \tag{3.16}$$

From Eq. (3.15) and (3.16) the impedance upstream of the hole is by definition

$$Z_{un} = \frac{p_n}{U_{un}} = \frac{\rho_0 c_0}{S} \frac{(A_1 + B_1)}{(A_1 - B_1)}. \tag{3.17}$$

Using Eq.(3.15), (3.16) and (3.17), the expression for pressure p_n at the region of the hole is

$$p_n = A_1 + B_1 = 2A_1 \left(\frac{Z_{un}}{Z_{un} + \rho_0 c_0 / S} \right). \tag{3.18}$$

In order to calculate the pressure of the next hole, focus is shifted towards the next region, defined by holes n and $n-1$. The acoustic pressures on either side (p_n and p_{n-1}) are written in terms of the forward travelling and reflected waves, of amplitudes A_2 and B_2 respectively as

$$p_n = A_2 + B_2 \tag{3.19}$$

$$p_{n-1} = A_2 e^{-jkl} + B_2 e^{jkl}. \tag{3.20}$$

Equivalently, the volume velocity downstream of hole n and upstream of hole $n-1$ is expressed as

$$U_{dn} = \frac{S}{\rho_0 c_0} (A_2 - B_2) \tag{3.21}$$

$$U_{un-1} = \frac{S}{\rho_0 c_0} \left(A_2 e^{-jkl} - B_2 e^{jkl} \right). \tag{3.22}$$

The acoustic pressure p_{n-1} can therefore be expressed in terms of p_n, Z_{un-1}, $Z_d n$ and the distance l between consecutive holes, taking the form

$$p_{n-1} = p_n \left\{ \frac{Z_{un-1} \left(\frac{\rho_0 c_0}{S} + Z_{dn} \right) \left[\cos(kl) - j \sin(kl) \right]}{Z_{dn} \left(\frac{\rho_0 c_0}{S} + Z_{un-1} \right)} \right\}. \tag{3.23}$$

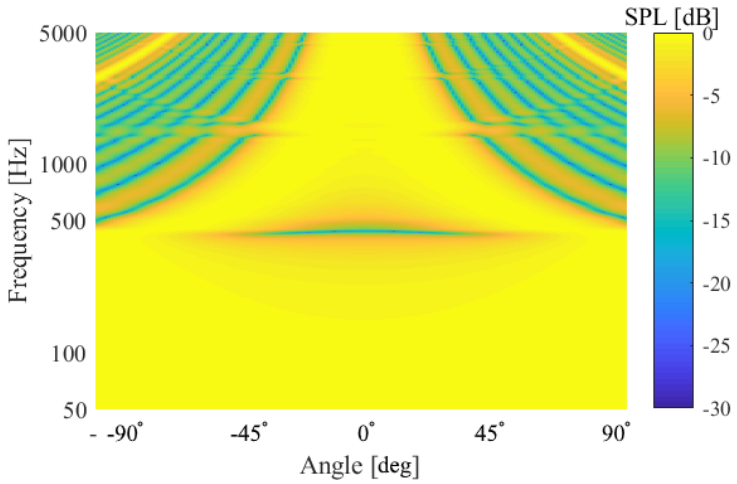

FIGURE 3.21: Normalised SPL frequency response as a function of the observation angle for a 1 m long endfire radiator equipped with eight 12 mm diameter holes.

Radiated Sound Field: Using Eq. (3.23), the acoustic pressure at every hole can be calculated using the known impedances. Volume velocity through each hole can then be calculated as

$$U_{bn} = \frac{p_n}{Z_{bn}}. \tag{3.24}$$

Approximating the radiation from each hole as a monopole source, the acoustic pressure at a point of distance r_n from the hole, which has volume velocity U_{bn} can be written as

$$p\left(r\right) = \frac{j\rho_0 c_0 k U_{bn}}{4\pi r_n} e^{-jkr_n}. \tag{3.25}$$

The total sound field radiated by N holes is equivalent to the sum of the sound fields radiated by each one individually; thus, considering that each hole acts as a separate source the total pressure at position r is estimated using Eq. (3.11).

An example of the resulting sound field from the simulated endfire acoustic radiator is shown in Fig. 3.21. Here, the SPL frequency response is shown as a function of the observation angle in the forward half plane, calculated at 180 measurement points located 2.8 m from the centre of the radiator. This measurement layout is identical to the one used in the evaluation of the loudspeaker array in Sec. 3.3. The SPL values have been normalised for a more convenient evaluation of the results. The simulated endfire acoustic radiator uses a 1 m long pipe of 4 cm internal diameter, with eight 12 mm diameter radiating holes.

Up to a specific frequency, which in the simulated example is around 480 Hz, the system generates an omnidirectional field. At 480 Hz, the sound pressure in the forward direction is reduced and instead the directivity is along the sides. This characteristic in the frequency response has been noted in (Holland and Fahy, 1991) and in (Cheer et al., 2013), and has been considered to mark the cut-on frequency for the endfire radiator, beyond which the system is directional. However, no explanation on its exact cause has been given. Beyond that limit, the directivity of the endfire radiator is seen to improve with frequency, although the presence of side lobes of a high SPL at frequencies above 3 kHz might negatively affect this performance.

Figure 3.22 shows the directivity of the system simulated above at specific frequencies. The frequencies have been chosen so as to be indicative of the behaviour

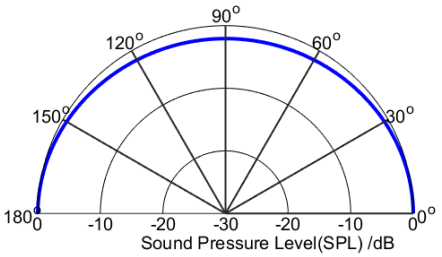

(A) Directivity at 300 Hz.

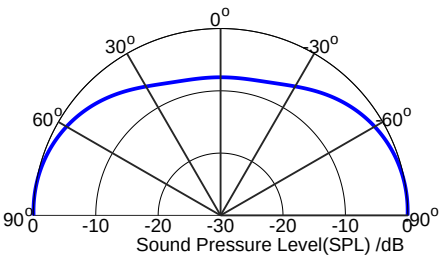

(B) Directivity at 400 Hz.

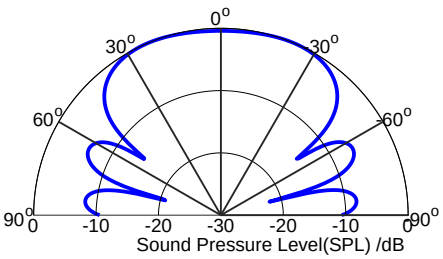

(C) Directivity at 1 kHz.

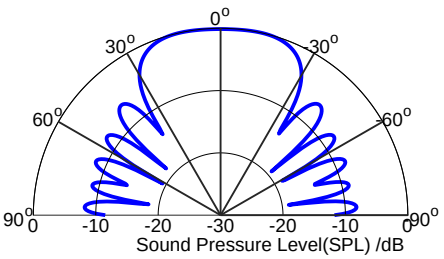

(D) Directivity at 2 kHz.

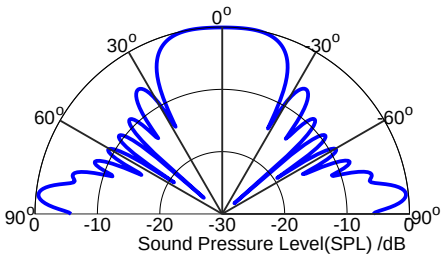

(E) Directivity at 3 kHz.

FIGURE 3.22: Directivity patterns of the endfire radiator with eight radiating holes of 6 mm radius.

of the radiator at characteristic points within the investigated range. At 300 Hz, the endfire acoustic radiator is almost omnidirectional, with a similar SPL in all directions. Right below the cut-on frequency limit observed in Fig. 3.21, at around 400 Hz, the radiation of the system is higher along the sides, which would correspond to a negative acoustic contrast value. After the cut-on frequency, the system achieves forward directivity, which can be seen in the examples for 1 kHz and 2 kHz. Within this range, the directivity increases with frequency, which translates to an increase in the achieved acoustic contrast levels. The presence of side lobes with comparable intensity to the main beam is evident in the 3 kHz example directivity plot. These side lobes reduce the overall directivity, and thus the level of acoustic contrast achieved.

Pipe Length:	No. of Holes:
0.6 m	6
0.8 m	8
1.0 m	10
1.2 m	12

TABLE 3.3: Different pipe lengths considered, and corresponding number of radiating holes, given a fixed 6 mm radius and 10 cm separation.

3.4.3 Parametric Study

A parametric study of the endfire acoustic radiator is carried out in order to understand the effect that each component of the design has on the resulting directivity, and to evaluate the proposed configuration as a whole. This involves a series of simulations performed using different values for a specific parameter. The difference in performance across the results will provide information on the contribution of the variable parameter to the beamforming performance. The parameters that will be investigated are the length of the pipe, the spacing between radiating holes and the size thereof.

The inner radius of the pipe, a_p, was chosen to be fixed at 2 cm. This is to avoid the possible onset of propagating higher modes, which, according to (Cheer et al., 2013), occur when $f > 400/a_p$. Using the value of 2 cm for a_p ensures that this frequency limit is at 5 kHz, which is the highest frequency investigated in this study. Another parameter that is kept fixed is the thickness of the pipe wall t_h, at 2 mm, which reflects a typical value for the type of PVC pipe which is expected to be used in such a device.

The directivity performance of the simulated system will be evaluated in terms of the acoustic contrast, calculated using Eq. (3.5) in conjunction with the sound pressure obtained via Eqs. (3.11) and (3.24), as well as the on-axis SPL frequency response. As the endfire acoustic radiator uses only a single source, it cannot be controlled to maximise its output in a specific bright zone using the acoustic contrast maximisation method of Sec. 3.2. The acoustic contrast is evaluated only in the forward direction, using the bright and dark zone distribution shown in Fig. 3.7a. As with the case of the loudspeaker array in Sec. 3.3, the investigated frequency range is between 100 Hz and 5 kHz, chosen to cover the requirements for EV warning sound components.

Pipe Length

The first parameter for investigation in the parametric study is the length of the pipe used by the endfire radiator. With the spacing between the radiating holes kept fixed at 10 cm, this constitutes a variation of the effective length of the source array. The lengths of pipe considered, along with the corresponding number of sound radiating holes, whose radius is fixed at 6 mm, are shown in Table 3.3.

Figure 3.23a shows the performance of the simulated configurations. Regarding the general behaviour across frequency for the endfire radiator, the acoustic contrast plot (Fig. 3.23a) shows the omnidirectional behaviour that characterises low frequencies up to the cut-on limit, where the sound field is focussed on the sides instead of forward, and causes a dip to negative values in contrast level. Beyond the cut-on frequency, the endfire radiator becomes more directional with frequency

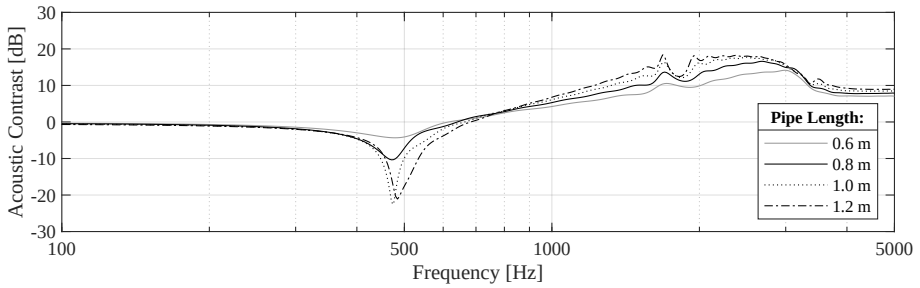

(A) Acoustic contrast frequency response.

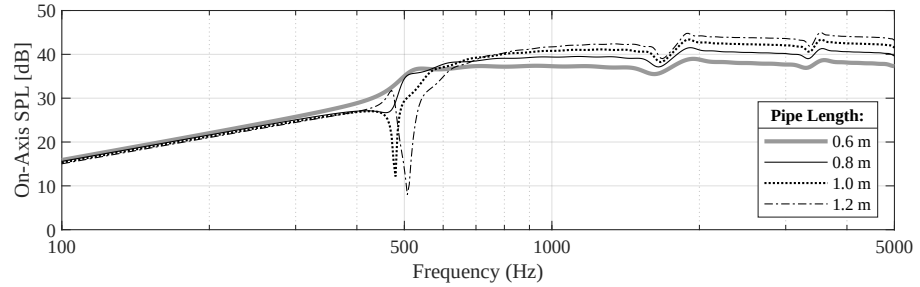

(B) On-axis SPL frequency response.

FIGURE 3.23: Acoustic contrast and on-axis SPL frequency responses for an endfire radiator of variable length, with 6 mm radius holes spaced at 10 cm.

until roughly 3 kHz, where the presence of side lobes reduce the level of acoustic contrast achieved.

The on-axis SPL response (Fig. 3.23b) the follows an initial roll on at frequencies where the system is omnidirectional, until a dip is observed at the cut-on frequency. After this, the response is mostly flat, with minor irregularities at frequencies that also correspond to shifts in the acoustic contrast. The fact that both responses display their different characteristics at the same frequencies is indicative of how the sound field generated by the endfire radiator is inherently directional.

Between the different simulated configurations, the responses are remarkably similar. Only a slight shift of the cut-on, albeit towards higher frequencies, and marginally higher contrast levels are evident to result from using a longer pipe. These results can be compared to the effects of overall array length in the case of the endfire array, investigated in Sec. 3.3. In that case, the longer arrays resulted in an improvement of the response at lower frequencies, and overall higher contrast levels. However for the endfire radiator there is very little difference in either response.

A possible explanation to this is in the increase in the number of radiating holes that corresponds to a longer pipe, given a fixed hole spacing. The amount of energy in the sound waves propagating inside the pipe decreases after part of it is radiated at each hole. Therefore, a greater number of holes means that a large portion of this initial energy is exhausted before the wave reaches the end of the pipe. This in turn means that, beyond a certain point, the effective array length does not change despite lengthening the pipe to facilitate more holes.

Considering the results above, it is worth investigating the effect of different pipe lengths that effectively dictate the length of the array of radiating sources. This can be done by keeping the number of holes fixed, instead of their separation, so that

Pipe Length:	Hole Spacing:
0.4 m	5 cm
0.8 m	10 cm
1.6 m	20 cm

TABLE 3.4: Different pipe lengths considered, and corresponding hole separation, given a fixed number of 10 radiating holes of 6 mm radius.

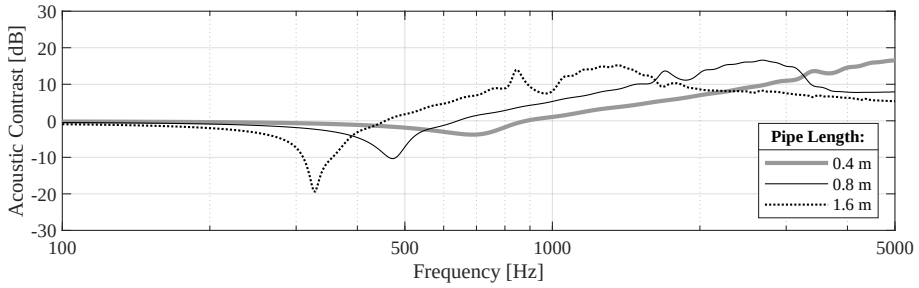

(A) Acoustic contrast frequency response.

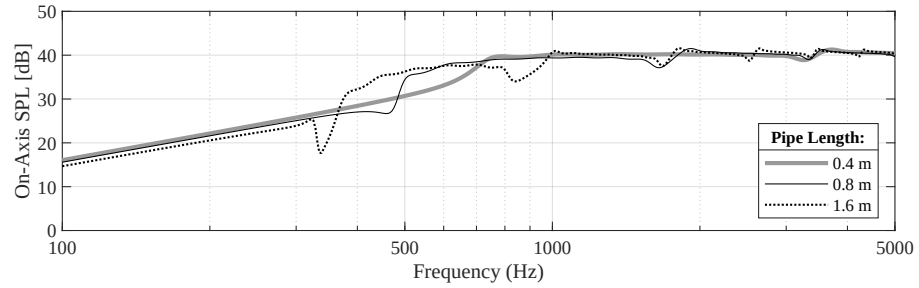

(B) On-axis SPL frequency response.

FIGURE 3.24: Acoustic contrast and on-axis SPL frequency responses for an endfire radiator of six 6 mm radius holes of variable length.

all holes are utilised as sources to the same extent across the investigated configurations.

The endfire radiator is thus simulated using different lengths of pipe and a fixed number of 10 radiating holes. The length values used, along with the corresponding hole spacings are shown in Table 3.4. Figure 3.24 presents the simulation results through the acoustic contrast and on-axis SPL frequency response. In this case, the improvement in the low frequency response due to the increase in effective array length is clearly evident, with the cut-on being shifted towards lower frequencies. This improvement, however, is accompanied by a decrease in the high frequency performance, which inevitably comes as a result of the wider spacing between the holes.

It can therefore be concluded that a longer pipe does indeed improve the low frequency limit of the endfire radiator, as long as the effective array length is likewise increased, by guaranteeing that waves travelling inside the pipe are capable of carrying the necessary amount of energy to the location of every radiating hole.

Hole Spacing:	No. of Holes:
5 cm	22
10 cm	11
20 cm	6
50 cm	3

TABLE 3.5: Different spacings between the holes of the endfire radiator considered, and the corresponding number of radiating holes, given a fixed 6 mm radius and 1 m effective array length.

Hole Spacing

By keeping the length of the pipe fixed at 1.1 m, and the hole radius at 6 mm, four configurations characterised by different spacing between the holes, and therefore a different number of holes, are simulated. It should be noted that the length of the pipe has been set considering a 5 cm interval between either end and the nearest hole, meaning that the array length in each case is 1 m. The spacing values considered, along with the corresponding number of holes in each case, are shown in Table. 3.5.

Figure 3.25 shows the performance of the simulated endfire radiators in terms of acoustic contrast and on-axis SPL. From the acoustic contrast response (Fig. 3.25a), it can be seen that a narrower spacing between the radiating holes results in improved directivity at higher frequencies and an increase in the maximum levels of contrast achieved, however it also increases the cut-on frequency. The same trend is observed in the on-axis SPL response (Fig. 3.25b), with the narrower spacing generating a higher maximum level, but shifting the response towards higher frequencies.

The improvement in the high frequency performance can be explained similarly to the case of the loudspeaker array, where a narrower spacing increases the frequency at which aliasing occurs, due to the wavelength being of comparable length to the interval between the radiating sources. In the case of the endfire radiator, however an increase in the cut-on frequency is also observed. This is due to the aforementioned fact that the energy of the sound waves propagating inside the pipe dissipates as sound is radiated from each hole. In this case, by keeping the length of the pipe fixed and decreasing the separation of holes, a larger number of holes is contained in a shorter length. Thus, the energy of the wave propagating inside the pipe dissipates quicker, and the effective length of the array decreases, as the holes that radiate sound are located within a shorter distance, which impacts upon the low frequency limit of the system.

Hole Size

Given the results of the parametric study so far, a trade-off exists between the low and high frequency limitations of the endfire radiator. A solution to the issue of energy dissipating while the sound waves propagate inside the pipe could be in adjusting the area of the radiating holes.

Figure 3.26 shows the effect of varying the hole radius while all remaining parameters are held constant. In particular, an endfire radiator of 1 m length and 20 cm separation between holes is simulated, for holes of 2.5 mm, 4 mm, 6 mm and 8 mm radius. Though the high frequency limit and maximum contrast achieved remain unaffected, the cut-on frequency is decreased when a smaller hole size is used. This result validates the assumption made in the previous parts of this study, as the

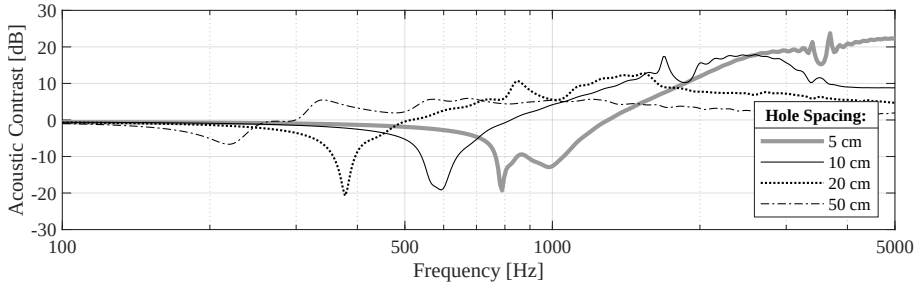

(A) Acoustic contrast frequency response.

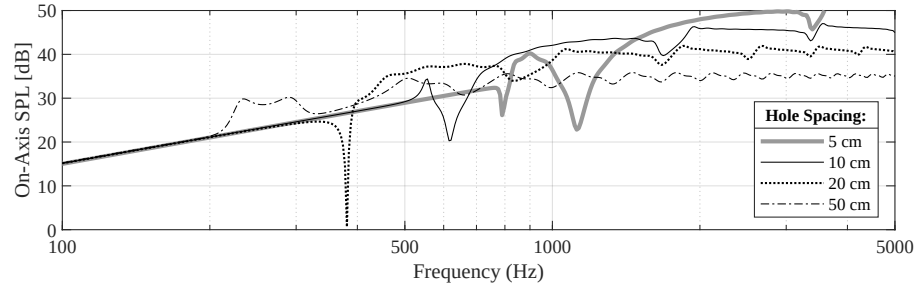

(B) On-axis SPL frequency response.

FIGURE 3.25: Acoustic contrast and on-axis SPL frequency responses for an endfire radiator with different numbers of holes.

smaller holes only allow for a limited amount of energy to be radiated as sound, therefore ensuring that the propagating wave inside the pipe maintains enough energy as it reaches the location of every hole forming the source array.

However, the smaller hole size comes with an anticipated drawback. As visible form the on-axis SPL response (Fig.3.26b), the smaller holes radiate less sound, and result in a decrease in the SPL generated, which might ultimately render the endfire radiator ineffective.

Conclusions

The parametric study of the endfire radiator has shown that, while such a system is simple and cost effective relative to a loudspeaker array, its performance is noticeably limited in comparison. The directivity of the endfire radiator is especially frequency specific, which imposes narrow limitations on the bandwidth available for a warning sound. Although the parameters of the system can be optimised to ensure an increased operational bandwidth, compromises in its performance in terms of actual sound output levels must be made. In addition, such a system cannot offer any form of control over its radiated sound field, and would need to be steered mechanically if selective beamforming were to be achieved.

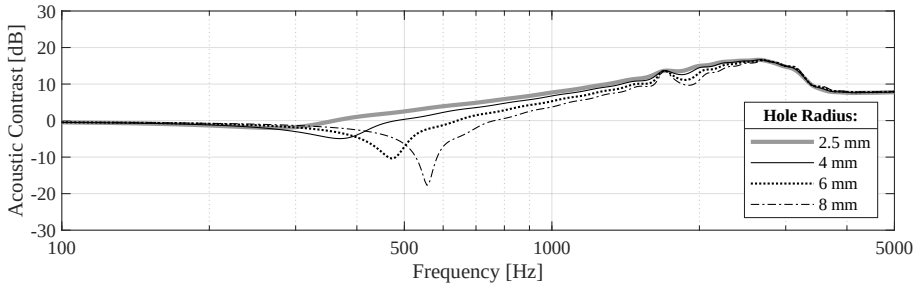

(A) Acoustic contrast frequency response.

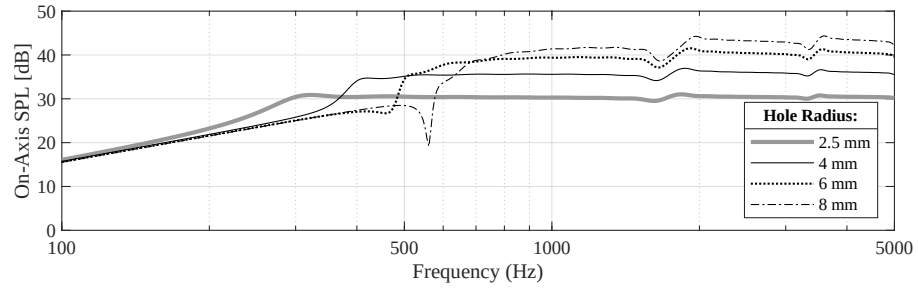

(B) On-axis SPL frequency response.

FIGURE 3.26: Acoustic contrast and on-axis SPL frequency responses for an endfire radiator of eight holes of variable radius.

3.5 Summary

This chapter has presented the concept of directivity as a characteristic of a sound system, providing a brief overview of methods that are used, or have been proposed for implementation as directional EV warning sound systems. In order to have a means of quantifying and comparing the directivity of a sound field, the acoustic contrast was defined. The acoustic contrast maximisation method was also presented as a process for controlling the directivity of a system characterised by multiple sound sources.

Focus was initially given to the loudspeaker array as the most straightforward directional sound system. A simulation-based parametric study was performed to obtain insights into its performance. The broadside loudspeaker array was able to generate and control a directional and steerable sound field. Longer arrays were shown to improve low frequency performance, and a narrow source separation was found to be necessary in order to achieve control at higher frequencies and increase the aliasing limit. Given these two factors, a significant number of loudspeakers are needed to ensure high directivity across a large bandwidth. However, practical issues such as the relatively high cost, weight, and sensitivity to environmental factors keep the loudspeaker array from being a generally viable solution for an EV warning sound system.

The concept of the low-cost endfire acoustic radiator was presented as a potential directional system that uses relatively few and simple components. An analytical model was formulated based on the literature, and the system was evaluated through a series of simulations. Despite its low manufacturing costs and mechanical robustness, results show that it ultimately struggles to cover a bandwidth suitable for the frequency content required for warning sounds, and is incapable of selective beamforming unless the entire system is physically moved.

Under consideration of the results from the studies presented in this chapter, the aim of a prospective directional warning sound system would be to match the performance of the broadside loudspeaker array, while improving upon the aspects of durability and physical robustness. In addition, it is important that the manufacturing and maintenance costs remain low, so as to present a practical and realisable solution for mass production and implementation. The solution to such a problem could be in the use of alternative means of sound generation, instead of loudspeaker drivers. The following chapters (Ch. 4, Ch. 5 and Ch. 6) will therefore be devoted to the conceptualisation and development of such a lower-cost, increased robustness, directional warning sound system.

Chapter 4

Structural Actuator Array: A Mathematical Model

In this chapter, the structural actuator array is introduced as a potential alternative to the loudspeaker array for implementation in a directional warning sound system, and an mathematical model for its theoretical investigation is presented. Section 4.1 provides an introduction to the concept, its principle of operation and the grounds on which it is being suggested as a viable alternative. Section 4.2 presents the formulation, through existing work on structural vibration and the radiation of sound, of an analytical model linking the effects of a distribution of forces upon a flat panel to the resulting sound pressure in the far field. This model can be used to perform a series of simulations, to investigate the theoretical capabilities of the proposed directional system, and determine the effect of its physical characteristics on its performance. A simulations-based parametric study of the structural actuator array is in turn conducted for this purpose, and is presented in Sec. 4.3. Parts of this chapter have been published as "A system for controlling the directivity of sound radiated from a structure" in the Journal of the Acoustical Society of America (Kournoutos and Cheer, 2019).

4.1 Principle of the Structural Actuator Array

In the investigation of directional systems presented in the previous chapter, it was shown that although the low-cost endfire acoustic radiator can be constructed for a fraction of the cost of a loudspeaker array, its performance severely lacks in both operational bandwidth and the ability to adapt the steering angle of the directional sound field. Moreover, as pointed out in Sec. 2.5.3 and Sec. 3.3, the implementation of such a solution in a vehicle raises the issue of finding suitable space to accommodate the radiator itself, requiring a placement that will allow the efficient radiation of the sound field, prevent the blocking of the radiating holes by dirt, water or debris and at the same time have a minimal impact on the overall design of the vehicle. Therefore, there remains a need for a practical alternative to the loudspeaker systems that is able to match the directivity performance of a loudspeaker array at comparable bandwidths, including beamforming control, but offer a reduced implementation cost and be more straightforward to implement in commercial vehicles.

Instead of using loudspeaker drivers, which may be too heavy, costly or fragile for the intended implementation, a sound radiating system can be designed around the vibration of a panel by introducing a controlled distribution of forces to the structure. A directional system based on such a structurally driven radiating surface could prove useful in applications where the exposure to specific environmental conditions could prove damaging to the loudspeaker drivers, or interventions to

the structure in order to install a conventional loudspeaker array would be cost inefficient. Dynamic force actuators are transducers that can be attached to a panel in order excite its structural response, which in turn generates acoustic radiation.

Also known as audio exciters or shakers, such transducers are widely available and affordable, which has rendered them popular for use in make-shift home audio systems(Meinke, 2016; Dayton Audio, 2019). These Distributed Mode Loudspeakers (DMLs), these have been shown to be capable of omnidirectional acoustic radiation over a greater bandwidth when compared to conventional loudspeakers using a cone to achieve acoustic radiation (Angus, 1999; Gontcharov and Hill, 2000), but with a reduced low frequency response (Newell and Holland, 2006). It has also been shown that this performance can be improved by using multiple optimally driven actuators on the panel (Anderson and Bocko, 2016). In addition, using a vibrating panel to radiate a directional sound field could increase the high frequency limit that occurs due to aliasing, which is associated with the discrete nature of a loudspeaker array and imposes a high frequency limit on the system (Rabenstein and Spors, 2006). By interpolating sound pressure between the locations of the actuators, a vibrating panel may potentially reduce these aliasing effects, although the radiated sound field is also likely to be affected by the modal vibration behaviour of the panel.

The field of active noise and vibration control has encompassed a significant amount of research on the subject of controlling the sound fields radiated through structural vibration. Utilising either piezoceramic (Fuller et al., 1991b) or inertial actuators (Paulitsch et al., 2006), studies have investigated the extent of control over radiation in the far field (Fuller et al., 1991a; Pan et al., 1992) and its directivity (Li and Thompson, 2019) that can be achieved by such means, with the intent of minimising the sound generated. When it comes to generating a localised sound field, the utilisation of structural vibration has been investigated for actuator distributions on OLED displays, such as flat screens on televisions and smart phones(Heilemann et al., 2017, 2019; Lee et al., 2020). It was shown that the screen itself can be used as the acoustic radiator, making it possible to focus the sound on the user, and offering a compact design without the necessity of additional room for speakers.

The system proposed in this chapter utilises an array of inertial actuators attached to a flat panel in order to radiate a sound field. The directivity of this field can be controlled through the manipulation of the relative phase and amplitude between the actuators. The choice of a flat panel as the vibrating structure is due to it being relatively straightforward to investigate and interpret the limits on performance. However, it should be stressed that the intention, and the focus of subsequent chapters, is the incorporation of the actuator array into an existing structure of the vehicle. As an initial stage of the investigation, a simulation-based parametric study will be conducted using an analytical mathematical model to provide an insight into the behaviour and capabilities of a simple system consisting of an actuator array attached to a flat, rectangular panel. Results of this study should indicate if there is potential in the proposed system to proceed with a physical experimental implementation.

4.2 Mathematical Model

Vibrating structures generate acoustic radiation by imposing fluctuations on the pressure field. These fluctuations depend on both the response of the structure and

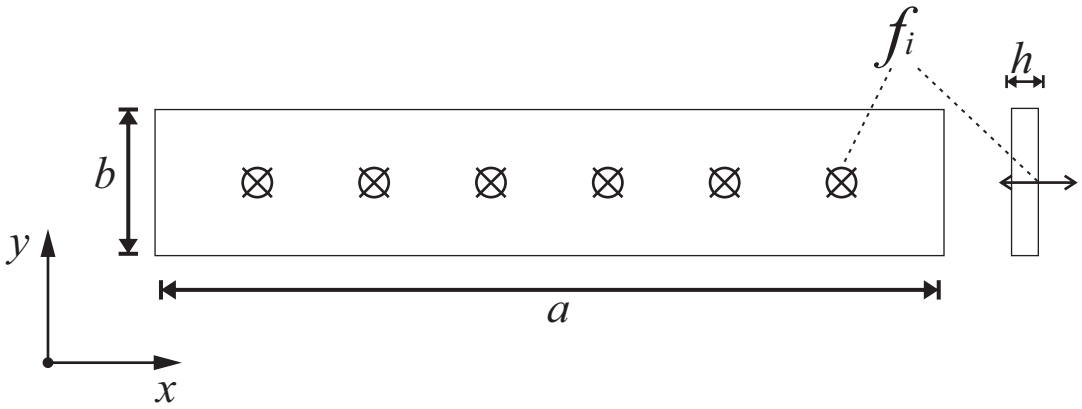

FIGURE 4.1: Schematic for the mathematical model of the structural actuator array. A rectangular plate of thickness h is excited by a number of individual point forces f_i perpendicular to the plane defined by the length a and width b of the plate.

on how the structure is excited. For example, a plate radiates differently depending on its construction, but also on the excitation force. Therefore, by controlling the vibration of a structure, it is possible to control how it radiates and this can be achieved using multiple inertial actuators mounted to the structure. In this section, models and equations from existing research on the forced vibration of plates, and the estimation of radiated pressure in the far field resulting from structural vibration, will be utilised to formulate an analytical model that can fully describe the proposed system and its function.

The proposed system can be approximated by a thin rectangular panel, simply supported along all four of its edges, with a distribution of points along its surface at which a transverse force, f_i, is applied. Figure 4.1 shows a schematic of this simplified system with six point forces distributed along the length of a panel with dimensions $a \times b \times h$. The model that will be used to estimate the pressure at locations in the far field due to the vibrating panel can be divided into two principal parts: the vibration of the panel by a force distribution, and the far field sound radiation that results from this vibration.

Vibration of a Simply Supported Thin Plate Excited by Point Forces

This first section of the mathematical model regards the structural vibration of the panel. What is sought after is an expression for the vibration of the panel in relation with the forces that are applied to its surface. The motion of a thin rectangular panel can be expressed in terms of its transverse displacement, w, as (Cremer and Heckl, 1988)

$$EI_M \left(\frac{\partial^4 w}{\partial x^4} + 2\frac{\partial^4 w}{\partial x^2 \partial y^2} + \frac{\partial^4 w}{\partial y^4} \right) + \rho h \frac{\partial^2 w}{\partial t^2} = -f(x, y, t), \tag{4.1}$$

where E is the Young's modulus, I_M is the moment of inertia, ρ is the density, x and y are the coordinate directions, t is the time, and $f(x, y, t)$ corresponds to the applied forcing function, which is zero in the case of free motion. The quantity EI_M is equivalent to the bending stiffness of the panel, and it is convenient to express this using the Poisson ratio of the panel material, ν, which gives

$$EI_M = \frac{h^3 E}{12(1 - \nu^2)}. \tag{4.2}$$

It is important to stress that for Eq.(4.1), the wavelength of vibration is assumed to be much greater than the thickness of the panel and no transverse shear or rotary inertia are taken into account. These approximations limit the accuracy of this mathematical model at high frequencies (Cremer and Heckl, 1988), which will be discussed further in Section 4.3.

A continuous system, such as the one formulated above and described by Eq. (4.1), can be approximated as a multiple degree of freedom system, as shown by Meirovitch (Meirovitch, 1967). A separable solution of the transverse modal displacement can be chosen for the free motion of a simply supported panel as

$$w_{mn}(x,y,t) = W_{mn}\sin(k_m x)\sin(k_n y)\mathrm{e}^{\mathrm{j}\omega t}, \tag{4.3}$$

where m and n are the modal indices for modes along the x and y axes respectively, and W_{mn} is the corresponding modal amplitude. The mode shapes of a panel have been thoroughly studied, and are dependent on its boundary conditions (Warburton, 1954). For simply supported boundaries of zero transverse displacement along the edges, the wavenumbers in each coordinate direction are

$$k_m = m\pi/a, \quad m = 1,2,3,... \tag{4.4a}$$

$$k_n = n\pi/b, \quad n = 1,2,3,... \tag{4.4b}$$

and the discrete frequencies at which the system resonates are given by

$$\omega_{mn} = \left(\frac{EI}{\rho h}\right)^{1/2}\left[k_m^2 + k_n^2\right]. \tag{4.5}$$

In order to represent the effects of an inertial actuator acting upon the panel, it is necessary to describe the response of the system to a harmonic force. This means that the right-hand side term in Eq. (4.1) becomes a two-dimensional forcing function $f(x,y)e^{\mathrm{j}\omega t}$. The forced response can then be written as a summation over the modes of the free response of the panel, vibrating at the forcing frequency, such that

$$w_{mn}(x,y,t) = \sum_{m=1}^{\infty}\sum_{n=1}^{\infty} W_{mn}\sin(k_m x)\sin(k_n y)\mathrm{e}^{\mathrm{j}\omega t}. \tag{4.6}$$

The most straightforward type of input is a point force input, expressed as $f_i(x,y,t) = F_i\delta(x-x_i)\delta(y-y_i)\mathrm{e}^{\mathrm{j}\omega t}$ and located at x_i, y_i. Under such conditions, the modal amplitudes are given by

$$W_{mn}(i) = \frac{4F_i \sin k_m x_i \sin k_n y_i}{M(\omega^2 - \omega_{mn}^2)}, \tag{4.7}$$

where $M = \rho hab$ is the total mass of the panel. This is the expression for the modal amplitudes from a point force offered by (Fuller et al., 1996). It is thus a straightforward task to find an expression for the modal amplitudes given a distribution of I point forces acting upon the panel, by performing a summation of the form

$$\sum_{i=1}^{I} W_{mn}(i) = \frac{4}{M(\omega^2 - \omega_{mn}^2)}\sum_{i=1}^{I} F_i \sin k_m x_i \sin k_n y_i. \tag{4.8}$$

Considering the above equation along with Eq. (4.6), the response of the panel excited by a distribution of I point forces, at a point on its surface can be given by

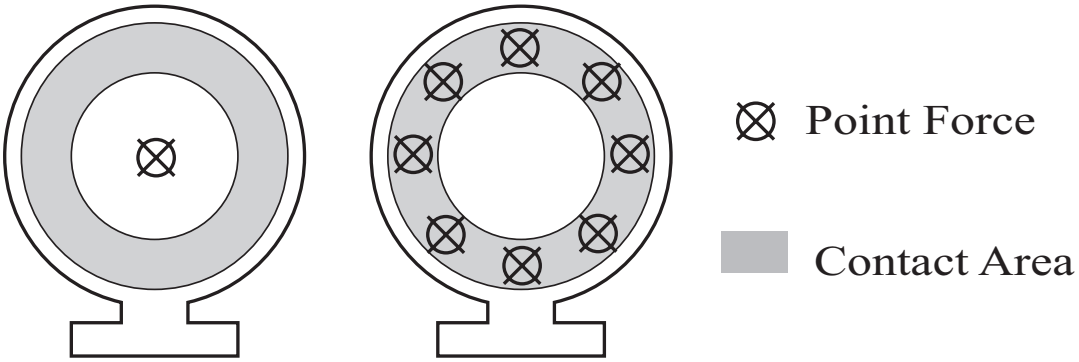

FIGURE 4.2: Approximation of an example actuator using either a single point force or a distribution of point forces acting over its contact area. The simulations presented in this chapter consider a circular contact area of 15 mm radius.

performing a triple summation over the number of modes along the x and y directions, and the number of forces, as

$$w_{mni}(x,y,t) = \sum_{i=1}^{I} \sum_{m=1}^{\infty} \sum_{n=1}^{\infty} W_{mn}(i) \sin(k_m x) \sin(k_n y) e^{j\omega t}. \tag{4.9}$$

Equation (4.9) presents an expression for the effect of a point force distribution on the transverse displacement of the panel. This solution is generally well suited to determine the global system response. However, it is not well suited to predict structural near-field effects at higher frequencies. To ensure accuracy at higher frequencies, a relatively high number of modes is necessary to approximate the sum in Eq. (4.6) when it is truncated in the calculation of the structural response (Fuller et al., 1996). To confirm that a sufficient number of modes have been included in the model in order to cover the frequency range of interest, a convergence study is necessary, and will be considered for the simulations presented in Sec. 4.3.

The effect of each inertial actuator on the thin panel can be approximated by a single point force acting at its respective location. However, as practical actuators have a finite area of contact with the panel, using a number of point forces distributed over this contact area, acting in phase and with the same amplitude would help in obtaining a more accurate model with little increase in its complexity. Figure 4.2 shows the approximation that will be used in the subsequent simulations, consisting of eight point forces distributed in a circle with a 15 mm radius, which represents the contact area of each actuator. A factor that has not been included in the model is the mass of the actuators, which may have an effect on the response of the panel due to mass loading. A more detailed model, which represents the actuators as mass-spring-damper systems has been explored in (Anderson et al., 2017). However, the effect of the added mass on the panel will not be considered further in the present model, and it is shown through the experimental results presented in Sec. 5.3 that this does not have a significant impact on its accuracy.

Sound Radiation

The second part of the mathematical model regards the radiation of sound generated by the vibrating panel to a point in the far field. For a flat vibrating surface that is part of an infinite, rigid baffle, such as the case of the system in this physical model, the acoustic pressure in the far field can be approximated using the Rayleigh integral.

This pressure, in terms of the complex transverse velocities $\dot{w}(\boldsymbol{r}_S)$ at points $\boldsymbol{r}_S$ on the surface S, is calculated at distance r from the centre of the panel as

$$p(\boldsymbol{r}) = \int_S \frac{\mathrm{j}\omega\rho_0 \dot{w}(\boldsymbol{r}_s)\mathrm{e}^{-\mathrm{j}kR}}{2\pi R}\mathrm{d}S, \tag{4.10}$$

where $R = |\boldsymbol{r} - \boldsymbol{r}_s|$, and the frequency dependence has been dropped for notational convenience. This formulation assumes that the panel is mounted in an infinite baffle. The complex velocity $\dot{w}(\boldsymbol{r}_S)$ derived from Eqs. (4.6) and (4.8) is

$$\dot{w}(\boldsymbol{r}_S) = \dot{W}_{mn} \sin\left(\frac{m\pi x}{a}\right) \sin\left(\frac{n\pi y}{b}\right) \qquad \left\{\substack{0\le x\le a \\ 0\le y\le b}\right\}. \tag{4.11}$$

The total acoustic pressure radiated from the panel due to vibration at its (m,n)-th mode at a point described by the coordinates (r,θ,ϕ) in the far field, is expressed upon evaluation of the integral in Eq. (4.10) using the transverse modal displacement of Eq. (4.6) as

$$p_{m,n}(r,\theta,\phi) = \frac{\mathrm{j}\omega\rho_0\dot{W}_{mn}\mathrm{e}^{-\mathrm{j}kr}}{2\pi r}\cdots \\ \cdots\int_0^b\int_0^a \sin\left(\frac{m\pi x}{a}\right)\sin\left(\frac{n\pi y}{b}\right)\mathrm{e}^{\mathrm{j}(\alpha x/a+\beta y/b)}\mathrm{d}x\,\mathrm{d}y, \tag{4.12}$$

where $\alpha = ka\sin\theta\cos\phi$ and $\beta = kb\sin\theta\sin\phi$. The above integral can be evaluated as in (Wallace, 1972), which yields the pressure due to the (m,n)-th mode as

$$p_{m,n}(r,\theta,\phi) = \frac{\mathrm{j}\omega\rho_0\dot{W}_{mn}\mathrm{e}^{-\mathrm{j}kr}}{2\pi r}\frac{ab}{mn\pi^2}\cdots \\ \cdots\left[\frac{(-1)^m\mathrm{e}^{-\mathrm{j}\alpha}-1}{(\alpha/m\pi)^2-1}\right]\left[\frac{(-1)^n\mathrm{e}^{-\mathrm{j}\beta}-1}{(\beta/n\pi)^2-1}\right]. \tag{4.13}$$

Taking into consideration a number of I point forces acting at coordinates (x_i,y_i), and M and N modes along the x and y directions, respectively, the above equation can be used in conjunction with Eq. (4.8) to calculate the pressure radiated from the panel due to the actuator array, provided a sufficient number of modes is used. This pressure is expressed as a triple summation of the form

$$p(r,\theta,\phi) = \sum_{i=1}^{I}\sum_{m=1}^{M}\sum_{n=1}^{N}\frac{\mathrm{j}\omega\rho_0\mathrm{e}^{-\mathrm{j}kr}}{2\pi r}\frac{ab}{mn\pi^2}\cdots \\ \cdots\left[\frac{(-1)^m\mathrm{e}^{-\mathrm{j}\alpha}-1}{(\alpha/m\pi)^2-1}\right]\left[\frac{(-1)^n\mathrm{e}^{-\mathrm{j}\beta}-1}{(\beta/n\pi)^2-1}\right]\dot{W}_{mn}(i). \tag{4.14}$$

In Eq.(4.14), a relation has been obtained linking the sound pressure obtained in a point of the far field to a distribution of forces on the surface of the panel. It is important to finally note that the mathematical model presented in this section assumes that the vibrating panel is set within an infinite baffle. As this configuration would not present a practical realization of the proposed array system, the simulations and measurements will only consider radiation in the forward half-space.

Critical Frequency

An important characteristic of the structural response when it comes to sound radiation is the critical frequency of the panel. This is the frequency at which the structural wavelength equals the acoustic wavelength in the surrounding medium, and in the case of a thin panel is calculated as (Cremer et al., 2007)

$$f_c = \frac{c^2}{1.8h}\sqrt{\frac{\rho}{E}}, \tag{4.15}$$

which, given that the surrounding medium is air, makes it dependent on the panel material, and its thickness, h. In practice, the critical frequency represents a limit above which the resonant modes of the plane are the predominant source of sound radiation to the far field (Norton and Karczub, 2003). The sound field that is generated by the controlled vibration of the panel through the distribution of forces on its surface is due to the near field vibration that occurs close to the positions where the forces are applied. Below the critical frequency, this vibration and the resulting interference effects on the surface of the panel are the primary factor in determining radiation efficiency (Fuller et al., 1996). It is therefore important for the system that the critical frequency of the panel lies beyond the frequency range within which directivity control needs to be achieved.

4.3 Parametric Study

In order to obtain insights into how each individual parameter affects the performance of the system, and perform a preliminary evaluation and optimisation of the structural actuator array prior to any physical testing, it is important to conduct a parametric study. The mathematical model that has been formulated in Sec. 4.2 can be used to simulate the radiated sound field of the actuator array and vibrating panel system. By varying a single design parameter while keeping all others constant at a time, this section will present a simulation based study into the effect parameters such as the panel dimensions and the actuator array distribution have on the directivity performance of the system. The performance for each case will be evaluated in terms of the acoustic contrast and on-axis SPL frequency responses, for a forward aimed and a steered directivity setting.

General Simulation Parameters

Table 4.1 contains the values for the parameters that are common between all of the simulations to be presented in this section. The panel is defined as a rectangular plate made of aluminium, a material that has been used by vehicle manufacturers, is relatively robust and lightweight. A frequency range from 100 Hz to 5 kHz has been chosen, as to be consistent with the current regulations, and is thus enough to cover the harmonic components of EV warning sounds in use and in development. All simulations consider 50 modes along the x-direction and 30 modes along the y-direction, giving a total of 1500 modes in the structural model of the panel. This number has been chosen after a convergence study so as to ensure an accurate approximation of the theoretically infinite summations in Eq. (4.6), and therefore an accurate representation of the structural response within the frequency range investigated in this study.

Air density ρ_0	1.225 kg/m^3
Speed of sound in air c_0	340.27 m/s
Panel density ρ	2700 kg/m^3
Young's modulus E	70 GPa
Poisson ratio ν	0.334
Damping η_s	0.04
Frequency range	100 Hz - 5 kHz
No. of modes considered (x-direction)	50
No. of modes considered (y-direction)	30
No. of pressure measurement points	180
Distance from centre of panel r	2.8 m
Bright zone angle coverage θ_B	36^o
Regularisation factor λ_2	10^{-6}

TABLE 4.1: Basic parameters set for the simulation of the structural actuator array.

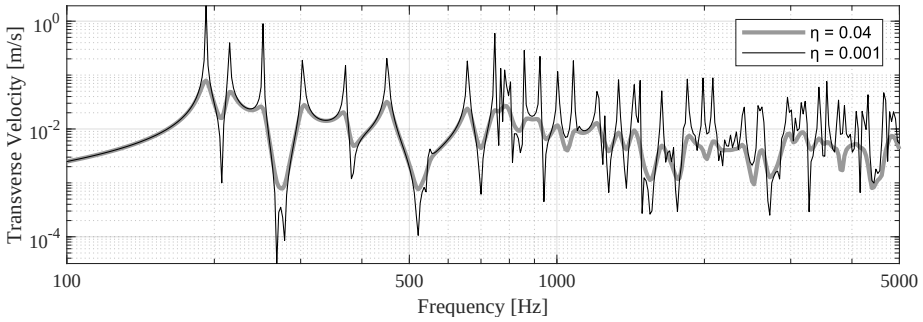

FIGURE 4.3: Frequency response function of a simply supported rectangular plate of dimensions 1 m×0.2 m×3 mm, cases for hysteretic damping values of $\eta_s = 0.04$ and $\eta_s = 0.001$. The material chosen for the plate is aluminium, the properties of which are displayed in Table 4.1.

To represent a more practical configuration, a hysteretic damping, $\eta_s = 0.04$, has been selected to limit the magnitude of peaks in the structural response at frequencies corresponding to the modes of the plate. Together with the modulus of elasticity this is expressed as

$$E' = (1 - j\eta_s)E. \tag{4.16}$$

Figure 4.3 shows the simulated frequency response of a 1 m×0.2 m×3 mm panel between 100 Hz and 5 kHz, for different values of hysteretic damping. The peaks that are visible correspond to the normal modes of the panel and it is clear that a higher damping serves to reduce the intensity of these peaks.

Another characteristic of the vibration of the panel which might provide insight into its behaviour is the distribution of velocity on its surface, when excited by external contact forces. Figure 4.4 shows the normalised velocity along the x-axis of the panel, excited by a pair of point forces, whose position on the x-axis is marked with an X symbol, at 300 Hz and 3 kHz. The near field vibration effects on the panel resulting from the actuator array are evident in both frequencies shown in this example. The vibration of the plate near the location of the sources and the resulting interference effects on its surface are the primary cause of sound radiation below the

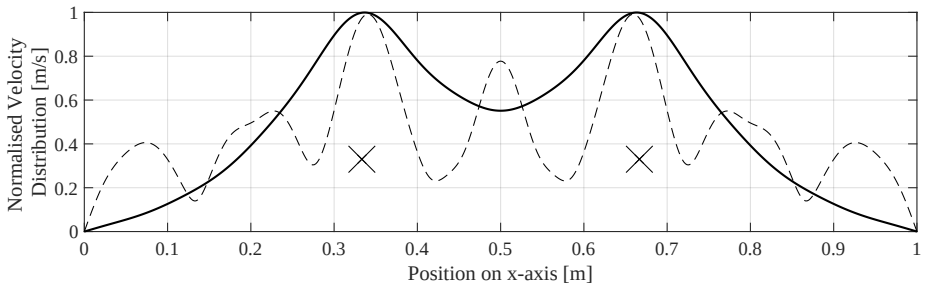

FIGURE 4.4: Normalised velocity distribution at 300 Hz (continuous line) and 3 kHz (dashed line) along the x-axis of a simply supported rectangular plate of dimensions 1 m×0.2 m×3 mm, excited by a pair of point forces, marked by X.

critical frequency. Modal vibration is observable in the higher frequency example. Below the critical frequency, f_c, sound generated from modal vibration like this is limited to the radiated near-field; for frequencies above f_c, modal vibration like this becomes highly efficient in sound radiation.

The far field sound pressure on the horizontal plane is measured at single degree increments on a 2.8 m radius half-circle in the designated forward half-space, centred around the array, making for a total of 180 measurement points. The distance from the centre of the array was chosen under consideration of the available space in the anechoic chamber which will be used for the experimental validation presented in Chapter 5. The control zone layout used in the simulations for the loudspeaker array and the low-cost endfire acoustic radiator in Secs. 3.3 and 3.4 is also used in this study as well, and the acoustic contrast control zones used in this study are shown in Figs. 3.7a and 3.7b. For all steering angle settings, the bright zone corresponds to a 36° arc, which is defined by 37 measurement points, with the remaining 143 measurement points comprising the dark zone. The regularisation factor, λ_2, used in Eq. (3.10) during the acoustic contrast maximisation process, must be assigned a high enough value in order to avoid the use of ill-conditioned matrices in the calculations. The chosen value for λ_2 is 10^{-6}, which is the lowest value ensuring robustness of the model under all of the conditions considered in the simulations presented in this chapter.

An example of the simulated SPL frequency response as a function of the observation angle in the forward half-plane is shown in Figure 4.5. The SPL values have been normalised to the maximum for clarity. The simulated array consists of eight actuators attached to a rectangular panel of dimensions 1 m×0.2 m×3 mm, with the rest of the parameters detailed in Table 4.1. The system is optimised using the acoustic contrast method described in Sec. 3.2, for bright zones in the forward direction, and steered by 45°. From these results it can be seen that the directivity is greatly dependent on frequency, with evidence for both a low and high frequency limit. To understand how each parameter of the structural array affects this behaviour, and to thus be able to optimise its performance, a study on the effect of the number of actuators, the actuator distribution, and the dimensions of the panel will be presented in the following sections.

4.3.1 Effects of Actuator Array Parameters

Given that each actuator is approximated by the 8-point force distribution shown in Fig.4.2, the main aspects that characterise a simulated array are the number of

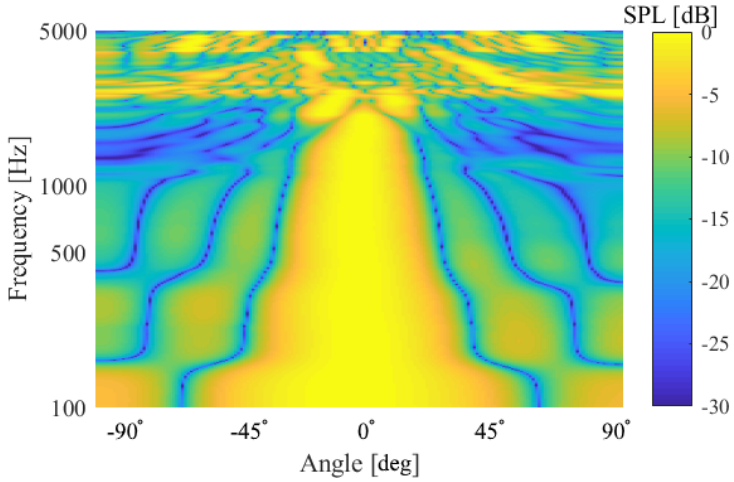

(A) Optimised for a forward bright zone.

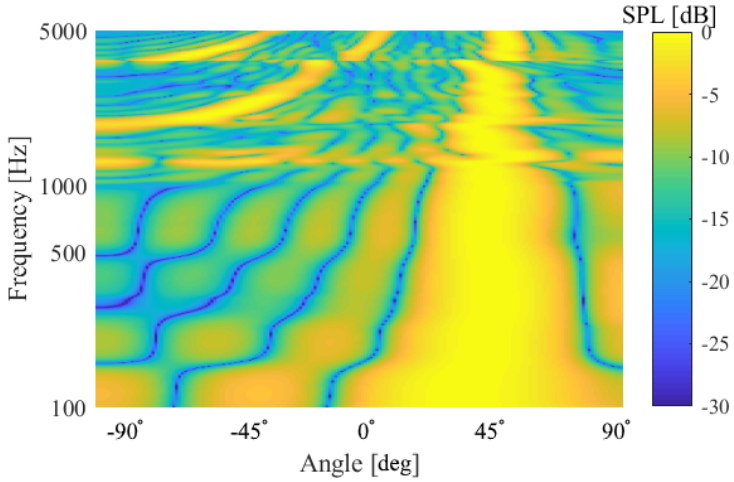

(B) Optimised for a bright zone steered by 45°.

FIGURE 4.5: Normalised SPL frequency response as a function of the observation angle for a structural array of eight actuators using a 1 m×0.2 m×3 mm panel.

actuators utilised and their distribution on the panel. This part of the parametric study considers a fixed panel size of dimensions 1 m×0.2 m×3 mm in addition to the parameter values defined in Table 4.1, and investigates the resulting sound field for different actuator distributions.

Prior to any in-depth analysis, it is useful to have a view of the resulting directivity and how it translates to a corresponding value of acoustic contrast. Figure 4.6 shows the directivity in terms of the normalised SPL at 100 Hz and 500 Hz, from a panel driven by a single actuator and an array of four actuators, evenly distributed along the panel. In the case of the single actuator the directivity is the natural directivity of the panel, whereas the four actuator array has been optimised to radiate in the forward direction, using the bright zone defined above. At 100 Hz, the panel displays an omnidirectional behaviour, which would correspond to an acoustic contrast of 0 dB. At 500 Hz, the natural directivity of the panel is along its sides on the defined x-axis of Fig. 4.1, and the resulting SPL is lower in level in the forward direction. This would correspond to a negative value of acoustic contrast. The four actuator array can be optimised to overcome the natural directivity of the panel,

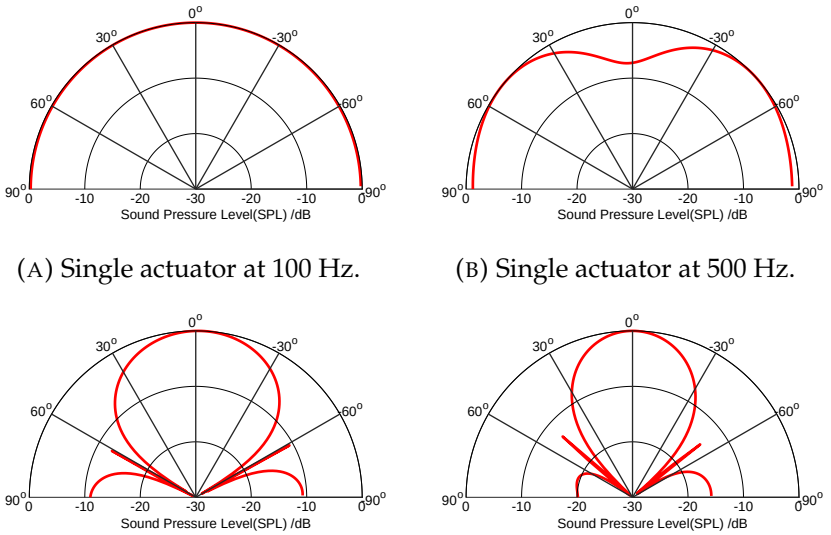

(A) Single actuator at 100 Hz.

(B) Single actuator at 500 Hz.

(C) Four actuators at 100 Hz.

(D) Four actuators at 500 Hz.

FIGURE 4.6: Directivity patterns at 100 Hz and 500 Hz from a 1 m×0.2 m×3 mm, excited by a single actuator and a four actuator array.

producing higher SPL in the designated bright zone compared to the dark zone. Comparing the patterns of the array at the two frequencies, the 500 Hz example displays higher directivity, which suggest that the level of acoustic contrast at 500 Hz is higher than at 100 Hz.

A first look into the effect of actuator number and distribution is shown in Fig. 4.7. The level of acoustic contrast, frequency averaged between 100 Hz and 5 kHz, is shown as a function of the spacing between the actuators in the array, for simulated arrays utilising different numbers of actuators. All simulated arrays display a uniform distribution of the actuators centred on the panel. It is evident that the overall directivity that can be achieved is higher when increasing the number of actuators in the array. At least four actuators are required to achieve a level of acoustic contrast above 10 dB. The increase in actuator spacing appears to affect the directivity performance, though at this first reading no general trend is clear. In order to obtain a more in-depth view of these effects, it is important to look into the directivity performance across frequency.

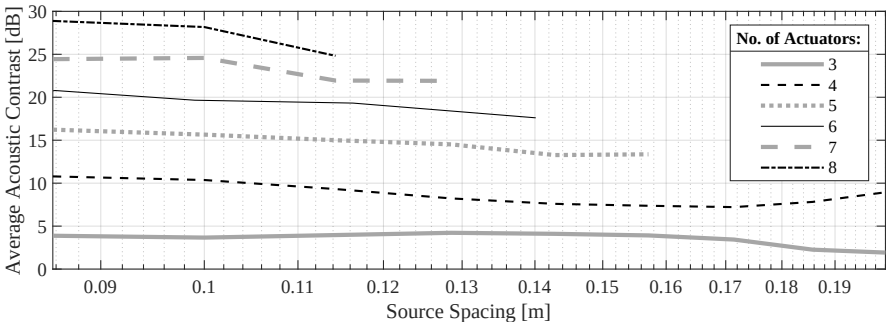

FIGURE 4.7: Frequency averaged acoustic contrast resulting from different numbers of actuators in the array, as a function of the spacing between actuators. The values concern simulated arrays optimised to radiate in the forward direction.

No. of Actuators	Forward bright zone		45° steered bright zone	
4	7.6 dB	±5.1 dB	7.4 dB	±2.2 dB
5	13.3 dB	±7.7 dB	9.9 dB	±2.8 dB
6	17.6 dB	±10.9 dB	13.9 dB	±5.0 dB

TABLE 4.2: Frequency averaged acoustic contrast and standard deviation between 100 Hz and 5 kHz, for arrays using different numbers of actuators.

Number of Actuators

The performance of structural actuator arrays using different numbers of actuators, in terms of acoustic contrast and on-axis SPL as a function of frequency, is shown in Fig 4.8. The simulated arrays consist of four, five and six actuators with a 14 cm spacing, which corresponds to an array length of 42 cm, 56 cm and 70 cm respectively. Figure 4.8a shows the acoustic contrast across frequency at the forward directed setting. It is evident that an overall improvement in contrast is achieved as the actuator number increases. Between the four and five actuator configurations, a notable increase in contrast is observed within the 200 Hz to 2 kHz range. Comparing the five and six actuator cases, the increase in contrast achieved is contained within the 700 Hz to 2 kHz range. The low frequency limit is only improved between the four and five actuator configuration, and a performance cut-off at 2 kHz persists for all three investigated cases. Despite the low frequency limitation in terms of directivity, the on-axis SPL response, shown in Fig. 4.8b, shows that the four actuator array can produce a higher SPL in the 140 Hz to 300 Hz range. However, no clear trend is discernible in terms of on-axis SPL.

The acoustic contrast response of the same three configurations at a steered setting is shown in Fig. 4.8c, where the arrays have been optimised using a bright zone steered by 45°. An overall improvement is observed as a greater number of actuators is used, particularly within the 200 Hz to 1.5 kHz range. The low frequency limit is again only improved between the four and five actuator cases. However, at this setting, no cut-off in directivity is evident within the investigated range. The on-axis SPL response for the steered setting (Fig. 4.8d) is generally similar between the configurations, only with the four actuator array producing a higher SPL at frequencies between 200 Hz and 400 Hz. The effects of anti-resonances appear more significant when more actuators are used, with greater drops in SPL at specific frequencies.

The frequency averaged acoustic contrast and its standard deviation calculated between 100 Hz and 5 kHz for this study are displayed in Table 4.2. It is clear that a greater number of actuators is capable of higher directivity in both directivity settings. The average acoustic contrast is lower at the steered setting, as the orientation is shifted from the natural directivity of the panel and the array, and the effective aperture size defined by the vibrating panel is reduced. The increase in the standard deviation is due to the 2 kHz cut-off in acoustic contrast existing for all three cases, regardless of the levels achieved at lower frequencies. This means that an array with more actuators is characterised by a greater variation in maximum possible contrast depending on frequency.

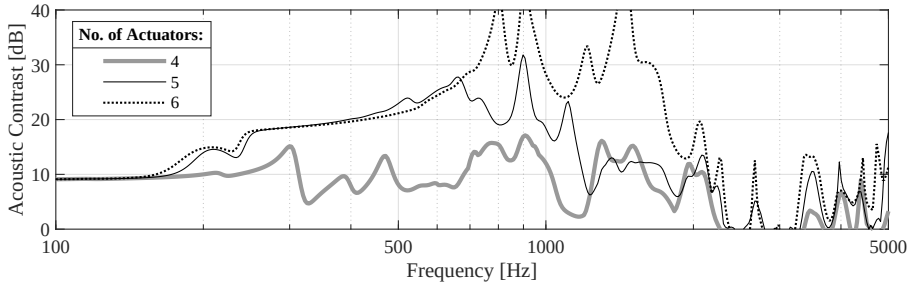

(A) Acoustic contrast at the forward setting.

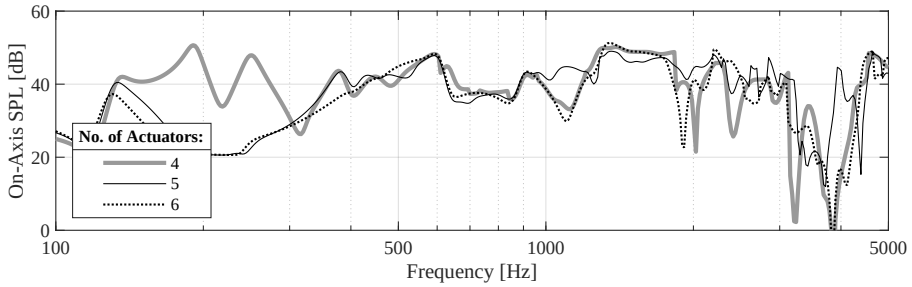

(B) On-axis SPL at the forward setting.

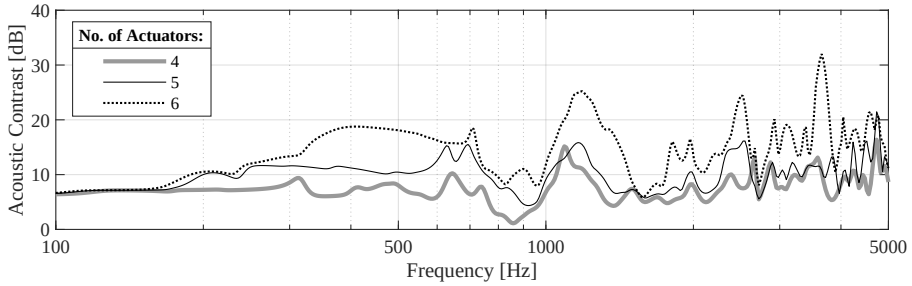

(C) Acoustic contrast at the steered setting.

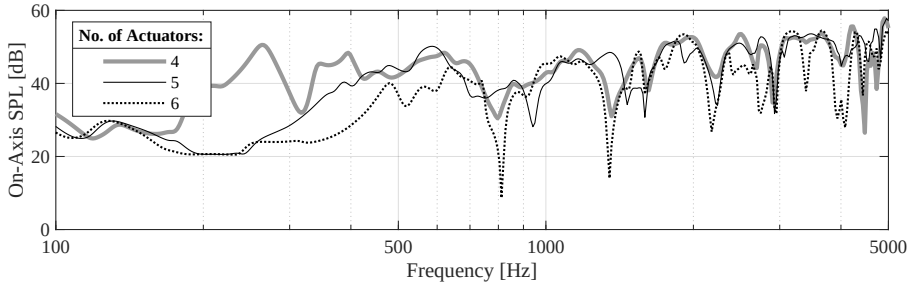

(D) On-axis SPL at the steered setting.

FIGURE 4.8: Performance across frequency for simulated arrays consisting of 4, 5 and 6 actuators, using a 1 m$\times$0.2 m$\times$3 mm panel. The arrays have been optimised using bright zones in the forward direction, and steered by 45°.

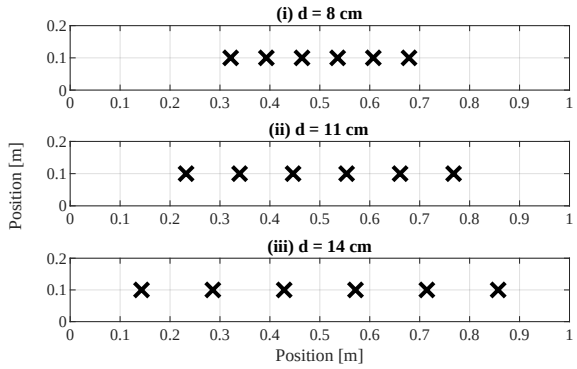

FIGURE 4.9: Schematic of arrays using six actuators with different spacing on a 1 m×20 cm×3 mm panel.

Actuator Spacing

In order to examine the effect that the spacing between actuators has on performance, three arrays using six actuators are simulated, each with a different spacing, as shown in Fig. 4.9. The spacing values of 8 cm, 11 cm and 14 cm correspond to overall array lengths of 40 cm, 55 cm and 70 cm, respectively.

Figure 4.10 shows the performance across the investigated frequency range for the arrays described above, at different steering settings. The acoustic contrast frequency response for the forward directed setting (Fig. 4.10a) shows a decrease in overall contrast levels as the spacing increases, which is in agreement with the trend observed in Fig. 4.7. At the same time, a shift of the entire response towards lower frequencies is also observed, with the low frequency limit being improved and the cut-off frequency reduced for a larger spacing value. The on-axis SPL response when using a forward bright zone is shown in Fig. 4.10b, however, no clear trend is observed in this case.

Contrary to the forward directed setting, the acoustic contrast frequency response for the steered setting (Fig. 4.10c) appears to show an overall improvement when the spacing between actuators increases. As seen in the comparison between different numbers of actuators used (Fig. 4.8c), the cut-off at higher frequencies is not apparent in the steered setting response. An improvement in the low frequency limit is achieved by using a larger spacing. The steered on-axis SPL is displayed in Fig. 4.10d, and shows a shift of anti-resonances towards lower frequencies as the spacing increases.

Table 4.3 contains the frequency averaged contrast and standard deviation for the cases investigated above. Although the shorter arrays are seen to be more effective in generating a forward focussed sound field, a longer array displays better performance at steered directivity settings. In the investigated example, the longer array is not only characterised by larger spacing between the actuators, but also by the fact that it covers the entire length of the 1 m long panel. In order to conclude whether the performance improvement at steered settings is determined primarily by the spacing between actuators, or their distribution relative to the panel dimensions, it is important to consider these results together with the investigation of different panel lengths for a given array size, which will be presented in Sec. 4.3.2.

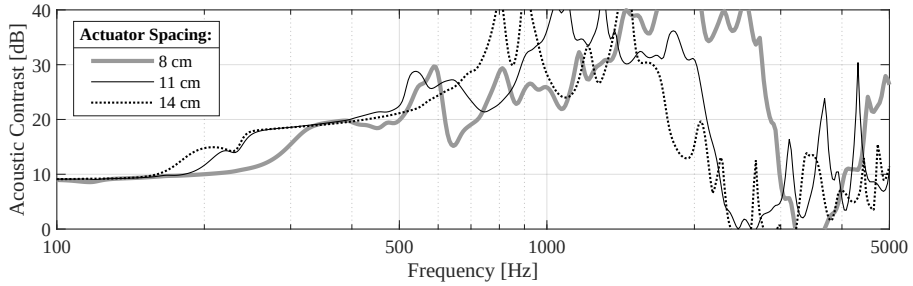

(A) Acoustic contrast at the forward setting.

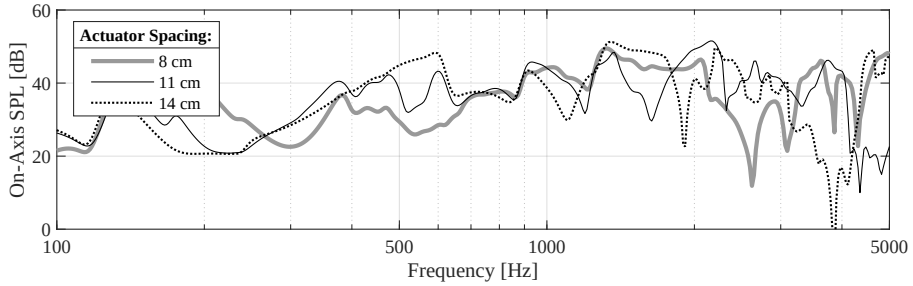

(B) On-axis SPL at the forward setting.

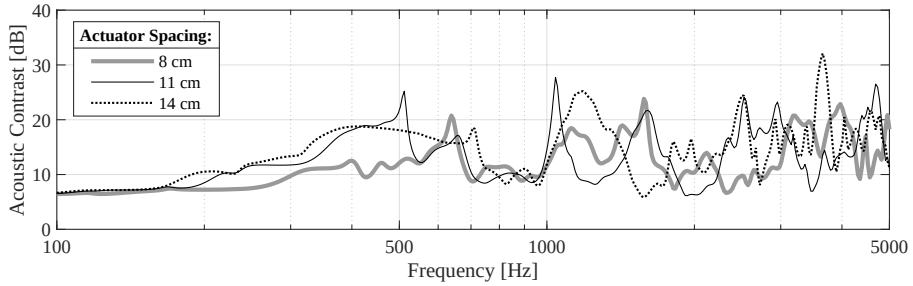

(C) Acoustic contrast at the steered setting.

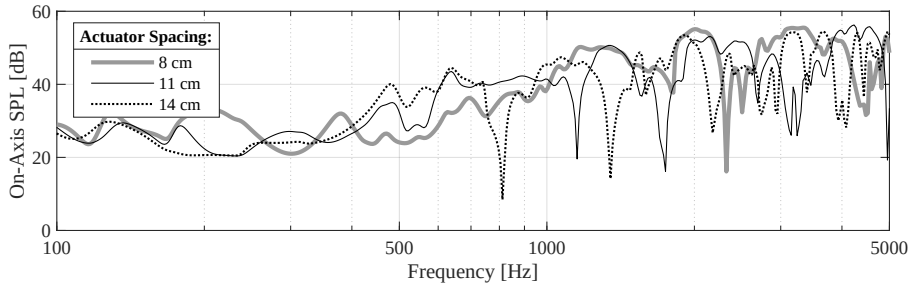

(D) On-axis SPL at the steered setting.

FIGURE 4.10: Performance across frequency for simulated arrays consisting of six actuators, using a 1 m×0.2 m×3 mm panel, with different spacing between the actuators. The arrays have been optimised using bright zones in the forward direction, and steered by 45°.

Actuator Spacing	Forward bright zone		45° steered bright zone	
8 cm	20.5 dB	±12.3 dB	10.4 dB	±4.2 dB
11 cm	19.0 dB	±10.6 dB	12.1 dB	±4.8 dB
14 cm	17.6 dB	±10.9 dB	13.9 dB	±5.0 dB

TABLE 4.3: Frequency averaged acoustic contrast and standard deviation between 100 Hz and 5 kHz, for arrays using six actuators at different spacings.

FIGURE 4.11: Schematic of non-uniform actuator distributions compared to a uniform distribution of equal overall length on a 1 m×20 cm×3 mm panel.

Non-Uniform Spacings

The study into the effect of actuator spacing has so far suggested that, while narrow arrays are more effective at producing a forward directed sound field (Fig. 4.10a), a larger spacing yields better results at steered settings (4.10c). It is therefore worth raising the question whether a distribution containing certain actuators positioned closer to each other and others at a greater distance would reach a beneficial trade-off and be capable of improved performance in all directivity settings. Two different non-uniform distributions have been tested, which are shown in Fig.4.11. In both cases, named Type I and Type II for convention, the spacing values have been chosen following a roughly logarithmic increment. In Type I, the spacing sequence is 21 cm, 11 cm, 6 cm, 11 cm and 21 cm, with the actuators being closer together in the center of the panel. In Type II, the sequence is 6 cm, 11 cm, 36 cm, 11 cm and 6 cm, with the actuators being concentrated at the edges of the panel. Both distributions have an overall array length of 70 cm.

Figure 4.12 shows the performance across frequency for the uniformly spaced array and the two alternative distributions, for the two different steering settings. In terms of acoustic contrast in the forward directivity setting (Fig. 4.12a), the Type I distribution displays an almost identical low frequency response to the uniform spaced array and a marginal improvement over the cut-off at around 2 kHz, but is significantly outperformed by the uniform array within the 600 Hz to 2 kHz range. The Type II distribution generally displays a reduced low frequency performance and a shift in the cut-off limit towards higher frequencies around 3 kHz. The response of both non-uniform distributions is generally similar within the 350 Hz to 2 kHz range. Looking into the on-axis SPL performance (Fig. 4.12b), the non-uniform spacing distributions display an advantage over the uniform arrangement in reducing the dips in performance, particularly at the higher frequencies within the investigated range.

The acoustic contrast frequency response of the same three array configurations, optimised for a bright zone steered by 45°, is displayed in Fig. 4.12c. As with the forward setting, the Type I distribution has a similar low frequency response to the uniform distribution, while Type II produces a reduced level of acoustic contrast. However, both Type I and the uniform distribution display generally similar levels of overall contrast achieved throughout the investigated range, albeit with increases in performance occurring at different frequency bands. The on-axis SPL frequency

Actuator Distribution	Forward bright zone		45° steered bright zone	
Uniform	17.6 dB	±10.9 dB	13.9 dB	±5.0 dB
Type I	13.8 dB	±6.1 dB	13.4 dB	±4.5 dB
Type II	14.2 dB	±6.2 dB	12.2 dB	±3.8 dB

TABLE 4.4: Frequency averaged acoustic contrast and standard deviation between 100 Hz and 5 kHz, for arrays using six actuators at different spacings.

response (Fig. 4.12d) is generally similar, with the non-uniform distributions displaying a reduction over the drops in performance caused by anti-resonances at specific frequencies.

The acoustic contrast, averaged across frequency between 100 Hz and 5 kHz, along with its standard deviation, are shown in Table 4.4 for the distributions investigated above. For the forward setting, the uniformly spaced array has a clear advantage over the alternative distributions, albeit with a significantly higher deviation, due to the cut-off at around 2 kHz. For the bright zone steered by 45°, all configurations display similar performance, though even in this case, the uniform distribution shows a slight advantage in average contrast achieved. It can therefore be concluded that the uniform force distribution is more effective at controlling the radiated sound field compared to the considered non-uniformly spaced arrays and, since the considered non-uniform arrays span the range of possible configurations, it appears unlikely that alternative arrangements would generate significantly different results.

Position on the y-Axis

The last parameter to be investigated relating to the distribution of the actuators on the panel regards their position along the y-axis. As the directivity control is limited to the xz plane, it is anticipated that the shape of the radiated sound field on this plane is primarily determined by the excitation of the panel modes along the x-axis, hence the focus of this study on different actuator distributions along the length of the panel. However, as changing the position of excitation on the y-axis can potentially lead to a different structural response, it is useful to obtain an insight into how the radiated sound field caused by the vibration of the panel might be affected by this parameter. Figure 4.13 shows a schematic of the different array positions relative to the panel simulated in this study.

Figure 4.14 shows the performance across frequency for instances of a six actuator array centred along the x-axis of a 1 m$\times$0.2 m$\times$3 mm panel, and positioned centred, displaced by 3 cm and by 6 cm along its y-axis. From the acoustic contrast response in the forward direction (Fig. 4.14a), it can be seen that moving the array off-centre results in a slight shift in its response towards higher frequencies, with a reduction in its low frequency response and limited improvement in the contrast achieved beyond the cut off at around 2 kHz. The on-axis SPL frequency responses (Fig. 4.14b) display general similarities with small shifts across frequency. However, no clear trend is observed.

The acoustic contrast across frequency for the above configurations, when optimised for a bright zone steered by 45° is shown in Fig. 4.14c. In this setting, the system shows a general decrease in contrast levels when shifted from the centre of the y-axis, with a reduced low frequency performance and narrower regions of high

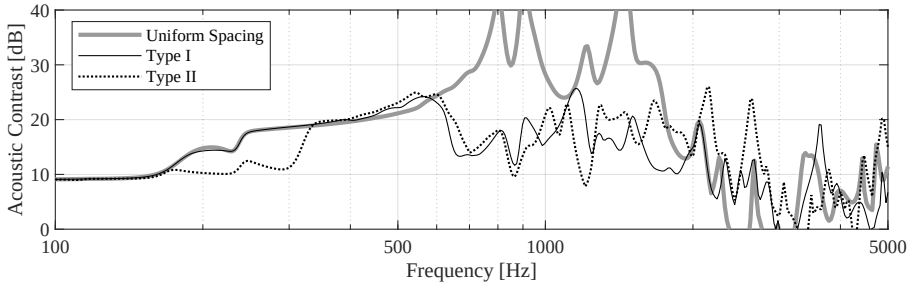

(A) Acoustic contrast at the forward setting.

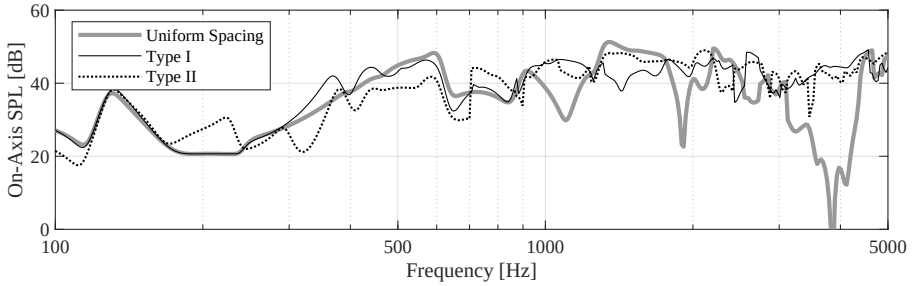

(B) On-axis SPL frequency at the forward setting.

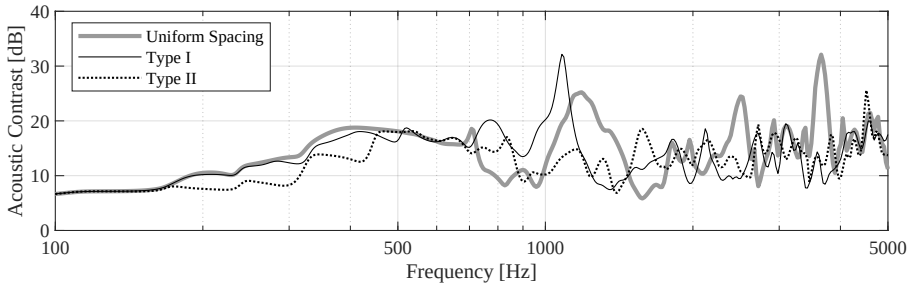

(C) Acoustic contrast at the steered setting.

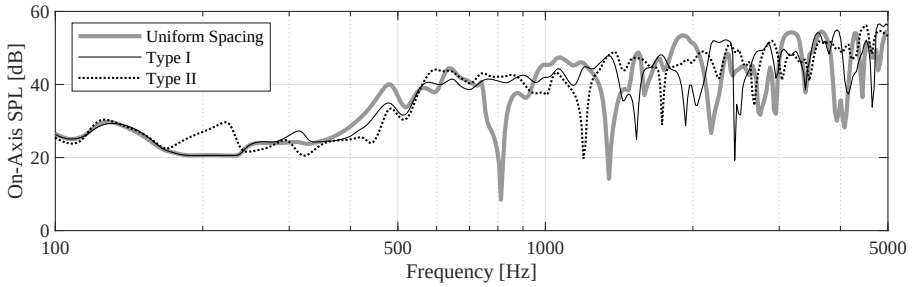

(D) On-axis SPL at the steered setting.

FIGURE 4.12: Performance across frequency for simulated arrays consisting of six actuators, using a 1 m×0.2 m×3 mm panel, with a total length of 70 cm and different spacing between the actuators. The arrays have been optimised using bright zones in the forward direction, and steered by 45°.

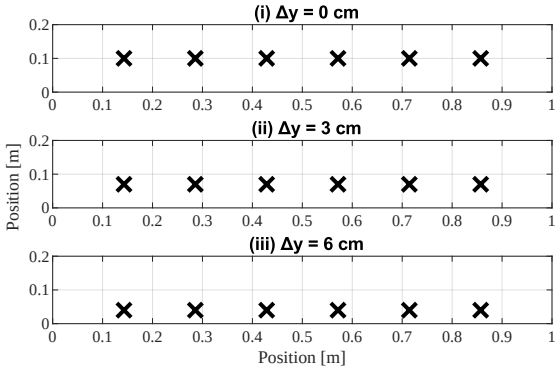

FIGURE 4.13: Schematic of arrays using six actuators positioned at different points along the y-axis of a 1 m×20 cm×3 mm panel.

y-axis displacement	Forward bright zone		45° steered bright zone	
0 cm	17.6 dB	±10.9 dB	13.9 dB	±5.0 dB
3 cm	17.5 dB	±11.9 dB	13.1 dB	±5.2 dB
6 cm	17.6 dB	±11.5 dB	12.5 dB	±4.8 dB

TABLE 4.5: Frequency averaged acoustic contrast and standard deviation between 100 Hz and 5 kHz, for arrays using six actuators at different positions on the y-axis.

contrast at higher frequencies. The on-axis SPL (Fig. 4.14d) shows general similarities for all three cases, and, as with the forward directed setting, no distinct trend is evident. Overall, the position of the array on the y-axis has been shown to not have a significant effect in directivity.

Table 4.5 shows the frequency averaged acoustic contrast and standard deviation between 100 Hz and 5 kHz for the three cases investigated above. The limited extent of the effects from shifting the actuator positions along the y-axis is evident, as average contrast and deviation values are similar for all cases in either steering setting. A difference in average contrast of 1.4 dB is the greatest observed, between the centred and the 6 cm off-centre arrays at the steered setting.

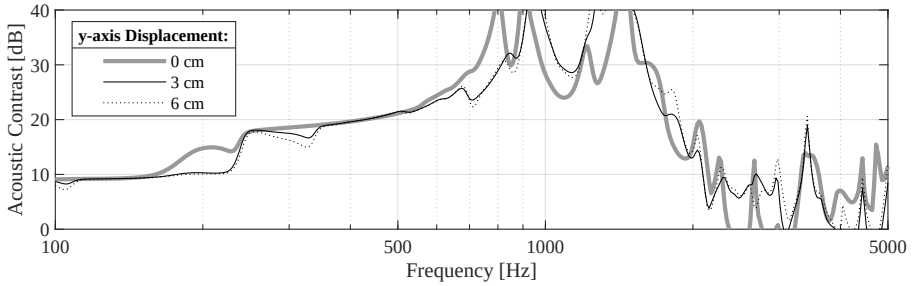

(A) Acoustic contrast at the forward setting.

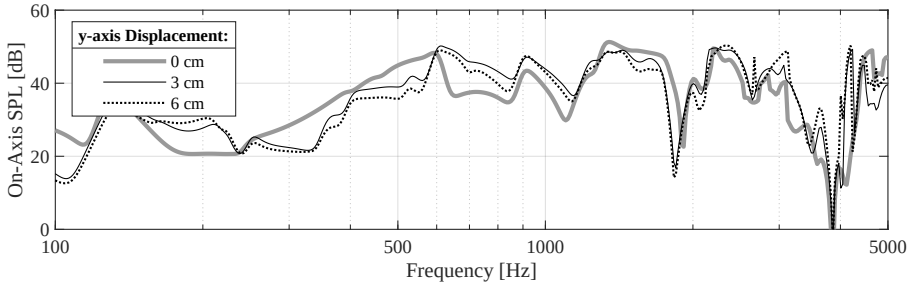

(B) On-axis SPL at the forward setting.

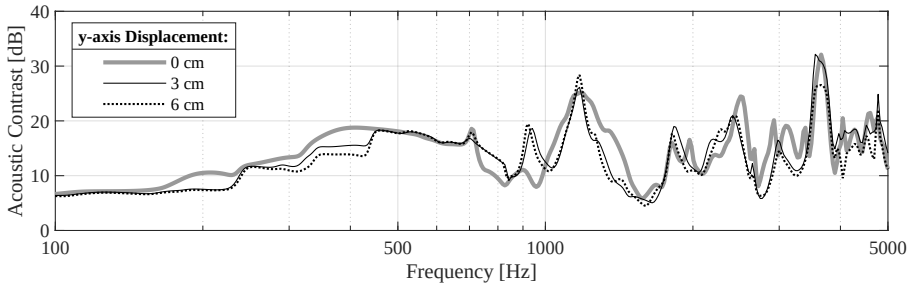

(C) Acoustic contrast at the steered setting.

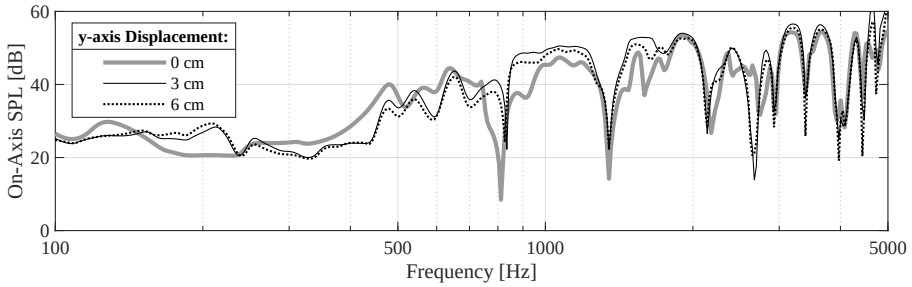

(D) On-axis SPL at the steered setting.

FIGURE 4.14: Performance across frequency for simulated arrays consisting of six actuators and a fixed array length of 70 cm, using a 1 m×0.2 m×3 mm panel, at different positions on the y-axis. The arrays have been optimised using bright zones in the forward direction, and steered by 45°.

4.3.2 Effects of Panel Size Parameters

The second part of the parametric study of the structural actuator array focuses on the effects that the size of the panel used has on the performance of the system. As the radiated sound field is primarily determined by the vibration of the panel, it is the structural modes of the panel and coupling of the actuators to these modes that plays a key part in the overall performance of the system. Therefore, it is also essential to study the effects of basic panel properties to fully evaluate the structural actuator array. In the subsequent simulations the effect of each panel dimension on the system performance is investigated. The fixed parameters, along with those listed in Table 4.1, regard the actuator array, which consists of six actuators, spaced at 8 cm from each other. This gives an effective array length of 40 cm, which serves to allow for the testing of a broader range of panel lengths.

Panel Length

Figure 4.15 shows the performance of the system across frequency when using panels of different length. Examining the acoustic contrast response (Fig. 4.15a), it is evident that the low frequency limit is improved by the increase in panel length, although the overall contrast levels do not appear to be greatly affected by this change. All investigated cases are characterised by the same cut-off in contrast at around 2 kHz, which indicates that the length of the panel does not determine the high frequency limit of the system. The on-axis SPL frequency response (Fig. 4.17b) is relatively irregular and a comparison between the results does not indicate any clear trends.

The acoustic contrast frequency response of the same arrays when optimised using a bright zone steered by 45° is shown in Fig. 4.15c. The improvement in performance at lower frequencies is also visible in this setting. Although longer panels are seen to be capable of higher contrast over isolated frequency bands within the 300 Hz to 2 kHz range, the shorter panel displays a flatter response with no significant dips in performance. This different response, also evident in the forward setting (Fig. 4.15a), is likely due to the actuator array covering the entire length of the panel, providing better control over its vibration, and also due to the fact that a shorter panel length results in a shift of the modes in frequency. At frequencies above 2 kHz, all investigated cases display very similar behaviour. Looking at the on-axis SPL response (Fig. 4.15d), one can group together the three longer panel cases as displaying similar behaviour, with the response of the shortest panel being an outlier. Between the three longer panels, a shift of the response in both acoustic contrast and SPL towards lower frequencies is observed as the length of the panel increases.

The frequency averaged acoustic contrast and its standard deviation between 100 Hz and 5 kHz for the arrays simulated above are displayed in Table 4.6. The values of average contrast are indicative of how, despite the small differences observed in the response of the different panel lengths, particularly at lower frequencies, the overall performance is relatively similar across all investigated cases. In conjunction with the results from the study on actuator spacing in Sec. 4.3.1, it can be concluded that it is the spacing between the actuators that holds a greater influence over the resulting directivity, compared to the relative size of the panel.

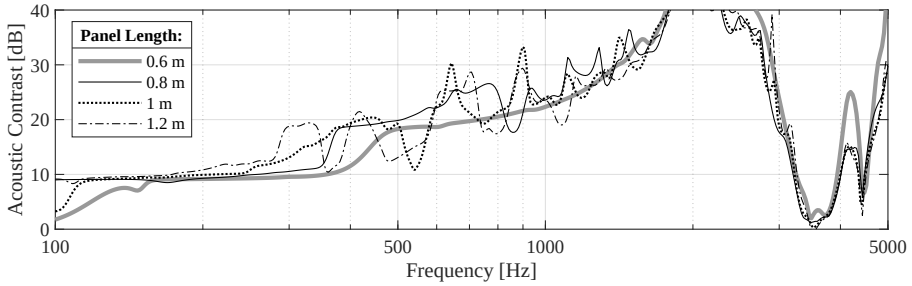

(A) Acoustic contrast at the forward setting.

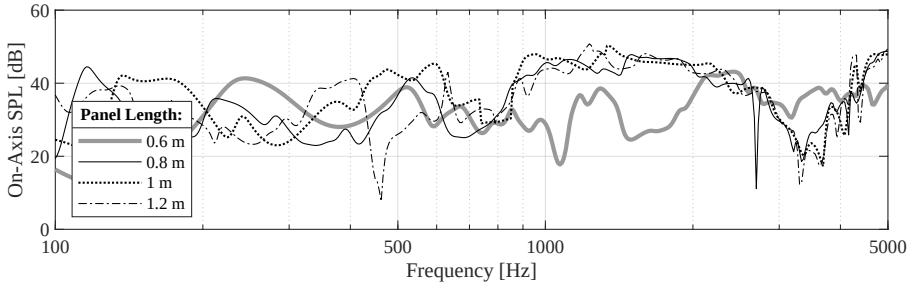

(B) On-axis SPL at the forward setting.

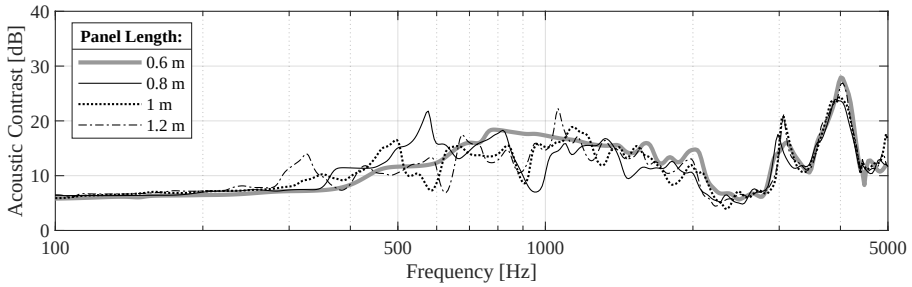

(C) Acoustic contrast at the steered setting.

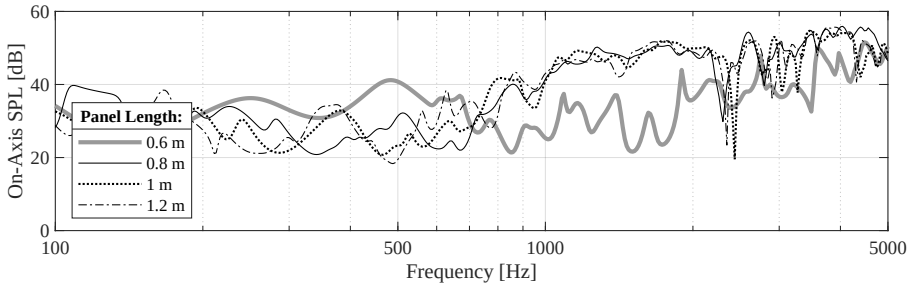

(D) On-axis SPL at the steered setting.

FIGURE 4.15: Performance across frequency for simulated arrays consisting of six actuators and a fixed array length of 40 cm, using a panel of 0.2 m width, 3 mm thickness and varying length. The arrays have been optimised using bright zones in the forward direction, and steered by 45°.

Panel Length	Forward bright zone		45° steered bright zone	
0.6 m	19.9 dB	±14.2 dB	11.3 dB	±4.8 dB
0.8 m	19.8 dB	±11.5 dB	10.9 dB	±4.3 dB
1 m	20.5 dB	±12.3 dB	10.4 dB	±4.2 dB
1.2 m	20.0 dB	±11.3 dB	11.1 dB	±4.3 dB

TABLE 4.6: Frequency averaged acoustic contrast and standard deviation between 100 Hz and 5 kHz, for arrays of six actuators using panels of different length.

Panel Width	Forward bright zone		45° steered bright zone	
10 cm	18.8 dB	±10.7 dB	11.8 dB	±4.7 dB
20 cm	20.5 dB	±12.3 dB	10.4 dB	±4.2 dB
40 cm	20.5 dB	±11.6 dB	11.0 dB	±4.2 dB

TABLE 4.7: Frequency averaged acoustic contrast and standard deviation between 100 Hz and 5 kHz, for arrays of six actuators using panels of different width.

Panel Width

Keeping the actuator array centred on the panel, the performance of systems utilising panels of varying size along the y-axis is investigated. Figure 4.16 shows the performance across frequency for three cases of identical arrays using panels of 10 cm, 20 cm and 30 cm width. In this instance, the behaviour of the system displays little variation among the investigated cases. Only the 10 cm wide panel appears to achieve a lower level of contrast for the majority of the investigated frequencies at the forward setting. The on-axis SPL responses are likewise similar between the three panel widths in both steering settings. The frequency averaged values for contrast reflect the similarity in the results, with the greatest difference in average contrast being 1.7 dB between the 10 cm and 40 cm wide panels. The results from this study, in conjunction with the results from the study on the position of actuators on the y-axis presented above, indicate that the activation of modes along the y-axis of the panel does not have a significant impact on the directivity of the radiated sound field on the xz plane.

Panel Thickness

The thickness of the panel is the last parameter regarding panel size to be investigated in this study. The performance across frequency for arrays consisting of six actuators, utilising 3 mm, 5 mm and 6 mm thick panels, is shown in Figure 4.17. In terms of acoustic contrast (Figs. 4.17a, 4.17c), increasing the thickness of the panel results in a shift in the response towards higher frequencies. A thinner panel improves the low frequency response, particularly for the forward setting. Conversely, increasing the thickness shifts the cut-off which characterises the forward directed case towards higher frequencies, and also reduces the resulting drop in contrast. This is due the thickness of the panel affecting the modal response through the quantity EI, as given by equation (4.2). Therefore, the modal frequencies determined by equation (4.5) shift higher with an increase in thickness. The on-axis SPL frequency responses (Figs. 4.17b, 4.17d) are generally similar in each steering setting among the different configurations, with shifts in the location of resonances and anti-resonances that do not follow a clear trend. Table 4.8 shows the average contrast and standard

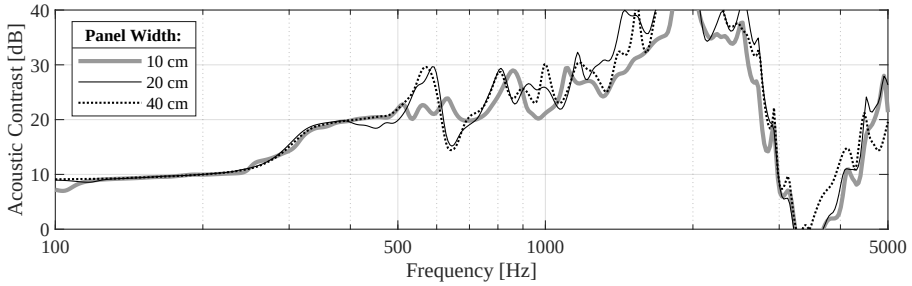

(A) Acoustic contrast at the forward setting.

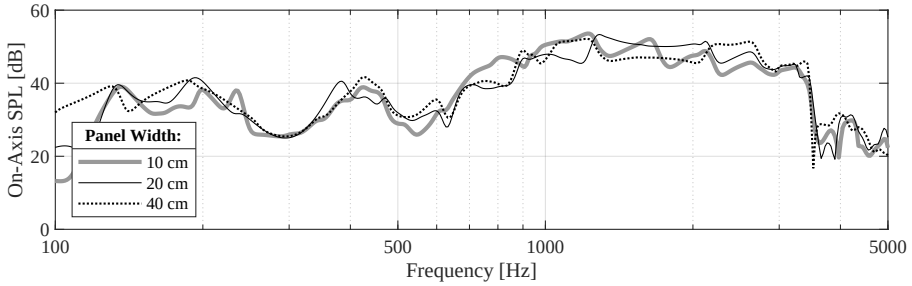

(B) On-axis SPL at the forward setting.

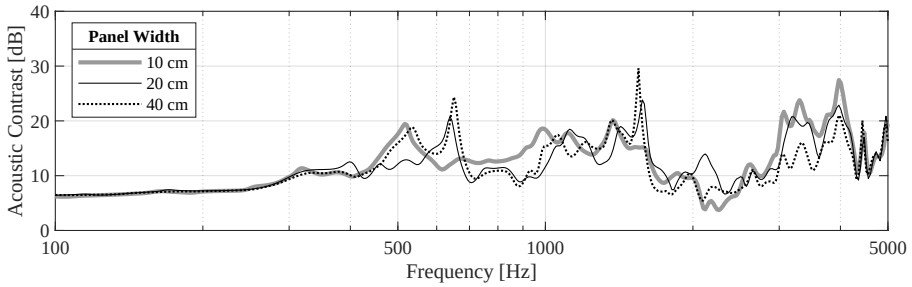

(C) Acoustic contrast at the steered setting.

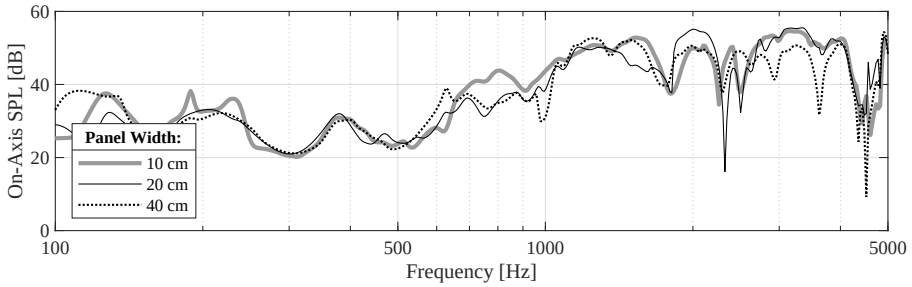

(D) On-axis SPL at the steered setting.

FIGURE 4.16: Performance across frequency for simulated arrays consisting of six actuators and a fixed array length of 40 cm, using a panel of 1 m length, 3 mm thickness and varying width. The arrays have been optimised using bright zones in the forward direction, and steered by $45^{/}circ$.

Panel Thickness	Forward bright zone		45° steered bright zone	
3 mm	20.5 dB	±12.3 dB	10.4 dB	±4.2 dB
5 mm	20.8 dB	±11.6 dB	10.7 dB	±4.3 dB
8 mm	19.6 dB	±11.0 dB	11.8 dB	±6.1 dB

TABLE 4.8: Frequency averaged acoustic contrast and standard deviation between 100 Hz and 5 kHz, for arrays of six actuators using panels of different thickness.

deviation calculated between 100 Hz and 5 kHz for the three panels investigated. The proximity between resulting contrast values for both directivity settings reflects the similar behaviour of the acoustic contrast frequency responses.

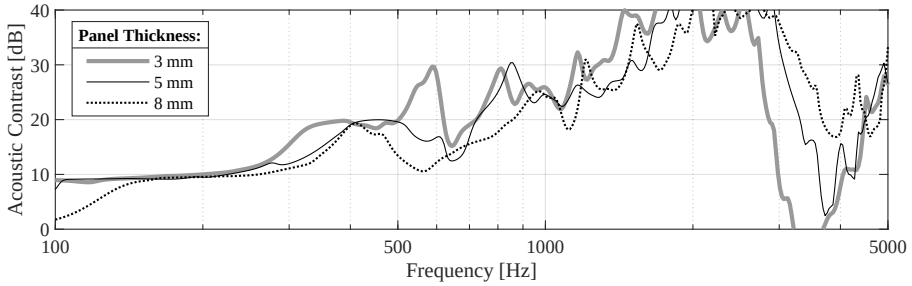

(A) Acoustic contrast at the forward setting.

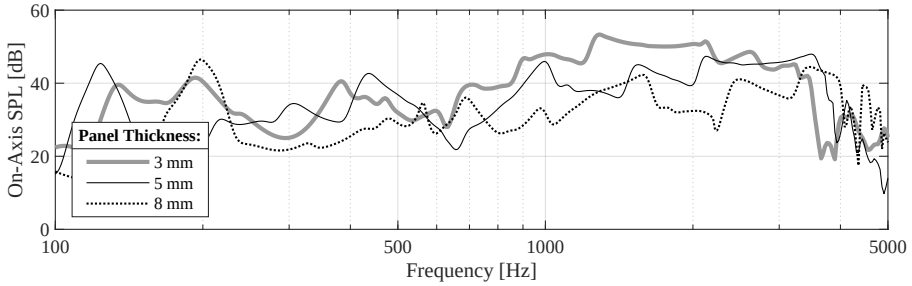

(B) On-axis SPL at the forward setting.

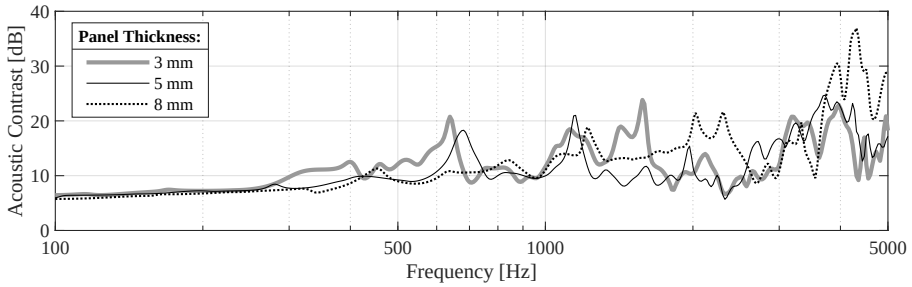

(C) Acoustic contrast at the steered setting.

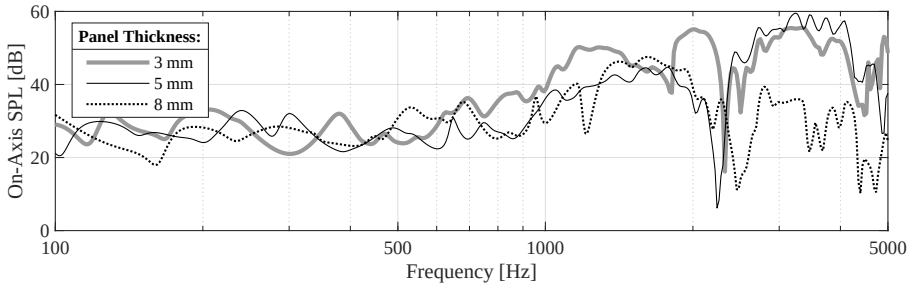

(D) On-axis SPL at the steered setting.

FIGURE 4.17: Performance across frequency for arrays consisting of six actuators and a fixed array length of 40 cm, using a panel of 1m length, 20 cm width and varying thickness. Results are shown for arrays optimised to radiate in a forward bright zone and a bright zone steered by 45°.

4.4 Summary

In this chapter, the concept of the structural actuator array was introduced. Through existing models of vibration resulting from forced excitation of plates, and sound radiation through structural vibration, a mathematical model for the operation of the proposed system was formulated. Based on the approximation of inertial actuators as a distribution of point forces acting on a thin plate, this model offered an expression of the sound pressure that can be measured in the far field, resulting from the forced excitation of a flat panel by a known force distribution. The structural actuator array was simulated using these approximations, facilitating a parametric study on its performance, and its dependency on the physical parameters of the panel and geometry of the array used.

The investigation showed that the number of actuators used in the array is the most important parameter in determining directivity performance, with a greater number achieving higher directivity. The spacing between actuators also has a significant effect in performance. A shorter spacing produces a higher overall level of acoustic contrast in the forward direction, whereas a longer spacing improves the response at low frequencies, and is capable of higher directivity at steered settings. A comparison of results for uniform and non-uniform actuator distributions of equal total length shows that the former is capable of a higher acoustic contrast performance. The resulting directivity was shown to be primarily dependent on the distribution of the actuators along the length of the panel. The physical dimensions of the panel were shown to generally have a limited effect on the directivity capabilities of the system.

Overall, the structural actuator array appears capable of producing a high level of directivity, albeit with a high dependence on frequency. The distribution of actuators can be optimised to set the operational bandwidth of the system, but in general, improving the low frequency response comes at the cost of reduced high frequency performance and vice versa. In order to ensure the largest possible operational bandwidth, both the length of the array–and of the panel necessary to accommodate it, needs to be maximised, and the spacing between actuators minimised. This leads to an increase in the total number of actuators used in the array. Moreover, the distribution of actuators should be even along the length of the panel to ensure a more consistent performance between the different beamforming settings. Under consideration of these conclusions, the specifications for a physical prototype of the structural actuator array can be obtained. The evaluation of such a prototype will be presented in Chapter 5.

Chapter 5

Structural Actuator Array: Experimental Validation

This chapter is devoted to the experimental validation of the mathematical model which was formulated and used to simulate the structural actuator array. For this purpose, a prototype is built using a flat rectangular panel and an array of inertial actuators. This prototype system is tested by measuring its directivity performance in an anechoic environment. The parameters of the system have been chosen under consideration of the parametric study performed in Sec. 4.3, in order to provide a high directivity performance across a significant bandwidth within the frequency range designated for warning sounds, while ensuring that the dimensions of the system render it suitable for a potential in-vehicle integration. Section 5.1 presents the components and specifications under which the prototype is built, as well as the measurement set-up in the anechoic chamber. The implementation of the acoustic contrast maximisation process for directivity control is described in Sec. 5.2. The results of this study are shown, commented on, and compared to the corresponding simulations performed using the mathematical model, in Sec. 5.3. The experiments and results presented in this chapter have been published as part of the paper "A system for controlling the directivity of sound radiated from a structure" in the Journal of the Acoustical Society of America (Kournoutos and Cheer, 2019).

5.1 Experimental Set-Up

Based on the understanding gained from the parametric study presented in Chapter 4, a prototype system has been assembled and is shown in Fig. 5.1. The materials, components, and specifications considered for the measurements performed in the anechoic chamber are fully listed in Table 5.1.

Structural Actuator Array

The parametric study performed in Secs. 4.3.1 and 4.3.2 allows for the optimisation of the basic parameters of the prototype in order to maximise its performance given the intended application of the system. The vibrating surface is a flat, rectangular panel, constructed from an aluminium (Al 6082), of dimensions 1 m$\times$0.2 m$\times$3 mm. This configuration was chosen as to best reach a compromise between the simple geometry simulated through the mathematical model, and the available surfaces and materials found on an actual vehicle. The panel itself is set upon a wooden mounting, which creates an enclosure of dimensions 1 m$\times$0.2 m$\times$0.18 m, as shown in Fig. 5.1b.

The number of actuators and length of the array determine its performance across frequency for the given panel characteristics. Six inertial actuators (model TEAX25C05-8 round audio exciters) form the array, with an overall weight of 360 g and a nominal frequency range of 200 Hz to 20 kHz. Examples of the actuators used are shown in Fig. 5.1a. Although a higher number of actuators would be expected to result in better directivity performance, it would also lead to an increase in the total mass and their total area of contact with the panel. As these parameters are not included, or only approximated by the mathematical model, this would potentially lead to higher inaccuracies in the simulations, and thus a less effective comparison. Moreover, a six actuator array offers a more direct comparison with the eVADER warning sound system, which employs an array of six loudspeaker drivers.

As it was shown that the system cannot produce a high level of acoustic contrast across the entire bandwidth designated for potential warning sounds, the prototype must be optimised under consideration of the warning sound used and its frequency components. A spacing of 14 cm between actuators was chosen, which ensures a higher performance in terms of acoustic contrast at steered directivity settings, and at lower frequencies in the forward direction, as indicated by results in Sec. 4.3.1. This choice of spacing is expected to reduce the cut-off frequency for the forward directed setting, however, the resulting bandwidth should still be sufficient to cover all components of warning sounds such as the one used in the eVADER system(Quinn et al., 2014), which is also intended to be emitted directionally.

Given the relevant properties for aluminium displayed in Table 4.1, and the thickness of the panel used, h, at 3 mm, the critical frequency, f_c, is calculated from Eq. (4.15) to be 4369 Hz. As mentioned in Sec. 4.2, this means that beyond this frequency, it is the bending waves on the panel that contribute to sound radiation rather than the near field vibration at the location of the actuators. Although the resulting critical frequency lies within the investigated frequency range, it remains well above the cut-off limit estimated by the simulations for the six actuator configuration, and is therefore not expected to compromise the evaluation of the system.

Measurement Arrangements

The anechoic chamber has dimensions 9.15 m$\times$9.15 m$\times$7.32 m, which are further limited by the acoustic diffusers attached to the walls. The prototype structural actuator array is placed for measurement inside the chamber, positioned at the centre of the chamber and supported at a height of 1.2 m. Three compact stereo amplifiers are used to drive the actuators. The resulting sound pressure is measured using a circular array of eleven omni-directional microphones, placed at a distance of 2.8 m from the centre of the panel, at a height of 1.2 m, and covering an angle of 180°, corresponding to the forward half-plane. Figure 5.1c provides a view of the microphone array positions relative to the prototype inside the anechoic chamber. Control of the signal sent to each amplifier channel, and data acquisition from the microphone array are handled by a compact data acquisition system which is connected to the computer with the necessary software and scripts.

Constraints on the frequency range within which the system can be reliably evaluated and compared with the mathematical model are primarily imposed by the additional mass loading on the panel due to the weight of the actuators at lower frequencies and by the number of modes included in the model at higher frequencies. The experiments using the prototype presented in this chapter are intended to both validate the results presented in the previous section and to assess the potential

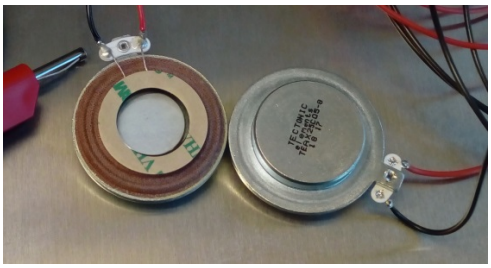

(A) Example pair of the inertial actuators used in the prototype system.

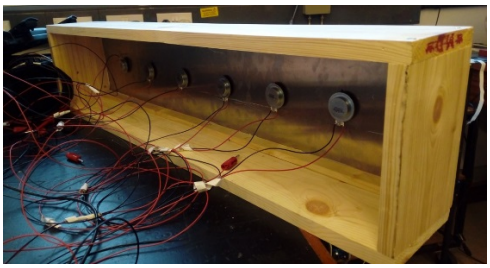

(B) The actuator array as attached to the panel, and its wooden mounting.

(C) Measurement set-up in the anechoic chamber.

FIGURE 5.1: Pictures of the components and measurement set-up used to build and test the prototype system.

performance of the proposed directional structural actuator array system in practice.

5.2 Implementation of Directivity Control

As explained in Chapter 4, the directivity of the sound field resulting from the vibration of the structure is determined by controlling the relative phase and amplitude between the actuators of the array, two properties that are contained in the complex input vector, $\boldsymbol{u}$, introduced in Sec. 3.2. In practice, this can be achieved by filtering the base signal of the warning sound to be emitted through a filter characterised by the appropriate magnitude and phase response, before driving each actuator. Such filters are designed using information from each individual actuator's transfer response, obtained through an initial measurement in the anechoic chamber. The process for this implementation of directivity control, from the stage of obtaining the response of each actuator to driving the system to radiate a directional sound field, is presented in a four-step flowchart, shown in Fig. 5.2.

In detail, the steps taken for the directivity control implementation process are as follows:

1. Each actuator in the array of I elements is driven with a test signal, in this case a sine sweep of 45 s duration, covering the frequency range from 10 Hz to 10 kHz. The resulting radiated sound pressure is measured by the sensor array, which is formed by M microphones.

2. The acoustic contrast maximization process is implemented in the next stage. The recorded data is used to calculate the matrices of transfer responses corresponding to the bright and dark zones, $\boldsymbol{G}_B$ and $\boldsymbol{G}_D$. These matrices must

Panel	
Material	Al 6082 alloy
Dimensions	1000 mm×200 mm×3 mm
Mass	1.62 kg
Critical frequency	4369 Hz
Enclosure dimensions	1 m×0.2 m×3 mm
Placement height	1.2 m
Actuators	
Brand	Tectonic Elements
Model	TEAX25C05-8
Frequency response	200 Hz - 20 kHz
Weight	60 g
Number	6
Spacing	14.3 cm
Amplifiers	
Brand	Sure Electronics
Model	TPA3110
Class	D
Channels	2
Power	15 W
Number	3
Microphones	
Brand	PCB Piezotronics
Model	130F20
Number	11
Distance	2.8 m
Increment	18°
Height	1.2 m
Data Acquisition	
Type	Multiple module DAQ system
Brand	National Instruments
Model	cDAQ-9178
Measurement	
Control zone coverage	180°
Bright zone width	36°
Investigated frequency range	100 Hz - 5 kHz

TABLE 5.1: List of materials, components and other specifications for the testing of the prototype structural actuator array.

be calculated for the N frequency bins used in the analysis. Then, the optimal source strength vector for each actuator, $\boldsymbol{u}$, is obtained at each frequency according to Eq. (3.10). The regularization factor, λ_2, is chosen accordingly to ensure a relatively smooth frequency response, avoiding spikes in excess of 5 dB in acoustic contrast level to ensure robust performance.

3. These optimal source strength frequency responses are then used to calculate a set of I FIR filters that match the frequency responses of $\boldsymbol{u}$. However, in order to do this, a time delay, τ, needs to be introduced to the optimal source strengths in order to produce a realizable causal filter. In the frequency domain, this can be expressed as $\boldsymbol{u}e^{-i2\pi f\tau}$, where f denotes the frequency. As warning sounds tend to be continuous signals, this delay does not have a significant impact on the effectiveness of the system.

4. A directional sound field that focuses on the assigned bright zone and minimizes the pressure in the dark zone can be produced by filtering a base signal, which would be the desired warning sound signal, through the optimal filter set, before using it to drive the actuator array.

Utilizing this method, a real-time implementation would require a number of predefined filter sets to be stored, each corresponding to a specific steering angle, that could be implemented in order to control the direction to which the beamformer is focused.

As has been already mentioned, only the forward half-plane is considered during the experiments presented in this chapter, to ensure consistency with the mathematical model based simulations, as the assumption of an infinite baffle in the formulation of the model is expected to have different effects compared to the frame upon which the prototype is mounted. Using eleven microphones to cover an angular width of 180° means that there is a 18° increment between neighbouring microphones. For each directivity setting, the bright zone is defined by the positions of three microphones, which cover a 36° angle. Figure 5.3 shows an example of the control zones used, with the bright and dark zones chosen to maximize directivity in the forward direction in the depicted instance.

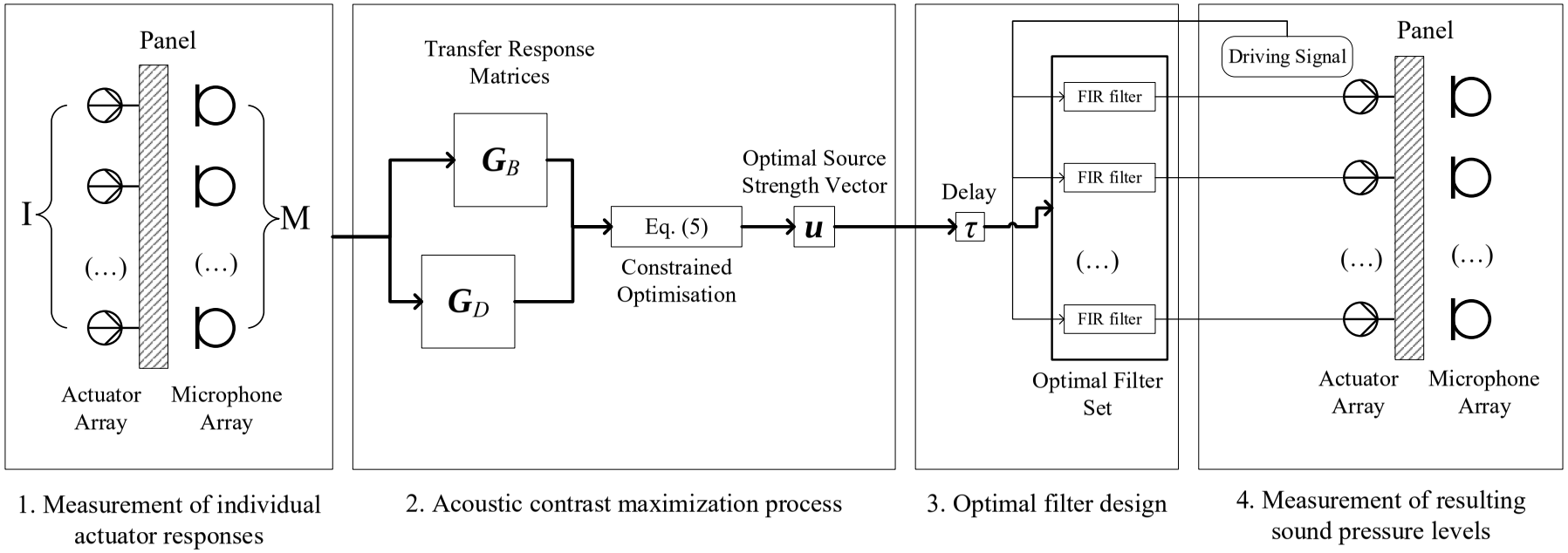

FIGURE 5.2: Flowchart showing the implementation of the directivity control process.

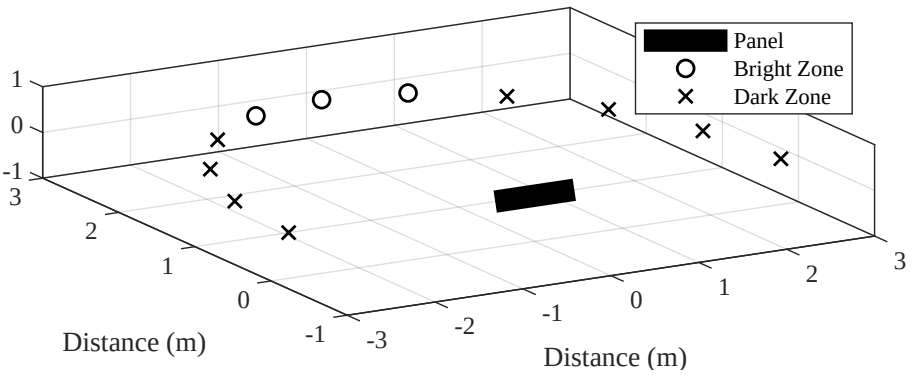

FIGURE 5.3: Schematic of the control zone used for the measurements in the anechoic chamber. Open circles represent microphones comprising the bright zone, and black dots represent the dark zone microphones. The dark line denotes the space occupied by the prototype system, which is consistent with the simulation study presented in Chapter 4.

5.3 Experimental Results

Structural Response

Prior to any sound field measurements, it is useful to obtain a view of the structural response of the panel when it is excited by the inertial actuators. This can provide an early insight into the accuracy of the mathematical model, and in particular, the approximations taken to describe the vibration of the plate. By attaching an accelerometer to the panel, the structural response can be obtained for that specific point. Figure 5.4 shows the response of the system when driven by a single actuator, measured using an accelerometer located at a point with coordinates (0.24 m, 0.07 m), and as simulated for the same point using the mathematical model, as described by Eq. (4.6). The comparison between the simulated and measured results shows that the model matches the behaviour of the physical system well for frequencies ranging from 400 Hz to roughly 3 kHz. At lower frequencies, differences between the simulated and measured responses are more noticeable. This is because the analytical model does not consider the mass of the actuators. In reality, this additional mass loading on the panel has an effect on its response at these frequencies. Potential causes for other discrepancies between the measurement and simulation results across the entire frequency range are the representation of the actuators by distributions of point forces, which might lead to a different excitation of modes at high frequencies, where the wavelength might be comparable to the dimensions of the actuator. Additionally, the infinite baffle assumption is significantly different from the experimental set-up, and might lead to differences in the resulting sound pressure at higher angles. Lastly, the model assumes simply supported boundary conditions, but in reality, the boundary conditions only approximate this theoretical condition.

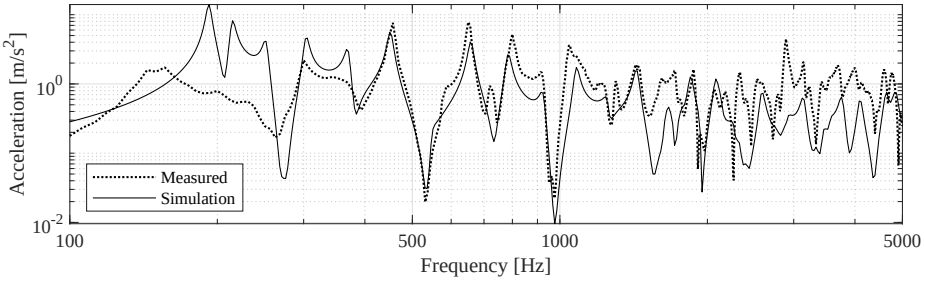

FIGURE 5.4: Structural response of the system, as measured at a point of coordinates (0.24 m, 0.07 m) on the panel. Comparison between simulation and measured data using the prototype system.

Sound Pressure Levels

The on-axis sound pressure level frequency response, measured at a distance of 2.8 m from the centre of the panel is evaluated and the measurement is compared to the simulation, calculated from Eq. (4.14), in Fig. 5.5. The array was driven so as to generate an a-weighted overall SPL across the 100 Hz to 5 kHz frequency range of 60 dB, at the position of the microphone located in front of the panel. Distortion effects were only discernible at frequencies below 100 Hz and can therefore be disregarded. Although the dimensions of the anechoic chamber did not allow for the measurement positions to be located as per the AVAS evaluation guidelines given

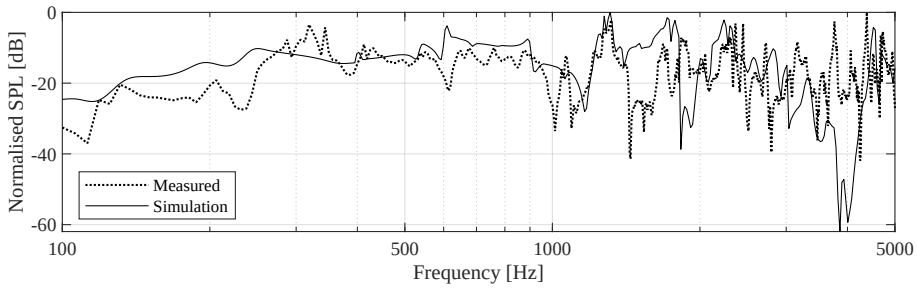

FIGURE 5.5: On-axis sound pressure level frequency response at a distance of 2.8 m. Comparison between simulation and measured data.

in (UNECE, 2017), this level is indicative of the target SPL when considering the effect of distance. Comparison of the results shows that for frequencies above 400 Hz the response of the model effectively follows the trends of the physical prototype. The primary cause for differences between the simulated response and that measured from the prototype at lower frequencies is the infinite baffle assumption that was considered in the model. Additional causes of discrepancies are, as previously stated, due to neglecting the mass of the actuators, and other approximations such as the simply supported boundary conditions.

Directivity control is achieved using the prototype system by driving the actuators with a sine sweep signal filtered through their respective FIR filters, as described in Section 5.2. The sound pressure level measured by the microphone array is used to calculate the acoustic contrast using Eq. (3.5). In Figure 5.6, the average measured sound pressure level calculated between 300 Hz and 3 kHz, is shown for different steering settings: aimed forward, and at angles of 36°, 54° and 72°. In all cases the bright zone has the previously defined coverage width of 36°. Microphone positions are marked by dots and the bright zone used is noted by a dashed line. The frequency limits in this instance were chosen to lie within the effective operating bandwidth of the prototype and be indicative of the performance of the system. It is evident from these plots that the system is capable of controlled directional radiation. To obtain a more detailed insight into the performance of the system, it is necessary to quantify directivity and evaluate it in terms of the acoustic contrast.

Acoustic Contrast

The acoustic contrast is calculated at each frequency bin using Eq. (3.5). This calculation is performed for the measured sound pressure in the anechoic chamber, and the sound pressure as estimated using the mathematical model of Chapter 4 to simulate the prototype array. The regularization factor, λ_2, used in the measurements, is chosen to ensure a relatively smooth response, as elaborated in Sec. 3.2. Figure 5.7 displays the resulting array effort, calculated through Eq. (3.8) with a reference signal, u_m, corresponding to the signal required for a single monopole source located at the centre of the array to produce the same mean square pressure in the forward bright zone. This array effort is used to set the value for λ_2 in the simulations, so that the simulated system requires equal array effort to the measured system. This is done to ensure a consistent comparison.

Table 5.2 shows the frequency averaged acoustic contrast and its standard deviation within the 100 Hz to 5 kHz range, for both measurements and simulations at

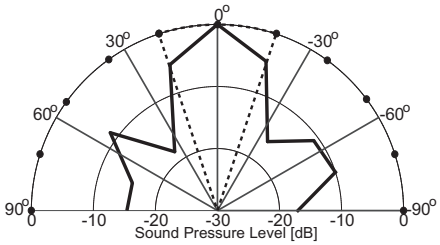

(A) Bright zone directed forward.

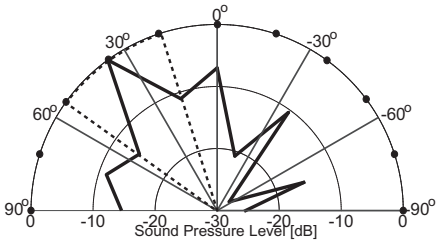

(B) Bright zone steered by 36°.

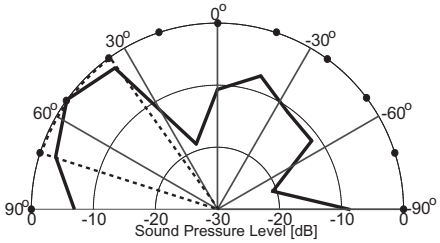

(C) Bright zone steered by 54°.

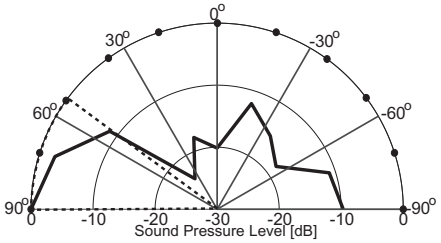

(D) Bright zone steered by 72°.

FIGURE 5.6: Directivity from the prototype structural actuator array, as measured within the anechoic chamber for different steering settings. The measured SPL has been normalised and frequency averaged between 300 Hz and 3 kHz.

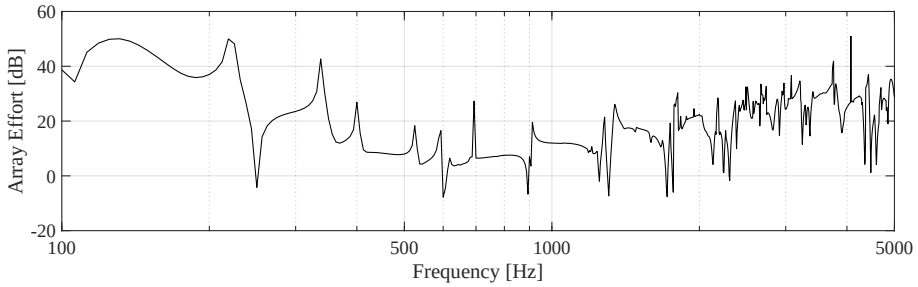

FIGURE 5.7: Array effort frequency response for the physical prototype of the structural actuator array. The array effort has been calculated with respect to the effort required for a single monopole source to produce the same mean square pressure in the forward bright zone.

Steering angle	Measured		Simulation	
0°	7.2 dB	±6.9 dB	10.9 dB	±8.5 dB
36°	8.1 dB	±5.9 dB	9.2 dB	±6.2 dB
54°	8.1 dB	±5.0 dB	9.6 dB	±3.3 dB
72°	12.0 dB	±5.5 dB	11.9 dB	±3.4 dB

TABLE 5.2: Frequency averaged acoustic contrast and standard deviation between 100 Hz and 5 kHz, at different bright zone steering settings. Comparison of results between measurements of the prototype array and simulations using the model presented in Chapter 4.

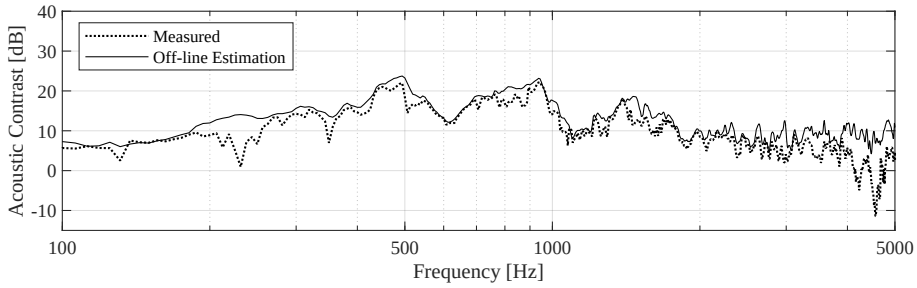

FIGURE 5.8: Acoustic contrast frequency response, as calculated off-line using the estimated transfer matrices, and as measured directly in the anechoic chamber, by driving the array using the designed FIR filters, corresponding to the forward setting.

different bright zone steering settings. Results from the measurement indicate a generally lower acoustic contrast compared to the simulation, albeit by a small margin. An exception is the 70° steered setting, where measurement and simulation achieve a very similar average value for contrast, with only 0.1 dB of difference. However, the high standard deviation across all cases suggests that the acoustic contrast is greatly dependent on frequency. Therefore, in order to obtain an in-depth view of the performance, it is necessary to examine the directional characteristic as a function of frequency.

To ensure that the optimal filter application for the directivity control process is implemented properly and yields reliable results, a comparison of the acoustic contrast frequency response for the forward directed setting between the on-line measurements in the chamber and the off-line estimation using the transfer matrices obtained in Sec. 5.2 is shown in Fig. 5.8. Both responses display a very similar behaviour at the majority of the investigated frequency range, with an average difference of 1.54 dB. Disparities at specific frequencies, particularly around 220 Hz and above 4 kHz are likely due to differences in the excitation of modes when all six actuators are simultaneously forcing the vibration of the panel. It can be thus concluded that the method produces sufficiently accurate results, and an effective experimental evaluation of the prototype system, and a comparison with the mathematical model, can be reliably performed.

Figure 5.9 shows the acoustic contrast over frequency, calculated according to Eq. (3.5). For the simulation and measurement results of the prototype system, for different directivity settings. In all cases, the model is effective at predicting the trends exhibited by the physical system over frequency. The accuracy of the predictions appears to diminish as the steering angle increases, particularly at the lower end of the investigated frequency range.

The system achieves the highest average acoustic contrast over the investigated

frequency range, as well as the highest value for contrast at an isolated frequency, for the forward setting. As the steering angle is shifted to 36° and then to 54°, the average contrast decreases, which is due to the effective decrease in the aperture size. It is worth noting however, that a limited increase in contrast is visible for frequencies above 2 kHz. For the 72° steered setting, along with the increase at higher frequencies, there is also a significant improvement in performance at lower frequencies around the 500 Hz mark. As the steering angle approaches 90°, the arrangement of actuators begins to resemble that of sound sources in an end-fire instead of broadside configuration, which is also capable of high directivity. However, due to the finite size of the plate, standing waves occur and the resulting modal behaviour imposes a limitation on the end-fire capabilities of the system, which would otherwise require an infinite surface.

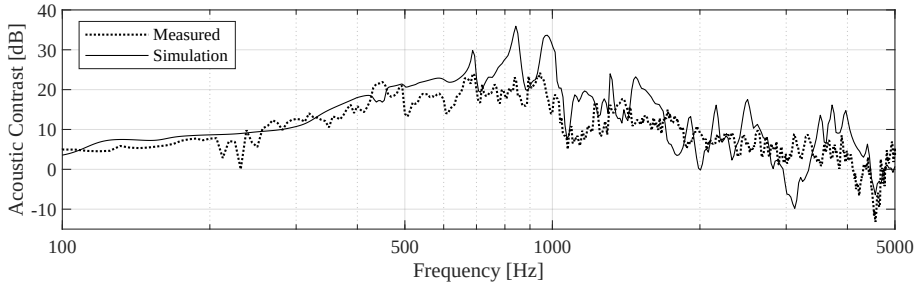

(A) Bright zone aimed in the forward direction.

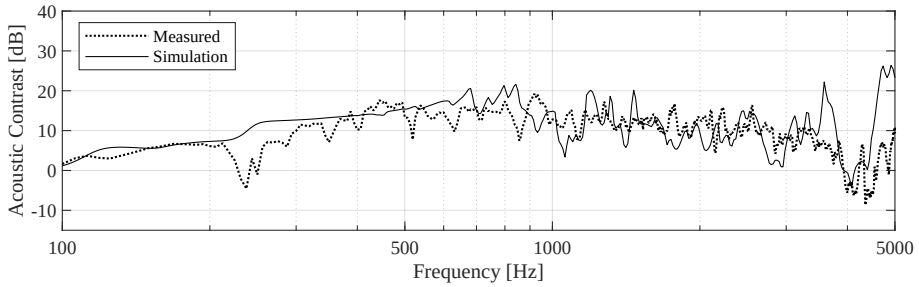

(B) Bright zone steered by 36°.

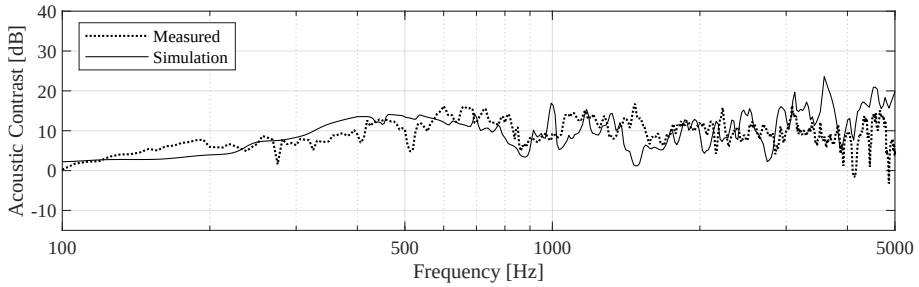

(C) Bright zone steered by 54°.

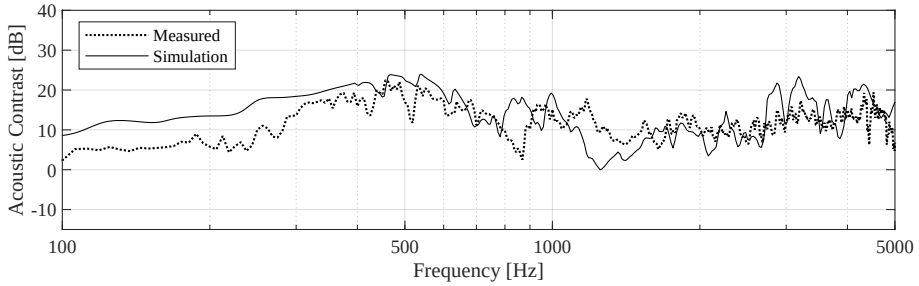

(D) Bright zone steered by 72°.

FIGURE 5.9: Comparison of the acoustic contrast response over frequency between simulations and measurements for a 36° wide bright zone at different steering angles.

5.4 Summary and Conclusions

A prototype system comprising of an aluminium panel mounted within a wooden enclosure, with an array of six inertial actuators was assembled and tested in an anechoic environment. The directivity performance of the system was shown to be frequency dependent, and most effective when steered in the forward direction. Comparison between the measured results and the simulation results originally presented in Chapter 4 indicated that the model provides a useful indication of the expected behaviour of the system within the 400 Hz to 3 kHz frequency range. Inaccuracies between the model and the measurements did occur, however, particularly at lower frequencies, which were due to the infinite baffle assumption used in the model. Other factors were physical characteristics not considered in the model, such as the size and mass of the inertial actuators, as well as the simply supported boundary conditions used in the model. The boundary conditions were also the primary cause of higher frequencies discrepancies in the 3 kHz to 5 kHz range.

Overall, the proposed structural actuator array system has been shown to be capable of radiating a directional sound field. The analytical model presented in Chapter 4 can be used to determine appropriate design parameters for the system to maximize its performance within a desired frequency range, whilst considering practical limitations on panel size and number of actuators.

Chapter 6

Structural Actuator Array: In-Vehicle Implementation

The previous chapter demonstrated that structural vibration can be controlled to produced a directional sound field. The next step in the investigation of the structural actuator array, presented in this chapter, is to investigate if the system is capable of the same performance in its intended role as a vehicle warning sound system. For this purpose, the array was installed on a production vehicle in different configurations, facilitating a series of measurements to determine the optimum configuration for the system and evaluate its performance. The experiments took place in the facilities of Applus+IDIADA in Tarragona, Spain. Experiments and results presented in this chapter have been published as "Investigation of a directional warning sound system for electric vehicles based on structural vibration" in the Journal of the Acoustical Society of America (Kournoutos and Cheer, 2020).

Section 6.1 presents the methodology and set-up for the experiments with the vehicle placed in a semi-anechoic environment. The different configurations of the actuators on the vehicle tested are also shown in detail. The measurements can be separated into four different main studies, which are presented in Sec. 6.2. The first study presented regards the effect that the number of actuators has on the resulting directivity for each of the considered configurations on the vehicle. This is done via a series of off-line estimations performed using the measured responses from each individual actuator used. Next, the directivity performance of the different configurations is evaluated from on-line measurements of the resulting SPL and acoustic contrast. Lastly, the suitability of each configuration is further evaluated by evaluating the resulting sound leakage into the interior of the vehicle.

6.1 Measurement Set-Up

The measurements have been carried out in a semi-anechoic chamber, with fully anechoic walls and ceiling and a concrete floor. The test vehicle was placed in the centre of the chamber, as shown in Fig. 6.1. The directional sound system was integrated into the vehicle by attaching inertial actuators onto its body to form an array. The actuators used (Tectonic Elements TEAX32C20-8) have an individual weight of 150 g, a diameter of 51.2 mm and a nominal rated power of 10 W. The frequency range of the actuators is between 100 Hz and 15 kHz. Up to six actuators are used simultaneously, powered by compact two-channel class D amplifiers (Sure Electronics TPA3110). These actuators are different to the ones used in the experiments presented in Chapter 5, chosen with a higher rated power to ensure that they prove adequate in exciting panels of the vehicle on which they are attached, that may be

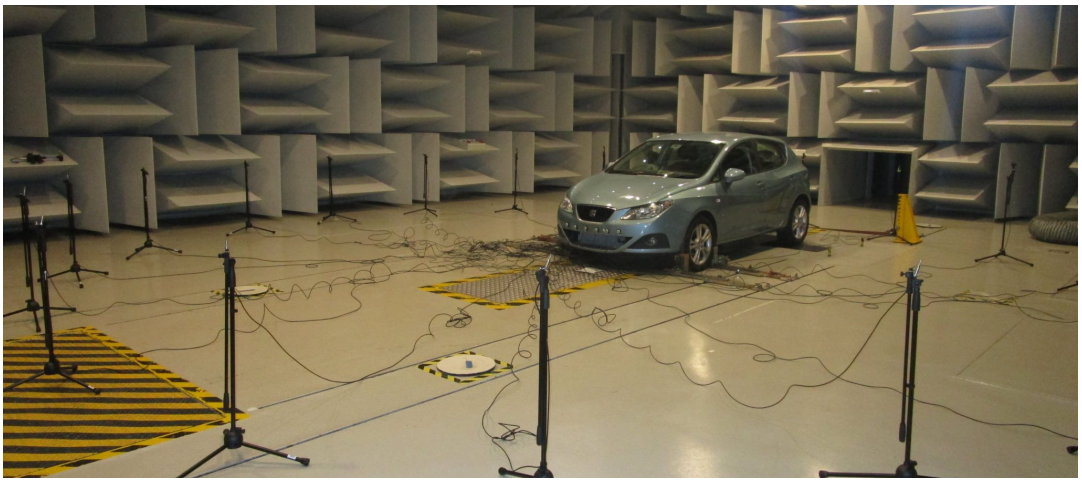

FIGURE 6.1: Test vehicle and measurement set-up in the semianechoic chamber.

characterised by a greater damping. The sound pressure is monitored by a circular array of twenty omnidirectional microphones (PCB 130F20), centred around the front end of the vehicle. The dimensions of the chamber limit the radius of this circle to 5m, and the microphones are placed at a height of 1.2m. Figure 6.1 shows the measurement set-up with the test vehicle in relation to the microphone array. Control of the actuators and data acquisition are both performed by a compact data acquisition system (National Instruments cDAQ-9178).

Control Zones

As mentioned above, the sensor array consists of twenty microphones arranged in a circle to offer 360° of coverage, which means an 18° interval between consecutive microphones. Similarly to the experiments performed using the prototype array in Chapter 5, the width of the bright zones used for the testing of the vehicle configurations is defined by the angle covered by three microphones at a time, making for a width of 36°. Unlike the previous study, the control zones cover the entire plane of travel, with the dark zone defined by the explementary angle of the bright zone. As the prototype investigation intended to compare results with the mathematical model, which was formulated using an infinite baffle hypothesis, only the forward half-plane was considered. At this stage, however, it is important to obtain an overview of the radiated sound field all around the vehicle, as the beamforming is intended to focus on specific vulnerable road users in the potential path of the vehicle.

Figure 6.2 shows the bright and dark zones used to evaluate the directivity at different steering settings, aimed forward, at a 36° angle and at a 72° angle. These three settings are considered in the investigation of the different array configurations on the vehicle which will be presented in the subsequent section.

Investigated Configurations

In order to investigate how effectively different panels on the vehicle can be driven to generate a directional sound field, the actuator array is installed and tested on a number of different components of the vehicle. Figure 6.3 displays the four different configurations that are considered in this study as potential practically realisable

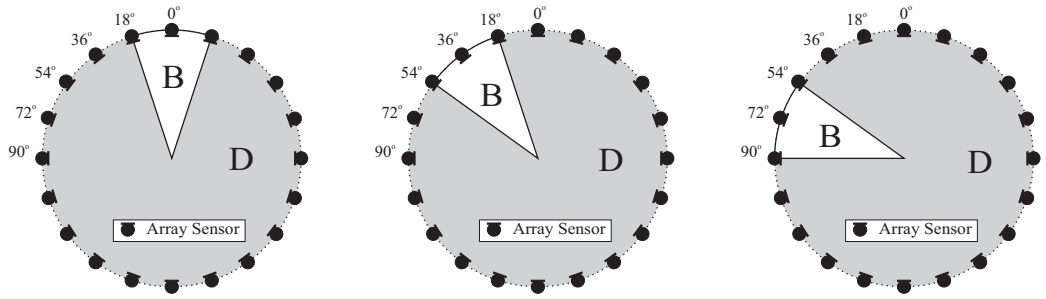

(A) Bright zone in the forward direction.

(B) Bright zone steered by 36°.

(C) Bright zone steered by 72°.

FIGURE 6.2: Directivity control zones used in the experiments.

options. Specifically, the array is placed on the bonnet, the front door, and the front bumper of the vehicle. The spacing between actuators in each case is chosen to ensure the maximum overall array length, based on the findings of the parametric study in Sec. 4.3. As the bonnet offers the largest area available for actuator placement, two configurations are tested: one in a broadside arrangement, with the actuators distributed along the width of the vehicle, as shown in Fig. 6.3a, and one in an end-fire arrangement, shown in Fig. 6.3b, with the distribution of the actuators along its length. The spacing between actuators is 15.6 cm for the broadside, and 13.9 cm for the end-fire case. The door configuration uses only four actuators spaced at 17.8 cm, as shown in Fig. 6.3c, due to limitations on their possible placement imposed by the curvature of the structure. Lastly, a six actuator array is installed along the front bumper of the car, with a 13.7 cm interval between actuators and a 68.5 cm overall length, as shown in Fig. 6.3d. It is worth noting, that for the bonnet and door configurations, the material upon which the actuators are attached is metal, whereas in the case of the bumper the material is plastic.

6.2 Experimental Results

This section will present and comment on the results of the experimental investigation of the actuator-based directional sound generation system. The different configurations are evaluated in terms of directivity performance in conjunction with their efficiency and leakage of noise into the vehicle cabin, through measurements of the resulting sound pressure levels in the interior and exterior of the vehicle. In all measurements, the investigated frequency range over which the system is to be evaluated is between 100 Hz and 5 kHz. This was chosen to cover the bandwidth used by current warning sounds as well as the guidelines on the frequency components of warning sounds set by regulations world-wide NHTSA (2016); UNECE (2017).

Off-line Investigation of Different Configurations

By measuring the response from individual actuators in each of the configurations tested, the information necessary to construct the corresponding transfer response matrices is obtained, as per the process presented in Sec. 5.2. Using this data, the acoustic contrast performance can be estimated off-line for arrays consisting of specific actuator placements, by choosing the appropriate matrices, $\boldsymbol{G}_B$ and $\boldsymbol{G}_D$, to solve Eq. (3.10) and use the resulting optimal source strength vector in Eq. (3.5). This

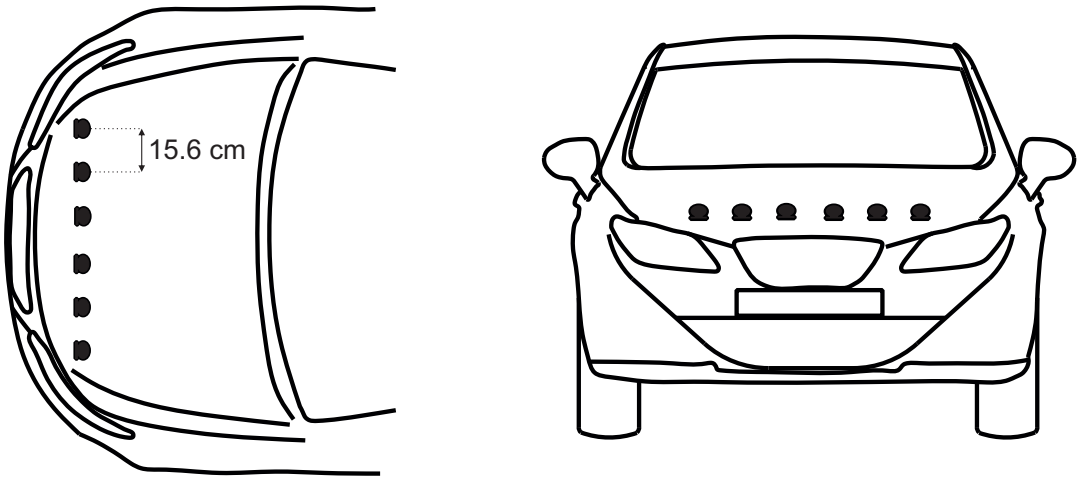

(A) Array on bonnet in broadside configuration.

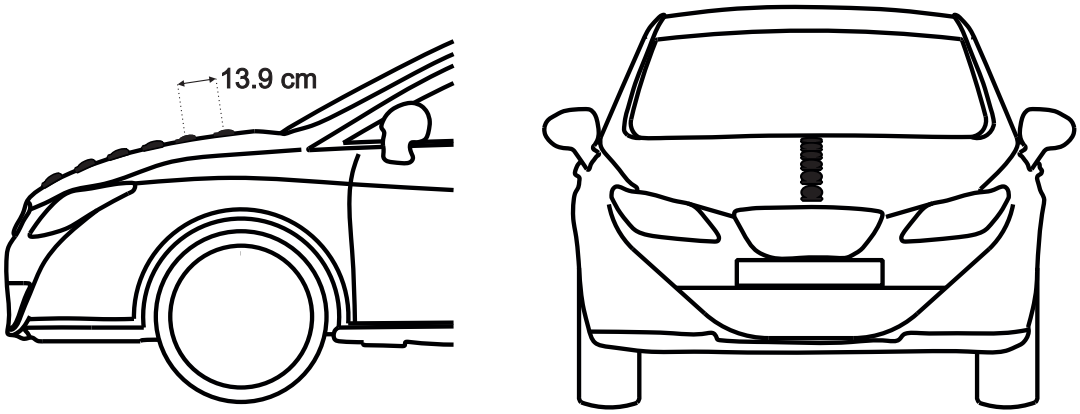

(B) Array on bonnet in endfire configuration.

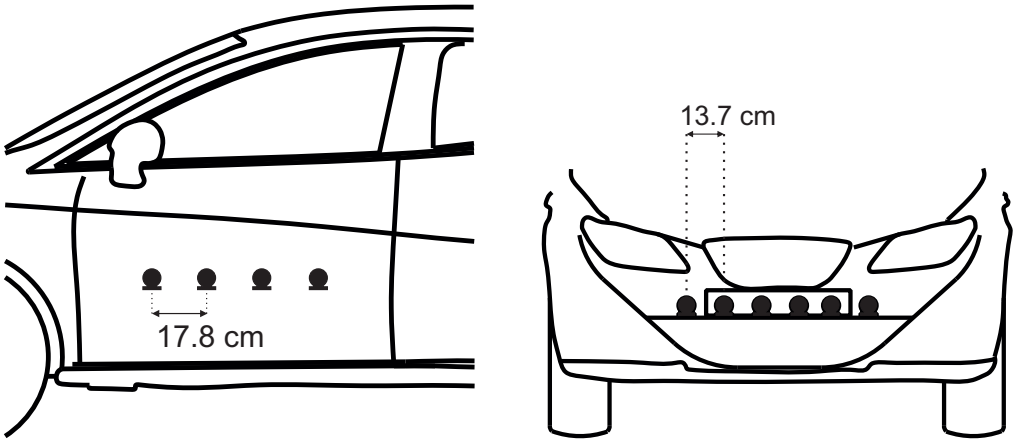

(C) Array on the front door. (D) Array on the front bumper.

FIGURE 6.3: Schematic of the different array configurations tested on the vehicle.

allows for an off-line investigation into the effect that different numbers of actuators in each configuration have on the performance of the system. Figure 6.4 shows the estimated acoustic contrast, frequency averaged between 100 Hz and 5 kHz, for different numbers of actuators in each array configuration tested, for the different steering settings. A trend apparent across all cases is that a higher number of actuators in a configuration guarantees better directivity performance, as expected from understanding the design of loudspeaker arrays, but also from the investigations presented in Chapters 4 and 5, also published in (Kournoutos and Cheer, 2019).

For the forward setting, shown in Fig. 6.4a, the bumper configuration is consistently the most effective out of the four, as it is capable of an average contrast above 10 dB when using four or more actuators. There is little difference between using a broadside or end-fire configuration on the bonnet, with the 10 dB mark only approached marginally when using all six actuators. The door configuration only manages a positive contrast value for four actuators, proving incapable of generating a forward directed sound field. At a steered setting of 36°, as shown by Fig. 6.4b, there is less difference between the performance of the different configurations for the same number of actuators. However, the most effective configuration differs depending on the number of actuators used. The highest level of contrast is achieved by the bumper configuration with 6 actuators.

For the highest considered steering angle of 72°, the door-mounted array becomes the most efficient at achieving the desired directional control with the highest average contrast when compared to all other configurations using the same number of actuators. Specifically, the door-mounted array achieves in excess of 10 dB of broadband averaged contrast when using three and four actuators. The three other configurations all display similar performance at an increased steering, and manage to achieve a broadband averaged contrast of 10 dB when utilising six actuators.

Hybrid Actuator Configurations

Considering that different array configurations provide the highest directivity depending on the bright zone that is used, it might prove useful to investigate a hybrid configuration, which contains actuators in multiple different parts of the vehicle's body. In particular, as the bumper and door arrays achieve the highest average contrast at forward and steered settings (Fig. 6.4), a configuration which includes actuators on the front bumper and on both front doors could be capable of improved performance in all steering settings. Due to limitations on the equipment available during the experiments, this investigation is limited to off-line estimations of the acoustic contrast achievable by these hybrid configurations using the transfer responses obtained from individual actuators.

Figure 6.5 shows the frequency averaged acoustic contrast between 100 Hz and 5 kHz, estimated off-line for arrays which contain four actuators on the front bumper and different numbers of actuators on each door. It is evident that the door actuators are unable to assist the bumper array in forming a sound field maximised in the forward and 36° bright zones. The highest increase is in the order of roughly 0.5 dB on the average contrast, which is achieved by having four actuators on each door. At the 72° setting, the contribution of the door actuators is substantial, though even in this setting, at least three actuators are required to increase the average contrast achieved. This would mean that the system would require at least ten actuators in total, which would lead to an increase of its potential cost, and thus question its viability as an alternative to other directional systems.

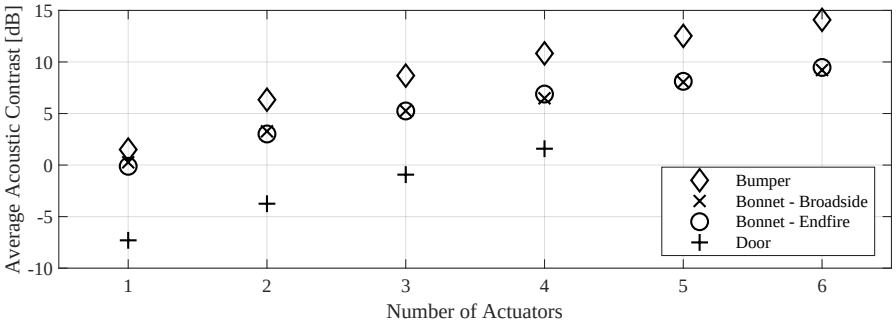

(A) Bright zone in the forward direction.

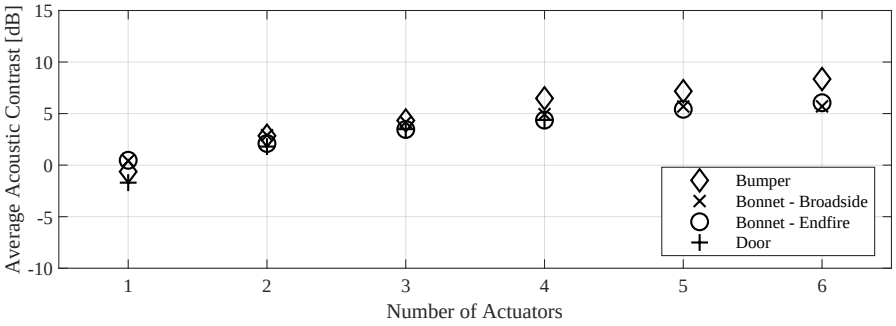

(B) Bright zone steered by 36°.

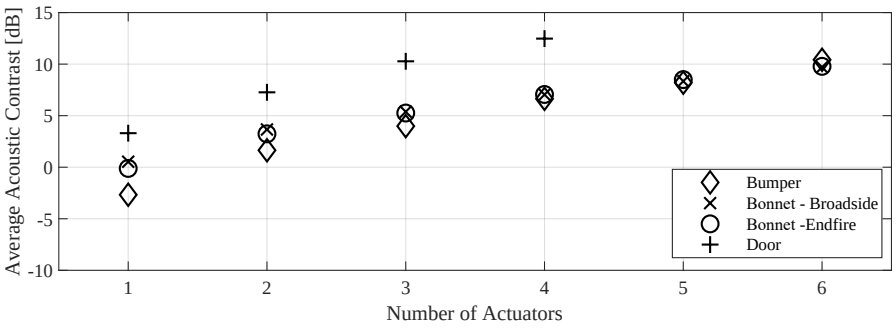

(C) Bright zone steered by 72°.

FIGURE 6.4: Frequency averaged acoustic contrast between 100 Hz and 5 kHz, as estimated for different array configuration.

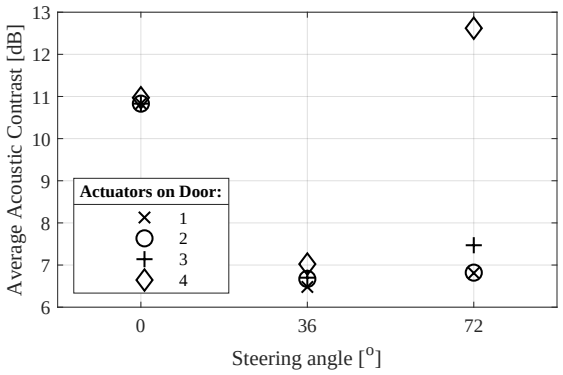

FIGURE 6.5: Off-line estimation of the frequency averaged acoustic contrast between 100 Hz and 5 kHz achieved at different bright zone steering settings, for arrays using four actuators on the front bumper and a varying number of actuators on each front door.

Overall, from the results shown in Figs. 6.4 and 6.5, it can be concluded that the mixed actuator distribution proves relatively inefficient, as installing the same overall number of actuators on the front bumper of the vehicle leads to better directivity performance. Although the hybrid array can display an advantage for highly steered bright zones, it requires at least four actuators on each door to achieve this, and this performance is inconsistent when compared to the contrast achieved at other steering settings.

On-line Measurements: Sound Pressure Levels

With the off-line investigation offering a view of the potential performance for each array configuration, and its dependence on the number of actuators used, the next part of the study is to evaluate the system via a series of on-line measurements. This is done by driving the array using the optimal filters to produce a directional sound field in the semi-anechoic chamber, and obtaining the resulting sound pressure measured from the microphone array. As the off-line results show that a higher acoustic contrast is achieved by a greater number of actuators in the array across all configurations, the on-line measurements are performed using the maximum number of actuators available in each case, which is four for the door-mounted array and six for the rest of the positions. Similar to the experiments presented in Chapter 5, each configuration has been optimised to generate an A-weighted overall SPL of 60 dB without noticeable distortion within the investigated frequency range, in line with the standards set by (UNECE, 2017).

The resulting directivity is shown in Fig. 6.6. The measured SPL resulting from each investigated configuration is displayed, normalised and frequency averaged between 100 Hz and 5 kHz. The results of different steering angle settings, controlled through the optimal filter implementation are displayed separately. Microphone positions are indicated by dots and the extent of the bright zone used in each cases corresponds to the shaded area. It can be seen that the bumper array is capable of the highest forward directivity with an SPL at least 10 dB higher in the bright zone than in the dark zone. A considerable degree of directivity is achieved at both the 36° and 72° steering angle settings, with the bright zone in both cases also approaching an SPL higher by 10 dB than the dark zone. Conversely, the door configuration appears only capable of producing a directional sound field, characterised by an SPL in the bright zone higher by 10 dB, at the 72° steering angle setting. Both bonnet configurations display comparable performance to the bumper array at steered settings, however, their forward directivity is noticeably lower.

On-line Measurements: Acoustic Contrast

A better understanding of the performance of the system can be obtained by investigating its directivity across frequency. This is most efficiently done by calculating the acoustic contrast frequency response of each configuration. Figure 6.7 shows the acoustic contrast across frequency, calculated from the measured sound pressure resulting from each array configuration, at the different steering angle settings.

Both bonnet-mounted arrays display a similar performance, shown in Figs. 6.7a and 6.7b, which is relatively stable at a level of about 10 dB. The inability of the door configuration to produce a forward directed sound field is visible in Fig. 6.7c, where the level of the acoustic contrast for the forward setting is in the negative values for a number of frequencies between 500 Hz and 3 kHz. This configuration is, however, capable of the highest acoustic contrast level at both steered settings,

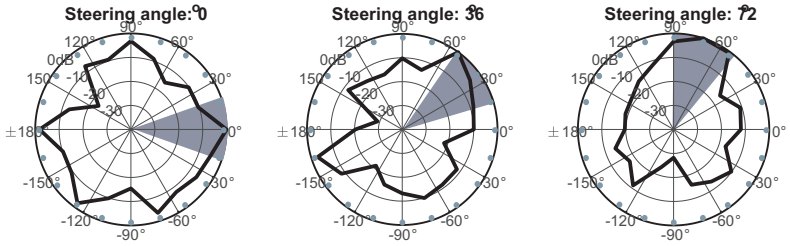

(A) Array on bonnet in broadside configuration.

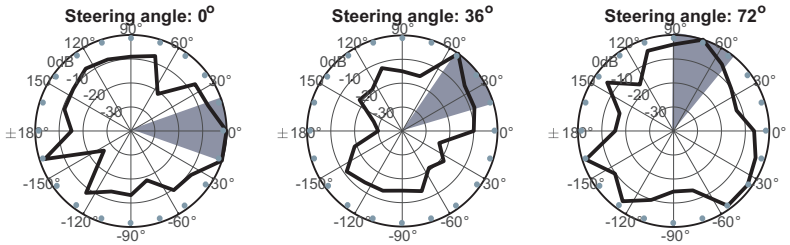

(B) Array on bonnet in endfire configuration.

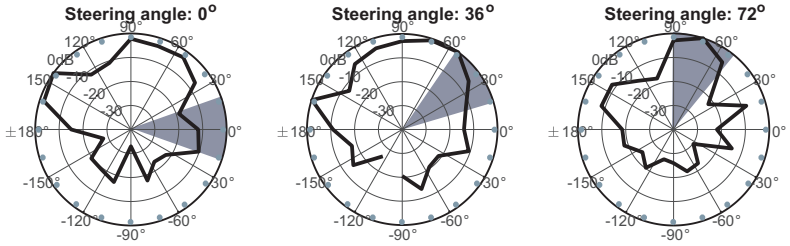

(C) Array on the front door.

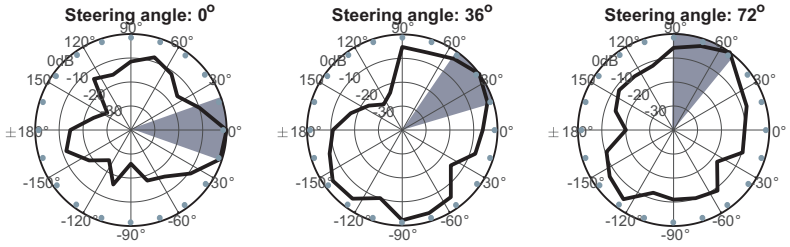

(D) Array on the front bumper.

FIGURE 6.6: Directivity patterns at steering angle settings in the forward direction and angles of 36° and 72°, from different configurations. The normalised SPL displayed has been frequency averaged between 100 Hz and 5 kHz.

exceeding the 10 dB mark for most of the investigated frequencies. The response of the bumper array displays the greatest frequency dependence. At frequencies below 200 Hz, this configuration appears to be incapable of producing a directional sound field towards a designated bright zone. The array becomes directional above 200 Hz, and proves capable of producing an acoustic contrast of over 10 dB in level. In particular, this performance reaches 20 dB in acoustic contrast level within the 1 kHz to 2 kHz range, for the forward and 36° settings. The achieved level drops at the higher steering angle of 72° to 10 dB, similar to that of the bonnet configurations. This is due to the natural directivity of the bumper being in the forward direction.

The average contrast achieved within the 300 Hz to 5 kHz bandwidth for the bumper configuration is consistently above 10 dB, which is comparable to the performance of loudspeaker-based systems (Quinn et al., 2014). This bandwidth sufficiently covers the frequency requirements set by regulations (NHTSA, 2016), with the exception of the 160 Hz and 200 Hz one-third octave bands allowed by ECE (UN-ECE, 2017), within which the system is not sufficiently directional. However, these low frequency bands are generally not opted for in the design of warning sounds, as documented AVAS-compliant sounds in current use (Konet et al., 2011) do not typically contain frequency components below the 315 Hz third-octave band. Therefore, the bandwidth offered by the actuator array can be considered sufficient to accommodate the components of an AVAS sound, including the shifts in frequency that are used to simulate acceleration of the vehicle.

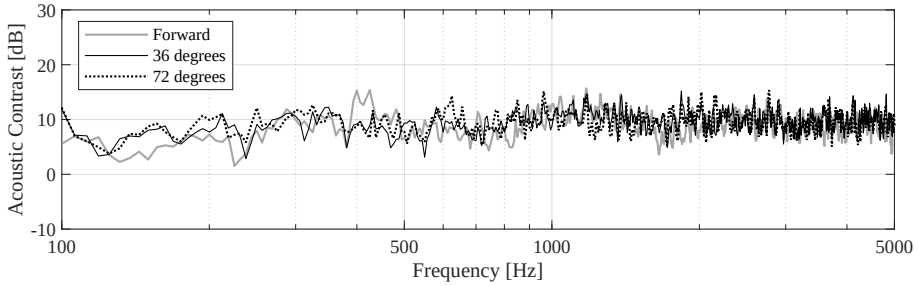

(A) Array on bonnet in broadside configuration.

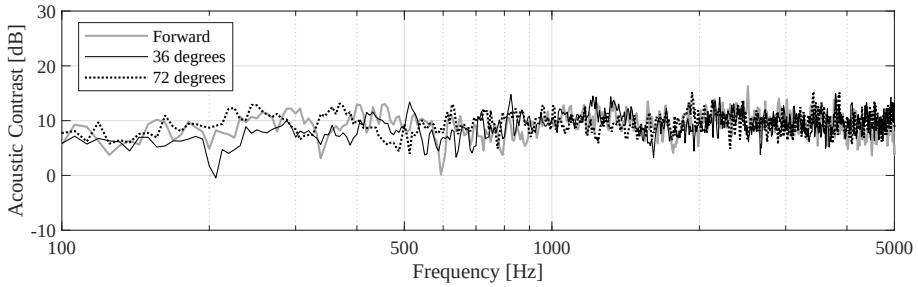

(B) Array on bonnet in endfire configuration.

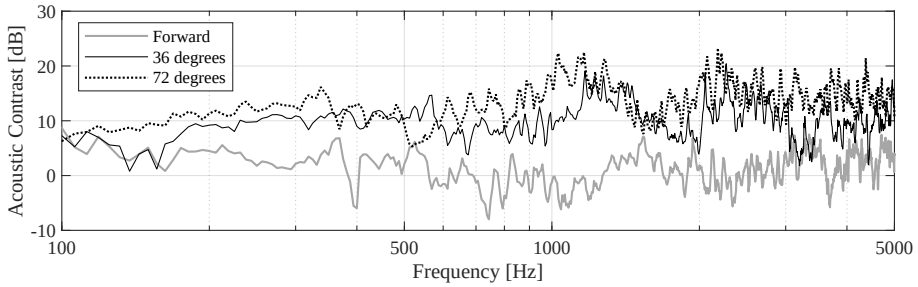

(C) Array on the front door.

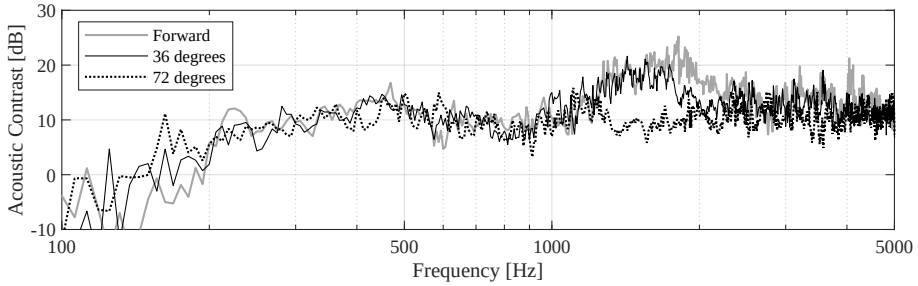

(D) Array on the front bumper.

FIGURE 6.7: Acoustic contrast frequency response for steering settings directed forward and at angles of 36° and 72°, as resulting using different array configurations.

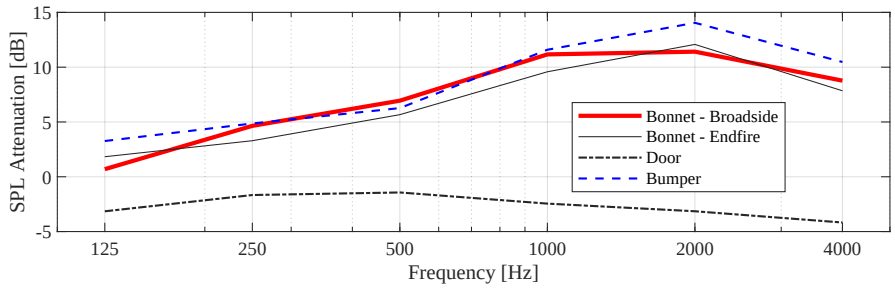

FIGURE 6.8: Attenuation of generated SPL between an external point and in the vehicle cabin, for the different array configurations tested on the vehicle. In all cases the array has been driven for a forward-facing bright zone.

Sound Leakage into the Vehicle Interior

Another factor that is key to evaluating the suitability of the proposed system for practical implementation, and can be readily investigated in this study, is the separation between the resulting external and internal sound fields. The system is intended to convey a warning sound to vulnerable road users in the path of the vehicle, but it should not be intrusive to the driver and passengers. Therefore, it is important to ensure that the sound radiated from the rear of the structural actuator array into the car cabin is sufficiently attenuated by the construction of the vehicle. If this is not the case, then it may be necessary to modify the construction of the vehicle to provide higher levels of attenuation or utilise more complex array designs that minimise the sound radiated from the rear of the panel. However, both of these measures will clearly increase the cost of implementation and, therefore, the appeal of the proposed system.

Figure 6.8 provides insight into the sound leakage into the vehicle cabin in the form of the attenuation achieved across frequency for the different configurations, when they are all steered towards the forward direction. The level of attenuation across frequency is defined in this instance as the difference in level between the SPL in each frequency bin measured by a microphone placed at the driver's car seat headrest and the SPL measured at a microphone placed 5 m in front of the vehicle, defining the centre of the bright zone. Furthermore, the calculated attenuation has been scaled using octave bands to provide a convenience of comparison, as the frequency response would normally be characterised by peaks and notches that may be caused by ground reflection and car-body diffraction effects. It is evident that the bumper configuration displays the highest level of attenuation between the externally and internally generated sound pressures. This is probably due to the presence of the engine compartment between the array and the cabin and the significant levels of attenuation that this provides. For both bonnet configurations, the attenuation achieved approaches a level of around 10 dB at frequencies above 1 kHz, however, it is significantly lower at lower frequencies. The results obtained for the door configuration indicate that the placement of the array on the door results in similar sound levels at the target exterior position and in the interior of the vehicle. The lack of attenuation between the door panel vibration and the interior sound field is perhaps not surprising, given the lightweight nature of modern vehicles and the low levels of noise transmission loss typically required through the door panel. This fact also constitutes a further reason on why a hybrid configuration employing actuators on the doors of the vehicle would be unsuitable.

6.3 Summary and Conclusions

This chapter presented the experimental evaluation of the structural actuator array installed on a vehicle and utilising the vibration of the vehicle's body to radiate a directionally controllable sound field. The proposed system was physically evaluated by installing the actuator array in a test vehicle and performing measurements in a semi-anechoic environment. Control over the directivity of the array was achieved through the implementation of filter sets corresponding to different steering angles, constructed using the acoustic contrast maximisation process.

Different arrangements of the actuator arrays on the vehicle were tested to obtain guidance into the most efficient placement for such a system. An off-line study first provided insights into the effect that the number of actuators in the array has on the system performance. The directivity performance was then evaluated through on-line measurements in the semi-anechoic chamber. Examining the frequency averaged directivity patterns and calculating the acoustic contrast across the investigated frequency spectrum provided an in-depth view of the capabilities of each configuration. In addition to the directivity investigation, the level of sound leakage from the array into the vehicle cabin was considered to determine the suitability of the system.

Overall, a six-actuator array positioned on the front bumper was shown to provide the overall best performance out of the configurations tested. Measurements of the real-time performance of this bumper array showed that the system can be successfully controlled to focus its radiated sound field towards the defined bright zones, maintaining an acoustic contrast level of over 10 dB throughout the 300 Hz to 5 kHz frequency range. In addition, its position on the bumper of the vehicle ensures the least amount of leakage to the cabin, making it the most appropriate for a practical implementation of the system. When compared to the published results from the loudspeaker-based eVADER system (Quinn et al., 2014), shown in Fig. 2.18, the investigated system demonstrates a comparable performance. Though the beamforming in eVADER is focussed on a narrower target zone, the structural actuator array is generally capable of the same 10 dB level of contrast between its defined bright and dark zones at different steering settings. Combining this performance with the potential for a cost-efficient integration in the vehicle, and its increased robustness, the proposed structural actuator array constitutes a viable solution for a directional warning sound system.

Chapter 7

Environmentally Adaptive Warning Sound System

This chapter presents a complementary approach to achieving both detectability and pass-by noise minimisation. The proposed method of minimising the generated pass-by noise whilst still ensuring that the system conveys the required auditory warning, is to adapt the warning sound itself so that it is rendered as audible as necessary, given the potentially changing sonic environment. Through a full implementation of the proposed system, it may be possible to modify not only the level, but also the spectral content of the warning sound, taking into account the masking effects stemming from the environmental noise. Such a system can be used in conjunction with a directional system, such as the structural actuator array presented previously, or with more basic warning sound emitters.

Section 7.1 provides an introduction to the concepts presented in this chapter, addressing issues with current implementations of adaptive warning sound systems, and providing a brief overview of auditory masking, upon which the operation of the proposed adaptive system is based. The design of the proposed system and its principles of operation are presented in Sec. 7.2. This section includes a description of the different stages of processing for the input signals, and the methods used to estimate the audibility thresholds and to accordingly adapt the warning sound. Section 7.3 presents results from the implementation of the adaptive system using pre-recorded samples of environmental noise. Finally, a methodology for the evaluation of the effectiveness of the adaptive system is proposed in Sec. 7.4.

7.1 Warning sounds and auditory masking

The research presented in this thesis has, up to this point, approached the task of conveying an auditory warning to vulnerable road users while minimising environmental noise emissions through the control of the spatial characteristics of the sound field. An alternative approach is to adapt the warning sound itself depending on the current environmental noise, to ensure that it is rendered detectable without being unnecessarily loud in any situation. Such solutions have been partly investigated in the past (Berge and Haukland, 2019b,a), as mentioned in Sec. 2.5; however, despite the inclusion of such features even in the eVADER system (Quinn et al., 2014), a thorough documentation of the algorithms behind these systems has not been presented in published research.

Moreover, the adaptation of the warning sound in these existing implementations is performed via adjustment of its overall level relative to that of the environmental noise. This means that the distinct tonal and narrow band components that comprise the warning sound are uniformly amplified or attenuated, to a level that is

determined by the overall level of the background noise. An important factor in the perception of an auditory stimulus that is not considered in this overall level adaptation process is the *masking* of frequency components by existing noise that may or may not exceed them in level within the respective frequency band.

Auditory masking refers to the perception of a sound being affected by the presence of another sound, which may not necessarily be of the same frequency, time occurrence or pressure level. The term *simultaneous masking* or *spectral masking* is used when the simultaneous sounding of a *masker*, which may be a broad band noise or a tone, prevents another sound to be perceived by the human auditory system. Masking can be total or partial, depending on the degree to which the masked sound remains audible. The masked threshold is the SPL of a test sound necessary to be just audible in the presence of a masker, and is generally above the threshold in quiet, although it may be equal to the threshold in quiet when the frequencies of masker and test sound are very different (Fastl and Zwicker, 2007).

Masking is directly linked with loudness, the attribute of auditory sensation in terms of which sounds can be ordered on a scale extending from quiet to loud (ANSI, 1973). Loudness perception is related to sound pressure level, frequency and the duration of a sound, with the sensitivity of the human ear changing as a function of frequency. Likewise, the quietest level of a signal perceived when combined with a masker, defined as the masking threshold, varies with frequency. Figure 7.1 shows examples of simultaneous masking either by broad band (a) or critical band white noise (b). In the first case it is shown how higher frequencies are more obscured by a broad band masker of a specific level; in particular, an increase in the threshold by 10 dB per frequency decade is visible above 1 kHz. The second case illustrates how a critical band masker noise can affect the perception of nearby frequencies, and how that behaviour changes depending on the frequencies of the masker and the masked sound.

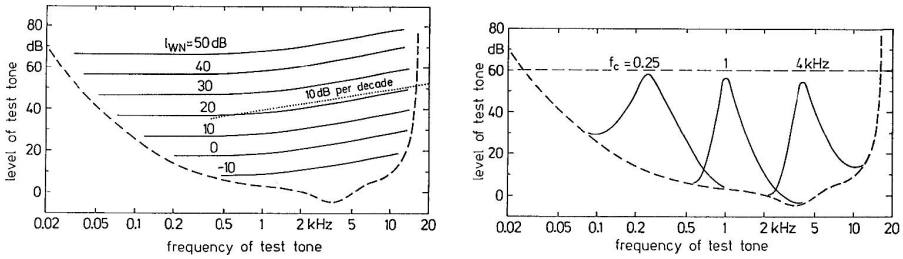

(A) Masking of test tone by white noise.

(B) Masking of test tone by critical band wide noise.

FIGURE 7.1: Level of test tone just masked by white noise of density level I_{WN} (a), and by critical band wide noise with a level of 60 dB and centre frequencies of 0.25, 1, and 4 kHz (b). The dashed curve indicates the threshold in quiet (Fastl and Zwicker, 2007).

As mentioned above, two sounds need not be of the same frequency in order to cause perceptual interference. Auditory filters inside the human ear can distinguish one sound from the other, however, when the difference in frequency between two tones becomes less than a critical bandwidth, they become perceived as a single noise. Apart from simultaneous masking, a type of auditory masking exists named *temporal* or *non-simultaneous* masking. This occurs when the audibility of a sound is affected by a masker that occurs immediately before or after the sound of interest. Masking is indicative of the limits of frequency distinction that the auditory system

can perform. Experimentation with conditions under which a sound masks an otherwise audible signal can be used to test the frequency sensitivity of the auditory system (Moore, 1998).

Auditory masking has been known as a concept, and research on it has been carried out as far back as 1924(Wegel and Lane, 1924). The majority of research on the understanding of this process has been to investigate its impact in the perception of sounds and particularly intelligibility of speech (Hawkins Jr and Stevens, 1950), with more recent work incorporating auditory masking in the study of speech enhancement technologies (Hansen et al., 2006). Masking effects have also been investigated in the context of applications such as sound quality in digital audio coding (Ambikairajah et al., 1997), and, perhaps more related to the subject of this thesis, the prospect of utilising this process to mask unwanted sounds in urban environments (Nilsson et al., 2010).

Among the findings of this last study was that the noise of traffic appears to be a particularly effective masker of harmonic and narrow band sounds, which indicates that the perceptibility of warning sounds might be greatly dependent on auditory masking. The surveys on the perception of EV warning sounds that were presented in Secs. 2.4 and 2.5 evaluated the different sounds in various environments for their effectiveness through subjective criteria. In this context, so far it has only been the study of Lee (Lee et al., 2017) that has considered the effects of auditory masking in a similar evaluation, offering an objective criterion in the assessment of how detectable a warning sound can be when put to actual use. It is therefore worth investigating the utilisation of an auditory masking model when it comes to rendering a warning sound effective, while minimising its contribution to the perceived levels of noise, in a varying environment.

7.2 Overview of the Proposed System

As addressed in the previous section, the algorithms employed in the environmental adaptation of warning sounds so far do not explicitly account for the effects of auditory masking, or any other factors affecting the perceptibility of sounds across the frequency spectrum. This suggests that there remains potential for substantial improvement in the development of such sound adaptation algorithms.

A system can be conceptualised that is capable of performing an adaptation not only of the level, but the spectral content of a warning sound in order to render it audible in any environment, without producing an unnecessarily high level of noise at any frequency band. If, for example, the vehicle were travelling in a quiet rural setting, it would be sufficient for the the warning sound level to be minimal, whereas if the vehicle were driving in a noisy city centre, it would be necessary to amplify the warning sound in order to overcome the existing background noise. One thing to note about this function is that the level of the adaptation would have to be bounded, so that the level of the warning sound does not increase without limitation, which would be particularly relevant in a setting containing multiple EVs equipped with similar warning sounds.

Such an algorithm could by itself constitute an independent solution to the issue of balancing detectability with minimisation of noise emissions, or could readily be used in conjunction with the structural actuator array presented in the previous chapters, or any other directional sound source, in order to maximise the efficiency and effectiveness of the warning sound system. This section aims to present an

overview of the general operation of the proposed system, from the physical components required to the signal processing stages and the implementation of a masking model for the calculation of the audibility thresholds.

7.2.1 Principle of operation

An environmentally adaptive warning sound system should, as its primary principle, be able to analyse the sonic environment that the EV finds itself in, and make modifications to the warning sound that is to be emitted according to the information it has gathered. The envisioned adaptive system would thus require components to monitor the sonic environment, to perform the necessary signal processing, and finally to radiate the warning sound appropriately. Figure 7.2 illustrates the principal sequence that this system follows from receiver, to the processing and finally to the warning sound emitter. In detail these are:

- A sound receiver, which could be a single microphone or an array thereof, either dedicated solely to the warning sound system, or possibly doubling up as a component of a different vehicle system. The receiver should be able to detect environmental noise successfully without being affected by factors such as wind due to the speed of the vehicle; this may require careful acoustical design or additional signal processing, however, this will not be considered here.
- The hardware and software necessary to process the signal(s) from the receiver(s) to estimate the precise level and, with an array, the directionality of the environmental noise, determine the audibility thresholds and adapt the gain equalisation of the warning sound so that it is appropriately audible.
- A sound emitter for the emission of the warning sound; this could potentially be a single loudspeaker, the structural actuator array or one of the directional systems mentioned in Chapter 3, or a different kind of sound source deemed suitable for use.

Additional elements such as cameras and GPS trackers could be used to obtain detailed information on the location of noise sources and of vulnerable road users, which can in turn be considered during the process of warning sound adaptation. The proposed adaptive system can operate in conjunction with such systems to achieve a more finely tuned result, but the essential components necessary for its function remain the three listed above.

Figure 7.3 illustrates the principles of operation for the proposed system through a processing block diagram. The symbols used in the diagram to denote sound pressures and signals are listed in Table 7.1. The function of the system is intended to follow this sequence:

1. The receiver measures an overall pressure, which corresponds to the environmental noise, p_{Er}, plus the warning sound, p_{Wr}, emitted from the vehicle, as measured at its location, and sends the signal to the **Signal Processing Block**.
2. The estimated warning sound component at the receiver, $\hat{p}_{Wr}$, is then subtracted from the received signal in order to isolate the signal corresponding to the environmental noise, $\hat{p}_{Er}$.
3. Further processing can be performed at this stage to estimate the environmental noise level, $\hat{p}_{Ep}$, and the level of the warning sound, $\hat{p}_{Wp}$, at the position of the intended target (a pedestrian or other vulnerable road user).

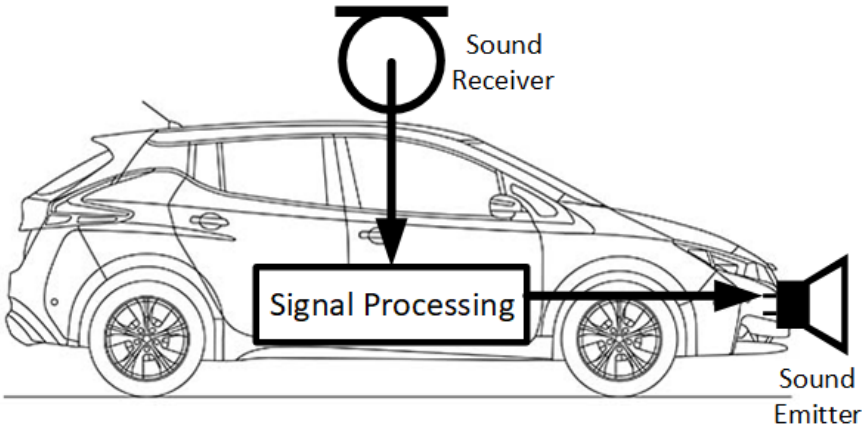

FIGURE 7.2: Diagram of the basic implementation principle of the adaptive system in an EV.

4. The above signal is then sent to the **Warning Sound Adaptation Block**. Here, thresholds of audibility due to the ambient wide band background noise, $\hat{p}_{Ep}$, are estimated using a masking model algorithm, and are compared to $\hat{p}_{Wp}$. The base warning sound, s_W, is adapted using the information obtained from the masking model, by adjusting the amplitude of its frequency components so that it will be rendered appropriately audible at the position of the target.

5. The adapted warning sound signal, $\tilde{s}_W$, is then simultaneously sent to the emitter and to be processed further:

   (a) The emitter receives the signal $\tilde{s}_W$ from the processing block, and produces the sound output.

   (b) At the same time, the transfer function corresponding to an estimate of the path from emitter to receiver is applied to $\tilde{s}_W$ so that it may be subtracted as the warning sound component, $\hat{p}_{Wr}$, from the overall input signal, $\hat{p}_{Er} + \hat{p}_{Wr}$.

Symbol	Content
p_{En}	Environmental SPL at location of its source
p_{Er}	Environmental SPL at receiver location
p_{We}	Warning SPL at emitter location
p_{Wr}	Warning SPL at receiver location
$\hat{p}_{Ep}$	Estimated environmental SPL at pedestrian location
$\hat{p}_{Er}$	Estimated environmental SPL at receiver location
$\hat{p}_{Wp}$	Estimated warning SPL at pedestrian location
$\hat{p}_{Wr}$	Estimated warning SPL at receiver location
s_W	Base warning sound signal
$\tilde{s}_W$	Adapted warning sound signal

TABLE 7.1: Nomenclature for the block diagram (Figure 7.3) of the proposed adaptive sound system.

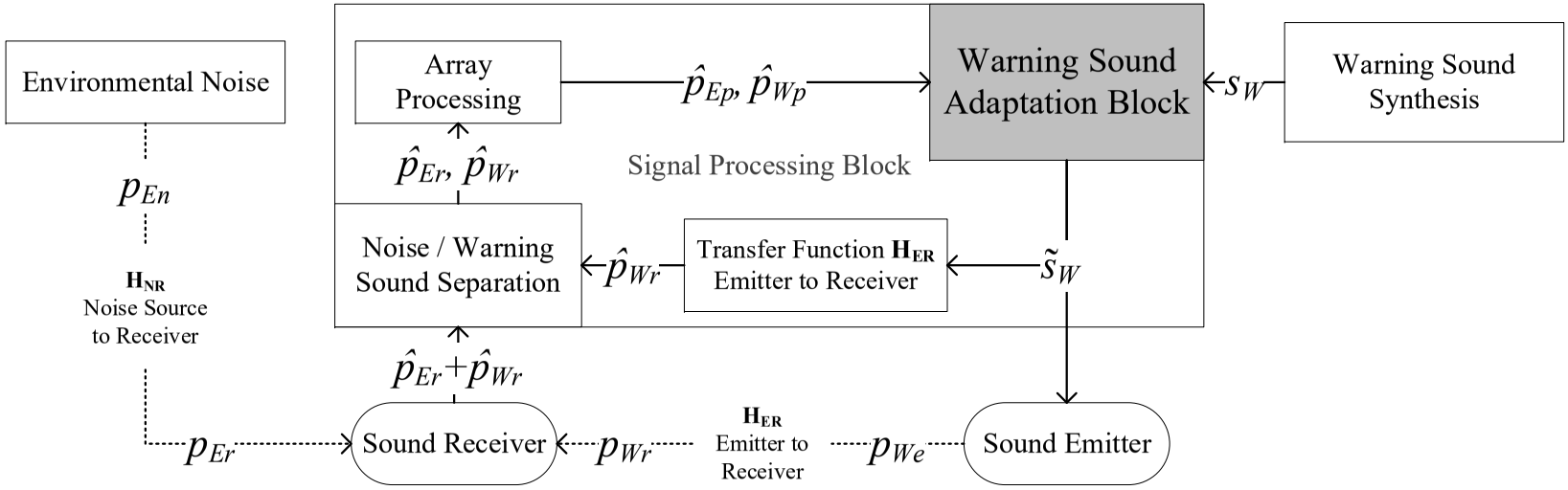

FIGURE 7.3: Block diagram of the adaptive system concept.

7.2.2 Signal processing block

The processing block in Fig: 7.3 contains all of the signal processing that is to be performed by the system, from the initial stage where an input signal is sent from the receiver, to the final stage when the output signal is sent to the emitter. Within this block are defined an inner processing stage, noted as the warning sound adaptation block in Fig. 7.3, where the sound adaptation takes place, and a peripheral stage, which includes all of the processing operations that the signals go through; these processing stages will be explained in the following subsections.

Separation of input signals

As described in the above section, and illustrated in Figure 7.3, the input to the system is the signal measured by the receiver that contains all information related to the acoustic environment. This comprises of the environmental noise, p_{Er}, plus the warning sound produced by the vehicle itself, p_{Wr}.

In order to calculate the audibility thresholds for the current environmental noise, it is therefore necessary to first remove the part of the signal which contains the warning sound. As the warning sound is generated directly by the system, its spectral content is fully known and, therefore, can be subtracted from the measured pressure. However, the warning sound, p_{Wr}, at the location of the receiver will differ from that at the location of the emitter, p_{We}, and this difference can be accounted for by the transfer function, H_{er}, corresponding to the path between the emitter and the receiver. It is possible to compensate for this path by calculating an estimate of its response, as

$$\hat{p}_{Er} = [p_{Er} + p_{Wr}] - H_{er} s_W. \tag{7.1}$$

Array processing

After the subtraction of the warning sound component from the signal measured by the receiver, it is assumed that the remaining signal contains an estimate of the environmental noise levels at the location of the receiver, $\hat{p}_{Er}$. If a receiver capable of detecting directional information on the aspects of the environmental noise is used, a more accurate estimate can be calculated. These estimates, however, still differ from the environmental noise level as perceived by the pedestrian, represented by a signal $\hat{p}_{Ep}$. An additional transfer function, H_{rp}, would therefore be necessary, to estimate the environmental noise at the pedestrian location through the acquired information at the location of the receiver, obtained through the relation

$$\hat{p}_{Ep} = H_{rp} \hat{p}_{Er}. \tag{7.2}$$

Depending on the type of the sound receiver used by the system, i.e. a single microphone or a microphone array, as well as the system used for the detection of vulnerable road users, methods of varying accuracy and complexity are possible to provide the required estimation.

7.2.3 Warning sound adaptation block

The key component of the adaptive warning sound system is the warning sound adaptation block, which is responsible for the audibility evaluation of the warning sound in the current sonic environment, and its respective adaptation. The block consists of a masking model algorithm which is used to calculate the audibility

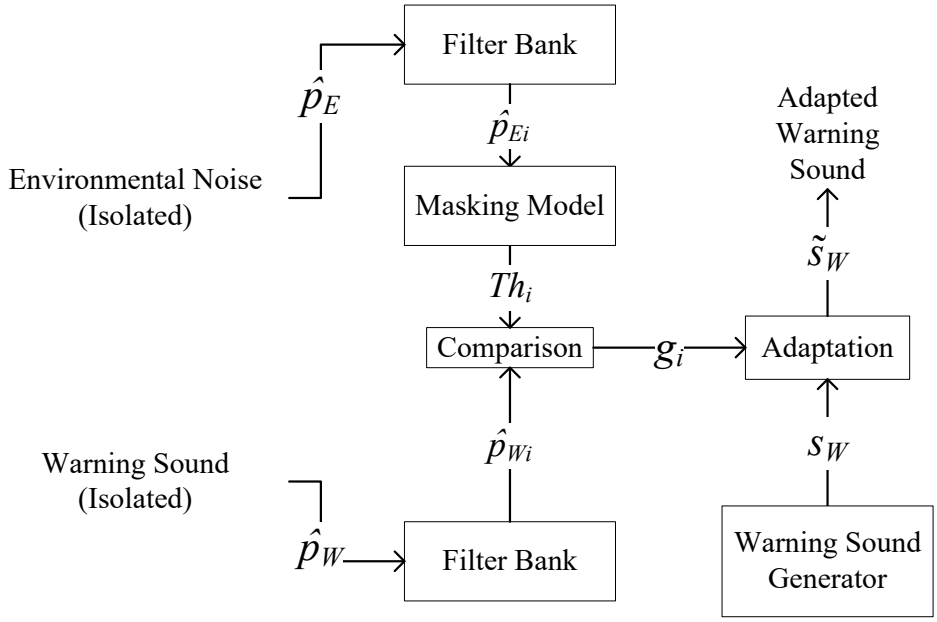

FIGURE 7.4: Block diagram of the generalised processes in the adaptation block.

thresholds for a given environmental noise, a process for the comparison of these thresholds with the levels of the warning sound, and a gain equalisation process which modifies the warning sound so that it is rendered appropriately audible.

Audibility thresholds

Figure 7.4 shows the processes that are performed in the adaptation block. The input signals $\hat{p}_E$ and $\hat{p}_W$ are the estimates of the environmental noise and the warning sound, isolated from one another, and, provided that the sound receiver configuration on the system allows it, estimated at the location of the pedestrian. As the purpose of the algorithm is to perform a frequency specific evaluation and adaptation, a filter bank of I filters is implemented on either signal, to provide an estimation of their level, $\hat{p}_{Ei}$ and $\hat{p}_{Wi}$, at each frequency band. The masking model is then implemented using the values of $\hat{p}_{Ei}$, to determine the levels that correspond to the audibility threshold for each respective frequency band, Th_i. These values are then used in conjunction with the level of the warning sound in each investigated band, $\hat{p}_{Wi}$, to indicate which frequency components of the warning sound need to be attenuated or amplified.

Gain adaptation

The comparison of $\hat{p}_{Wi}$ and Th_i allows for the calculation of the gain coefficients that need to be implemented to the base warning sound. There are two methods for achieving this under investigation for the development of the proposed system.

The first method assumes that the warning sound generator is semi-independent of the adaptation algorithm. In such a case, which is the one depicted in Fig. 7.4, the base warning sound is treated as an additional input signal, s_W. As the comparison

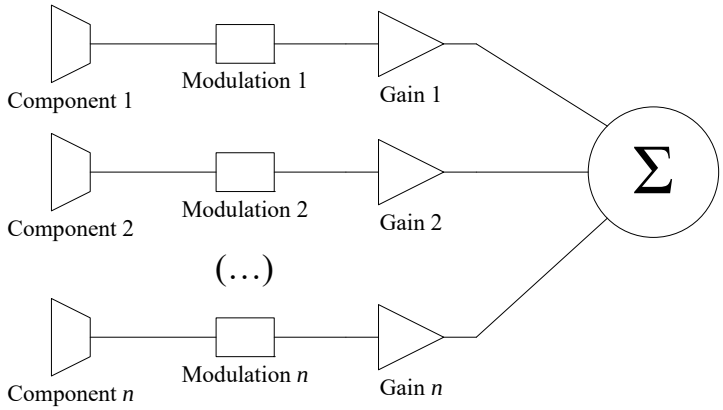

FIGURE 7.5: Diagram of the warning sound synthesis and integrated gain equalisation process. This example illustrates a warning sound comprised of n frequency components, each being separately modulated before having its gain adjusted and subsequently added together to generate the signal.

between the warning sound and the audibility threshold levels occurs over a number of i frequency bands, the result is I different gain coefficients, g_i, each corresponding to a specific frequency band. These gain coefficients indicate whether the level of the warning sound in a frequency band requires attenuation or amplification. The adaptation of the base warning sound is thus realised by filtering the signal s_W using the same filter bank as in the previous step, and implementing the values g_i within each respective band. Such a method allows the adaptation algorithm to operate independently of the warning sound generation method, and can therefore be utilised to test the system using a variety of warning sounds. A drawback however, is that the additional filtering process might lead to an increased computational complexity.

The second method would require the warning sound synthesis stage to be integrated into the adaptation algorithm. In such a configuration, the different frequency components of a warning sound would first be generated and have any modulation implemented like in any other instance, but the gain equalisation process would come before they are summed together to generate a uniform signal. Figure 7.5 illustrates this process for a hypothetical warning sound of n individually modulated frequency components. As the number of warning sound frequency components in this case does not necessarily coincide with the frequency bands over which the audibility thresholds are estimated, upon comparison of Th_i and $\hat{p}_{Wi}$, the algorithm must include a process to calculate n gain values to be used in the warning sound synthesis. Properties such as bandwidth and modulation, that characterise each frequency component of the warning sound need to be considered when calculating these gain values, in order for them to effectively determine the resulting level as intended. This approach would thus require the system to be designed and calibrated for a specific warning sound, making for a more efficient adaptation process, but would not allow for flexibility in choosing from a variety of warning sounds.

7.3 Simulation based application study

This section presents an investigation into the application of the proposed adaptive warning sound system to a warning sound that has been developed by industry and is currently widely used by EVs. The warning sound is used in conjunction with environmental noise soundscapes to provide the necessary input signals, and the full process described in Sec. 7.2 is implemented to process the signals and adapt the base warning sound. For this purpose, a number of transfer functions have been produced from physical measurements, and a model of auditory masking has been integrated into the algorithm. These elements facilitate an off-line simulation-based study that can offer a first insight into the capabilities of the proposed system.

7.3.1 Input signals

For the configuration used in this application study, the warning sound generation is treated as an external stage, meaning that the base warning sound constitutes one of the input signals to the system that is in turn adapted through a filter implementation, instead of being synthesized within the algorithm. This choice has been made to allow for flexibility in using the same adaptation algorithm in conjunction with different warning sounds and to allow industrial warning sounds to be utilised, for which the synthesis method is not openly available.

The warning sound used in this instance is the VSP, developed by Nissan for use in their EVs and HEVs (Tabata et al., 2011; Konet et al., 2011), previously mentioned in Sec.2.4. This choice was made due to the thorough documentation of this sound design that is openly available, and for the fact that its main frequency components cover a significant frequency range, making it suitable for a demonstration of the selective adaptation capabilities of the proposed algorithm. The VSP consists of two primary frequency components, f_{lo} and f_{hi}, one with a peak at 600 Hz and one with a peak in the 2.2 to 2.8 kHz region. The lower frequency component is also characterised by both frequency modulation and amplitude modulation to aid in its detectability. Between these two primary components the sound displays a dip in intensity, centred around the frequency of 1 kHz. An indication of changes in speed is achieved by shifting the pitch of the higher frequency component. Figure 7.6 shows a spectrogram of the warning sound, which has been generated in code using the description provided in (Tabata et al., 2011), within the investigated frequency range of 100 Hz to 5 kHz. In Fig. 7.6a, the warning sound represents a constant speed for the vehicle, and the higher frequency component, remains centred at $f_{hi} = 2.5$kHz. In Fig. 7.6b, an accelerating motion is simulated, with f_{hi} over time from 2.2 kHz to 2.8 kHz.

Three different sound samples are used to provide an indication of environmental noise levels under different situations where the vehicle might need to emit its warning sound. These samples were obtained using a portable digital recording device in various locations in the city of Southampton, with a sample rate of 44.1 kHz. They correspond to a high-volume traffic road, which includes lorries and other industrial vehicles, a light traffic road, where vehicle traffic consists of passenger cars travelling at low speeds, and nearby a city park, where the existing traffic noise is limited to low speed manoeuvres, such as cars parking. Figure 7.7 shows the noise levels across frequency for these three environments, expressed through the power spectral density of their respective signals calculated over a 5 s long sample. The frequency range investigated in this application study is 100 Hz to 5 kHz, which is consistent with the studies presented in the previous chapters, as this covers the

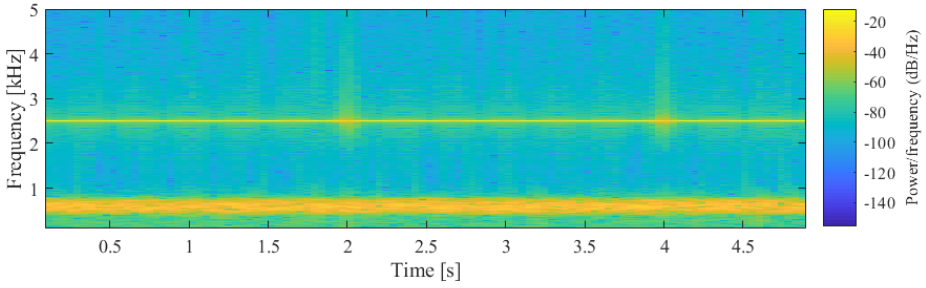

(A) Constant speed.

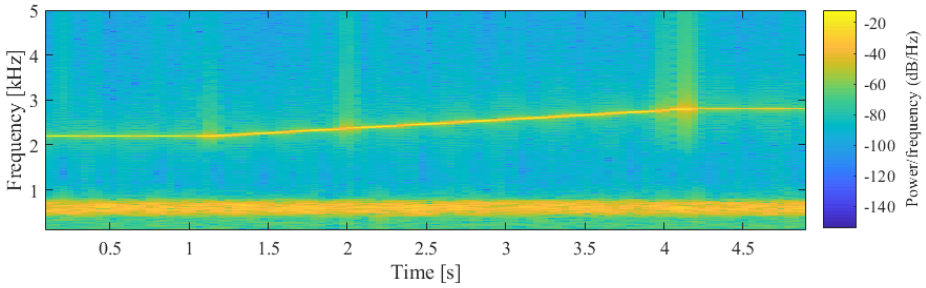

(B) Acceleration.

FIGURE 7.6: Spectrogram of the VSP warning sound generated based on the description provided in (Tabata et al., 2011), for a constant speed and an accelerating setting.

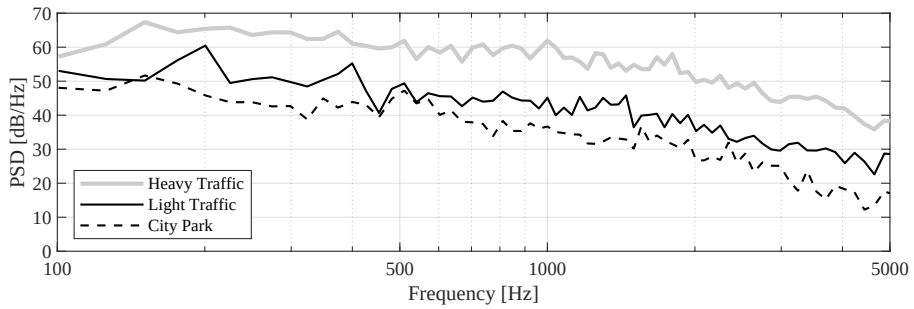

FIGURE 7.7: Power spectral density across frequency for the three samples of environmental noise used in this study.

bandwidth covered by warning sound guidelines (UNECE, 2017; NHTSA, 2016). It can be seen that the choice of samples corresponds to a variety of sonic environments that cover a wide range of noise levels, which allows for the evaluation of the effectiveness of the proposed system in both amplifying or attenuating the base warning sound.

7.3.2 Transfer functions

The signal processing block of the adaptive system requires the implementation of a number of transfer functions in order to obtain a more accurate estimate for the sounds as perceived in specific locations. Figure 7.8 shows a schematic of the measurement set-up that was used to obtain the transfer functions necessary for the full implementation of the algorithm. The same equipment, vehicle, and semi-anechoic environment were used as in the measurements presented in Chapter 6.

In order to recreate the characteristics of the relatively diffuse sound field expected for environmental sounds, the matrix of transfer functions, $\boldsymbol{H}_{nr}$, corresponding to the paths from each of the 20 measurement positions to the sound receiver shown in Fig. 7.8, is applied to the environmental noise samples described above. The resulting signals are then added together and scaled down to generate the measured environmental noise level, and the resulting signal constitutes the portion of the input signal corresponding to environmental noise, p_{Er}.

The transfer function corresponding to the path between the sound emitter and the receiver, H_{er}, can be directly obtained by measurement, as shown in Fig. 7.8. When applied to the adapted warning sound signal, $\tilde{s}_W$, H_{er} provides an estimate of the warning sound as measured by the sound receiver, $\hat{p}_{Wr}$ which is then used to subtract the corresponding component from the overall input, as per Eq. (7.1). This aims to effectively isolate the environmental noise $\hat{p}_{Er}$ measured by the receiver.

As mentioned in Sec. 7.2.2, a more accurate adaptation of the warning sound can be achieved if the audibility thresholds are estimated using information on the environmental noise levels at the location of the pedestrian to whom the auditory warning is meant to be conveyed, as well as the directional characteristics of the environmental noise. Such a function, however, requires the system to employ a virtual sensing method and an array of receiver microphones, elements which might significantly raise the cost of the system. Even in this case, the feasibility of calculating the exact transfer function at any potential location relative to the vehicle, given a changing environment, is in itself a subject that requires substantial research. This problem lies beyond the scope of this present study; therefore, the estimated $\hat{p}_{Er}$ will be considered as adequately similar to the actual environmental noise levels at the location of a potential vulnerable road user, p_{Ep}, to allow for an effective adaptation of the warning sound.

7.3.3 Adaptive algorithm

Having utilised the transfer functions above to obtain $\hat{p}_{Ep}$, the audibility thresholds given the environmental noise at the location of the pedestrian can be estimated through the implementation of a masking model. The specific masking model used in this study was introduced by Terhardt in 1979 (Terhardt, 1979; Terhardt et al., 1982) and was developed focussing on the detection of tonal components. Although many masking models, often of higher precision, have since been developed, this masking model has thus far been the only model used in a study evaluating the perceptibility of EV warning sounds considering masking effects (Lee et al., 2017), and its relatively simple implementation makes it suitable for this application study of the adaptive system.

The masking model of Terhardt considers only simultaneous masking of sounds, and does not produce any estimation on temporal masking effects. However, as the effect of temporal masking generally only lasts up to 100 ms, its duration is too brief relative to the timescales involved in the timely identification of a vehicle by a human recipient. Therefore, it is reasonable to conclude that an adaptive EV warning sound system only needs to consider the effects of simultaneous masking for its operation.

Power estimation

Figure 7.9 shows the block diagram of the adaptation process for the proposed system. The isolated environmental noise and warning sound components, $\hat{p}_{Ep}$ and

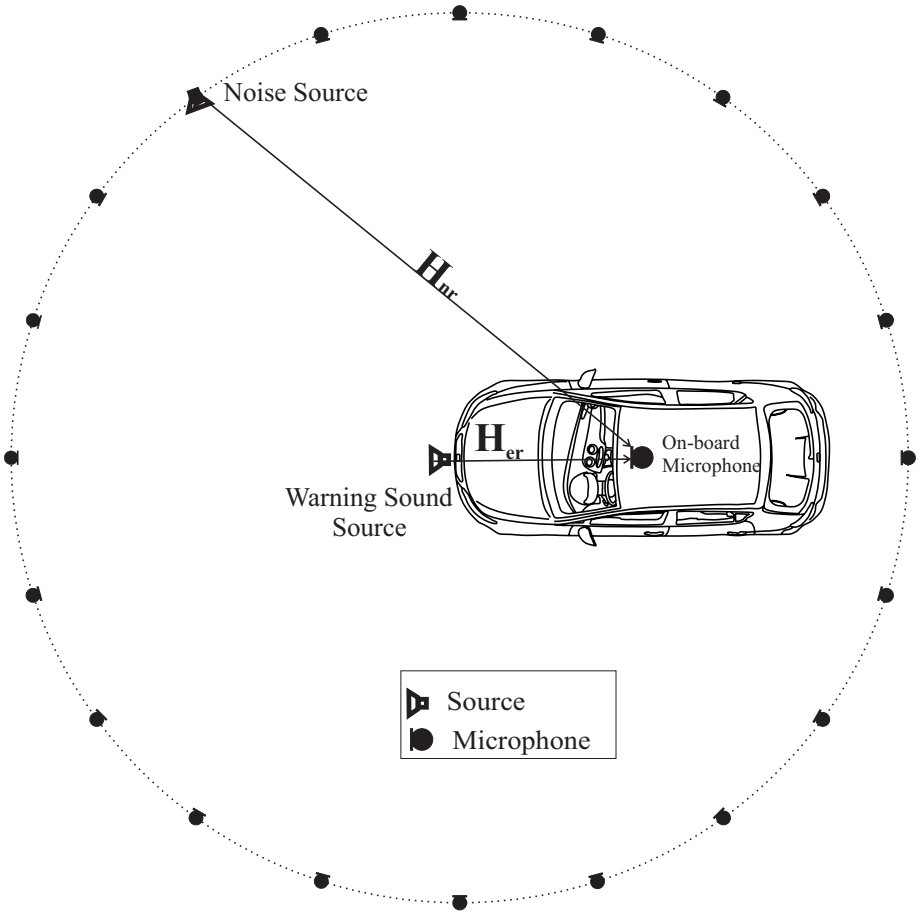

FIGURE 7.8: Measurement set-up for the calculation of the transfer functions used in the adaptation algorithm.

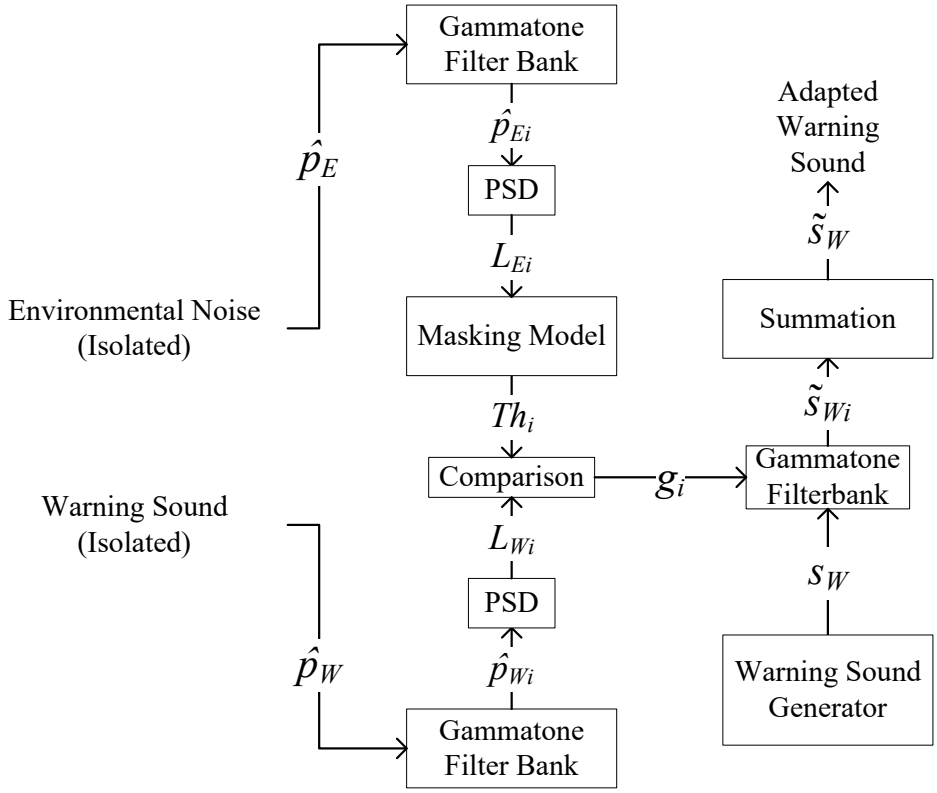

FIGURE 7.9: Block diagram of the proposed warning sound adaptation block.

$\hat{p}_{Wp}$, are the main input signals to the adaptation block. The level of these signals across frequency is necessary to determine the audibility thresholds through the masking model. To perform this task, a gammatone filter bank is used to allow estimation of the power spectral density of the signals at each frequency band. A gammatone filter is a linear filter, described by an impulse response that is the product of the gamma distribution, which is in turn based on the gamma function ($\Gamma(n) = (n-1)!$), and a sinusoidal tone. The gammatone impulse response is

$$g(t) = at^{n-1}\mathrm{e}^{-2\pi bt}\cos(2\pi ft + \phi), \tag{7.3}$$

where f is the centre frequency in Hz, ϕ is the phase of the carrier, a is the amplitude, n is the order of the filter, b bandwidth of the filter, and t is time.

The gammatone filter was utilised by Patterson and Holdsworth (Patterson et al., 1987) to construct an auditory filter bank capable of approximating the initial frequency analysis necessary in human hearing models. The implementation of a gammatone filter bank at this stage of the adaptative algorithm, can therefore be expected to increase the accuracy of the auditory threshold estimation. The filter bank used in this instance consists of 99 filters, with centre frequencies distributed between 60 Hz and 20 kHz. Out of these centre frequencies, 72 are within the investigated bandwidth of 100 Hz to 5 kHz. The output of this filtering process is a filtered signal corresponding to each frequency band. The power spectral density is estimated for each signal, given in dB as L_{Ei} and L_{Wi}.

Masking model implementation

As shown in Fig. 7.9, the masking model is implemented using the values L_{Ei}, corresponding to the level of the environmental noise at each frequency band, calculated through the power spectral density of the signal, to estimate the thresholds of audibility. Under Terhardt's model, the simultaneous masking of a tone, located at the i-th frequency band, by another, located at the k-th, may be approximated as being triangular in shape, with slopes given by

$$S_1 = 27\text{dB/Bark}, \quad f_i \leq f_k \tag{7.4a}$$

$$S_2 = [-24 - (0.23\text{kHz}/f_k) + (0.2L_k/\text{dB})]\text{dB/Bark}, \quad f_i \geq f_k, \tag{7.4b}$$

where L_k and f_k are the level and frequency of the masker, respectively, and f_i is the frequency of the masked tone. It should be noted that the calculation of these slopes makes use of the Bark scale, which is a psychoacoustical scale introduced in (Zwicker, 1961). This does not limit the choice of filters and centre frequencies considered in the filter bank used in this algorithm. The masker level produced is in turn estimated using the relation

$$L_{ki} = L_k - S_1(z_k - z_i), \quad f_i \leq f_k \tag{7.5a}$$

$$L_{ki} = L_k - S_2(z_i - z_k), \quad f_i \geq f_k, \tag{7.5b}$$

where z_i and z_k are the frequencies f_i and f_k expressed in Barks through the relation $z = 13.3\arctan(0.75f)$. For a total number of investigated frequency bands N, the resulting relative masker amplitude A_μ in the i-th band is

$$A_i = \sum_{k=1}^{i-1} 10^{L_{ki}/20\text{dB}} + \sum_{k=i+1}^{N} 10^{L_{ki}/20\text{dB}}. \tag{7.6}$$

Using this value, the audibility threshold in the i-th band is, according to (Terhardt et al., 1982), given as

$$Th_i = 20\log_{10} A_i - 5.5\text{dB}. \tag{7.7}$$

The output of the masking model is thus an array of the values Th_i, constituting the audibility thresholds across frequency.

Gain adaptation

The gain coefficient for the i-th frequency band is calculated using the estimated thresholds as

$$g_i = 10^{(Th_i - L_{Wi})/10}, \tag{7.8}$$

where L_{Wi} is the level of the warning sound estimated in the i-th frequency band.

As previously mentioned, and as shown in Fig. 7.9, the algorithm used in this study employs an external warning sound generator. This means that the base warning sound signal is treated as a tertiary input to the adaptive algorithm, and is adapted by being filtered through a gammatone filter bank, as described earlier in this section, with the gain values g_i applied to the corresponding filter. From Eq. (7.8), it can be seen that when $L_{Wi} < Th_i$, then $g_i < 1$, meaning that the signal in the i-th frequency band is attenuated, and when $L_{Wi} > Th_i$, $g_i > 1$, which amplifies the signal at the corresponding band. The resulting filtered signals are then added together to construct the adapted warning sound signal.

To keep the algorithm from unnecessarily attempting to match the level of the warning sound to the audibility thresholds at frequency bands where the former is not intended to produce an output, a limitation criterion, beyond which g_i is reset to 1, must be imposed. For this study, this has been defined as

$$Th_i - L_{Wi} \leq 1.5\Delta L_{max}, \tag{7.9}$$

where ΔL_{max} is given by

$$\Delta L_{max} = \max(|Th_j - L_{Wj}|). \tag{7.10}$$

In the above relation, the j subscript denotes the two bands with central frequencies closest to the two dominant frequency components of the VSP sound used in this study. ΔL_{max} is thus the maximum difference in level that the warning sound displays in either of these two frequency bands. Eq. (7.9) effectively means that the algorithm will only adapt the warning sound in bands where its level is below the audibility threshold by a difference of up to 1.5 times the value of ΔL_{max}. This choice of frequencies and scaling factor of 1.5 was made to ensure the most effective adaptation of the VSP sound, and such parameters are dependent on the warning sound used.

One more thing that is important to note, is that a warning sound is expected to shift its frequency content when the vehicle is accelerating to indicate its change in speed. The VSP warning sound used in this application, as shown in Fig. 7.6b, performs this by shifting the centre frequency, f_{hi}, of its higher frequency component. In such a case, the algorithm is able to perform the adaptation as described above, by taking this information into account and assigning the values of j in Eq. (7.10) to correspond to the appropriate frequency bands that are necessary to include both frequency components of the VSP at any moment.

7.3.4 Results

The system input consists of the environmental noise signal, p_{Er}, formed using the different environmental noise samples shown in Fig. 7.7 and the base warning sound signal, p_{Wr}, which is the VSP warning sound developed by Nissan (Tabata et al., 2011). Using this information, the algorithm performs an estimation of the audibility thresholds, and filters the base warning sound while implementing the gain values, g_i, calculated according to Eq. (7.8), to adapt the warning sound accordingly. Figure 7.10 shows results of the adaptation in terms of the power spectral density expressed in dB across frequency, for the given environmental noise signal, the base warning sound, the audibility thresholds estimated using the masking model of Terhardt, and the resulting adapted warning sound. The power spectral density has been calculated over a buffer of 1024 samples for each signal, at a sample rate of 44.1 kHz.

Across all cases, it can be seen that the effects of auditory masking have a noticeable impact on the audibility threshold level for frequencies beyond around 800 Hz. Looking at the response of the adapted warning sound, it can be seen that the level of each frequency component is independently adjusted to match the audibility threshold in the corresponding frequency band. In Fig. 7.10 (a), where the environmental noise is high enough to ensure the audibility thresholds lie above the level of the base warning sound, the adapted sound is amplified accordingly across all frequency bands. In the case shown in Fig. 7.10 (b), the low frequency component is

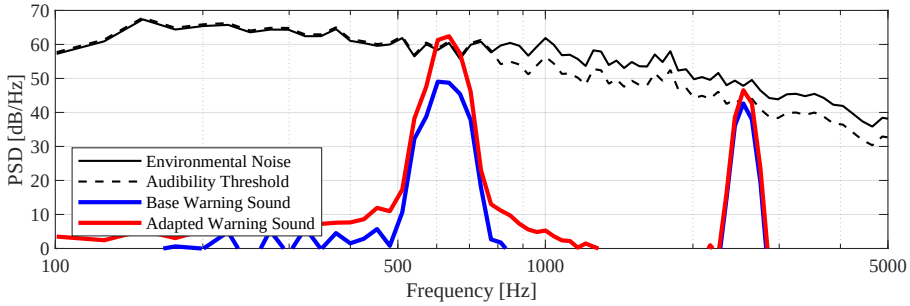

(A) Environmental noise recorded in a heavy traffic situation.

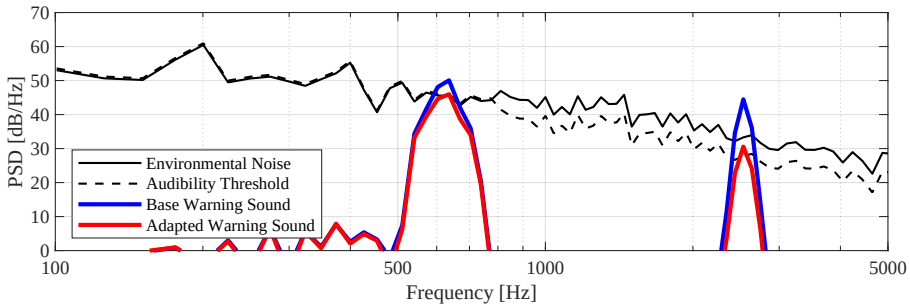

(B) Environmental noise recorded in a light traffic situation.

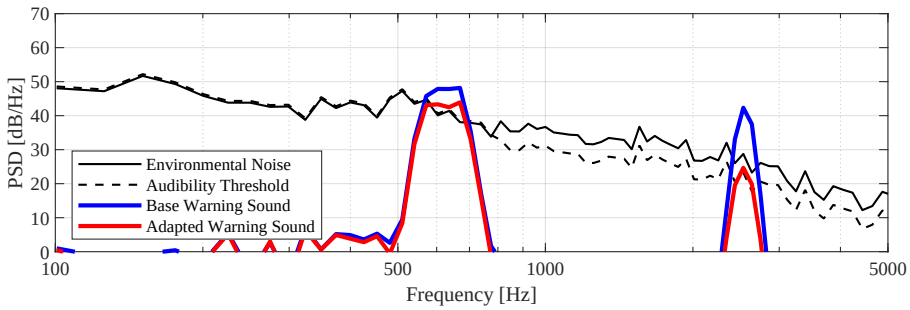

(C) Environmental noise recorded in a city park.

FIGURE 7.10: Power spectral density expressed in dB across frequency, calculated over a 1024 sample buffer for the environmental noise, estimated audibility thresholds, base warning sound, and adapted warning sound using different examples of environmental noise.

roughly at the level of the audibility threshold, therefore only a minimal attenuation is implemented on its centre frequency band. The high frequency component, being well above the threshold, is significantly attenuated. In the case shown in Fig. 7.10 (c), the background noise levels are low enough so that the base warning sound exceeds the audibility thresholds by a margin across all key frequency bands. The main components of the adapted sound are thus attenuated to match the estimated threshold levels. It can therefore be concluded that the proposed algorithm is successful in adapting a warning sound signal depending on the spectrum of the given background noise, to match the levels indicated by the implementation of an auditory masking model.

One factor in the adaptation process that has a significant effect on the adapted output signal and the overall performance of the system, is the size of the buffer chosen to partition the input signal. This buffer size also determines the update rate of the gain values, g_i, which is especially important in the adaptation of the warning

sound during acceleration, when its frequency content significantly changes over time. The effect of buffer size are thus evaluated in this application study for two different settings: one with a warning sound that remains static over time, characterised by the spectrogram shown in Fig. 7.6a, indicating a constant speed, and a setting corresponding to an accelerating motion of the vehicle, with the warning sound characterised by the spectrogram shown in Fig. 7.6b.

Figure 7.11 shows the waveforms of a five second sample of environmental noise, the base warning sound with no component specific gain adjustment, and the adapted warning sound, in the constant speed setting. In Fig. 7.11 (a), the buffer has a length of 1024 samples, while in Fig. 7.11 (b) a 4096 buffer has been used, to showcase the impact that the length of the buffer might have on the response of the system across time. Likewise, Fig. 7.12 shows the waveforms of the same environmental noise and the base and adapted warning sound for an accelerating setting, using the two different buffer lengths. The response obtained through the shorter buffer replicates fluctuations in the amplitude of environmental noise with a higher precision. Moreover, there is a longer delay in this response, as the greater buffer size means that the adaptation algorithm waits for a longer time period before determining the required gain values. This is particularly evident around region marked 1. in the figure, where the short buffer adapts the warning sound to respond to a spike in the environmental noise, whereas the longer buffer does not perform such an adaptation. It is also clear from these results, however, that there are fluctuations in the amplitude of the environmental noise that neither adapted waveform follows, such as the region marked 2., which suggests that they are either too short for even the 1024 sample buffer to respond to, or they stem from events at frequencies outside of the range specified by the filter bank used. Although the response of the adaptation relative to the environmental sonic stimuli can be seen in these figures, the differences between the adaptation of the constant speed and accelerating warning sounds are not evident, necessitating an investigation of the gain adaptation over time.

Figure 7.13 shows the calculated gain values, g_i, for the frequency bands corresponding to the dominant components of the warning sound at 600 Hz and 2.5 kHz, when using a 1024 sample buffer in (a) and a 4096 sample buffer in (b), for a constant speed setting. In the former case, the gain values display a relatively large variation between short time intervals, as the adaptation algorithm tends to match both signals. Although this analysis might indicate that the shortest possible buffer would yield the most effective adaptation, the optimum buffer length would be most suitably determined through listening tests. Large and rapid fluctuations in the warning sound might ultimately render the warning sound less detectable to the human listener or unnecessarily annoying, which would defeat the point of the proposed approach.

Figure 7.14 shows the values of g_i for the frequency bands at 600 Hz, 2.2 kHz and 2.8 kHz, in an accelerating scenario using the two different buffer lengths. The latter two bands were chosen as they constitute the limits of the range for the higher frequency component of the VSP warning sound during acceleration, shown in Fig. 7.6b. Through these two examples it is possible to demonstrate the selective gain adaptation described through Eqs. (7.9) and (7.10) in Sec. 7.3.3. The 2.2 kHz component is adapted up until the 3 s mark, beyond which it is no longer considered among the frequency bands used in Eq. (7.10), as spectral content of the warning sound is shifted towards higher frequencies due to the acceleration of the vehicle. Conversely, the 2.8 kHz component is only adapted after the 2 s mark, when the frequency

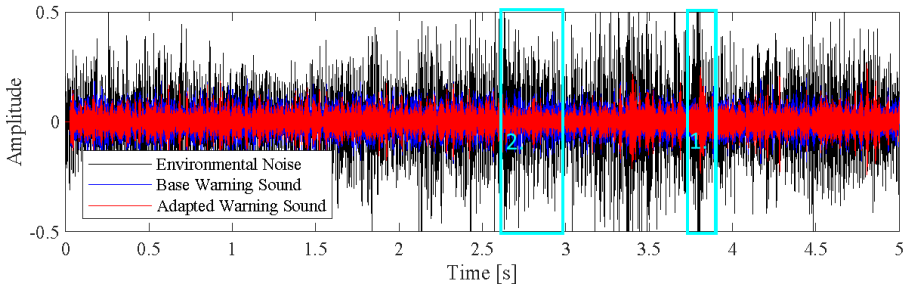

(A) Buffer size of 1024 samples.

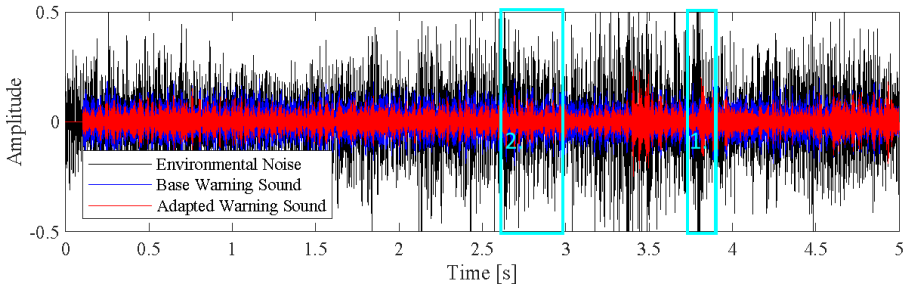

(B) Buffer size of 4096 samples.

FIGURE 7.11: Time history of the base warning sound, the environmental noise sample, and the resulting adapted warning sound for buffer sizes of 1024 samples and 4096 samples, for a constant vehicle speed.

component of the warning sound denoting acceleration approaches this higher frequency. Between the cases of the two buffer lengths used, the same conclusions can be drawn as with the constant speed scenario. Particularly for the accelerating scenario, however, the use of a shorter buffer is crucial in the accurate adaptation of the frequency component displaying the shift in time. If too long a buffer is used, the shift in pitch of the generated sound might place it outside the frequency bands considered in the gain adaptation process.

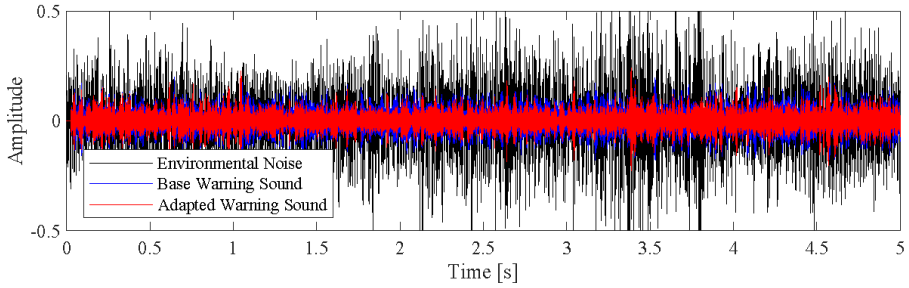

(A) Buffer size of 1024 samples.

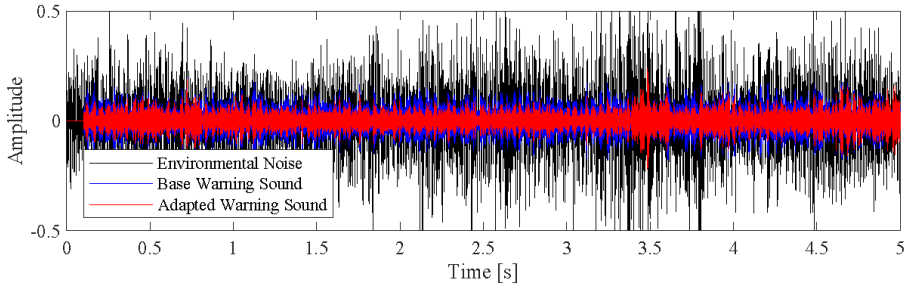

(B) Buffer size of 4096 samples.

FIGURE 7.12: Time history of the base warning sound, the environmental noise sample, and the resulting adapted warning sound for buffer sizes of 1024 samples and 4096 samples, for an accelerating vehicle.

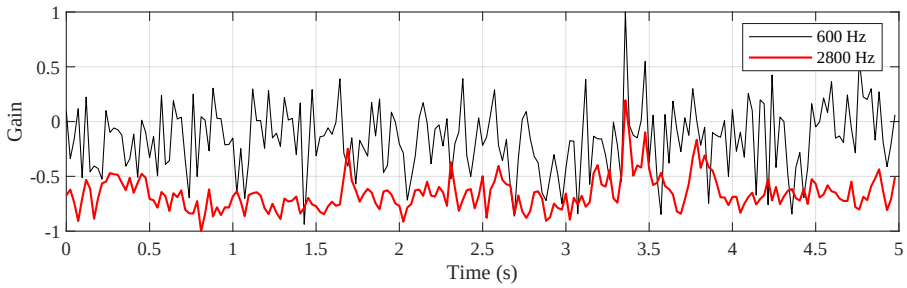

(A) Buffer size of 1024 samples.

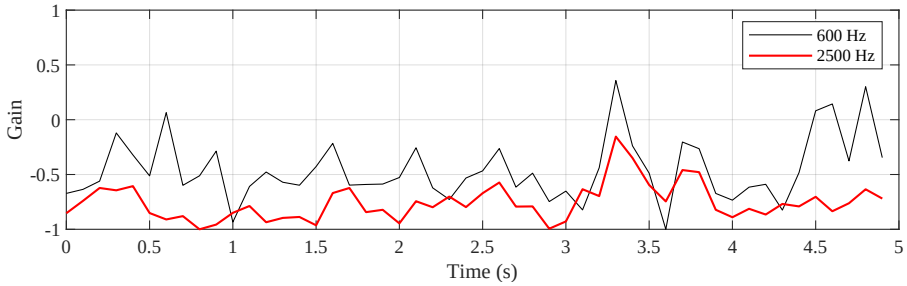

(B) Buffer size of 4096 samples.

FIGURE 7.13: Gain values for the frequency bands corresponding to the dominant components of the adapted warning sound over time for a constant vehicle speed, given the presence of environmental noise and the use of different buffer lengths.

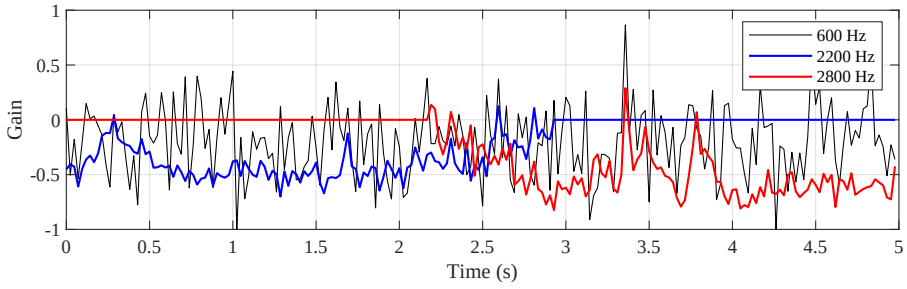

(A) Buffer size of 1024 samples.

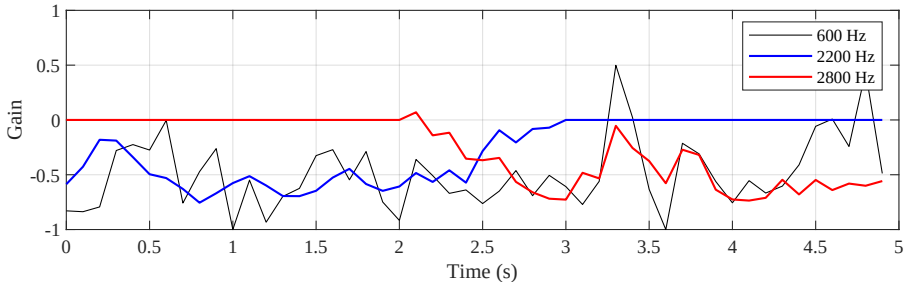

(B) Buffer size of 4096 samples.

FIGURE 7.14: Gain values for the frequency bands corresponding to the dominant components of the adapted warning sound over time for an accelerating vehicle, given the presence of environmental noise and the use of different buffer lengths.

7.4 Proposed evaluation method

It can be concluded, from the results of the application study presented in Sec. 7.3.4, that the adaptive system introduced in this chapter can successfully adapt the spectral content of a base warning sound depending on the context of the current environmental noise. However, the effectiveness of the system must be evaluated by its ability to render a vehicle detectable compared to a system that only adapts the overall gain of the warning sound, or even a non-adaptive warning sound.

Such an evaluation could be performed via a series of listening tests, in which participants are presented with a virtual scenario. In this scenario, an environmental background noise would be present, and a vehicle equipped with the investigated warning sound system would be approaching the listener. The listener would be asked to indicate when they have detected the vehicle by pressing of a button, and this would infer the distance at which the vehicle could be detected; no visual stimulus would be provided in order to ensure that the test only evaluated the efficacy of the warning sound system.

Using the same set-up, this listening test could be performed using different types of warning sound level adaptation, such as an overall gain adaptation, or a static warning sound level, dictated by the guidelines for the AVAS requirements (UN-ECE, 2017). This would facilitate the comparison of the different methods, with the effectiveness of the adapted sound being evaluated based on the difference in overall level generated compared to the static sound, in a setting that ensures the detectability of the vehicle at the same distance. Another important factor in the suitability of a warning sound that could be investigated through a subjective listening test is the annoyance associated with the sound, and how it varies when the same base sound is adapted through different methods.

Apart from the comparison between different warning sound systems, the effects of different parameters on the performance of the adaptive system could also be evaluated through these listening tests. Such parameters that require investigation via listening tests are:

- The impact of including transfer functions to provide estimates of the noise levels at the location of the pedestrian can be assessed. If it is found that such approximations do not result in a measurably more accurate adaptation, these processes can be omitted to simplify the system and reduce its computational requirements.

- The frequency resolution at which the spectral analysis of the signals is performed. As above, a lower resolution can reduce the computational cost of the system. Conversely, it might prove necessary to perform the analysis using a high frequency resolution to accurately isolate sounds in the environment that affect the detectability of the warning sound.

- The masking model used to determine the audibility thresholds. A number of masking models have been developed to evaluate the effects caused by different types of sounds. A series of listening tests could help to determine which model is most suitable for adapting a warning sound in the presence of environmental noise.

- The buffer size that determines the rate of update for the adapted sound. As pointed out in Sec. 7.3.4, a shorter buffer can adapt the sound to the changes in environmental noise more accurately, but beyond a point this might have an impact on its detectability or annoyance caused.

- The adaptation of frequency components in the warning sound indicating the acceleration of the vehicle. The shift in pitch of such components is crucial to the perception of the motion of the vehicle, and by itself serves towards the detectability of the warning sound. Its adaptation may prove to interfere with both these factors to a considerable extent, and it might also need to an increased complexity of the adaptation algorithm. Therefore it could be investigated if the adaptation would be more efficient when performed only on the static components of the warning sound.

Although these tests had been planned to a significant extent, they were not possible to realise within the scope of this project due to the outbreak of the COVID-19 pandemic. At the time of writing, the lockdown measures undertaken as safety precautions did not allow for the carrying out of any listening tests. Therefore, the plans presented above constitute a suggestion for potential future work on the development of the environmentally adaptive warning sound system.

7.5 Summary

This chapter presented an approach to minimising drive-by noise caused by the use of a warning sound in the form of an environmentally adaptive warning sound system. This system is intended to adjust the overall level and spectral content of a warning sound according to the sonic environment, so that it is rendered audible yet not unnecessarily intrusive. For this purpose, such a system must take into account the effects of auditory masking, which influence the perception of a warning sound in the presence of background noise.

An overview of the system structure was given, which separates it into a peripheral signal processing block, which includes the initial and final stages of signal processing to the input and output signals respectively, and a core sound adaptation block, which contains the sound adaptation process. This adaptation is performed by filtering the input signals, corresponding to the environmental noise and the initial warning sound levels, implementing a masking model to determine the thresholds of audibility, and adapting the warning sound to ensure that it exceeds these levels.

An off-line application study of the system was carried out using measured transfer functions to estimate the noise levels at the location of a pedestrian. The sound adaptation process was implemented using a gammatone filter bank along with an existing masking model previously utilised in the context of EV warning sounds. Results from this study show that the algorithm is capable of adapting the base warning sound so that its level at each frequency band exceeds the threshold of audibility imposed by the present background noise. Upon the successful implementation of this algorithm, a basic listening test was proposed for the evaluation of the effectiveness of the system, and of the impact that different parameters might bear upon its performance. However, it was not possible to carry out the listening test due to the impact of COVID-19 and it therefore remains a suggestion for future work.

Chapter 8

Conclusions and Future Work

8.1 Conclusions

The necessity of installing artificial warning sounds in quiet vehicles as a safety measure, and the effort to minimise the environmental noise emissions of vehicle traffic have lead to a conflict regarding the priorities in the design of EVs and HEVs. This thesis aimed to develop suggestions for realisable warning sound system designs that are capable of achieving both detectability and minimisation of drive-by noise emissions, while presenting a viable option for manufacturing and implementing in a wide production context.

EVs and HEVs have been found to be significantly quieter at speeds below the 30 km/h limit when compared to conventional ICE vehicles. This is due to the quiet operation of the electric motor compared to the ICE, and the absence of other significant noise sources such as the interaction between the road and the tyres, and the aerodynamics of the vehicle at such low speeds. Concerns over the potential risks that this absence of noise might bring have stressed the necessity of corresponding safety measures. Regulations have been planned globally, mandating the inclusion of artificial warning sounds on all EVs and HEVs, and providing guidelines for their implementation and evaluation. However, criticism of these new rules persists, citing the increase in environmental noise pollution it might cause. For this reason, the prospect of using a directional warning sound system has been suggested in previous research. In principle, such a system can shape the radiated sound field to emit the warning sound towards a pedestrian, while minimising its output in all other directions.

The acoustic contrast between two designated control zones was used as a means of quantifying directivity, in order to evaluate and compare the performance of directional sound systems. Simulation based parametric studies were performed for two systems that have been proposed as potential directional warning sound sources: the loudspeaker array and the endfire acoustic radiator. Results of these studies indicated that while the loudspeaker array can achieve the directivity performance necessary for the role, it may not be viable as a practical solution as it beholds a high manufacturing cost and involves potentially fragile loudspeaker drivers being exposed to adverse conditions. Conversely, the endfire radiator, while simple and easy to produce at a low cost, does not achieve directivity over a bandwidth that is sufficient to accommodate the warning sounds required by current legislation.

As a solution that offers the directivity control capabilities of the loudspeaker array at a lower cost and with increased robustness, the concept of the structural actuator array was introduced. This system consists of an array of inertial actuators, which are attached to a surface that could potentially be part of an existing structure in the vehicle. Control of the vibration of the structure, and the resulting radiated

sound field, is achieved through adjusting the relative amplitudes and phases of the signals driving each actuator. An analytical model was formulated to simulate the structural actuator array and provide insights into the effect of individual design parameters on its performance.

A simple prototype consisting of a flat panel and an array of six actuators was built to validate the analytical model. Directivity measurements conducted in an anechoic environment showed that the analytical model succeeds in simulating the behaviour of the physical system. As a directional system, the structural actuator array was shown to be capable of generating a controllable directional sound field over a bandwidth that can be used to emit the warning sound signal required by legislation. When compared to the two other directional systems investigated, the structural actuator array showed a significantly improved bandwidth compared to the endfire radiator, and a comparable directivity performance to the loudspeaker array, with a response characterised by an improved high frequency limit, but also affected by the resonances on the panel.

The structural actuator array was installed in a production vehicle to be evaluated in the full context of its intended implementation. The measurements, conducted in a semi-anechoic environment, included the testing of different configurations of the array on the vehicle to determine the most suitable position. The configuration which proved to be most suitable consisted of six actuators attached on the front bumper of the vehicle. This arrangement was capable of maintaining an acoustic contrast level of over 10 dB throughout the investigated frequency range. In addition, its position ensures the least amount of noise leakage into the cabin, making it the most appropriate for a practical implementation of the system. The directivity performance of the structural array is comparable to that achieved by loudspeaker-based systems, at the same time offering increased durability against environmental factors, and a more cost-effective integration in the vehicle.

In addition to the development of a directional system, a system for the environmental adaptation of the warning sound was conceptualised and investigated as a potential complementary or alternative method of ensuring detectability and the minimisation of unwanted environmental noise contributions. The proposed system uses a sound receiver on the vehicle to measure the environmental noise levels, and an algorithm is described that performs an adaptation of the warning sound based on the estimation of audibility thresholds per frequency band, using an auditory masking model. A basic simulation-based application study of the algorithm using a combination of soundscape recordings and measurements conducted on a vehicle in a controlled acoustic environment showed that it is capable of performing the adaptation to match the audibility thresholds for a variety of noise environments, and a plan was presented for a listening test based evaluation of the proposed system.

8.2 Review of Objectives and Contributions

Through the research presented in this doctoral thesis, the following contributions were made:

- The formulation of a physical model for a system based on structural vibration capable of generating a controllable directional sound field, based on existing models for plate vibration and the resulting radiation of sound.

- The control of the above system via the acoustic contrast maximisation method, which had been implemented in systems involving loudspeaker arrays. In this work, the acoustic contrast was utilised to control the directivity of the sound field generated by an array of inertial actuators forcing the vibration of a panel.
- The experimental validation of the physical model of the structural actuator array through the comparison of simulation results with measurements from a physical prototype system.
- The implementation of the structural actuator array as a warning sound system for EVs by installing the array in a vehicle and performing an experimental evaluation of its directivity performance through acoustical measurements.
- The design and simulations-based implementation study of a system for the adaptation of warning sound signals, based on the spectral content of the sonic environment and under consideration of frequency specific masking effects. Such a system ensures that the warning sound is rendered audible without becoming unnecessarily loud and intrusive, and can be used either independently or in conjunction with the directional system.

From the above contributions, the objectives set out at the beginning of this research have been addressed as follows:

- In developing the structural actuator array as a potential emitter of EV warning sounds, a system was realised that is capable of rendering the vehicle detectable to pedestrians and other vulnerable road users through auditory means, while at the same time minimising its own contribution to environmental noise levels by directing the generated sound field only at the intended target location.
- The operational bandwidth of the proposed system includes the frequency range from 200 Hz to 5 kHz, covering the bandwidth within which warning sounds contain their harmonic contents, in accordance to international regulations.
- As the actuator array can be simply attached on a structure, its installation to the body of a vehicle does not require modifications. Moreover, as the actuators are not exposed to environmental factors such as rain, wind and dust, the system offers an increased robustness and potential longevity. These factors make the structural actuator array a cost-effective solution in both its manufacturing and maintenance.
- The environmentally adaptive algorithm constitutes a method of ensuring the detectability of a vehicle through its warning sound while minimising its contribution to noise. It was demonstrated that the algorithm tested can match the audibility threshold by reducing the level of the warning sound at frequency bands that cover its harmonic contents.

Under consideration of the performance of the structural actuator array and the environmentally adaptive system, the adoption of these technologies from EV and HEV manufacturers can potentially reduce the drive-by noise emissions of slow moving traffic by up to 10 dB due to the directional warning sound system, and ensure an overall reduction of all environmental noise emissions. It can therefore be concluded that this thesis has successfully satisfied the objectives set, and has offered a viable solution towards instilling road safety for pedestrians through acoustic means, while ensuring a minimal contribution to noise pollution.

8.3 Suggestions for Future Work

Further work on the development of the proposed solution could progress in the following directions.

- The consideration of the design of the vehicle for the optimisation of the structural actuator array in regards to its positioning and the number of actuators to be used. The in-vehicle experiments presented in this thesis were carried out without prior knowledge of the test vehicle. The system could be more efficiently optimised through simulations, if full knowledge of the vehicle components available to accommodate the array are utilised together with methods such as finite element modelling. This could help identify the optimum positions and characteristics of the actuators that are necessary to ensure the best performance.

- Jury based testing and evaluation of the structural actuator array installed in a vehicle. The effectiveness of the system in effectively emitting the warning sound to a specific target in isolation from all other directions could be better determined in a multiple participant survey. In addition, such a study could help define the width of a sound maximisation zone necessary to convey a sufficient warning.

- Development of an environment-dependent spectral adaptation algorithm for the warning sound. Systems suggested in other research have included the aspect of adapting the level of the warning sound, if it is estimated to be too high or low compared to the levels of ambient noise. A more advanced algorithm could perform a spectral adaptation instead of an adjustment of the overall level, to overcome narrow band-specific masking effects and ensure audibility in all conditions. The evaluation of such an adaptive system could be performed by conducting a series of listening tests.

- The combination of both the structural array and the adaptive algorithm in a single warning system, that will be able to adapt its base warning sound depending on the current environment and emit it directionally through the array.

- Investigation of real-time steering methods for the array. The acoustic contrast maximisation method used in the presented investigation could be implemented in real-time through the use of pre-stored filter banks corresponding to specific directivity settings. However, instead of using preset settings, it would be beneficial to develop an algorithm that considers the detection of a vulnerable road user and controls the directivity in response to the situation. A compromise between computational efficiency and directivity performance arises from such an implementation, which would necessitate the comparison with simpler algorithms, like delay-and-sum beamforming, and higher accuracy methods such as the sound power minimisation used in eVADER.

- Application of the structural actuator array to other domains. For example, the proposed array could be beneficial in other applications where it is not possible or practical to accommodate the addition of loudspeakers, such as in flat panel television screens, advertising boards or personalised exhibition displays.

- Improvement on the sound quality of structural array. Although the intended implementation as a warning sound system in this thesis did not impose higher

requirements, a high fidelity version of the system could broaden the range of its potential applicability.

- Evaluation of the algorithm for the environmental adaptation of the warning sound through a series of listening tests. Such a study can help investigate the impact of individual internal parameters on the performance of the system, and facilitate a comparison between the effectiveness of the proposed method, the overall gain adaptation used in existing research, and the minimum warning sound SPL dictated in the AVAS guidelines.

Bibliography

F. Abbaléa, S. Andry, M. Baulac, M. C. Bérengier, B. Bonhomme, J. Defrance, J. P. Deparis, G. Dutilleux, D. Ecotière, and B. Gauvreau. Road noise prediction, 2—noise propagation computation method including meteorological effects (nmpb 2008). *Sétra edition*, 2009.

E. Allam, I. Ahmed, N. Hammad, and S. Abouel-Seoud. Noise characteristics for hybrid electric vehicle induction motor. Technical report, SAE Technical Paper, 2007.

E. Ambikairajah, A. Davis, and W. Wong. Auditory masking and mpeg-1 audio compression. *Electronics & communication engineering journal*, 9(4):165–175, 1997.

D. Anderson and M. F. Bocko. Modal crossover networks for flat-panel loudspeakers. *J. Audio Eng. Soc*, 64(4):229–240, 2016.

D. A. Anderson, M. C. Heilemann, and M. F. Bocko. Flat-panel loudspeaker simulation model with electromagnetic inertial exciters and enclosures. *J. Audio Eng. Soc*, 65(9):722–732, 2017.

J. A. S. Angus. Distributed mode loudspeaker polar patterns. In *Audio Engineering Society Convention 107*. Audio Engineering Society, 1999.

ANSI. American national psychoacoustical terminology. American National Standards Institute, 1973.

K. Arima. Electric cars: The role of standards in Japan and abroad. *Japan Industry News*, 2015.

M. B. Bennett and D. T. Blackstock. Parametric array in air. *The Journal of the Acoustical Society of America*, 57(3):562–568, 1975. doi: 10.1121/1.380484.

L. L. Beranek and T. Mellow. *Acoustics: sound fields and transducers*. Academic Press, 2012.

T. Berge and F. Haukland. The concept of adaptive avas-results from a small test program. In *INTER-NOISE and NOISE-CON Congress and Conference Proceedings*, volume 259, pages 335–346. Institute of Noise Control Engineering, 2019a.

T. S. Berge and F. Haukland. Adaptive acoustic vehicle alerting sound, avas, for electric vehicles results from field testing. *SINTEF Rapport*, 2019b.

A. Berkhoff and R. Van der Rots. Real-time steerable directional sound sources. In *Proceedings of the Conference on Acoustics AIA-DAGA 2013, including the 40th Italian (AIA) Annual Conference on Acoustics and the 39th German Annual Conference on Acoustics (DAGA)*, 2013.

T. Birchall, P. Clark, and J. Moran. Design and implementation of a directive electric car warning sound. Masters Group Design Project, University of Southampton, 2013.

M. Blanco Galindo, P. Coleman, and P. Jackson. Microphone array geometries for horizontal spatial audio object capture with beamforming. *Journal of the Audio Engineering Society (AES)*, 2020.

M. Brandstein and D. Ward. *Microphone arrays: signal processing techniques and applications*. Springer Science & Business Media, 2013.

H. Campello-Vicente, R. Peral-Orts, N. Campillo-Davo, and E. Velasco-Sanchez. The effect of electric vehicles on urban noise maps. *Applied Acoustics*, 116:59–64, 2017.

J. Cheer, S. J. Elliott, Y. Kim, and J.-W. Choi. The effect of finite sized baffles on mobile device personal audio. In *Audio Engineering Society Convention 130*. Audio Engineering Society, 2011.

J. Cheer, T. Birchall, P. Clark, and J. Moran. Design and implementation of a directive electric car warning sound. In *Proceedings of the Institute of Acoustics*, volume 35, 2013.

J.-W. Choi and Y.-H. Kim. Generation of an acoustically bright zone with an illuminated region using multiple sources. *The Journal of the Acoustical Society of America*, 111(4):1695–1700, 2002. doi: 10.1121/1.1456926.

Code of China. Acoustic vehicle alerting system of electric vehicles running at low speed (English Version), 2018. www.codeofchina.com/standard/GBT37153-2018.html.

P. Coleman, P. J. B. Jackson, M. Olik, M. Møller, M. Olsen, and J. Abildgaard Pedersen. Personal audio with a planar bright zone. *The Journal of the Acoustical Society of America*, 136(4):1725–1735, 2014. doi: 10.1121/1.4893909.

L. Cremer and M. Heckl. *Structure-borne sound: structural vibrations and sound radiation at audio frequencies*. Springer, 1988.

L. Cremer, M. Heckl, and B. A. T. Petersson. *Structure-Borne Sound*. Number 978-3-540-26514-6. Springer-Verlag Berlin Heidelberg, 3 edition, 2007.

Dayton Audio. Exciters & tactile transducers 101. https://www.daytonaudio.com/topic/excitersbuyerguide, 2019. Accessed: 2020-09-10.

Y. Egawa. A study of auditory warning alarms evaluation for automated guided vehicles. In *Proceedings of the First International Conference on Ergonomics of Hybrid Automated Systems I*, pages 529–536, 1988.

G. W. Elko. Superdirectional microphone arrays. In *Acoustic signal processing for telecommunication*, pages 181–237. Springer, 2000.

S. J. Elliott, J. Cheer, J. Choi, and Y. Kim. Robustness and regularization of personal audio systems. *IEEE Transactions on Audio, Speech, and Language Processing*, 20(7): 2123–2133, Sep. 2012. ISSN 1558-7916. doi: 10.1109/TASL.2012.2197613.

European Council. Regulation (EU) No 540/2014 of the European Parliament and of the Council of 16 April 2014 on the sound level of motor vehicles and of replacement silencing systems, and amending Directive 2007/46/EC and repealing Directive 70/157/EEC Text with EEA relevance. The European Parliament and The Council of the European Union, 2014.

L. Evans. Speed estimation from a moving automobile. *Ergonomics*, 13(2):219–230, 1970.

H. Fastl and E. Zwicker. *Psychoacoustics - Facts and Models*. Number 978-3-540-23159-2. Springer-Verlag Berlin Heidelberg, 3 edition, 2007.

S. Fleury et al. Effect of additional warning sounds on pedestrians' detection ofelectric vehicles: An ecological approach. *Accident Analysis and Prevention*, 2016.

J. Florentin, F. Durieux, Y. Kuriyama, and T. Yamamoto. Electric motor noise in a lightweight steel vehicle. Technical report, SAE Technical Paper, 2011.

Fortune. Electric vehicle (EV) market size, share & industry analysis, by type, vehicle type, and regional forecast, 2019-2026. https://www.fortunebusinessinsights.com/industry-reports/electric-vehicle-market-101678, 2019. Accessed: 2020-05-21.

C. Fuller, C. Hansen, and S. Snyder. Active control of sound radiation from a vibrating rectangular panel by sound sources and vibration inputs: An experimental comparison. *Journal of Sound and Vibration*, 145(2):195 – 215, 1991a. ISSN 0022-460X. doi: https://doi.org/10.1016/0022-460X(91)90587-A.

C. Fuller, C. Hansen, and S. Snyder. Experiments on active control of sound radiation from a panel using a piezoceramic actuator. *Journal of Sound and Vibration*, 150(2): 179 – 190, 1991b. ISSN 0022-460X. doi: https://doi.org/10.1016/0022-460X(91)90614-P.

C. C. Fuller, S. J. Elliott, and P. A. Nelson. *Active control of vibration*. Academic Press, 1996.

W.-S. Gan, J. Yang, and T. Kamakura. A review of parametric acoustic array in air. *Applied Acoustics*, 73(12):1211–1219, 2012.

A. R. George. Automobile aerodynamic noise. *SAE transactions*, pages 434–457, 1990.

V. P. Gontcharov and N. P. R. Hill. Diffusivity properties of distributed mode loudspeakers. In *Audio Engineering Society Convention 108*. Audio Engineering Society, 2000.

K. Govindswamy and G. Eisele. Sound character of electric vehicles. Technical report, SAE Technical Paper, 2011.

F. P. Grad, A. J. Rosenthal, L. R. Rockett, J. A. Fay, J. Heywood, J. F. Kain, G. K. Ingram, D. Harrison Jr, and T. Tietenberg. Automobile and the regulation of its impact on the environment. Technical report, University of Oklahoma Press, Norman, OK, 1975.

GRB. Proposal for guidelines on measures ensuring the audibility of hybrid and electric vehicles. Working Party on Noise (GRB), Economic Commission for Europe, 2011.

R. Haberkern. Soundlazer directional loudspeakers. https://www.soundlazer.com/, 2020. Accessed: 2020-05-27.

R. Hanna. Incidence of pedestrian and bicyclist crashes by hybrid electric passenger vehicles. Technical report, National Highway Traffic Safety Administration, Department of Transportation, US, 2009.

J. H. Hansen, V. Radhakrishnan, and K. H. Arehart. Speech enhancement based on generalized minimum mean square error estimators and masking properties of the auditory system. *IEEE Transactions on Audio, Speech, and Language Processing*, 14(6):2049–2063, 2006.

P. Harrop and F. Gonzalez. Electric vehicles 2018-2038: Forecasts, analysis and opportunities. Technical report, IDTechEx USA, October 2018.

J. Hawkins Jr and S. Stevens. The masking of pure tones and of speech by white noise. *The Journal of the Acoustical Society of America*, 22(1):6–13, 1950.

M. Heckl. Tyre noise generation. *Wear*, 113(1):157–170, 1986.

M. C. Heilemann, D. Anderson, and M. F. Bocko. Sound-source localization on flat-panel loudspeakers. *Journal of the Audio Engineering Society*, 65(3):168–177, 2017.

M. C. Heilemann, D. A. Anderson, and M. F. Bocko. Near-field object-based audio rendering on flat-panel displays. *Journal of the Audio Engineering Society*, 67(7/8): 531–539, 2019.

K. Holland and F. Fahy. A low cost endfire acoustic radiator. *Journal of the Audio Engineering Society*, 39(7/8):540–550, 1991.

S. Hong, K. Cho, and B. Ko. Investigation of probability of pedestrian crash based on auditory recognition distance due to a quiet vehicle in motor mode. *International journal of automotive technology*, 14(3):441–448, 2013.

L. M. Iversen, G. Marbjerg, and H. Bendtsen. Noise from electric vehicles-'state of the art'literature survey. In *INTER-NOISE and NOISE-CON Congress and Conference Proceedings*, volume 247, pages 267–271. Institute of Noise Control Engineering, 2013.

JASIC. A study on approach warning systems for hybrid vehicle in motor mode. Japan Automobile Standards Internationalization Center, 2009.

JASIC. Guidelines for measure against quietness problem of hybrid vehicles. LIT and Japan Automobiles Standards Internationalisaition Centre - Informal group on quiet road transport vehicles, Japan, 2010.

D. S. Kim, R. W. Emerson, K. Naghshineh, J. Pliskow, and K. Myers. Impact of adding artificially generated alert sound to hybrid electric vehicles on their detectability by pedestrians who are blind. *Journal of rehabilitation research and development*, 49 (3):381, 2012.

G. H. Kim and Y. S. Moon. Apparatus for warning pedestrians of oncoming vehicle, Oct. 7 2014. US Patent 8,854,229.

L. Kinsler and A. Frey. *Fundamentals of Acoustics*. Wiley, 1962.

H. Konet, M. Sato, T. Schiller, A. Christensen, T. Tabata, and T. Kanuma. Development of approaching vehicle sound for pedestrians (vsp) for quiet electric vehicles. *SAE International Journal of Engines*, 4(1):1217–1224, 2011.

N. Kournoutos and J. Cheer. A system for controlling the directivity of sound radiated from a structure. *The Journal of the Acoustical Society of America*, 147:231–241, 2019. doi: 10.1121/10.0000589.

N. Kournoutos and J. Cheer. Investigation of a directional warning sound system for electric vehicles based on structural vibration. *The Journal of the Acoustical Society of America*, 148(2):588–598, 2020. doi: 10.1121/10.0001681.

J. Kragh. User's Guide Nord2000 Road. Technical report, DELTA, 2006.

S. Lee, K. Park, and H.-W. Park. A study on the improvement of acoustic radiation characteristics of flat panel exciter speakers. In *2020 IEEE International Conference on Consumer Electronics (ICCE)*. IEEE, 2020.

S. K. Lee, S. M. Lee, T. Shin, and M. Han. Objective evaluation of the sound quality of the warning sound of electric vehicles with a consideration of the masking effect: Annoyance and detectability. *International Journal of Automotive Technology*, 18(4): 699–705, 2017.

J. Lelong and R. Michelet. Passenger cars. Power unit and tyre-road noise, driving behaviour: What are the stakes? In *INTER-NOISE and NOISE-CON Congress and Conference Proceedings*. Institute of Noise Control Engineering, 2001.

D. Lennström, T. Lindbom, and A. Nykänen. Prominence of tones in electric vehicle interior noise. In *International Congress and Exposition on Noise Control Engineering: 15/09/2013-18/09/2013*, volume 1, pages 508–515. ÖAL Österreichischer Arbeitsring für Lärmbekämpfung, 2013.

Q. Li and D. J. Thompson. Directivity of sound radiated from baffled rectangular plates and plate strips. *Applied Acoustics*, 155:309 – 324, 2019. ISSN 0003-682X. doi: https://doi.org/10.1016/j.apacoust.2019.05.018.

G. Marbjerg. Noise from electric vehicles - a literature survey. Technical report, COMPETT, 2013.

R. Meinke. Parts express project gallery: DML flat panel speaker. http://projectgallery.parts-express.com/speaker-projects/dml-flat-pannel/, 2016.

L. Meirovitch. *Analytical methods in vibrations*. McMillan, 1967.

B. C. J. Moore. *Cochlear Hearing Loss*. Number 978-1-861-56091-9. Wiley, 1998.

P. Morgan et al. Assessing the perceived safety risk from quiet electric and hybrid vehicles to vision-impaired pedestrians. Department for Transport, UK, 2011.

M. Muirhead and L. Walter. Analysis of stats19 data to examine the relationship between the rate of vehicle accidents involving pedestrians and type approval noise levels. Department for Transport, UK, 2011.

T. Nelson and T. Nilsson. Comparing headphone and speaker effects on simulated driving. *Accident Analysis and Prevention*, 22(6):523–529, 1990.

P. Newell and K. Holland. *Loudspeakers: For music recording and reproduction*. Routledge, 2006.

NHTSA. Minimum Sound Requirements for Hybrid and Electric Vehicles. National Highway Traffic Safety Administration, Department of Transportation, US, 2013.

NHTSA. Minimum Sound Requirements for Hybrid and Electric Vehicles - Final Rule. National Highway Traffic Safety Administration, Department of Transportation, US, 2016.

M. E. Nilsson, J. Alvarsson, M. Rådsten-Ekman, and K. Bolin. Auditory masking of wanted and unwanted sounds in a city park. *Noise Control Engineering Journal*, 58 (5):524–531, 2010.

M. P. Norton and D. G. Karczub. *Fundamentals of Noise and Vibration Analysis for Engineers*. Cambridge University Press, 2 edition, 2003. doi: 10.1017/CBO9781139163927.

P. Nyeste and M. Wogalter. On adding sound to quiet vehicles. *Proceedings of the Human Factors and Ergonomics Society Annual Meeting*, 52(21):1747–170, 2008.

C. Oestergaards. EC Tunes warning sound system for electric and hybrid vehicles - technical specification. http://www.ectunes.com/, 2013. Accessed: 2017-09-04.

O. Ojo, G. Dong, and Z. Wu. Pulse-width modulation for five-phase converters based on device turn-on times. In *Conference Record of the 2006 IEEE Industry Applications Conference Forty-First IAS Annual Meeting*, volume 2, pages 627–634. IEEE, 2006.

F. Olivieri, F. M. Fazi, M. Shin, and P. Nelson. Pressure-matching beamforming method for loudspeaker arrays with frequency dependent selection of control points. In *Audio Engineering Society Convention 138*, May 2015.

H. F. Olson. *Elements of acoustical engineering*. D. Van Nostrand Co., 1947.

H. F. Olson. Directional microphones. *Journal of the Audio Engineering Society*, 15(4): 420–430, 1967.

J. Pan, S. D. Snyder, C. H. Hansen, and C. R. Fuller. Active control of far field sound radiated by a rectangular panel –a general analysis. *The Journal of the Acoustical Society of America*, 91(4):2056–2066, 1992. doi: 10.1121/1.403691.

E. Parizet, W. Ellermeier, and R. Robart. Auditory warnings for electric vehicles: Detectability in normal-vision and visually-impaired listeners. *Applied Acoustics*, 86:50–58, 2014.

E. Parizet, K. Janssens, P. Poveda-Martínez, A. Pereira, J. Lorencki, and J. Ramis-Soriano. *NVH analysis techniques for design and optimization of hybrid and electric vehicles*, volume 4. Shaker Verlag Publications, 2016a.

E. Parizet et al. Additional efficient warning sounds for electric and hybrid vehicles. In Z. S. Michel André, editor, *Energy and Environment*, volume 1, pages 501–510. Wiley, 2016b. doi: 10.1002/9781119307761.ch32.

R. D. Patterson, I. Nimmo-Smith, J. Holdsworth, and P. Rice. An efficient auditory filterbank based on the gammatone function. In *a meeting of the IOC Speech Group on Auditory Modelling at RSRE*, volume 2, 1987.

C. Paulitsch, P. Gardonio, and S. J. Elliott. Active vibration control using an inertial actuator with internal damping. *The Journal of the Acoustical Society of America*, 119 (4):2131–2140, 2006. doi: 10.1121/1.2141228.

C. Peachy. Halosonic applications for electric vehicles. Lotus Engineering Presentation, 2013.

J. Petiot, B. Kristensen, and A. Maier. How should an electric vehicle sound? user and expert perception. *Proceedings of the ASME 2013 International Design Engineering Technical Conferences / Computers and Information in Engineering Conference IDETC/CIE*, 2013.

F. J. Pompei. The use of airborne ultrasonics for generating audible sound beams. *Journal of the Audio Engineering Society*, 47(9):726–731, 1999.

F. J. Pompei. Directional acoustic alerting system, 2006. US Patent 7,106,180.

P. Poveda-Martínez, R. Peral-Orts, N. Campillo-Davo, J. Nescolarde-Selva, M. Lloret-Climent, and J. Ramis-Soriano. Study of the effectiveness of electric vehicle warning sounds depending on the urban environment. *Applied Acoustics*, 116:317–328, 2017.

D. Quinn, J. Mitchell, P. Clark, and J. J. García. eVADER-Development and initial evaluation of a next generation pedestrian alert solution for quiet electric vehicles. In *Proc. FISITA*, page 111, 2014.

R. Rabenstein and S. Spors. Spatial aliasing artifacts produced by linear and circular loudspeaker arrays used for wave field synthesis. In *Audio Engineering Society Convention 120*. Audio Engineering Society, 2006.

G. Rimondi. Tire contribution in the context of automobile noise reduction. *Tire Science and Technology*, 23(3):189–208, 1995.

M. C. Robbins. The effectiveness of emergency vehicle audio warning systems. In *Proceedings of the Human Factors and Ergonomics Society Annual Meeting*, volume 39, pages 1004–1005. SAGE Publications Sage CA: Los Angeles, CA, 1995.

I. Sakamoto et al. Reviews on countermeasure to safety risk associated with quietness of hybrid or electric vehicles in japan. In *INTER-NOISE and NOISE-CON Congress and Conference Proceedings*, volume 244, pages 4285–4292. Institute of Noise Control Engineering, 2010.

I. Sakamoto et al. Report on basic research for standardization of measures for quiet vehicles in Japan (Intermit report). In *INTER-NOISE and NOISE-CON Congress and Conference Proceedings*, volume 246, pages 470–481. Institute of Noise Control Engineering, 2012.

U. Sandberg. Adding noise to quiet electric and hybrid vehicles: an electric issue. *Noise News Internation*, 2012.

U. Sandberg, L. Goubert, and P. Mioduszewski. Are vehicles driven in electric mode so quiet that they need acoustic warning signals? *Proceedings of 20th International Congress on Acoustics*, 2010.

M. F. Simón Gálvez, S. J. Elliott, and J. Cheer. A superdirective array of phase shift sources. *The Journal of the Acoustical Society of America*, 132(2):746–756, 2012. doi: 10.1121/1.4733556.

M. F. Simón Gálvez, S. J. Elliott, and J. Cheer. Personal audio loudspeaker array as a complementary tv sound system for the hard of hearing. *IEICE Transactions on Fundamentals of Electronics, Communications and Computer Sciences*, 97(9):1824–1831, 2014.

S. Singh, S. Payne, and P. Jennings. Detection and emotional evaluation of an electric vehicle's exterior sound in a simulated environment. In *INTER-NOISE and NOISE-CON Congress and Conference Proceedings*. Institute of Noise Control Engineering, 2013.

W. Soede, F. A. Bilsen, and A. J. Berkhout. Assessment of a directional microphone array for hearing impaired listeners. *The Journal of the Acoustical Society of America*, 94(2):799–808, 1993. doi: 10.1121/1.408181.

Soundracer AB. Soundracer Electric Vehicle Electronic Engine Sound Systems. https://www.soundracer.se/, 2017. Accessed: 2017-09-04.

A. Stelling-Konczak, G. van Wee, J. Commandeur, and M. Hagenzieker. Mobile phone conversations, listening to music and quiet (electric) cars: are traffic sounds important for safe cycling? *Accident Analysis & Prevention*, 106:10–22, 2017.

T. Tabata et al. Development of approaching vehicle sound for pedestrians (VSP) for quiet electric vehicles. *Nissan Motor Company*, 2011.

F. Takahashi, G. Watanabe, M. Nakada, H. Sakata, and M. Ikeda. Tyre/suspension system modelling for investigation of road noise characteristics. *International Journal of Vehicle Design*, 8(4-6):588–597, 1987.

N. Tanaka and M. Tanaka. Active noise control using a steerable parametric array loudspeaker. *The Journal of the Acoustical Society of America*, 127(6):3526–3537, 2010.

E. Terhardt. Calculating virtual pitch. *Hearing research*, 1(2):155–182, 1979.

E. Terhardt, G. Stoll, and M. Seewann. Algorithm for extraction of pitch and pitch salience from complex tonal signals. *The Journal of the Acoustical Society of America*, 71(3):679–688, 1982.

UNECE. Regulation No 138 of the Economic Commission for Europe of the United Nations (UNECE) — Uniform provisions concerning the approval of Quiet Road Transport Vehicles with regard to their reduced audibility. Economic Commission for Europe of the United Nations (UNECE), 2017.

R. van der Rots and A. Berkhoff. Directional loudspeaker arrays for acoustic warning systems with minimised noise pollution. *Applied acoustics*, 89:345–354, 2015.

E. Verheijen and J. Jabben. Effect of electric cars on traffic noise and safety. *National Institute for Public Health and the Environment, The Netherlands*, 2010.

VISATON GmbH & Co. KG. *MR 130 - 8 Ohm Fullrange System*, 2017.

I. Wagner. The U.S. electric vehicle industry - statistics & facts. https://www.statista.com/topics/4421/the-us-electric-vehicle-industry/, 2020. Accessed: 2020-05-21.

C. E. Wallace. Radiation resistance of a rectangular panel. *The Journal of the Acoustical Society of America*, 51:946–952, 1972. doi: 10.1121/1.1912943.

G. B. Warburton. The vibration of rectangular plates. *Proceedings of the Institution of Mechanical Engineers*, 168(1):371–384, 1954.

R. Wegel and C. Lane. The auditory masking of one pure tone by another and its probable relation to the dynamics of the inner ear. *Physical review*, 23(2):266, 1924.

P. J. Westervelt. Parametric acoustic array. *The Journal of the Acoustical Society of America*, 35(4):535–537, 1963. doi: 10.1121/1.1918525.

M. Wogalter, R. Ornan, R. Lim, and M. Chipley. On the risk of quiet vehicles to pedestrians and drivers. *Proceedings of the Human Factors and Ergonomics Society Annual Meeting*, 45(23):1685–1688, 2001.

J. Wu, R. Austin, and C.-L. Chen. Incidence rates of pedestrian and bicyclist crashes by hybrid electric passenger vehicles: An update. Technical report, National Highway Traffic Safety Administration, Department of Transportation, US, 2011.

K. Yamauchi. A discussion on the problem of quietness of hybrid and electric vehicles and additional warning sound for these vehicles. In *Proc. Forum Acusticum*, 2014.

J. K. You, M. H. Cho, and J. M. Lee. Pedestrian warning system and method for eco-friendly vehicle, Jan. 7 2020. US Patent 10,525,878.

E. Zwicker. Subdivision of the audible frequency range into critical bands (frequenzgruppen). *The Journal of the Acoustical Society of America*, 33(2):248–248, 1961.